Investigating the role of higher order chromatin structure and DNA damage complexity on ATM signalling and G2/M checkpoint arrest

A thesis submitted to the University of Sussex for the degree of Doctor of Philosophy

By

Holly Brunton

July 2011

Declaration

I hereby declare that thesis has not been and will not be, submitted in whole or in part to another University for the award of any other degree.

Holly Brunton

Acknowledgements

I would like to express my sincerest gratitude to Professor Penny Jeggo for support and guidance throughout my Doctorate studies. A special thank you is given to Dr Aaron Goodarzi and Dr Atsushi Shibata for their time and expertise in the laboratory. Both of whom made the work presented in this thesis possible. In addition, I would like to thank all members of the Jeggo laboratory for stimulating scientific discussions and of course friendship. A final thank you is given to my friends and family.

UNIVERSITY OF SUSSEX

HOLLY BRUNTON

DOCTOR OF PHILOSOPHY BIOCHEMISTRY

Investigating the role of higher order chromatin structure and DNA damage complexity on ATM signalling and G2/M checkpoint arrest

SUMMARY

In response to DNA double stranded breaks (DSBs), mammalian cells have evolved two major repair pathways, DNA Non Homologous End Joining (NHEJ) and Homologous Recombination (HR). The majority of DSB repair in G1 and G2 phase is repaired with fast kinetics by NHEJ in a pathway that involves the core NHEJ factors: Ku, DNA-PKcs, XLF, DNA Ligase IV and XRCC4. A subset of slow repairing DSBs also requires ATM and Artemis (Riballo *et al*, 2004). This slow component of repair represents DSBs that reside within highly compacted regions of the genome known as heterochromatin (HC) (Goodarzi *et al*, 2008). ATM functions at HC to mediate relaxation by phosphorylating the HC building factor KAP-1 (Goodarzi *et al*, 2008). Here I provide evidence that DSBs dependent upon Artemis for their repair also reside within regions of HC. However, unlike ATM, Artemis functions downstream of the HC relaxation process. In response to DSBs, ATM phosphorylates the histone variant H2AX (γH2AX). γH2AX acts as a docking site for the localized recruitment and activation of DNA Damage Response (DDR) proteins. The expansion of γH2AX can spread over megabases of DNA. Here I have shown that highly compacted KAP-1, MeCP2 and DNMT3B enriched chromatin acts as a barrier to IR induced γH2AX expansion. In patient cells deficient for MeCP2 or DNMT3B proteins, such as Rett syndrome (MeCP2 deficient) and Immunodeficiency centromeric-instability facial-anomalies syndrome (DNMT3B deficient), ATM and Chk2 signalling is heightened, which is reflected in a hypersensitive and prolonged G2/M checkpoint arrest. These findings suggest that higher order chromatin complexity is a barrier to ATM signalling to the checkpoint machinery. In the final section of my thesis, I addressed what affect DNA damage complexity exerts on checkpoint arrest. Using exposure to heavy ion irradiation, which induces complex DSBs, I observed larger γH2AX foci and prolonged G2/M checkpoint arrest.

Abbreviations

53BP1	p53 binding protein 1
9-1-1	Rad9-Rad1-Hus1
Alt-NHEJ	Alternative NHEJ
Asf1	Anti-silencing function 1
A-T	Ataxia telangiectasia
ATLD	Ataxia telangiectasia-like disorder
ATR	ATM and Rad3-related protein
ATRIP	ATR interacting protein
ATP	Adinosine Triphosphate
ATM	Ataxia Telangiectasia Mutated
ATMi	ATM inhibitor
ATR-SS	ATR-seckel syndrome
BARD1	BRCA1 associated RING domain protein 1
Bax	Bcl-2 associated x
Bcl-2	B-cell lymphoma 2
BER	Base Excision Repair
bp	Base pair
BRCA1	Breast cancer associated protein 1
BRCT	BRCA1 C-terminal domain
BSA	Bovine serum albumin
CAF-1	Chromatin assembly factor
CDK	Cyclin dependent kinase

CDK2	Cyclin dependent kinase 2
CENP-A	Centromere protein A
CENP-F	Centromere protein F
ChIP	Chromatin Immunoprecipitation
Chk1	Checkpoint protein 1
Chk2	Checkpoint protein 2
CK2	Caesin kinase 2
CSR	Class switch recombination
CT	Computed tomography
C-terminus	Carboxyl terminus
CtIP	C-terminal binding protein
DAPI	4’,6-diamidino-2-phenylindole
DDR	DNA Damage Response
DNA	Deoxyribonucleic acid
DNA-PK	DNA-dependent kinase
DNA-PKcs	DNA-dependent kinase catalytic subunit
DNMT	DNA methyltransferase
DSBs	Double Stranded Breaks
FACS	Fluorescence-activated cell sorting
FAT	FRAP-ATM-TRRAP domain
FATC	FRAP-ATM-TRRAP-C terminal
FCS	Foetal calf serum
Fe	Iron

FHA	Fork head associated domain
FSHD	Facioscapulohumeral muscular dystrophy
γH2AX	H2AX phosphorylated at Ser139
GAR	Glycine/arginine-rich region (GAR)
GCN5	Glucosamine-5-phosphate N-acetyltransferase
GCR	Galactic cosmic rays
GFP	Green Fluorescent Protein
GSI	Gesellschaft fur schrrerionedforschung Institute
Gy	Gray
H2A	Histone H2A
H2AX	Histone variant H2AX
H3	Histone H3
H4	Histone H4
HAT	Histone acetylase
HC	Heterochromatin
HDAC	Histone deacetylase
HEAT	Huntingtin, elongation factor 3 protein phosphatase 2A and TOR1
HERC2	Heat domain and RLD 2
HGPS	Hutchinson-Gilford progeria syndrome
HMG	High mobility group
HIMAC	Heavy Ion medical Accelerator in Chiba
HMGN1	High-mobility group nucleosome binding domain 1
HMT	Histone methyltransferase

HP1	Heterochromatin protein 1
HR	Homologous Recombination
HSC	Hematopoietic stem cell
HU	Hydroxyurea
ICF	Immunodeficiency Centromeric instability Facial anomalies syndrome
ICL	Inter-cross link repair
IF	Immunofluorescence
Igs	Immunoglobulin
IP	Immunoprecipitation
IR	Ionizing Radiation
IRIF	Ionizing radiation induced foci
K68	Ubiquitin chains
KAP-1	Kruppel box associated protein 1
Kb	Kilobases
KRAB	Kruppel associated box domain protein
LBR	Lamin B receptor
LET	Linear energy transfer
LIG4	Ligase IV syndrome
LMDS	Local multiple damaged sites
MAPK	Mitogen activated protein kinase
MBC	Methyl binding domain
MCM	minichromosome maintenance
MDC1	Mediator of DNA Damage Checkpoint protein 1

MDM2	Murine double minute 2
MeCP2	Methyl CpG binding protein 2
MEF	Murine / mouse embryonic fibroblast
MMR	Mismatch repair
MNase	Micrococcal nuclease
MRI	Magnetic resonance imaging
MRN	Mre11 / Rad50 / Nbs1 complex
mRNA	Messenger RNA
NBS	Nijmegen breakage syndrome
NCS	Neocarzinostatin
NES	Nuclear export signal
NER	Nucleotide Excision Repair
NFKβ	Nuclear factor kappa-light-chain-enhancer of activated B cells
NHEJ	Non-homologous end joining
NIH3T3	Mouse fibroblast cell line
NIRS	National Institute of Radiological Science
NLS	Nuclear localisation signal
NoRC	Nuclear remodelling complex
N-terminus	amino terminus
NTP	Nucleoside triphosphate
NuRD	Nucleosome Remodelling histone Deacetylase
OTUB1	OUT domain-containing ubiquitin aldehyde-binding protein 1
PAGE	Polyacrylomide gel electrophoresis

PALB2	Partner and localizer of BRCA2
PARP	Poly ADP-ribose Polymerase
PARPi	PARP inhibitor
PARP1	Poly ADP-ribose Polymerase 1
PARP2	Poly ADP-ribose Polymerase 2
pATM	ATM phosphorylated on serine 1981
PAZ	PIWI / Argonaute / Zwille domain
PBS	Phosphate buffered saline
PCC	Prematurely condensed chromosome
pChk1	Chk1 phosphorylated at serine 345
pChk2	Chk2 phosphorylated at threonine 68
PCNA	Proliferating cell nuclear antigen
PCNT-SS	Percentrin-mutated Seckel syndrome
PET	Position emission tomography
PFA	Paraformaldehyde
PFGE	Pulse field gel electrophoresis
pH3	Histone H3 phosphorylated on serine 10
PHD	Plant homeo domain
PIAS1	Protein inhibitor of activated STAT 1
PIAS4	Protein inhibitor of activated STAT 4
PIKK	Phosphoinositol 3-kinase like kinase
PIP	PCNA interacting protein motif
piRNA	PIWI interacting RNA

pKAP-1	KAP-1 phosphorylated on serine 824
PML	Pro myelocytic leukaemia
PP2A	Protein phosphatase 2A
PP5A	Protein phosphatase 5A
PRD	PIKK regulatory domain
PRMT1	Protein arginine N methyltransferase 1
PTIP	Pax2 Transactivating domain-interacting protein
PUMA	p53 up-regulated modulator of apoptosis
Rb	Retinoblastoma
RBE	Relative biological effectiveness
rDNA	Ribosomal DNA
RDS	Radioresistant DNA synthesis
RFC	Replication Factor C
RISC	RNA induced silencing complex
RNA	Ribonucleic acid
RNAi	RNA interference
RNF168	Ring-finger containing Nuclear Factor 168
RNF8	Ring-finger containing Nuclear Factor 8
ROS	Reactive oxygen species
RPA	Replication protein A
rRNA	Ribosomal RNA
RSC	Remodels the Structure of Chromatin
RSS	Recombination Signal Sequences

RSTS	Rubinstein-Tabi syndrome
RT	Radiotherapy
SCD	SQ/TQ motif
SCID	Severe combined immunodeficiency
SCIDA	Athabascan-type SCID
SDS	Sodium dodecyl sulphate
SET	Su(var)3-9, Enhancer of zeste and Trithorax domain
SETDB1	SET domain, bifurcated 1
SIPS	Stress induced premature senescence
siRNA	Short interfering RNA
SIRT1	Sirtuin 1
SOBP	Spread out Bragg peak
SSA	Single strand annealing
SSB	Single strand break
ssDNA	Single stranded DNA
SUMO	Small ubiquitin modifier
SAE	SUMO activating enzymes
SWI/SNF	Switching defective and Sucrose Non-Fermenting
TCR	T cell receptor
TRD	Transcriptional repressor domain
TRF	Telomere repeat binding factor
TOPBP1	Topoisomerase binding protein 1
TSA	Trichostatin A

Ub	Ubiquitin
UBC13	Ubiqutin conjugating enzyme 13
UIM	Ubiquitin interacting motif
UV	Ultraviolet light
VDAC	voltage-dependent anion channel
V(D)J	Variable (V), Diversity (D) and Joining (J) genes
WT	Wildtype
XCI	X chromosome inactivation
XLF	XRCC4-like factor
XRCC4	X-ray cross complementing group 4

List of Figures

List of Tables

Chapter 1: Introduction

1 Introduction

1.1 The importance of the DNA damage response

On a daily basis our genetic material is exposed to a variety of DNA damaging agents. Exposure to these agents poses a threat to the faithful transmission of our genetic material and to the survival of the individual. In response to these threats, mammalian cells have evolved an assortment of repair mechanisms which mechanistically preserve the genetic information encoded by DNA. The failure to repair or the misrepair of DNA alterations or lesions can result in apoptosis or chromosomal alterations including deletions, translocations, and chromosome fusions, which decrease genome stability and can subsequently lead to the development of cancer. Mammalian cells potentially experience 10^5 spontaneous DNA lesions per day (Hoeijmakers, 2009). Sources of DNA damage can arise both endogenously and exogenously. Endogenous sources of DNA damage include hydrolysis, oxidation, alkylation, and inaccurate replication of DNA (Lindahl and Barnes, 2000). Environmental sources of DNA damaging agents include ionizing radiation (IR), ultraviolet (UV) radiation and various chemotherapeutic drugs (Hakem, 2008) (Table 1.1). Given the range of DNA alterations potentially inflicted on a cell on a daily basis, it is no surprise that a variety of repair mechanisms specific for lesion type have evolved to counteract the DNA damage (Table 1.2). The most potentially threatening lesions posed to mammalian cells are DNA Double Stranded Breaks (DSBs). The signaling and repair mechanisms that are activated in response to these lesions will be the main focus of this thesis.

Activation of DNA repair pathways is a highly regulated process that ensures DNA repair at the right time and place. In response to replication stress and DNA damage the DNA Damage Response (DDR) signaling transduction pathway is activated (Jackson and Bartek, 2009). The DDR is primarily activated by members of the PIKK family – ATM, ATR and DNA-PK, and members of the poly (ADP-ribose) polymerase (PARP) family. ATM and DNA-PK respond to DSBs. ATR in complex with ATRIP is activated following recruitment to RPA coated single stranded (ss) DNA regions which can occur at stalled replication forks and resected DSBs (Cimprich and Cortez, 2008a). PARP is activated in response to single stranded breaks (SSBs) and catalyzes the addition of poly (ADP-ribose) chains on proteins to recruit DDR factors to chromatin at single stranded (ss) breaks (Schreiber et al., 2006). The PARP family has 16 members, but only PARP1 and PARP2 have been implicated in the DDR (Schreiber et al., 2006). ATM and ATR are required for DSB repair as well as repair of replication associated damage. In

this general introduction I have given a mechanistic overview of points relevant to my thesis. Each chapter has a more specific and detailed discussion of arguments significant to each chapter.

1.2 DSB repair

At least 4 independent pathways of DSB repair exist, these being NHEJ, HR, alternative NHEJ (alt-NHEJ) and single strand annealing (SSA). A factor mainly influencing pathway choice is the extent of DNA end processing. NHEJ does not require end processing or resection, whereas alt-NHEJ, HR and SSA are dependent on DSB end resection prior to repair (Hartlerode and Scully, 2009). Four different DSB sensors also exist: Ku70/Ku80, Mre11/Rad50/Nbs1 (MRN) and RPA, which direct repair down different repair pathways. The major pathways of DSB repair that predominate are NHEJ and HR.

1.2.1 Non Homologous End joining (NHEJ)

In mammalian cells the majority of DSBs in both G1 and G2 phases of the cell cycle are repaired by NHEJ (Beucher et al., 2009). The initiating step of NHEJ involves the binding of the heterodimer Ku70/80, which forms a ring like structure around each end of the broken DNA molecule (Walker *et al*, 2001). Ku70/80 binds DSB ends with high affinity and localizes at the site of damage within seconds (Smith et al., 1999). The DNA-dependent protein kinase catalytic subunit (DNA-PKcs), a serine/threonine protein kinase, is activated following recruitment to the DSB by Ku70/80 (Gottlieb and Jackson, 1993). This interaction between Ku and DNA-PKcs is thought to be mediated by the Ku80 carboxyl-terminus (Singleton et al., 1999). DNA-PKcs contains two clusters of autophosphorylation, known as the ABCDE (aa 2609 – 2647) and PQR (aa 2023 – 2056) (Cui et al., 2005). The DNA-PK holoenzyme (DNA-PKcs and Ku70/80) is thought to be important for tethering DNA ends. The initial presence of the unphosphorylated DNA-PK effectively blocks access to DNA termini by processing enzymes and ligases. It has been postulated that this blocking event functions to regulate repair pathway choice between NHEJ and HR, since an increased incidence of HR was observed in DNA-PK deficient cells (Allen et al., 2003). Autophosphorylation of DNA-PK on the ABCDE cluster results in destabilization of DNA-PKcs interaction with the DNA ends thus relieving this blockage (Chan et al., 2002). If the DSB termini are refractory to direct ligation, nucleases are subsequently recruited to process

the DNA ends prior to ligation. A 10-25% sub-fraction of DSBs are specifically dependent on processing by the endonuclease Artemis, in an ATM dependent NHEJ repair pathway. One question I wish to address in my thesis is the nature of these lesions dependent on Artemis for repair. Ligation of blunt or processed ends is catalyzed by the ATP utilizing Ligase IV, XRCC4 and XLF complex. The carboxy terminus of ligase IV contains two regions that harbor BRCA1 carboxy-terminus like (BRCT) motifs, a sequence known to be involved in protein-protein interactions, especially with BRCT domains in other proteins (Zhang et al., 1998). It has been suggested that the BRCT motifs of ligase IV may be involved in the interaction of ligase IV/ XRCC4/ XLF complex with Ku70/80 (Costantini et al., 2007), resulting in its recruitment to the DSB. Ligation is mediated by the donation of an AMP onto the exposed 5' phosphate by the DNA ligase-adenylate complex. It has been proposed that XLF re-adenylates ligase IV following the ligation event, which recharges ligase IV for further ligations (Riballo et al., 2009) (Figure 1.1). The majority of NHEJ repair is ATM independent and repaired with fast kinetics (Riballo et al., 2004b). Only 10-25 % of ionizing radiation (IR) induced DSBs in G0/G1 phase of the cell cycle require ATM activity and this sub-fraction represents the slow repair component of NHEJ. This slow component of DSB repair also requires the mediator protein 53BP1, γH2AX, the Mre11/Rad50/Nbs1 (MRN) complex and the endonuclease Artemis (Riballo et al., 2004). Further details of the slow and fast repair kinetics of DSB repair are given in chapter 4. Extensive characterization of ATM and Artemis has shown that cells lacking either of these two proteins manifest an epistatic repair defect whereby 10-20% of IR induced DSB remain un-repaired (Riballo et al., 2004), strongly suggesting that they function within a common pathway. The role of Artemis in DSB repair is evaluated in chapter 5.

1.2.2 Homologous Recombination (HR)

DSBs can be recognised by the Mre11/Rad50/Nbs1 complex, which promotes activation of ATM (Williams and Tainer, 2007). MRE11 has endonuclease and exonuclease activities that are important for the initial steps of DNA end resection, which are essential to initiate HR repair (Williams et al., 2007) (Figure 1.1). The NBS1 subunit of the MRN complex interacts with ATM via its C-terminal region, which promotes the recruitment of ATM to DSBs (Jazayeri et al., 2008). DNA resection, which is required to mediate HR, is regulated by ATM dependent phosphorylation and subsequent activation of CtIP (Shibata et al., 2011). CtIP interacts with BRCA1 and the MRN complex, interactions of which are likely to be important for CtIP recruitment to damage sites (Huen et al., 2010). CtIP is an endonuclease that promotes DNA

end resection (Sartori et al., 2007). CtIP activity is regulated by CDK2 phosphorylation, levels of which are low in G1 phase cells (You and Bailis, 2010). Since HR is dependent on resection and a homologous sister chromatid to act as a template for repair, this repair pathway is restricted to S and G2 phases of the cell cycle (You & Boulis, 2010). In S and G2, CtIP associates with BRCA1, which ubiquitinates CtIP and facilitates its association with damaged sites (Huen et al., 2010). Repair pathway choice is thought to be regulated by resection. Indeed DSB resection promoted by CtIP and ATM can be inhibited by 53BP1 in BRCA1 deficient cells (Bunting et al., 2010). 53BP1 was shown to block HR by preventing end resection. Here the knockdown of 53BP1 in BRCA1 deficient cells rescued the sensitivity of BRCA1 cells to PARPi, suggesting that 53BP1 blocks HR. BRCA1 and 53BP1 deficient cells inhibited for ATM were also sensitive to PARPi, since ATM cannot initiate CtIP mediated resection despite DNA ends being available for resection. BRCA1 is known to possess ubiquitin ligase activity, but this function is not essential for maintaining genomic stability (Reid et al., 2008). Bunting et al (2010), propose that BRCA1 may function to remove proteins which are inhibitory to HR. For example the retention of Ku (Postow et al., 2008) and 53BP1 (Watanabe et al., 2009) is dependent on DSB induced ubiquitination of these factors. Following DSB resection and formation of 3'ssDNA ends, the heterotrimeric RPA complex, which is composed of 3 tightly associated subunits of 70, 32 and 14 KDa, binds the ssDNA region (Wold, 1997). RPA is required for NER, BER, MMR and DSB repair (Wold, 1997). RPA is hyperphosphorylated in response to UV or IR (Liu and Weaver, 1993). The unstressed cell cycle dependent phosphorylation of RPA occurs during G1/S transition and in M phase at CDK phosphorylation sites Ser23 and Ser29 at the N-terminus of RPA32 subunit (Din et al., 1990). Stress induces RPA hyperphosphorylation. RPA coated single stranded DNA regions recruit the PIKK family member ATR. ATR binds RPA via the ATR interacting protein (ATRIP) (Zou and Elledge, 2003). ATR phosphorylates components of the replication fork including the MCM helicase complex, which facilitates DNA strand opening (Cortez et al., 2004). ATR also phosphorylates Chk1 at the site of a DSB (Lukas et al., 2003). Chk1 phosphorylates protein involved in HR repair, including RAD51. Chk1 dependent RAD51 phosphorylation at Thr309 is essential for RAD51 foci formation after replication associated damage (Sorensen et al., 2005). Rad51 filaments assemble on RPA coated ssDNA a process which is mediated through BRCA2 leading to HR repair (West, 2003). RPA and Rad51 form IR induced foci, which have been suggested to represent sites of resected DSBs (Miyazaki et al., 2004). The interaction between Rad51 and BRCA2 C-terminus is dependent on CDK dependent phosphorylation of BRCA2, and is therefore limited to S and G2 phases of the cell cycle (Esashi et al., 2005). Rad51 filaments mediate the process of strand invasion, a process which searches the sister chromatid for homologous sequences to use as a template for repair. There are

several outcomes from this process, including extension of the 3' invading strand by DNA polymerase followed by reannealing to the processed second strand of the break (West, 2003). Alternatively, Holiday junction intermediates can be formed after ligation of the invading strand with the second DNA end following branch migration (West, 2003). A variety of process can function to resolve the Holliday junction intermediate structures (Wechsler et al., 2011). Proteins involved in Holiday junction resolution include MUS81-EME1 (Chen et al., 2001), SLX1-SLX4 (Andersen et al., 2009) and GEN1 (Rass et al., 2010), which function in endonucleolytic cleavage. Topological DNA problems that arise during DNA replication or repair can be resolved by topoisomerase enzyme I or II. Topoisomerases are enzymes that bind single or double stranded DNA and induce a transient nick in the DNA phosphate backbone. This allows the DNA to unwind and relax around the nick and subsequently removes the topological problem.

A role for CtIP has recently been established in the removal of DNA interstrand crosslinks. CtIP functions in G1 phase cells along with the MRN complex to remove etoposide induced lesions (Quennet et al., 2010). Knockdown of CtIP in XLF deficient cells was not additive suggesting that CtIP directed repair of etoposide (a drug which inhibits topoisomerase II) induced DSBs via NHEJ. It was proposed that CtIP functions in G1 with the MRN complex to remove topoisomerase II from DSBs prior to repair by NHEJ (Quennet et al., 2010).

Loss of ATRIP leads to an almost identical phenotype as observed when ATR is deleted (Cortez et al., 2001). ATRIP binds to RPA coated ssDNA directly (Zou and Elledge, 2003). γH2AX after UV is dependent on ATR (O'Driscoll et al., 2003b; Ward and Chen, 2001). CtIP is not phosphorylated after UV (Foray et al., 2003). ATM is not activated in response to UV (Khanna et al., 2001).

1.2.3 Alternative NHEJ

PARP also senses DSBs and acts to promote alt-NHEJ, which functions as a "backup" repair pathway to classical NHEJ in the absence of Ku (Wang et al., 2006a). Alt-NHEJ is characterized by repair junctions bearing regions of microhomology, excessive deletions (Roth and Wilson, 1986) and chromosomal translocations (Bennardo et al., 2008). Chromosomal translocations are characteristic of cancer cells, thus understanding translocation formation is important for preventing tumorigenesis. An alternative NHEJ pathway was suggested to function to promote translocation formation given that translocations are not observed with HR proficient cells (Zhang and Rowley, 2006) and the elimination of Ku or DNA ligase IV–XRCC4 promotes the

frequency that chromosomal translocations occur (Simsek and Jasin, 2010). Alt-NHEJ uses a region of microhomology to align the broken DNA strands before joining. To reveal a region of microhomology suitable to mediate alt-NHEJ, 5'-3' nucleolytic resection is required to degrade the ends at the DSB which results in loss of DNA sequence (McVey and Lee, 2008). A candidate nuclease is CtIP, since CtIP depleted cells have a decreased frequency of chromosomal translocation (Li et al., 2000). Recently CtIP has been established to have an essential role in alt-NHEJ. CtIP depletion in $Ku70^{-/-}$ cells resulted in an 80% reduction in translocations. Ku normally suppresses chromosomal translocations by inhibiting the resection step of alt-NHEJ and directing repair by NHEJ. Additionally CtIP knockdown cells were observed to have shorter microhomology repair junctions (Zhang & Jasin, 2010). Therefore alt-NHEJ is a DSB repair pathway that is independent of Ku and XRCC4 but dependent on PARP and CtIP.

1.3 Signalling molecules and modifications

1.3.1 Phosphorylation

Post translational modifications such as protein phosphorylation in response to DNA damage is an important mechanism which orchestrates and regulates the DDR. Phosphorylation is the addition of a phosphate (PO_4) group onto a protein. Phosphorylation activates or deactivates many protein enzymes. Phosphorylation on serine is the most common residue modified by phosphate addition, followed by threonine, then tyrosine (Burnett and Kennedy, 1954). The addition of a phosphate group to a protein is carried out by protein kinases. Kinases are enzymes that transfer the phosphate group from donor molecules such as ATP to specific substrates. Eukaryotic protein kinases belong to an extensive protein family that share a conserved catalytic core (Hanks and Hunter, 1995). The N-terminal of the catalytic domain has a stretch of glycine residues with a lysine amino acid which is important for ATP binding. The catalytic domain also contains an aspartic acid which is important for the catalytic activity of the kinase (Knighton et al., 1991). Serine/Threonine protein kinases phosphorylate the OH group of serine or threonine. ATM, ATR, and DNA-PKcs are all serine/threonine protein kinases and are central to damage response signalling.

1.3.2 Ubiquitination and SUMOylation

In addition to phosphorylation, ubiquitination and SUMOylation have recently been established as additional modifications important for DDR regulation. Ubiquitin is a small highly conserved regulatory protein. The ubiquitination of target proteins works using three functional components, namely an E1 ubiquitin activating enzyme, an E2 ubiquitin conjugating enzyme and an E3 ubiquitin ligase (Figure 1.3). The E1 ubiquitin ligase catalyzes the activation of ubiquitin by using ATP to transfer ubiquitin to the E2 enzyme. The E2 enzyme interacts with a specific E3. The E3 ligase is responsible for transferring the ubiquitin to a specific target by catalysing the attachment of ubiquitin to a lysine on a target protein via an isopepetide bond. Polyubiquitinated proteins are often targeted for degradation by the proteasome. Mono-ubiquitinated proteins are not targeted for degradation, but instead are altered in their cellular location or function. Additionally, different lysine residues targeted for ubiquitination can direct events down different pathways, for example Lys48 polyubiquitin chains target proteins for proteosomal degradation, whereas Lys68 polyubiquitin chains are important for DSB repair (reviewed in A-Hakim et al., 2010).

SUMO is a small ubiquitin-like modifier. Although SUMO has very little sequence identity with ubiquitin at the amino acid level, it has a nearly identical structural fold. Three SUMO isoforms in humans exists: SUMO1, SUMO2 and SUMO3. SUMO2 and SUMO3 are highly similar (Saitoh and Hinchey, 2000). Mixed chains of SUMO1 and SUMO2/3 can be formed. SUMO1 lacks the internal SUMO consensus site found in SUMO2/3, and is thought to terminate polySUMO chains (Matic et al., 2008). SUMOylation is directed by an enzymatic cascade analogous to that involved in ubiquitination. First the C-terminal peptide of SUMO is cleaved by a sentrin-specific (SENP) protease using ATP to reveal a di-glycine motif. Next SUMO becomes bound to an E1 SUMO activating enzyme (SAE). SUMO is then passed to an E2 conjugating enzyme, Ubc9 in mammalian cells. An E3 ligase, either protein inhibitor of activated STAT 4 (PIAS4) or PIAS1 in mammalian cells, then attaches the SUMO to a target protein (Hay, 2005).

1.4 Protein–protein interacting motifs: 14-3-3, FHA and BRCT domains

Protein phosphate modifications are not only important for the activation of many proteins involved in the DDR but are also important for the formation of phosphopeptide signalling complexes and protein–protein interactions. Certain proteins and domains specifically

recognize short amino acid sequences surrounding a central phosphorylated serine or threonine residue. Three families of phosphoserine/threonine binding domains function in the DDR: 14-3-3 proteins, FHA domains and BRCT domains. The first phosphothreonine/serine binding protein identified was the 14-3-3 complex (Muslin et al., 1996). 14-3-3 proteins are highly conserved and are found in all eukaryotes (Mohammad and Yaffe, 2009). 14-3-3 proteins mainly function in the cell cycle to supress cyclin-cdk activity through directly binding and sequestering the CDC25 family of phosphatases in the cytoplasm (Dalal et al., 2004) (see 1.10.2 for details). FHA domains are phosphothreonine binding motifs found in hundreds of prokaryotic and eukaryotic proteins involved in transcription, DDR signalling and cell cycle control (Mohammad & Yaffe, 2009). DDR proteins MDC1, RNF8, NBS1 and Chk2 all contain an FHA domain. BRCT domains are found in multiple DDR proteins and are often in tandem arrays. There are roughly 30 BRCT domain containing proteins in mammalian cells (Callebaut and Mornon, 1997). The phosphopeptide binding activity of BRCT domains requires the presence of two BRCT domains in tandem. The N-terminal BRCT primarily stabilizes the phosphoserine, while the tandem BRCT domain fold forms a hydrophobic pocket which stabilizes the phosho-ligand (Clapperton et al., 2004). Cancer associated mutations of BRCA1 often disrupt the BRCT domain of Breast cancer and ovarian type 1 (BRCA1) (Castilla et al., 1994), reflecting the importance of this domain in the DDR.

1.5 The mediator proteins

1.5.1 BRCA1

BRCA1 is a multifunctional protein that functions to maintain genome stability primarily through its involvement in DSB repair and cell cycle control. BRCA1 contains a highly conserved RING domain and two BRCT domains (Figure 1.2). The RING domain is found in many E3 ubiquitin ligases and mediates protein ubiquitination. The BRCT domains bind phosphorylated proteins and mediate protein-protein interactions (Manke et al., 2003), (Yu et al., 2003). The RING domain of BRCA1 mediates its stable association with BRCA1-associated RING domain protein 1 (BARD1) (Meza et al., 1999). BARD1 has a similar domain organization to BRCA1, comprising an N-terminal RING domain and tandem C-terminal BRCT domain. BRCA1 exists as a stable heterodimer with BARD1 (Wu et al., 1996). BRCA1 participates in G2/M checkpoint control partly by regulating Chk1 phosphorylation (Yarden et al., 2002). The mechanism is unclear; it is possible that BRCA1 may modify local chromatin architecture through substrate

ubiquitination surrounding a DSB to enhance ATM signalling. Alternatively BRCA1 may act as a scaffold for Chk1 phosphorylation (Huen et al., 2010). BRCA1 is known to be required for CtIP dependent resection which leads to RPA recruitment and Chk1 activation. Therefore BRCA1 may regulate G2/M checkpoint arrest indirectly by initiating resection which subsequently leads to Chk1 activation. For example, CtIP interacts with the BRCT domain of BRCA1 (Yu and Chen, 2004), and is modified with ubiquitin chains by BRCA1. CtIP promotes resection by stimulating the MRN complex (Sartori et al., 2007). CtIP is phosphorylated at Ser327 and interacts with BRCA1 during S and G2 phase (Yu & Chen, 2004). CtIP phosphorylation mutants that cannot bind BRCA1 exhibit defects in Chk1 phosphorylation and G2/M checkpoint arrest (Yu et al., 2006). Therefore it is possible that BRCA1 regulates the G2/M checkpoint by mediating CtIP dependent resection and subsequent Chk1 activation. BRCA1 also has a direct role in DSB repair through interacting with partner & localizer of BRCA2 (PALB2). PALB2 recruits BRCA2 to sites of DSBs (Xia et al., 2006). BRCA2 loads Rad51 which forms filaments capable of performing a homology search in a sister chromatid to facilitate repair by HR.

1.5.2 53BP1

p53 binding protein 1 (53BP1) is another mediator protein that is important for relaying signalling between sensor and transducer proteins. 53BP1 also contains two BRCT domains which are involved in protein interactions. Upstream of the BRCT domain, 53BP1 contains a tudor domain (Charier et al., 2004) (Figure 1.2). Tudor domains interact with methylated histone residues, and are possibly used by 53BP1 for recruitment to regions of damaged DNA. 53BP1 also contains a glycine/arginine-rich region (GAR), which is methylated by the enzyme PRMT1 (protein arginine N methyltransferase 1) and has been implicated as a possible DNA binding function for 53BP1 (Boisvert et al., 2005). 53BP1 contains 32 PIKK S/TQ consensus sites (Jowsey et al., 2007). Abrogation of 53BP1 results in a modest defect in G2/M checkpoint arrest which is only detectable after low doses IR and not after higher doses (DiTullio et al., 2002), reflecting an essential role of 53BP1 in signal amplification after low doses IR. 53BP1 is necessary for efficient Chk2 phosphorylation (Wang et al., 2002). In DSB repair, 53BP1 is required for ATM dependent DSB repair (Riballo et al., 2004). These DSBs are repaired with slower kinetics and represent breaks that reside at regions of heterochromatin (Goodarzi et al., 2008a), (Noon et al., 2010). 53BP1 also influences chromatin mobility at the environment surrounding a DNA damaged focus. For example, the presence of 53BP1 at deprotected telomeres increases chromatin mobility, thereby increasing the likelihood that two ends will

come together for repair by NHEJ (Dimitriva et al., 2008). 53BP1 also enhances the rate of class switch recombination (Manis et al., 2004; Ward et al., 2004) and long range V(D)J recombination (Difilippantonio et al., 2008), both end joining processes that involve DNA ends that are not in close proximity. Difilippantonio et al (2008), suggest that 53BP1 may promote chromatin mobility possibly via interacting with dynein motor proteins (Lo et al., 2005).

1.5.3 MDC1

Mediator of DNA damage checkpoint protein 1 (MDC1) is another mediator protein with a BRCT and FHA domain (Figure 1.2). MDC1 rapidly binds Ser139 phosphorylated H2AX to promote the recruitment of repair proteins to DSBs (Stewart et al., 2003). MDC1 deficient cells are sensitive to IR, and MDC1 controls the formation of 53BP1, BRCA1 and MRN by promoting efficient H2AX phosphorylation (Stewart et al., 2003) (see 1.6 for further discussion).

1.6 γH2AX phosphorylation and DDR signalling cascade

In response to DSBs, ATM and ATR phosphorylate a plethora of proteins that mediate the DDR signalling response. One initial target of these kinases is the histone variant H2AX. ATM, ATR and DNA-PKcs can directly phosphorylate H2AX at Ser139, a histone modification that is commonly referred to as γH2AX (Rogakou et al., 1998) (Figure 1.4). Following H2AX phosphorylation, MCD1 directly binds H2AX via its C-terminal BRCT repeat domain (Lukas et al., 2004). MDC1 also binds the FHA and BRCT domains of the MRN complex subunit Nbs1 (Chapman and Jackson, 2008). Nbs1 directly binds and tethers ATM at the site of a DSB, which functions to localize the kinase activity of ATM. MDC1 also binds ATM through its FHA domain which further propagates H2AX spreading (Lou et al., 2006). The initial localization of DDR proteins such as NBS1, BRCA1 and 53BP1 are not dependent on γH2AX phosphorylation, but sustained DDR signalling and maintenance of these factors at a DSB is dependent on extensive γH2AX spreading (Celeste et al., 2002). Additionally chromatin remodelling factors such as INO80 and SWI/SNF family are recruited to DSBs in a γH2AX dependent manner (Lee et al., 2010). Recruitment of several DDR proteins is dependent on ubiquitination. The ubiquitin ligase RING finger containing nuclear factor 8 (RNF8) associates with MDC1 via an N-terminal FHA domain which propagates K63 linked ubiquitin (Ub) chains on neighbouring H2A and H2AX histones (Huen et al., 2007; Mailand et al., 2007). The E3 ligase RING finger containing nuclear

factor 168 (RNF168) binds these Ub chains and stimulates K63 ubiquitination (Stewart et al., 2009). Heat domain & RLD 2 (HERC2), a recently identified E3 ubiquitin ligase interacts with RNF8 and facilitates the assembly of the RNF8 and ubiquitin conjugating enzyme 13 (UBC13) complex which further stimulates K63-linked ubiquitin chain synthesis (Bekker-Jensen and Mailand, 2010). K63 Ub chains generated by RNF8 are recognized by RAP80, which subsequently recruits the E3 ligase BRCA1 via an interaction with the scaffold protein ABRA1 (Huen et al., 2007). RNF168 dependent ubiquitination is regulated by inhibition of UBC13 by the deubiquiting enzyme OTUB1 (Nakada et al., 2010).

SUMO mediated modifications are also important for DDR protein recruitment. Protein inhibitor of activated STAT4 (PIAS4), an E3 SUMOylating protein kinase, has been shown to stimulate the Ub ligase activity of the RNF8/UBC13 complex (a ubiquitin E3 and SUMO E2 complex respectively), thus promoting the recruitment of RNF168 and BRCA1 to site of damage (Galantly et al., 2009). A related kinase PIAS1 and PIAS4 are capable of directly SUMOylating BRCA1 to stimulate its Ub ligase activity (Galanty et al., 2009). A related protein, PIAS1 and PIAS4 are capable of directly SUMOylating BRCA1 to stimulate its Ub ligase activity (Galanty et al., 2009). Additionally 53BP1 recruitment is dependent on PIAS4 (Galantly et al., 2009). However 53BP1 has no Ub binding domain. It has been proposed that RNF8/RNF168 dependent ubiquitination events mediate chromatin relaxation which subsequently exposes dimethyl H4K20 and H3K79 residues, which are recognized by 53BP1 tudor domains (FitzGerald et al., 2009). The accumulation of these proteins into repair foci can be easily visualized under a microscope using fluorescently tagged antibodies to identify any one of these proteins. Monitoring the disappearance of these repair foci is commonly used as a biomarker for DSB repair and is a technique employed in this thesis.

1.7 PIKK family

The coordinated regulation of the DDR is controlled and initiated by three related kinases ATM, ATR and DNA-PK. These kinases belong to the PIKK (phospatidylionositol-3-kinase) related family (Shiloh, 2003). These enzymes phosphorylate proteins rather than lipids like the related PI3K family. All members are large proteins over 300 KDa's in size with related domain structures. At the N-terminus all members have a large repeated domain known as a huntingtin, elongation factor3, protein phosphatase 2A & TOR1 (HEAT) domain, followed by a FRAP-ATM-TRRAP (FAT) domain, a catalytic domain homologous to the PI-3 kinase domain, a

PIKK regulatory domain (PRD) and a FATC domain at the C-terminus (Lovejoy and Cortez, 2009). The HEAT, FAT and FATC domains are involved in protein and substrate interaction (Lavin, 2008). The consensus phosphorylation site for PIKK substrates is a serine or threonine residue followed by glutamine (SQ/TQ) motif. ATM and ATR have a wide substrate scope, with over 900 substrates having been identified (Matsuoka et al., 2007).

1.8 ATM activation

Ataxia telangiectasia mutated (ATM) is central to the DSB signal transduction cascade. ATM exists as an inactive dimer in undamaged cells. In response to DSBs, ATM undergoes autophosphorylation, which results in dimer dissociation and kinase activation (Bakkenist and Kastan, 2003).

1.8.1 ATM autophosphorylation and activation

The most widely studied ATM auto-phosphorylation, Ser1981, is an SQ motif located in the amino-terminal region of the FAT domain and is rapidly phosphorylated in response to IR (Bakkenist & Kastan, 2003). Other phosphorylation sites on ATM have also been demonstrated to be important for ATM activation such as Ser367 and Ser1893 (Kozlor et al., 2006). Expression of mutated versions of ATM harboring nonphosphorylateable residues in cells from A-T patients resulted in increased radiosensitivity. However the literature remains controversial over the importance of ATM autophosphorylation events. Nussenweig and co-workers demonstrated that expression of an S1987 (analogous to human S1981A) allele in ATM mouse yielded normal ATM dependent phosphorylation events after DNA damage and normal ATM localization at DSBs (Pellegrini et al., 2006). Furthermore, the Ser1981 autophosphorylation site is not conserved in all ATM homologs, for example it is not present in Arabidopsis, Drosophila, budding yeast or fission yeast. Therefore the importance of ATM autophosphorylation in mediating ATM kinase activation may differ between species. Despite this distinction between species, ATM autophosphorylation in human cells does correlate with ATM activation and is used in this thesis to monitor ATM activation.

1.8.2 PP2A mediated dephosphorylation of ATM

The de-activation of ATM's kinase activity is also important for the down regulation of DSB induced signaling events and to allow cell cycle re-entry. Protein phosphatases have been demonstrated to affect ATM activity in vivo, in particular PP2A and PP5A (Ali et al., 2004; Goodarzi et al., 2004). PP2A is a member of the protein/threonine phosphatase family and is composed of a catalytic (C) subunit, a scaffolding (A) subunit and a regulatory (B) subunit. ATM directly interacts with the A subunit of PP2A, and in unirradiated cells, A and C subunits of PP2A directly co-immunoprecipitate with ATM (Goodarzi et al., 2004). Following IR these subunits dissociate from ATM, suggesting that ATM may be constitutively dephosphorylated by PP2A in undamaged cells (Goodarzi et al., 2004).

1.8.3 ATM activation and signal amplification

Ataxia telangiectasia like disorder (ATLD) and Nijmegen Breakage Syndrome (NBS) express hypomorphic alleles of Mre11 and Nbs1, respectively and are deficient in ATM activation. The clinical similarities between these syndromes and A-T suggest that the MRN complex plays an important role in ATM activation (Lee and Paull, 2005; Uziel et al., 2003). MRN is now an established upstream activator and substrate of ATM. Evidence of this was established from studies analyzing ATM signaling in Nbs1 or Mre11 deficient cell lines, where ATM autophosphorylation at Ser1981 was found to be compromised (Uziel et al., 2003). MRN was later shown to interact with ATM via the C-terminus of Nbs1, which is required for the recruitment of ATM at the site of a DSB (Falck et al., 2005; Nakada et al., 2003). Cells expressing a complex which targets MRN for degradation known as endovine E1655k/E4crf6 have abrogated ATM autophosphorylation, and BRCA1 and Chk2 phosphorylation, implying that MRN is required for ATM mediated phosphorylation of downstream repair factors (Carson et al., 2003). In Nbs1 defective cells, Chk2 phosphorylation is reduced or absent but p53 phosphorylation by ATM is unaffected (Lee et al., 2003). This data suggests that the MRN complex is required for tethering ATM's kinase activity at the break, whereas ATM targets which do not form IR induce foci, such as p53, can be readily phosphorylated in the absence of MRN mediated ATM tethering. The mediator proteins MDC1 and 53BP1 have a dose dependent role in amplifying ATM signalling. After low doses of IR, cells deficient for 53BP1 or MDC1 are unable to initiate a full checkpoint response, however after doses above 6 Gy IR cells

are checkpoint proficient (Fernandez-Capetillo et al., 2002; Peng and Chen, 2003). This data presents a role for the mediator proteins in amplifying low dose damage signalling.

1.8.4 ATM activation and chromatin remodeling

In 2003 Kastan and Bakkenist (2003), reported that ATM activation following chloroquine induced chromatin relaxation independently of IR. A role for the chromatin modifying protein high-mobility group nucleosome binding domain 1 (HMGN1) has been shown to be important for ATM activation (Kim et al., 2009). HMGN1 is a member of the HMG superfamily of nuclear proteins that bind nucleosome core particles and affect chromatin superstructure (Bianchi and Agresti, 2005). *Hmgn1*$^{-/-}$ MEFs revealed that loss of HMGN1 significantly reduces the IR induced autophosphorylation of Ser1987 (Ser1981 homolog) (Kim et al., 2009). However the IR induced formation of Nbs1, MDC1, 53BP1 and γH2AX foci were all normal in *Hmgn1*$^{-/-}$ cells, implying that the reduced ATM activation observed in these cells was not due to defective recruitment of DSB mediator proteins to damaged sites. Loss of HMG1 reduced the amount of ATM Ser1987 phosphorylation found bound at chromatin. However, HMGN1 and ATM do not co-localize when analyzed by immunofluorescence, indicating that ATM does not bind HMGN1 enriched chromatin (Kim et al., 2009). This implied that defective ATM activation in *Hmgn1*$^{-/-}$ cells was due to global changes in chromatin organization rather than a direct interaction between HMGN1 and ATM. Additionally, global acetylation of Lys14 of histone H3 (H3K14) after IR increased in WT cells but less so in *Hmgn1*$^{-/-}$ cells. The authors suggest that HMGN1 affects global organization of ATM throughout the nucleus through a mechanism involving H3K14 chromatin modification (Kim et al., 2009).

Tip60 is a histone acetyl transferase (HAT) which adds acetyl groups to lysine residues on histone tails. DSB induced activation of Tip60 leads to Tip60 dependent acetylation and activation of ATM (Sun et al., 2005; Sun et al., 2007). Mutations in the chromodomain, a conserved domain which interacts with methyl groups on methylated lysine residues, abolishes Tip60 dependent acetylation and autophosphorylation of ATM (Sun et al., 2009). Chk2 phosphorylation is also defective in Tip60 chromodomain mutants. Tip60 acetyltransferase activity and ATM activation is also significantly impaired in Suv39H1/2 MEFs (Sun et al., 2009). Suv39H1 and H2 are histone methyltransferases responsible for tri-methylating lysine 9 on histone H3, a chromatin modification associated with regions of heterochromatin. Following treatment of cells with a demethylating drug which specifically demethylates H3K9me3 and H3K36me3 (Klose et al., 2006; Whetstine et al., 2006), the

demethylation of H3K9, H3K27 and H3K36 was found not to affect γH2AX foci or MRN recruitment to the site of a DSB. Tip60 was also recruited to DSBs in cells in which TriMeK9 H3 was reduced, suggesting that the interaction of Tip60's chromodomain and methylated histones is not required for Tip60 recruitment to a DSB (Sun et al., 2009). However demethylation of H3K9 sensitized cells to IR (Sun et al., 2009). Most TriMeK9 H3 has been shown by NMR spectroscopy to be bound by heterochromatin protein 1 (HP1), three isoforms of which exist (Nielsen et al., 2002). Following treatment with IR, the chromodomain of HP1β is phosphorylated by casein kinase 2 (Ck2), which results in the release of HP1β from TriMeK9 histone H3 (Ayoub et al., 2008). Inhibiting cells for Ck2 prevents the release of HP1β from chromatin and results in defective Tip60 acetyltransferase activity and impairs Chk2 phosphorylation (Ayoub et al., 2008). This implies that TriMeK9 histone H3 tail modifications are required for activation of Tip60 acetyltransferase activity. Tip60 acetyltransferase activity and acetylation of ATM is also reduced in MRN deficient cells (Sun et al., 2009). Sun et al (2009), proposed that ATM and Tip60 are recruited to DSBs via the MRN complex as an inactive complex. Price and co-workers have proposed a model for ATM activation that involves first the ejection of HP1β from chromatin exposing TriMeK9 H3, followed by MRN association with DSBs, the recruitment of inactive ATM-Tip60 complex to Nbs1, the localized recruitment of Tip60 and TriMeK9 resulting in activation of Tip60's acetyltransferase activity, followed by acetylation and finally activation of ATM.

1.9 ATR signaling

The DDR is also stimulated by regions of ssDNA that can be generated at stalled or collapsed replication forks and by resected DSBs. The DDR in response to these lesions is coordinated by ATR. ATR responds to a wide range of DNA damage including replication stress, base adducts, UV induced nucleotide damage and DSBs. The response of ATR to IR, unlike ATM, is restricted to S and G2 phases of the cell cycle (Jazayeri et al., 2006). This is likely a consequence of resection mediated ssDNA generation being regulated by proteins which are regulated by CDK mediated stimulation, levels of which are low in G1 and M phase and high in S and G2 phase (Paull and Gellert, 1998; Sartori et al., 2007). The initiating step in ATR activation is the generation of ssDNA (Figure 1.5). ssDNA regions rapidly become coated in RPA which recruit the ATR-ATRIP (ATR-interacting protein) complex (Cortez et al., 2001). ATR and ATRIP are constitutively bound and loss of either complex results in the same DDR defect (Cimprich and Cortez, 2008b). To activate ATR kinase activity it must interact with TopBP1 (Kumagai et al.,

2006). TopBP1 recruitment to ssDNA regions is also mediated by RPA (Majka et al., 2006). Here the clamp loader Rad17, which has homology to the replication factor C (RFC) that loads proliferating cell nuclear antigen (PCNA) at replication forks, is first recruited. Rad17 subsequently loads the PCNA like heterotrimeric ring Rad9-Rad1-Hus1 (9-1-1) complex to damage sites (Yang and Zou, 2006). The 9-1-1 complex is responsible for recruiting topoisomerase binding protein 1 (TopBP1) bringing TopBP1 and ATR in close proximity leads to ATR activation (Lee et al., 2007). The mediator protein Claspin is also recruited via Rad17 (Wang et al., 2006b). Claspin is required to mediate ATR kinase activity towards the check point kinase Chk1 (Kumagai and Dunphy, 2003). In G2 phase cells, ATM and MRN are required to initiate resection to form ssDNA substrates which lead to RPA recruitment and subsequent ATR activation. In this scenario, ATM phosphorylates and activates the exonuclease CtIP.

1.10 Cell cycle checkpoint control

An overview of cell cycle checkpoint arrest is given here. A more detailed discussion of how DNA damage and heterochromatin affect checkpoint arrest is given in chapter 3, 4 and 6. The cell cycle is monitored by surveillance mechanisms that arrest further progression if a crucial process has not been completed or if a cell has sustained DNA damage. The G1 and S phase checkpoints prevent replication of damaged DNA, whereas the G2 checkpoint prevents segregation of damaged chromosomes to daughter cells. Cell cycle checkpoint arrest is regulated by ATM and ATR. The downstream effector kinases that transduce ATM and ATR mediated signaling to initiate checkpoint arrest are the checkpoint kinases Chk2 and Chk1, respectively. Chk2 and Chk1 act as transducers of the DNA damage signal, phosphorylating a multitude of substrates in the DDR. Chk2 and Chk2 have a number of overlapping substrates, but have independent roles in directing the cellular response to DNA damage. ATM responds to DSBs and ATM and Chk2 can contribute to the regulation of all checkpoints. ATR responds to replication associated DNA damage, UV induced DNA damage, DNA crosslinks and resected DSBs. Given that DNA resection is restricted in G1 due to low CDK levels preventing the activation of endonucleases and that SSBs do not activate ATM or ATR, G1/S checkpoint arrest is dependent on ATM signaling only. Both ATM and ATR can function to initiate arrest at the intra-S phase and G2/M checkpoints. Similar to ATR, Chk1 activation is restricted to S and G2 phase (Huertas and Jackson, 2009) (Figure 1.6).

1.10.1 Chk1 and Chk2

Chk2 is a highly phosphorylated protein with more than 25 phosphorylation sites identified to date, some of which are important for regulation and stability (Ahn et al., 2004; Gabant et al., 2008; Kass et al., 2007; Lovly et al., 2008). A well-studied Chk2 phosphorylation is the phosphorylation of Thr68 by ATM in response to DSBs (Ahn et al., 2000; Matsuoka et al., 2000). Phosphorylation at Thr68 promotes the binding of the SQ/TQ motif of one Chk2 to the FHA domain of another Chk2. This dimerization event initiates the autophosphorylation of Chk2's T loop at Thr383 and Thr387 residues, resulting in full Chk2 activation (Ahn et al., 2002; Xu et al., 2002). Protein phosphatases PP2A, PP2C and WIP1 bind and dephosphorylate Thr68 on Chk2. Once the T loop is phosphorylated, Thr68 is not required to maintain Chk2 activation (Ahn and Prives, 2002). Chk2 mice are viable and develop normally after birth (Hirao et al., 2000). Despite G2/M checkpoint initiation after IR being normal in Chk2 -/- deficient cells, conflicting results regarding G2/M checkpoint maintenance have been reported. At IR doses of 10 Gy, Chk2 deficient cells maintain checkpoint arrest for up to 6 hours (Takai et al., 2002). However at lower doses IR (5 Gy), Chk2 deficient cells are released from the G2/M checkpoint prematurely (Hirao et al., 2000). It is likely that at higher doses IR enough DDR signaling is generated to maintain arrest. At lower dose IR there is a role for the mediator proteins MDC1 and 53BP1 to tether and amplifying the DDR.

Chk1 expression is largely restricted to S and G2 phase (Lukas et al., 2001) and is active as a kinase even in unperturbed cells (Gatei et al., 2003). Chk1 is characterized by 4 functional domains: an N-terminal kinase domain, followed by an SCD domain, a bipartite nuclear localization signal, and a PCNA interacting protein (PIP) motif (Scorah et al., 2008). The C-terminal of Chk1 has been proposed to function as an auto-inhibitory region, as C-terminally truncated isoforms of Chk1 have increased activity (Katsuragi and Sagata, 2004). Chk1 activation is primarily downstream of ATR in response to genotoxic insult. In undamaged cells a large proportion of Chk1 is chromatin bound (Smits et al., 2006). Phosphorylation of Chk1 appears to affect its subcellular localization. For example, phosphorylation of Chk1 on Ser317 is required for chromatin release as well as G2 checkpoint arrest, as Ser317 mutants and Chk1 tethered to chromatin cannot activate G2/M checkpoint responses (Niida et al., 2007; Smits et al., 2006).

The checkpoint kinases phosphorylate numerous proteins that influence diverse aspects of the DDR to promote genome integrity. Chk1 and Chk2 influence diverse aspects of the DDR primarily, but not exclusively, via their influence on transcription. For example, Shimada et al (2008), reported a novel function for Chk1 in chromatin modification. Here Chk1

was shown to mediate phosphorylation of histone H3 on residue Thr11 (H3-Thr11). Using radiolabelled phosphorous, Chk1 but not kinase dead Chk1 incorporated phosphorous into H3 in vivo. In addition, Chk1 chromatin dissociation after DNA damage correlated with H3-Thr11 dephosphorylation and a reduction of Cdk1 and cyclin B1 transcript levels. GCN5 (a histone acetyltransferase (HAT) that promotes transcription) binds H3 peptides and phosphorylation of H3-Thr11 was found to enhance GCN5 chromatin binding (Shimada et al., 2008). The authors proposed a model whereby in unperturbed cells Chk1 is chromatin bound and histone H3 is phosphorylated at Thr11 in a Chk1 dependent manner. This phosphorylation event promotes the recruitment of GCN5 to specific genes. Following DNA damage, Chk1 is phosphorylated by ATR or ATM, resulting in Chk1 dissociation from chromatin and a subsequent reduction in H3-Thr11 phosphorylation. GCN5 is no longer recruited to target genes and transcription is turned off (Shimada et al., 2008).

Chk1, unlike Chk2, is an essential gene, and $Chk1^{-/-}$ mice are embryonic lethal (Takai et al., 2000). $Chk1^{-/-}$ embryos fail to arrest in response to replication blocking agent aphidicolin or DNA damage induced by UV or X-ray. The lethality of these mice suggests that Chk2 cannot redundantly function to replace Chk1 and likely reflects the role of Chk1 activation in response to replication associated DNA damage. Human cells lacking Chk1 exhibit defects in both IR induced S and G2 phase checkpoints.

1.10.2 G1/S checkpoint

The G1/S checkpoint is essential to prevent any lesions that may arise in G0/G1 phase reaching the replication fork. If left undetected, these lesions could potentially become heritable mutations, which later compromise genetic integrity. In G1 phase cells the main protein regulating checkpoint arrest, identified by (Kastan et al., 1992), is p53. p53 levels vary throughout the cell cycle; levels are high in G1 but are low for the rest of the cells cycle (Kastan et al., 1992). The turnover of p53 is regulated by the murine double minute 2 (MDM2) protein, which binds the N-terminus of p53 and functions as a ubiquitin E3 ligase to promote p53 degradation by proteosomes (Zhang and Xiong, 2001). MDM2 mono-ubiquitinates the C-terminal of p53. This ubiquitination event exposes the leucine rich nuclear export signal (NES) of p53 stimulating the nuclear export and degradation of p53 in the cytoplasm (Boyd et al., 2000; Stommel et al., 1999). Following damage induction, ATM phosphorylates p53 at Ser15 in vivo (Siliciano et al., 1997). This phosphorylation event precludes MDM2 binding of p53. Consequently p53 is not ubiquitinated and degradation is prevented (Chen et al., 2005). ATM

also directly phosphorylates MDM2, which inhibits the transport of p53 by MDM2 out of the nucleus for degradation (Maya et al., 2001). Furthermore, in addition to ATM phosphorylation of p53 on Ser15, both Chk1 and Chk2 phosphorylate p53 on Ser20, which adds to the disruption of p53's association with the ubiquitin ligase MDM2, again promoting p53 stability (Banin et al., 1998; Canman et al., 1998; Shieh et al., 2000).

Following p53 stabilization and increased activation, transcriptional targets such as p21 are up-regulated. p21 is a cyclin dependent kinase (CDK) inhibitor (Xie et al., 1998). CDKs are serine-threonine kinases that only become active on association with cyclins. CDK-cyclin complexes regulate the progression through the cell cycle. IR induced enhanced expression of p21 inhibits activation of the CDK-cyclin complexes cyclin E/Cdk2 and cyclin D/cdk4. Failure to activate cyclin E/Cdk2 and cyclin D/cdk4 maintains E2F (a DNA binding transcription factor) sequestration by retinoblastoma (Rb) and impedes cell cycle progression through G1 (Elledge, 1996). The Rb tumour suppressor protein binds to E2F preventing it from interacting with the transcription machinery. In the absence of Rb, E2F mediates the transcription of proteins involved in DNA replication (Chen et al., 2009). G1/S checkpoint arrest is also triggered by activated Chk2 following its phosphorylation at Thr68 by ATM. Phosphorylated dimers or monomers of Chk2 are active in phosphorylating substrates such as CDC25A. CDC25A is a protein phosphatase that removes phosphate groups from phosphorylated tyrosine or serine/threonine residues. Three isoforms of CDC25 exist: A, B and C. Phosphorylation of CDC25 isoforms targets them for degradation, preventing them from phosphorylating and activating of CDKs, and thereby inhibiting cell cycle progression (Boutros and Byrne, 2005). Phosphorylation of the effector protein CDC25A, primes it for ubiquitination and proteasome destruction (Mailand et al., 2002). The degradation of CDC25A allows the inhibitory phosphorylation on cyclin dependent kinase 4 (cdk4) at Tyr14 to be maintained, which prevents S-phase entry (Terada et al., 1995). ATM activation of Chk2 also activates and stabilizes p53. The p53 dependent block in G1 maintains arrest initiated by the CDC25A pathway to allow sufficient time for complete DNA repair. The high frequency of p53 mutations in human cancers highlights its role as a tumour suppressor.

1.10.3 The intra-S phase checkpoint

The intra-S phase checkpoint results in a slowing of cell cycle progression rather than a complete arrest. In response to DNA damage in S phase, CDC25A is phosphorylated on Ser123, Ser178, Ser276 and Ser292 by ATM, Chk1 and Chk2, leading to its rapid degradation (Lukas et

al., 2001; Sorensen et al., 2003). Degradation of CDC25A during S phase is regulated by the F-box protein β-TrCP, which is phosphorylated after DNA damage. β-TrCP binds CDC25A after its phosphorylation by Chk1/Chk2, marking it for ubiquitin mediated proteolysis (Busino et al., 2003). This prevents the dephosphorylation of Thr14/Tyr15 on CDK2 by CDC25A. Maintenance of the inhibitory phosphorylations on CDK2 prevent loading of the origin binding factor CDC45. Lack of CDC45 loading at origins precludes recruitment of DNA polymerase and thereby blocks the initiation of DNA replication from unfired origins (Takisawa et al., 2000). Chk1 and CDC5A levels are positively regulated by E2F when cells enter S-phase.

1.10.4 G2/M phase checkpoint arrest

The G2/M checkpoint functions to prevent DNA damage caused during G2 phase being segregated into daughter cells during M phase. Regulation of the G2/M checkpoint is controlled by both Chk2 and Chk1 and depends on the inhibition of cyclin dependent protein kinase 1 (Cdk1) (Yu et al., 1998). Cdk1 prepares cells for entry into mitosis by phosphorylating key proteins required for replication including RNA polymerase II and histone H1 (Hartwell and Kastan, 1994). Regulation of Cdk1 activity involves Cdk1 catalytic subunits associating with cyclins. Activation of Cdk1 is a multistep process. First inhibitory Cdk1 phosphorylations on Thr14 and Tyr15, which are carried out by the protein kinase WEE1 (McGowan and Russell, 1995) and Myt1 (Booher et al., 1997) respectively, must be removed prior to its association with cyclin B (Morgan, 1995). Cdk1 is inactive under these circumstances because phosphorylation of Thr14 and Tyr15 block the ATP binding site of the kinase. During G2/M transition, CDC25 activates the kinase by dephosphorylating Thr14 and Tyr15 (Morgan, 1995). In response to genotoxic stress, Chk1 and Chk2 both can function to phosphorylate CDC25 at serine 216 (Sanchez et al., 1997). Phosphorylation of CDC25 creates a binding site for 14-3-3 proteins. 14-3-3 proteins are members of a phosphoserine binding family of proteins which, when bound to CDC25, sequester CDC25 in the cytoplasm. This sequestering event prevents CDC25 dephosphorylating and activating the mitotic cyclin B-Cdk1 kinase. Inactivation of cyclinB-Cdk1 kinase prevents damaged cells from entering mitosis. Despite both Chk2 and Chk1 functioning to phosphorylate CDC25, Chk1 appears to have a prominent role in this process. Jin et al (2008), found that, when the human colon cancer cell line HCT116 was engineered to lack Chk2, cells displayed no defects in CDC25 degradation in response to IR. In contrast depletion of Chk1 resulted in strong stabilization of CDC25 in response to IR and

continued cell cycle progression. Therefore Chk1 is believed to be the major kinase controlling CDC25 degradation in response to IR.

1.11 ATM dependent apoptosis

When the amount of damage in a cell is not repairable it can trigger apoptosis. Apoptosis is the process of programmed cell death. Biochemical events lead to characteristic cell changes such as loss of cell membrane asymmetry and attachment, cell shrinkage, nuclear fragmentation and chromatin condensation (Kerr et al., 1972). The process of apoptosis is controlled by a diverse range of cellular signals. There are two major pathways of apoptosis, one of which is mitochondrial based involving caspases (Fesik and Shi, 2001) and the other ligand based involving the attachment of receptors onto cell surfaces (Dejean et al., 2006; Kurose et al., 2006). ATM defective cells are resistant to IR induced apoptosis (Duchaud et al., 1996; Takagi et al., 1998), implying that ATM is important for apoptotic signalling after IR. Here I will briefly mention some of the ATM dependent apoptotic pathways, but other pathways of apoptosis exist that are both dependent and independent of ATM.

ATM phosphorylation of p53 induces transcriptional activation of pro-apoptotic factors such as p53 up-regulated modulator of apoptosis (PUMA). PUMA is a member of the B-cell lymphoma 2 (Bcl-2) protein family which are a family of apoptotic regulatory proteins. p53 also up-regulates the Bcl-2 associated x (Bax) protein (Lane, 1992). Bax is believed to interact with and induce the opening of the mitochondrial voltage-dependent anion channel (VDAC). Alternatively Bax has been suggested to insert into the mitochondrial membrane to form a pore (Wolter et al., 1997). Opening of the mitochondrial membrane results in the release of cytochrome c (a protein associated with the inner mitochondrial membrane which is involved in electron transfer (Tafani et al., 2002) and other pro-apoptotic factors from the mitochondria leading to the activation of caspases. Caspases are a family of proteases that degrade proteins.

Chk2 can promote apoptosis independent of p53 in response to IR by phosphorylating Ser117 of the tumour suppressor pro myelocytic leukaemia (PML), which is another protein that functions to promote apoptosis. PML can also promote autophosphorylation and activation of Chk2 (Yang et al., 2006), resulting in an auto-activatory loop. ATM also phosphorylates nuclear factor kappa-light-chain-enhancer of activated B cells (NFKβ), a transcription factor which activates expression of the apoptotic FAS receptor (a receptor on the surface of cells that leads to apoptosis) (Stagni et al., 2008). The FAS receptor along with other proteins forms a complex on the cell surface which becomes internalized. On cellular

entry, the FAS receptor promotes the degradation of organelles via the action of caspases (Huang et al., 1996).

1.12 Senescence

Senescence is a form of permanent cell cycle arrest, evasion of which is a common theme in cancer cells. Solid tumors derived from epithelial cells show extensive resistance to apoptosis after IR (Dewey et al., 1995; Hendry et al., 1995; Ross, 1999). Senescent cells adopt a large and flattened morphology, positively stain for senescent associated β-galactosidase activity, terminate DNA synthesis and accumulate p53, p21 and p16 (Naka et al., 2004). p38 mitogen activated protein kinase (MAPK) signals to induce senescence. Senescence is mainly stimulated by RB and p16 (Kiyono et al., 1998). Oncogenic stress induced senescence results when overexpression of certain oncogenes such as Ras and Raf trigger a permanent and irreversible cell cycle arrest (Serrano and Blasco, 2001; Zhu et al., 1998). Growth inhibitors such as p53 and p16 are important for oncogenic suppression in the presence of oncogenic stimuli (Serrano and Blasco, 2001). DNA damage checkpoints can be permanently activated as a consequence of irreparable DNA damage or exposed telomeric ends.

1.12.1 Replicative senescence

The Hayflick limit describes the proliferative potential of human cells to a finite number of doublings (Hayflick and Moorhead, 1961). The replicative potential of a cell is dependent on the telomere length of each chromosome. Telomeric DNA is composed of tandem repeat DNA sequences, consisting of 6 bases (TTAGGG in humans) and a 3’ overhang ss telomeric DNA (~300 bases) (de Lange, 2004). The 3’ overhang is embedded in the telomeric DNA, and with the help of telomere repeat binding factors (TRF) forms a loop structure known as the t-loop. This capping event prevents telomere end fusions. Due to the end replication problem which results from incomplete DNA replication on either DNA end, telomeres gradually erode with each cell doubling, which eventually leads to critical shortening (Yang et al., 1998). Shortened telomeres eventually lose their cap and exposed telomere ends activate a DDR, leading to p53 activation and permanent G1 arrest.

1.12.2 Stress induced premature senescence (SIPS)

In addition to replicative senescence, normal diploid fibroblasts can undergo stress induced premature senescence (SIPS) in response to DNA damage. SIPS is not prevented by telomere elongation such as hTERT expression, therefore is not triggered by telomere shortening like replicative senescence (Gorbunova et al., 2002). SIPS is induced in various types of cancer (Chang et al., 2002). Normally after 6 hours after IR the p53 response wanes, however in SIPS, these responses have been observed for at least 10 days (Suzuki et al., 2001). Telomerase is expressed in ~ 90% of cancer cells; therefore replicative senescence is not normally induced (Kim et al., 1994). Lack of correct cell cycle regulation in cancer cells loses the ability to induce SIPS in cancer cells.

1.13 The DDR and human disease

Human diseases with defects in components of the DDR typically have defects associated with neuron homeostasis, immunity, fertility and aging (Table 1.3).

1.13.1 Ataxia

A common defect associated with loss of some components of the DDR is ataxia. Ataxia is a neurological symptom that involves lack of coordinated muscle movements. Cerebellar ataxia describes ataxia due to dysfunction of the cerebellum, as opposed to defects in peripheral neurons. Several DDR disorders have defects in the cerebellum, which is the part of the brain which controls motor coordination. The cerebellum is composed of 3 classes of neurons – granule cells, Purkinjie cells and interneurons, which is about 50% of neurons of the whole brain (Katyal and McKinnon, 2008). Ataxia normally correlates with defective SSB repair not DSB repair. However since neurons exhibit high mitochondrial respiration which can result in oxidative stress and subsequent DNA damage, the accumulation of SSBs in close proximity and on opposite DNA strands could produce DSB(s), in this sineario defective DSB repair would of particular risk to the maintenance of post-mitotic brain health. Additionally neurons do not divide therefore repair of DSBs is dependent on error prone NHEJ. Defects in regulation of oxidative stress and repair of DNA lesions often results in neuronal death and

neurodegeneration. Ataxia telangiectasia (A-T) patients which have mutations in *ATM* develop profound progressive ataxia due to progressive loss of granule and Purkinjie cells.

1.13.2 Microcephaly

The DDR also has a critical role during brain development. Consequently a large number of DDR disorders display microcephaly. Microcephaly is a neurodevelopmental disorder in which the circumference of the head is more than two standard deviations smaller than average for the individual's age and sex. Defective proliferation of neurogenitor cells during fetal development accounts for microcephaly (O'Driscoll and Jeggo, 2008). Seckel syndrome patients with mutations in *ATR* typically display microcephaly. Nijmegen breakage syndrome (NBS) patients which have mutations in *NBS1* display microcephaly; similarly Nijmegen breakage syndrome- like disorder (NBS-LD) patients who have mutations in *RAD50* also display microcephaly. However some patients with mutations in *Mre11*, another component of the MRN complex, do not have microcephaly but instead display ataxia. This can be explained by the role of Mre11 in activating apoptosis. For example Mre11 defective mice which display a similar phenotype to A-TLD lose their ability to undergo ATM dependent apoptosis in the nervous system after DNA damage. This potentially results in the incorporation of damaged cells in the brain and subsequent neurodegeneration (Ciccia and Elledge, 2010). NBS mutants however still exhibit ATM dependent apoptosis which could consequently result in cell loss and microcephaly (Shull et al., 2009). Therefore residual ATM activity in the brain might determine the outcome between neurodegeneration and microcephaly.

1.13.3 Ataxia telangiectasia (A-T)

A-T is an autosomal recessive disorder caused by mutations in the *ATM* gene located on chromosome 11q22-23 (Savitsky et al., 1995). A-T patients have low or undetectable levels of ATM protein. A-T is characterized by early onset progressive cerebellar ataxia, ocular apraxia, telangiectasia of the eyes and skin (which is the appearance of prominent blood vessels), immunodeficiency and chromosomal instability. Cells derived from A-T patients display severe radiosensitivity and defects in G1/S, S and G2/M phase checkpoint arrest following exposure to IR (Lavin, 1999).

1.13.4 ATR-Seckel

Seckel syndrome is a genetically heterogeneous autosomal recessive disorder characterized by profound proportionate growth retardation, dwarfism, microcephaly and mental retardation. One type of Seckel syndrome is caused by mutations in the gene encoding *ATR* which maps to 3q22.1-q24. ATR-SS patient cells exhibit increased sensitivity to DNA replication fork stalling, have a defective ATR-dependent G2/M checkpoint arrest specifically after UV-irradiation and contain cells with supernumerary centrosomes (Alderton et al., 2004). Centrosomes are organelles that function as microtubule organizing centres in the cell and are important for cell cycle regulation. The centrosome is normally replicated once per cell cycle in S phase (Stearns, 2001). Cells containing multiple centrosomes incur difficulties in chromosome segregation during mitosis.

Despite the complete knockout of ATR being lethal (de Klein et al., 2000), hypomorphic mutations in ATR which reduce the abundance of ATR but do not completely abolish it have been reported in Seckel syndrome patients (O'Driscoll et al., 2003a). Therefore low levels of ATR expression are compatible with survival. Murga et al (2009) took advantage of this mutation, and replaced the mouse genomic ATR fragment with the human counterpart containing the Seckel mutation to generate a humanized mouse model. These mice recapitulated many of the human Seckel syndrome phenotypes, such as severe dwarfism, microcephaly and premature aging. Interestingly an elevated incidence of malignancy is not observed in ATR knockout mice (Murga et al., 2009). Therefore below a certain threshold of ATR activity allows the accumulation of genomic instabilities that lead to tumor formation. It has been suggested that malignant transformation may depend on the amount of residual ATR activity (Murga et al., 2009).

Pericentrin-mutated Seckel syndrome (PCNT-SS) is another form of Seckel syndrome where patients have a similar phenotype as ATR-SS patients, but the mutated gene is percentrin (PCNT). PCNT is a large protein that has a structural role in centrosome formation. Centrosome function is known to be essential for normal brain development by mediating the correct balance between symmetric and asymmetric division in the neuroepithelial stem cell layer (Lu et al., 2000). When dividing the neuroepithlial stem cells undergo a proliferative division producing two identical cells (symmetric divisions). After this division, the daughter cells produce another identical daughter cell as well as a non-stem cell progenitor cell which

forms a neuron (asymmetric division). Therefore impaired ATR signaling could potentially impair normal centrosome function and impact on brain development for example by exhausting neuroepithelial stem cells too early if symmetric and asymmetric divisions are unbalanced, potentially resulting in microcephaly (Kerzendorfer and O'Driscoll, 2009). Additionally, mitotic promoting factor Cdk1-cyclinB is activated at the centrosome and Chk1 localization at the centrosome has been shown to be important for its ability to arrest cells following DNA damage (Kramer et al., 2004). Therefore irregular centrosome formation could potentially affect the activation of ATR's downstream target kinase Chk1.

1.13.5 Infertility and Immune deficiencies

The generation of gametes during meiosis requires the exchange of genetic material between homologous chromosomes, which involves the formation of DSBs by the nuclease SPO11 and their subsequent repair by homologous recombination (Keeney and Neale, 2006). Therefore defective DSB repair during meiosis can result in infertility. A-T and FA patients display infertility (Biton et al., 2008).

To maintain immunity against the barrage of foreign pathogens a cell is exposed to each day, mammalian cells have developed an immune system which is capable of generating a wide number of unique immunoglobins and T cell receptors. B and T lymphocytes recognise foreign antigens through specialized receptors known as immunoglobins and TCR, respectively. These receptors are composed of V(D)J segments. Variation of these receptors is generated by recombination of these segments prior to antibody expression. Each V(D)J segment is flanked by a 12 or 23 bp recombination signal sequence (RSS). The process of recombination is initiated when Recombination Activating Gene 1 (RAG1) and Recombination Activating Gene 2 (RAG2) along with Human Mobility Group 1 (HMG1) or Human Mobility Group 2 (HMG2) proteins form a complex known as the RAG complex, which binds RSS sequences (Hiom and Gellert, 1997). The RAG complex endonucleolytically nicks the DNA at the RSS. Mutations in RAG1 and RAG2 have been identified in patients with severe combined immunodeficiency (SCID) caused by profound lymphopenia with diminished or absent immunoglobins (Sobacchi et al., 2006). Following RAG cleavage, the free 3' hydroxyl on each V, D, J coding end then attacks the antiparallel DNA strand and via transesterification a DNA hairpin is generated at each V, D and J coding end. The RSS end (signal end) is blunt. After generation of two hairpinned coding ends and two signal ends, the four DNA ends are held together by the RAG complex in a post-cleavage complex (Agrawal and Schatz, 1997). The hairpins are then cleaved

by Artemis (Ma et al., 2002). The loss of Artemis hairpin endonuclease activity results in the immunodeficient phenotype that is observed in Artemis patients. The subsequent re-joining of the V(D)J ends is carried out by NHEJ. Diversification of V(D)J variable domains is further achieved by class switch recombination (CSR) (Stavnezer et al., 2008a). CSR is triggered by the AID enzyme, which deaminates cytosines to uracil (Stavnezer et al., 2008b). DNA breaks are then generated by the combined action of the uracil DNA glycosylase UNG and the AP endonuclease APE1. NHEJ then leads to the exchange of the antibody constant regions.

1.13.6 Premature aging and cancer

Cancer is a major age-related disease in humans. In the absence of cancer, aging is mostly characterized by tissue atrophy and degeneration since older genomes have a higher incidence of accumulated DNA damage due to ongoing damage induction and less proficiency in repair (Weissman et al., 2007). p53 eliminates or arrests the proliferation of damaged or mutant cells by the process of apoptosis and senescence. Patients with inherited DDR defects often display features of premature aging. Most mammalian tissue can be described as being comprised of two major cellular components either: 1) stem or progenitor cells, which are responsible for regenerative capacity or repair after injury, or 2) differentiated somatic cells, which are responsible for adult stem cell support and specialized tissue/organ functions. Tissue degeneration with age can be accounted for by two major mechanisms: loss of stem cell pool division potential and loss of differentiated somatic cell function. Depending on cell type and damage amount, cellular senescence can be initiated by p53 signalling (Lowe et al., 1993). Senescent cells can no longer participate in tissue renewal and repair. Thus senescence can deplete both stem (Janzen et al., 2006) and stromal cell pools (Herbig et al., 2006). Unlike apoptotic cells, senescent cells persist, and have the ability to alter their surrounding tissue microenvironment (Campisi, 2005). Depletion of hematopoietic stem cells (HSC) has been observed in a variety of mouse models defective for DDR components, including ATM, BRCA2, Ku80 and LIG4. Ku80 null mice exhibit accelerated aging phenotypes, including skin atrophy, osteopenia, hepatocellular degeneration and shortened lifespan (Vogel et al., 1999). Ku80-/- MEFs undergo p53 dependent premature replicative senescence. However, loss of p53 in these cells was able to rescue the replicative senescence phenotype (Lim et al., 2000). This suggested that increased DNA damage and therefore p53 signalling was responsible for the accelerated aging phenotype of the Ku80-/- MEFs. Zmpste24 is a metalloproteinase that participates in the maturation of Lamin A, a protein component of the nuclear envelop.

Defects in Lamin A can cause premature aging phenotypes in humans and mice (Sullivan et al., 1999). Some Hutchinson-Gilford progeria syndrome (HGPS) patients harbor mutations in ZMPST24 (Eriksson et al., 2003). Zmpste24-/- mice have upregulated activation of many p53 targets (Varela et al., 2005), such as pChk1 and γH2AX (Liu et al., 2006). Analysis of DSB repair by neutral comet assay after IR revealed that Zmpste24-/- MEFs and HGPS cells repair DSBs with slower kinetics than wild type cells (Lui et al., 2005). Recruitment of Rad51 to DSBs is also impaired in these cells (Lui et al., 2005). It has been proposed that nuclear envelope abnormalities and defect in DSB repair in Zmpste24-/- mice and HGPS patients activate p53. Loss of p53 in the Zmpste24-/- background partially rescued the aging phenotype characteristic of Zmpste24 deficiency (Variela et al., 2005). Therefore despite p53 mediated apoptosis and senescence promoting tumor suppression, both can lead to aging phenotypes possibly by depleting important stem cells and other stroma cell pools. Therefore p53 dependent signalling has been optimized to balance the beneficial effects of tumor suppression against the detrimental effects of tissue degeneration.

1.14 Chromatin modification

It is becoming increasingly clear that chromatin structure impacts the DDR and is modulated in response to DNA damage. The best characterized example of this is the ATM/ATR/DNA-PK mediated phosphorylation of Ser139 of the histone H2A variant H2AX on chromatin flanking DSBs. H2AX is a histone variant, comprising roughly 10% of the histone H2A complement in mammalian cells, on average being placed 1 in every 10 nucleosomes. The percentage of H2AX content varies depending on cell type. For example the H2AX complement in lymphocytes and Hela cells has been reported to be as little as 2%, whereas 20 % of nucleosomes in SF268 human glioma cells contain H2AX (Rogakou et al., 1998). Following the induction of a DSB, within seconds, H2AX becomes rapidly phosphorylated at Serine 139 (Ser139). This phosphorylation event is mainly dependent on ATM, but DNA-PK can also play a redundant role (Stiff et al., 2004). ATR mediated phosphorylation of H2AX has been shown to be important during homologous recombination mediated repair in response to DNA damage that would slow or stall replication forks (Bonner et al., 2008). ATM independent H2AX phosphorylation also plays multiple roles during apoptosis. For example, DNA-PKcs mediated phosphorylation of H2AX at Ser139 mediates apoptotic DNA fragmentation (Rogakou et al., 2000). Phosphorylation of H2AX by c-Jun N-terminus kinase (JNK) has also been associated with the induction of apoptosis (Lu et al., 2006).

1.15 Chromatin structure

Genomic DNA and histones form a highly condensed structure known as chromatin. The major building blocks of chromatin are the histone proteins. These are small proteins containing a high proportion of basic amino acids (arginine and lysine) that facilitate binding to the negatively charged DNA molecule. There are five major types of histones, H1, H2A, H2B, H3, and H4 which assemble to form one octameric nucleosome core particle by wrapping 146 base pairs of DNA around the histone complex in a 1.65 left-handed super-helical turn (Suto et al., 2000). The linker histone H1 binds the nucleosome and the entry and exit sites of the DNA, thus locking the DNA into place and allowing the formation of a higher order structure. Chromatin is organized into two major types in the cell, euchromatin and heterochromatin. Euchromatin is associated with transcriptionally active regions of the genome and is said to be in an “open” conformation, whereas heterochromatin is associated with silenced regions and is transcriptionally inactive.

1.16 Types of heterochromatin

There are two main types of heterochromatin:

1.16.1 Constitutive heterochromatin

Constitutive heterochromatin contains a particular type of DNA called satellite DNA, which consists of large numbers of short tandemly repeated sequences known as alpha-satellite DNA, DNA satellite I, II and III. These satellite DNA sequences are able to fold on themselves and may have an important role in the formation of the highly compact structure of the constitutive heterochromatin (Metzler-Guillemain et al., 2003). Constitutive heterochromatin is stable and conserves its heterochromatic properties during all stages of development and in all tissues. It is highly polymorphic, which is likely a consequence of the instability of the satellite DNA; this polymorphism can affect not only the size but also the localization of the heterochromatin (Metzler-Guillemain et al., 2003).

1.16.2 Facultative heterochromatin

Facultative heterochromatin is reversible, its heterochromatic state depending on the stage of development or the cell type examined.

Some examples of heterochromatic regions in mammalian cells include:

(1) **Centromeres** – composed of tandem repeats known as satellite DNA. Centromeres are marked for epigenetic silencing by centromere protein–A (CENP-A), (Palmer et al., 1991). CENP-A contains a histone H3 related histone fold which replaces one or both copies of H3 in the $(H3\text{-}H4)^2$ tetrameric core of nucleosomes found at centromeres (Palmer et al., 1991). CENP-A is believed to confer conformational rigidity to nucleosomes, marking centromeres as constitutive heterochromatin (Black and Bassett, 2008).

(2) **Telomeres** – composed of TTAGGG repeats. Epigenetic regulation of telomere length is maintained by suppressor of variegation 3-9 homolog 1 (Suv39h1) (an enzyme that adds methyl residues to chromatin) and Suv39h2 in mammalian cells (Garcia-Cao et al., 2004).

(3) **Ribosomal DNA** (rDNA) – In eukaryotes, there are hundreds of rDNA genes tandemly repeated head to tail within nucleolus organizer regions (NORs), (Preuss and Pikaard, 2007). Their expression is in accordance with the physiological need for ribosomes (Preuss & Pikaard, 2007). One mechanism for transcriptional regulation is an epigenetic on/off switch which facilitates whether the rDNA sequences are silenced through heterochromatic formation (Preuss & Pikaard, 2007). A protein complex of eNoSc with sirtuin 1 (SIRT1) and Suv39h1has been described to sense both energy status and control rDNA transcription (Murayama et al., 2008). Low physiological energy levels induce the eNoSc/SIRT1/Suv39h complex to bind H3-K9 residues in rDNA, initiating methylation of these residues and consequently resulting in heterochromatin formation and gene silencing (Murayama et al., 2008).

1.17 Heterochromatin modification

To establish a highly compacted chromatin structure, chromatin must be modified. Two main classes of enzymes that modify chromatin structure have been identified: the first class

function through covalent modifications of histone tails. These modifications include methylation, acetylation, phosphorylation, ubiquitination, sumoylation, citrullination and ADP-ribosylation (Marmorstein, 2001). The second class, are large multi protein ATP-hydrolyzing complexes that utilize ATP to charge the alteration of nucleosome structure (Lusser and Kadonaga, 2003) (Table 1.4).

1.17.1 Histone Deacetylases (HDACs)

Histone deacetylases (HDACs) are key players in heterochromatin formation and can be recruited by transcriptional repressors (which are sequence specific transcription factors that, following binding at promoter sequences, initiate the accumulation of repression specific factors), co-repressors, and proteins that methylate DNA (Richards and Elgin, 2002). HDACs function by catalyzing the removal of acetyl groups from ε-N-acetyl lysine amino acids on histones (de Ruijter et al., 2003). Their action is opposite to that of histone acetyltransferase. Histone acetylation plays an important role in the regulation of gene expression. Hyperacetylated chromatin is associated with transcriptionally active areas of the genome and hypoacetylated areas with transcriptional silencing (Strahl and Allis, 2000).

1.17.2 Histone Methyltransferases (HMTs)

Histone methylation at lysine residues is central to epigenetic regulation of gene expression and is carried out by histone methyltransferases (HMT) (Sims et al., 2003). Common histone residues involved in HMT associated repression include H3 lysine 9 (H3-K9), H3-K27 and H4-K20 (Sims et al., 2003). At present the best understood histone modification is methylation of H3-K9, which is catalyzed by Suv39h1 and Suv39h2 in mammalian cells, and is responsible for most of the H3-K9 methylation at pericentric heterochromatin (Peters et al., 2001)

1.17.3 DNA Methyltransferases (DNMTs)

Mammalian DNA is modified by the addition of a methyl residue at position 5 of certain cytosine residues. This modification is predominantly carried out at CpG dinucleotides. Approximately 80% of CpG dinucleotides are modified in the human genome (Cooper & Krawczak, 1989). DNA methylation is important for embryonic development (Li et al., 1992),

imprinting (Sleutels et al., 2000) and X chromosome inactivation (Csankovski et al., 2001). DNA methyltransferases (DNMTs) are a family of enzymes that catalyze the transfer of a methyl group to DNA (Kaneda et al., 2004). Four active DNMTs have been identified in mammals, DNMT1, DNMT2, DNMT3A and DNMT3B. DNMT1 is the most abundant methyltransferase, which functions as a maintenance methyltransferase by copying DNA methylation patterns from the paternal to the daughter strand following DNA replication (Bestor, 2000). DNMT3A and DNMT3B are referred to as de novo DNA methyltransferases which are essential for methylation patterns established in the embryonic genome shortly after fertilization (Li, 2002). The function of DNMT2 is currently unknown. Heterochromatin, including centromeres, repetitive DNA sequences and telomeres tend to be hypermethylated and transcriptionally silent (Jenuwein, 2001)

1.17.4 Heterochromatin Protein 1 (HP1)

Heterochromatin protein 1 (HP1) is a structural component of heterochromatin which can bind both methylated histone residues and the HMTs responsible for the residue methylation (Craig, 2005). HP1 is associated with many types of heterochromatin such as telomeres, centromeres, silenced gene promoters and triplet repeat expansions (Kellum, 2003). Mammals have 3 isoforms – HP1α, HP1β and HP1γ (Craig, 2005). HP1 can bind to both Suv39h and H3-K9. The recruitment of Suv39h results in methylation of adjacent nucleosomes and the spread of heterochromatin (Kellum, 2003).

1.17.5 ATP-Dependent Chromatin Remodelers

ATP-dependent chromatin remodelers can be recruited to chromatin by repressors and co-repressors. However unlike the above proteins that alter chromatin structure through covalent modification, ATP-dependent remodelers use ATP to drive nucleosome remodeling. ATP-dependent remodelers function as ATP driven motors that translocate along DNA and destabilize protein-DNA interactions (Pazin and Kadonaga, 1997). One model suggests ATP hydrolysis is used to traverse a nucleosome in a wave like manner that results in partial disruption of the nucleosome (Pazin & Kadonaga, 1997). A well-known family of ATP-dependent chromatin remodelers is the SWI/SNF (switch/sucrose non-fermentable) family. The SWI/SNF polypeptides contain seven conserved motifs that are characteristic of a large

group of nucleoside triphosphate (NTP) – binding proteins that include DNA and RNA helicases (Kruger et al., 1995). Many orthologs of the yeast SWI/SNF family are present in higher eukaryotes. Other known mammalian remodelers include: the ISWI containing RSF (remodeling and spacing factor) which mediates nucleosome deposition and generates regularly spaced nucleosome arrays (Loyola et al., 2003); and the nucleosome remodeling histone deacetylation (NuRD) complex, which has both ATP power nucleosome remodeling capabilities and histone deacetylation activity (Feng and Zhang, 2003).

1.18 siRNA mediated protein knockdown

Knockdown of protein expression by Small interfering RNAs (siRNA) mediated transfection is a useful tool for analysing protein function and is a technique employed in this thesis. siRNAs are a type of double stranded RNA molecule (typically 20-25 nucleotides in length) that play a variety of roles in biology including: gene silencing, transposon control, centromere function and silencing impaired sex chromosomes during meiosis. These small regulatory RNAs represent an ancient regulatory mechanism as mirrored by their presence in organisms ranging from plants to yeast and mammals. The source of the initial dsRNA can be either exogenous (e.g. from viral replication) or endogenous. Expression of endogenous siRNA is often tissue or developmental stage specific. siRNAs are generally derived from dsRNA, which is fragmented by Dicer an endonuclease in the RNase III family that cleaves dsRNA into ~21 nucleotide siRNA. The siRNA is then bound by Argonaute protein. Argonaute proteins are small RNA binding proteins that are characterized by the presence of three domains: the PIWI/Argonaute/Zwille (PAZ) domain, the Middle (MID) domain and the P-element induced wimpy testis (PIWI) domain. The PAZ domain forms a binding pocket for the 3’ end of the small RNA, whereas the 5’ terminal nucleotide is bound by the MID domain (Boland et al., 2010). The PIWI domain has catalytic endonuclease activity referred to as slicing. The slicer activity allows Argonaute to degrade one of the strands of the dsRNA, thereby exposing the ssRNA and allowing it to detect its complementary target sequence (Leuschner et al., 2006; Matranga et al., 2005). The genomes of most organisms encode multiple Argonaute proteins, which typically bind to one specific type of siRNA either a microRNA (miRNA) which arise from imperfectly based paired miRNA hairpins, or siRNAs which arise from perfectly based paired long dsRNA, or PIWI interacting RNAs (piRNA) which is a germline enriched class of small RNA typically 24-30 nucleotides in length. The Argonoute and siRNA form the core RNA induced silencing complex (RISC) and target messenger RNA (mRNA) for silencing by mediating

transcript degradation. Targeting the mRNA by the RISC complex can induce the synthesis of secondary siRNA due to the formation of dsRNA on siRNA and mRNA association. In this sinareo RISC recruits RNA dependent RNA polymerase (RdRP), an enzyme that catalyzes the replication of RNA from an RNA template. RdRP synthesizes a new RNA that is antisense to the RNA template. The newly formed dsRNA is then fragmented by Dicer.

1.19 Aims of this thesis

The impact of higher order chromatin structure on DSB repair is now well established, but its impact on DDR signalling is less well understood. For example, can IR induced γH2AX foci expansion increase when heterochromatin associated barriers are reduced? What impact does this have on checkpoint arrest? Additionally do human disorders with known defects in chromatin organization respond hyperactively to IR? And if so, is this attributable to enhanced DDR signalling per γH2AX focus? Heavy ion radiotherapy is becoming of increasing importance for treating tumours that reside within vital organs which are not readily accessible by other means of radiotherapy, such as X-rays. For example, heavy charged particles offer a sharp increase in dose in a well-defined depth with a rapid loss of dose beyond the maximum output point, meaning that neighbouring tissues remain largely unaffected. This is of particular importance when treating brain tumours. However, given that heavy ion irradiation produces more complex DNA damage compared to X-ray, and complex DNA damage is more likely to take longer to repair, it is unknown whether this manifests as a prolonged checkpoint arrest? Also the number of heavy ion induced γH2AX clusters that are required to maintain checkpoint arrest is also unknown. A number of questions remain as to the mechanism by which Artemis functions to enable repair of a subset of ATM dependent DSBs in G0/G1. ATM and Artemis both have epistatic repair defects, but does Artemis like ATM function to repair HC associated DSBs? In this thesis I have addressed 3 main questions (see below) which all relate to the interplay between ATM signalling, checkpoint arrest and repair. How heterochromatin impacts on these endpoints is central to this work.

1.19.1 Addressing how human syndromes with disordered heterochromatin structure respond to IR.

Previously global chromatin compaction induced by histone H1 has been shown to limit the strength of the DNA damage signalling response (Murga et al., 2007). Additionally, transcriptionally active regions have been shown to inhibit γH2AX expansion (Iacovoni et al., 2010). However whether heterochromatin affects ATM signalling is yet to be examined. In chapters 3 and 4, I investigate how heterochromatin superstructure influences damage response signalling focussing on the impact of disordered chromatin found in human syndromes.

1.19.2 Addressing the function of Artemis in DSB repair

ATM and Artemis have an epistatic repair defect (Riballo et al., 2004a). The role of ATM in the repair of a subset of IR induced DSBs has recently been established. ATM was demonstrated to function in the repair of heterochromatin associated DSBs by mediating chromatin relaxation via phosphorylation of the heterochromatin building factor KAP-1 (Goodarzi et al., 2008b; Ziv et al., 2006). The function of Artemis in this process has not yet been established. In chapter 5, I address whether Artemis dependent DSBs also reside within regions of heterochromatin.

1.19.3 Addressing checkpoint arrest after heavy ion irradiation

Chapter 6 arose from an opportunity to visit the National Institute of Radiological Science (NIRS) in Chiba, Japan. The NIRS is home to one of three worldwide heavy ion accelerators. The ion accelerator at the NIRS is used for both patient radiotherapy treatments and scientific research. In chapters 3 and 4 of this thesis it was established that chromatin complexity influences the duration and sensitivity of G2/M checkpoint arrest. In this chapter I addressed how damage complexity after heavy ion irradiation influences this. The G2/M checkpoint has previously been shown to have a defined sensitivity threshold which requires at least 10-15 DSS to initiate arrest (Deckbar et al., 2007; Fernet et al., 2010). As a consequence, cells released from checkpoint arrest harbour 1-2 chromosome breaks in mitosis. Since heavy ion irradiation produces more complex clustered DSBs, in this chapter I addressed whether checkpoint arrest could be maintained until only a few clustered γH2AX foci remained.

Chapter 2: Materials and Methods

Materials and Methods

1.20 Cells and tissue culture

1.20.1 Cell lines

NIH 3T3 cells and mouse embryonic fibroblasts (MEFs): WT, AT, & Art-/- were cultured in MEM supplemented with 10% v/v foetal calf serum (FCS), 1% v/v Penicillin/Streptomycin solution and 1% v/v L-Glutamine. 1BR (wildtype), 48BR (wildtype), PT3 (ICF/DNMT3B) and CJ179 (Art) transformed human fibroblasts (hTRETs) were cultured in MEM supplemented as above. 48BR (wildtype), 1BR3 (wildtype), GM11271 (Rett/MeCP2), GM11272 (Rett/MeCP2), and GM16548 (Rett/MeCP2) primary human fibroblasts were grown in MEM and supplemented with 15% FCS and 1% v/v Penicillin/Streptomycin solution and 1% v/v L-Glutamine. GM02188 (wildtype), GM16848 (Rett/MeCP2), GM08714 (ICF/DNMT3B) & AG10801 (HGPS/Lamin A) are lymphoblastoid cell lines (LBLs) and were cultured in RPMI supplemented with 10% FCS, 1% v/v L-Glutamine and 1% v/v Penicillin/Streptomycin solution. All cells were grown at 37 ^{o}C in a humidified atmosphere containing 5% carbon dioxide.

1.20.2 Tissue culture

To maintain cells in a healthy and proliferating condition, cultures were divided every 4-5 days. For passaging, cells were washed once with 1X PBS followed by the addition of trypsin (200 mg/ml trypsin dissolved is PBS, followed by filter sterilization). Cells were incubated with trypsin for 2-5 minutes in a 37°C incubator, and collected and pelleted by centrifugation at 1500 rpm for 5 minutes at RT. The pellet was then resuspended in the desired volume of

media. To establish frozen cell stocks, a confluent 75 cm^2 flask was trypsinized, pelleted and resuspended in 1 ml FCS with 10% v/v DMSO. Vials were slowly cooled to -80°C and transferred to liquid nitrogen tanks for permanent storage.

1.20.3 Drug treatments and IR

10 µM ATM inhibitor (Calbiochem) was added 30 minutes before IR. 4 µM aphidicolin was added immediately after IR to block entry of irradiated S phase cells into G2 during analysis. Cells were irradiated in medium using either a ^{137}Cs gamma-source (dose rate, 7.5 Gy/min) or 250kV X-rays delivered at 12 mA (dose rate 0.5 Gy/min). For irradiation with heavy ions cells were seeded into Nunc glass chamber slides. Heavy ion irradiation with Carbon (290 MeV/nucleon, LET 70 KeV/µm) and Iron (500 MeV/nucleon, LET 200 KeV/µm) beams were performed at the Heavy Ion Medical Accelerator (HIMAC) facility at the National Institute of Radiological Sciences (NIRS), Chiba, Japan. Heavy ion irradiation was delivered at a dose rate of 1 Gy/min.

1.21 Immunofluorescence

Cells grown on cover-slips were fixed for 10 minutes with fixative (3% (w/v) PFA, 2 % (w/v) sucrose and 1X PBS) and permeabilised for 3 minutes with 0.2% Triton X-100 in PBS. Cells were washed with PBS and incubated with primary antibody diluted in 2% (w/v) BSA + PBS, for one hour at room temperature. Cells were washed three times with PBS before incubating with the appropriate secondary antibody (diluted in 2 % (w/v) BSA + PBS (Green = FITC, red = cy3 or TRITC, conjugated antibodies), for 1 hour at room temperature in the dark. 4', 6-diamidino-2-phenylindole (DAPI) (1mg/ml) was then applied for 10 minutes followed by three washes with PBS. Cover-slips were then mounted on microscope slides using Vectashield. Slides were visualized on a Zeiss Axioplan microscope or An Applied Precision Delta Vision RT Lympus 1X70 deconvolution microscope. (See table 2.1 for antibody dilutions).

1.21.1 Sequential staining for pChk1, pChk2 and pATM

Cells were fixed with 3 % PFA for 10 minutes, washed twice with PBS and incubated with 0.2 % Triton-X for 3 minutes. Cells were washed 2X with PSB and incubated with primary phospho-antibodies for 30 minutes at 37°C. Cells were washed 3X with PBS before incubating with the secondary antibody rabbit Cy3 or mouse FITC for 30 minutes at 37°. Cells were washed 3X with PBS and incubated with primary CENP-F antibody for 30 minutes at 37°. Cells were then washed 3X with PBS and incubated with secondary Alexa fluroflore 488 for 30 minutes at 37°. 4', 6-diamidino-2-phenylindole (DAPI) (1mg/ml) was then applied for 10 minutes followed by three washes with PBS. Cover-slips were then mounted on microscope slides using Vectashield and visualised using a Zeiss Axioplan microscope. (See table 2.1 for dilutions)

1.21.2 Pre-extraction for RPA foci

Before irradiating cells, aphidicolin was added to prevent S phase cells progressing into G2 phase during analysis. Cells were irradiated and processed 1 hour later. Media was removed and cells were washed with 1X PBS. To pre-extract, 1 ml PBS + 0.2% Triton-X was added to each sample for 60 seconds. Triton-X solution was removed by aspiration and cells were fixed with 1 ml 3% PFA for 10 minutes. Staining was continued as described before.

Table 2.1 Antibodies used for Immunofluorescence (IF) and Western Blotting (WB)

A

Antibody	Size (KDa)	Species and supplier	Application
CENP-F	330	Rabbit (Abcam)	IF 1:1000
pSer1981 ATM	330	Rabbit (Epitomics)	IF 1:100, WB 1:500
ATM	330	Rabbit	WB 1:500
ATR	309	Goat	WB 1:500
53BP1	220	Rabbit (Abcam)	IF 1:800, WB 1:1000
KAP-1	100	Rabbit (Abcam)	IF 1:800, WB 1:1000
KAP-1	100	Mouse (Abcam)	IF 1:800, WB 1:1000
KAP-1	100	Goat (Abcam)	IF 1:300
pSer824 KAP-1	100	Rabbit (Noon *et al*, 2010)	IF 1:200 (+ 1:1000 peptide)
DNMT3B	98	Rabbit (Invitrogen)	IF 1:800, WB 1:500
Ku80	80	Rabbit (Sata Cruz)	WB 1:2000
pThr68 Chk2	68	Rabbit (Cell signalling)	WB 1:500
Chk2	68	Rabbit (cell signalling)	WB 1:500
pChk1	56	Rabbit (Cell signalling)	WB 1:500
Chk1	56	Rabbit (cell signalling)	WB 1:500
HDAC1	55	Mouse (Abcam)	IF 1:300, WB 1:1000
pP53	53	Mouse (Cell signalling)	WB 1:1000
MeCP2	53	Rabbit (Invitrogen)	IF 1:800, WB 1:500
P53	53	Mouse	WB 1:1000
pSer10 H3	16	Rabbit (upstate biotechnology)	IF 1:400
γH2AX	16	Mouse (Abcam/ Upstate)	IF 1:800, WB 1:500
TriMeK9 H3	~16	Rabbit (Abcam)	IF 1:800, WB 1:500
RPA	34	Mouse	IF 1:100
Actin	42	Mouse (Abcam)	WB 1:3000

B

Antibody	Supplier	Application
Anti-Mouse FITC conjugated	Sigma	IF 1:200
Anti-Rabbit Cy3 conjugated	Sigma	IF 1:200
Anti-Goat Cy3 conjugated	Sigma	IF 1:200
Anti-Mouse HRP conjugated	Dako	WB 1:2000
Anti-Rabbit HRP conjugated	Dako	WB 1:2000

(A) Primary antibodies used for immunofluorescence (IF) and western blotting (WB).

(B) Secondary antibodies used for immunofluorescence (IF) and western blotting (WB).

1.22 siRNA transfection

siRNA transfections were carried out using HiPerfect (Qiagen) or Metafectene-Pro (Biontex) mediated transfection reagents according to the manufacturer's instructions. 50-100 pmol of 25 mM stock siRNA solutions were incubated with 2.5-5 µl of transfection reagent and optiMEM for 10 minutes at RT. Following incubation, the siRNA mix was applied onto glass coverslips in 3.5 cm dishes followed by 2 ml of 2 x 10^5 cell stocks. Cells were incubated for 48 hours prior to conducting experiments. Where a double knock down was required to achieve efficient knockdown of protein expression, siRNA transfections were set up as described above. 24 hours after incubation cells were trypsinized from the dishes, centrifuged at 1500 rpm for 5 minutes and resuspended in 2 ml media/ dish. siRNA transfections were set up again and the previously transfected cells were incubated with a fresh siRNA transfection for a further 48 hours. (See table 2.2 for siRNA sequences used for transfections).

Table 2.2 Oligonucleotides used for siRNA transfections

siRNA target	Sequence 5'-3'	Supplier
HDAC1 (human cDNA nt 224-249)	UCUUGCGCUCCAUCCGUCCAGAUAA	Invitrogen
HDAC2 (human cDNA nt 1381-1406)	CACCUGGUGUCCAGAUGCAAGCUAU	Invitrogen
KAP-1 'A' (human cDNA nt 450-475)	CAGTGCTGCCACTAGCTGTGAGGATA	Invitrogen
KAP-1 'C' (mouse cDNA nt 1297-1322)	AAGATGCAGTGAGGAACCAACGTAA	Invitrogen
Artemis 'A' (mouse cDNA nt 684-709)	CCACGUCGUGUGGCUGAACUGUAAA	Invitrogen
Artemis 'B' (mouse cDNA nt 1705-1729)	UUUACAGUUCAGCCACACACGACGGUGG	Invitrogen
MeCP2 (mouse)	CCUGAAGGUUGGACACGAA	Dharmacon
MeCP2 (human)	GACACAUCCCUGGACCCUAAUGAUU	Invitrogen
DNMT3B (mouse) (SMARTpool)	GAGGAGUGCAUUAUCGUUA UCAGGAUGAUAAAGAGUUU GCAAUGAUCUCUCUAACGU GGAAUGCGCUGGGUACAGU	Dharmacon
DNMT3B (human)	CCACCUUCAAUAAGCUCGUCUCCUA	Invitrogen
siGENOME Non-targetting siRNA pools	Cat. no. D-001206-13	Dharmacon

1.23 Protein techniques

Stock solutions:

Acrylamide gels:

30% w/v Acrylamide

2% w/v Bis-Acrylamide

20% w/v sodium Dodecyl Sulphate (SDS)

1M Tris pH 8.8

10% Ammonium Persulphate

ddH_20

TEMED

Gel stack:

30% w/v acrylamide

20% w/v Bis-acrylamide

1M Tris pH 6.8

20% SDS

10% APS

TEMED

ddH_20

NETN lysis buffer:

50 mM Tris pH 7.5

150 mM NaCl

0.2 mM EDTA

1% NP-40

ddH_20

1 protein phosphatase table

6X SDS sample loading buffer (for 30 ml):

15 ml Glycerol

12 ml 1M Tris pH 6.8

3g SDS

Bromophenol Blue

Gently warm to dissolve

Add 1.5 ml β-mercaptoethanol

1.23.1 Protein extraction

Media was removed and cells were washed with PBS + 1 mM EDTA. Cells were trypsinized in 500 µl trypsin (0.25%) for 3 minutes. Cell aggregates were removed by pipetting up and down, and transferred to eppendorfs. Samples were kept on ice. Cells were centrifuged at 2000 rpm for 2 minutes at 4°C. Pelleted cells were washed twice in 1 ml ice cold 1X PBS. Cells were centrifuged at 2000 rpm for 4 minutes at 4°C. To the pellet a 5X Pellet cell volume (PCV) of NETN + NaCl + protease inhibitors + phosphatase inhibitors was added. Pellets were

suspended in the NETN by pipetting strongly. Samples were sonicated in a water bath for 5 minutes. Samples were left on ice for 30 minutes. BIO-RAD protein quantification was then carried out on the samples to determine protein concentrations. For quantification, 5 µl of each sample + 10 µl NETN + N buffer was added to 75 µl reagent A (BIO-RAD) + 600 µl reagent B (BIO-RAD), incubated at room temperature for 15 minutes and spectrophrometically quantified using a Beckman spectrophotometer. For the blank standardization sample 15 µl of NETN + N buffer was used. Appropriate sample volumes were boiled for 3 minutes in 6X SDS loading buffer and centrifuged briefly before gel loading. Samples were loaded alongside a 250 kDa Precision Plus Protein Standards marker from BIO-RAD.

1.23.2 Poly-Acrylamide Gel Electrphoresis (PAGE)

Acrylamide gels of appropriate percentage (see table 2.3) were made from stock solutions and polymerized at RT for at least 30 minutes. Gel stacks were then made fresh from stock solutions and added to the gel to polymerize for 15 minutes prior to removing the well comb. Gels were run in an Invitrogen Novex mini-cell tank.

Table 2.3: Loading concentrations for different percentage SDS-PAGE gels.

	6 %	**8 %**	**10 %**	**12 %**
dH_2O	5.4 ml	4.7 ml	4.1 ml	3.4 ml
30% Acrylamide	2 ml	2.7 ml	3.3 ml	4 ml
1M Tris (8.8)	2.5 ml	2.5 ml	2.5 ml	2.5 ml
20 % SDS	50 ul	50 ul	50 ul	50 ul
10 % APS	50 ul	50 ul	50 ul	50 ul
TEMED	5 ul	5 ul	5 ul	5 ul

1.23.3 Western blotting

Transfer buffer (1L):

5.8g Tris

2.93g Glycine

800 ml ddH_20

200 ml methanol

(For high molecular weight proteins 1,8 ml 20% SDS was also added).

10X Tris-buffered saline (TBS:1L):

12.11g Tris

81.82g NaCl

ddH_20 to 1L

pH to 7.4

Working 1X TBS/Tween-20 wash buffer:

50 ml 10X TBS

0.5 ml Tween 20

450 ml ddH_20

Following protein separation by SDS-PAGE, samples were transferred onto a 0.45 µm nitrocellulose membrane using the BIO-RAD Mini Trans-Blot Cell. Proteins were transferred for 1 hour at 100V in chilled electroblot buffer. To visualize that proteins had successfully

transferred to the membrane, a non-permanent Poceau stain (0.1% w/v Poceau S in 5% v/v acetic acid) was applied to the membrane for 1 minute. The stain was removed by washing in 1X TBS/Tween. The membrane was then blocked for 1 hour in 5% BSA made up in 1X TBS/Tween. Primary antibodies (see table) were diluted in 5% BSA solution and incubated with the membrane at 4°C for 24 hours with gentle shaking. After incubation, the membrane was given three 20 minute washes in 1X TBS/Tween. Secondary HRP conjugated antibodies (see table) were diluted in 5% BSA and incubated with the membrane for 1 hour at RT with gentle shaking. The membrane was washed a further three times for 30 minutes (each wash) in 1X TBS/Tween. To visualize the protein bands, membranes were incubated with enhanced chemiluminescence (ECL) immunoblotting agent (Amersham Biosciences) for 2-5 minutes and exposed onto autoradiography blue sensitive film (GE healthcare). A Xograph Compact 4 automatic X-ray film processor was used to develop the film.

1.23.4 Stripping a western membrane for re-probing

To reuse a membrane which had already been developed in ECL, it was first rinsed in water. The membrane was then incubated with 50 ml 1X stripping buffer (2X: 30 ml 1M Tris HCL pH 6.8, 50 ml 2% SDS made to 250 ml with water) + 350 µl beta-merceptoethanol at 60° for 30 minutes in the fume hood. The buffer was removed and the blot was washed twice for 10 minutes with TBS/Tween in a fume hood. The membrane was re-blocked with 5% BSA for 1 hour and incubated with primary antibody. The western blot procedure was then continued as before.

1.24 Immunoprecipitation (IP)

Nucleosome prep and chromatin segregation assay buffers:

Low Salt Buffer (LSB)

10 mM HEPES pH 7.4

25 mM KCl

10 mM NaCl

1 mM MgCl2

0.1 mM EDTA

High Salt Buffer (HSB)

50 mM Tris-HCL pH 8

5% glycerol

1 mM EDTA

10 mM MgCl2

400 mM KCl

1X protease inhibitor

0.1 µM MC-LR

Nuclease buffer

10 mM HEPES

10 mM KCl

1 mM CaCl2

1.5 mM MgCl2

0.34 sucrose

10% glycerol

1 mM DDT

0.1% Triton X-100

Wash Buffer

Nuclease buffer

1% NP-40,

1% Triton X-100

300 mM NaCl

Solubilisation Buffer

Nuclease buffer

2% NP-40

2% Triton X-100

600 mM NaCl

Denaturing Buffer

50 mM Tris pH 6.8

1% SDS

100 mM DTT

10% glycerol

1.24.1 Fixation trials for IP

2 x T25 flasks were used per cell type. Cells were irradiated with 10 Gy IR and PFA treated 30 minutes later. Cells were fixed with 2 ml fixative for 3 minutes under the following conditions: (1) No fixative (PBS), (2) 0.1% PFA, (3) 0.3% PFA, (4) 1% PFA, (5) 3% PFA. Fixative was poured off and cells were washed with 1X PBS. Media was added back to the flask and the cells were collected by scraping. Collected cells were centrifuged at 2000 rpm for 2 minutes. The supernatant was removed and the pellets were washed with 1X PBS and transferred to eppendorfs. Pellets were then washed with 1X LSB (0.5 ml), centrifuged at 2000 rpm for 2 mins and resuspended in 5X pellet cell volume (PCV)) of LSB + PI + PPI + Microcystin-LR (MCLR – protein phosphatase inhibitor).

1.24.2 Nucleosome solubilization and γH2AX IP

Cells were fixed with 0.1% PFA for 3 minutes, then washed with PBS and once with low salt buffer (LSB: 10 mM HEPES (pH 7.4), 25 mM KCl, 10 mM NaCl, 1 mM $MgCl_2$, 0.1 mM EDTA). Pellet cells were resuspended in five times the packed cell volume (PCV) of LSB + 0.1 um MC-LR and 1X protease inhibitor cocktail (Sigma-Aldrich, UK) and snap frozen in liquid nitrogen. Cells were quick thawed and centrifuged at 10,000 rpm for 10 minutes. The pellet was resuspended in 2 times the PCV of nuclease buffer (10 mM HEPES (pH 7.9), 10 mM KCl, 1.0 mM $CaCl_2$, 1.5 mM $MgCl_2$, 0.34 M sucrose, 10% glycerol, 1 mM DTT, 0.1 % (v/v) Triton X-100) containing 100U/ml MNase. Samples were incubated at 37 degrees for 45 minutes. A PCV of solubilization buffer (nuclease buffer + 2% (v/v) NP-40, 2% (v/v) Triton X-100, 600 mM NaCl) was then added. Samples were sonicated and centrifuged at 10,000 rpm for 10 minutes. The final supernatant was incubated with 2 µl of anti-γH2AX monoclonal antibody overnight at 4 degrees. 30 µl of protein G-sepharose was added and incubated overnight to pull down immunocomplexes followed by 3 washes with wash buffer (nuclease buffer + 1% (v/v) NP-40, 1% (v/v) Triton X-100, 300 mM NaCl. Samples were boiled for 2 minutes following the addition of 20 µl 2X SDS sample buffer. Samples were separated on a 12.5 % SDS PAGE gel.

1.24.3 DNA extraction following γH2AX IP

γH2AX IP was carried out as described above. 20 µg DNase-free RNase A was added to each sample and incubated at 37°C for 30 minutes. 250 µl IP elution buffer (1% SDS + 0.1 M NaHCO3) was added to each sample and incubated at room temperature for 15 minutes. Samples were vortexed occasionally throughout the incubation. The supernatant was collected in a screw cap eppendorf and the elution process repeated once. Supernatants were pooled. To revert the cross-linking, 200 mM NaCl was added to the eluted samples and samples were incubated at 85°C for 2 hours. Protein and DNA samples were precipitated with the addition of 1 ml 99% ethanol. Samples were incubated with ethanol overnight at -20°C. 24 hours later, samples were centrifuged at 3000 rpm for 15 minutes at 4°C. Pellets were washed with cold 70% ethanol. Samples were centrifuged again at 3000 rpm for 15 minutes at 4°C. The pellet was air dried at room temperature. The pellet was then dissolved in 100 µl ddH_2O pH 8. To each pellet, 11 µl of 10X proteinase K buffer + 1 µl of 20 µg/µl of proteinase K was added and incubated at 50°C for 30 minutes. DNA was then extracted with phenol/chloroform/isoamyl alcohol, using the same volume that was used to originally dissolve the pellet. Samples were shaken by hand and centrifuged at 3000 rpm for 10 minutes at room temperature. The upper aqueous layer (DNA) was removed. This was repeated 2X and the upper aqueous layers pooled. The DNA was ethanol precipitated in 1ml 99.9% ethanol at -20°C overnight. 24 hours later, samples were centrifuged at 10,000 rpm for 10 minutes. The final pellet was dissolved in 50 – 100 µl of water. A fraction of the sample was loaded on an agarose gel.

1.24.4 DNA agarose gel

Stock solutions:

1X TAE:

0.4M Tris acetate

1mM EDTA pH 8

6X loading buffer:

25 mg Xylene cyanol FF

25 mg Bromophenol blue

3 ml Glycine

Make up to 10 ml with ddH_20

Store at 4°C

To prepare agarose gels the appropriate concentration (w/v) of agarose was dissolved in 1X TAE buffer by heating in a microwave. The agarose was cooled and ethidium bromide (0.5µg/ml) was added prior to pouring. Gels were left to polymerize at RT. Prior to sample loading the gel was immersed in TAE buffer for 10 minutes. Samples wer loaded with sample loading buffer alongside a 1Kb DNA marker (Invitrogen). Electrophoresis was carried out at 85V for 40 minutes. Ethidium bromide incorporated DNA was visualized with a UV light box.

1.25 Chromatin fractionation assay

Cells were irradiated with 40 Gy IR, trypsinzied and washed with 1ml PBS. Cells were centrifuged at 1500 rpm for 1 min. The cells pellet was resuspended in 1X PCV of nuclease buffer (no MNase). Sample were again spun at 1500 rpm for 1 min (supernatant = C0). The pellet was then resuspended in nuclease buffer (same V as PCV) containing 10 U/ml MNase and incubated at 37° for 10 mins. Samples were then centrifuged for 3 minutes at 2,000 rpm (supernatant = C1). The pellet was then resuspended in nuclease buffer (same V used for PCV) containing 100 U/ml MNase and incubated at 37°C for 45 minutes. The same volume of solublization buffer (nuclease buffer + 2% NP-40, 2% Triton X-100, 600 mM NaCl) was then added to the pellet. Samples were then briefly vortexed and centrifuged for 5 minutes at 10,000 rpm (supernatant = C2). The remaining pellet was resuspended in solubilization buffer (same V as HSB) and an equal volume of denaturing buffer (50 mM Tris pH 6.8, 1% SDS, 100 mM DTT, 10 % glycerol). Finally, the remaining sample was sonicated, boiled for 5 minutes and

centrifuged for 5 minutes at 10,000 rpm (supernatant = C3). (A very small pellet will remain which is the insoluble cell membrane)

1.26 Flow cytometry

Cells were grown in dishes at a concentration of 2 x 10^5 cells/ml for 48 hours. Cells were trypinized in 0.4% trypsin and centrifuged at 1500 rpm for 3 minutes. The cell pellet was washed in 10 ml PBS + 1mm EDTA and again centrifuged at 1500 rpm for 3 minutes. The PBS was then removed. The pellet was resuspended in 2 mls PBS with a pipette to have a population of single cells. 1 ml 2% PFA was added slowly to the sample while vortexing. Samples were fixed in PFA (2%) for 10 minutes. The pellet was centrifuged at 3000 rpm for 3 minutes, resuspended in PBS and stored at 4°C. 200 µl PI buffer (20 µl 1 mg/ml Propidiun iodine (PI), 2 µl 30 mg/ml RNase, 180 µl PBS) was added to each sample. Samples were then transferred to a FACS tube. Samples were read using a FACS canto cell sorting calibrator.

1.27 Clonogenic survival

On day one, 1 x T25 flask was set up with 2 x 10^5 cells per cell line. 15 X 9 cm Petri dishes per cell line with 6 x 10^4 feeder cells were also set up. Feeder cells were irradiated with 35 Gy (IR) before plating into MEM + NBCS + supplements (10 ml/dish). On day two, the T25 flasks were trypsinized and counted. Serial dilutions were made from these cells. Cells were irradiated and plated onto feeder cells. On day 21, 1 ml of methylene blue was added to each dish for 45 minutes. The solution was poured off and plates were left to dry at room temperature for 24 hours. The plates were then gently washed with water and again left to dry. Colonies with more than 50 cells were counted.

1.28 Delta vision microscope

1.28.1 SoftWoRx® Suite software analysis

Quantitative measurements of γH2AX and DAPI overlap were obtained and visualized as a red signal using softWoRx® Suite software. The size of overlapping regions per cell was quantified by ImageJ. The number of chromocentres was analysed. The size of overlap per chromocentre was normalized following these analyses. The volume of the interior signal was visualized and measured by Huygens Professional, Scientific Volume Imaging. Similar to the analysis of overlap, the volume per chromocentre was normalized to the number of chromocentres.

1.28.2 Measuring fluroflore signal intensity using ImageJ software.

The signal intensity of FITC and DAPI per YH2AX focus was quantified with ImageJ. To measure pATM signal intensity, the untreated nuclear intensity was subtracted from the IR induced nuclear signal intensity. The images were taken by the Zeiss Axioplan microscope with identical exposure time. The size of γH2AX foci at chromocentres was quantified with ImageJ after deconvolution with softWoRx® Suite software.

1.28.3 softWoRx® Suite software analysis

Quantitative measurements of γH2AX and DAPI overlap were obtained and visualized as a red signal using softWoRx® Suite software. The size of overlapping regions per cell was quantified by ImageJ. The number of chromocentres was analysed. The size of overlap per chromocentre was normalized following these analyses. The volume of the interior signal was visualized and measured by Huygens Professional, Scientific Volume Imaging. Similar to the analysis of overlap, the volume per chromocentre was normalized to the number of chromocentres.

1.29 γH2AX foci and G2/M checkpoint analysis

DSB repair was monitored by disappearance of γH2AX foci (Lobrich et al., 2010). G1 and G2 phase cells were identified using the cell cycle marker, anti-CENPF in human cells and anti- p-H3 Ser10 in mouse cells, respectively (Beucher et al., 2009). For initiation of G2/M checkpoint analysis, cells were fixed 1 or 2 h after IR, and stained for p-H3 Ser10 and DAPI. p-H3 Ser10 positive and condensed chromatin cells were scored as mitotic cells. >400 cells were scored per condition. For DSB repair in cycling cells and maintenance of G2/M checkpoint analysis, 4 μM aphidicolin was added immediately after IR to block entry of irradiated S phase cells into G2 during analysis. Aphidicolin does not impact upon DSB repair and signaling in G1 and G2 phase (Beucher et al., 2009; Lobrich et al., 2010; Shibata et al., 2010). The mitotic idex represents the number of mitotic cells per 100 cells.

Chapter 3: The impact of higher order chromatin structure on G2/M checkpoint arrest and ATM signalling

The impact of higher order chromatin structure on G2/M checkpoint arrest and ATM signalling

1.30 Introduction

ATM is a DNA damage inducible protein kinase, which phosphorylates a plethora of substrates participating in the DNA damage response, including proteins involved in DNA repair and cell cycle checkpoint arrest. An early detectable ATM substrate is the histone variant γH2AX which acts as a docking site for the recruitment and retention of damage response proteins into repair foci. The accumulation and spread of these repair foci can travel over megabases of DNA. γH2AX foci formation is required for ATM-dependent DSB repair but its influence on ATM signalling appears to be modest since loss of H2AX confers only a mild defect in ATM phosphorylation of downstream substrates – most specifically impacting at low doses. Given that chromatin architecture plays an important role in regulating DNA replication, transcription, recombination and repair; the impact that heterochromatin poses to DDR signalling is unknown. This is of particular importance because there are human syndromes with disordered heterochromatin. In this chapter I will focus on how changes to heterochromatin that occur in human disorders influence ATM signalling. Specifically, I will focus on how reduced heterochromatin organization impacts upon the expansion of IR induced γH2AX foci and G2/M checkpoint initiation.

1.30.1 The impact of chromatin on DSB repair

Over two decades ago, changes in DNA packaging following DNA damage was recognized by changes in accessibility of DNA binding dyes and DNA nucleosome digestibility (Takahashi and Kaneko, 1985). The re-emergence of interest in this field has put heterochromatin in vogue,

and many recent publications analyzing the impact of chromatin structure on DSB repair have shed light on how the damage response machinery manoeuvres nucleosomes to allow access to the DNA repair machinery. It was first suggested in yeast that upon DNA damage histone remodelling complexes initiate structural changes at the site of a lesion (Downs et al., 2004). In yeast a subunit of the histone remodelling complex NuA4 was found to directly interact with H2A S129 (analogous to mammalian H2AX S139) following DNA damage (Downs et al., 2004), suggesting that nucleosome remodelling occurs at the site of a DSB. Further experiments in yeast found that the stability of histone H2B or H3 association with chromatin decreases after DSB induction (Tsukuda et al., 2005). Chromatin surrounding the DSB region also becomes more accessible to MNase digestion, implying that the chromatin superstructure at these localities relaxes (Tsukuda et al., 2005). In mammalian cells, delayed recruitment and focal accumulation of 53BP1 and Rad51 has been observed in cells defective for the histone Acetyltransferase (HAT) co-factor Trrap (Murr et al., 2006). HATs typically modify histone tails with acetyl residues to promote nucleosomal relaxation. Using ChIP, a reduction of H4 acetylation at the site of an I-Sce1 induced DSB in Trrap deficient cells was observed. Depletion of Trrap also abolished the association of another HAT known as Tip60 with the DSB site (Murr et al., 2006). Following chemically induced chromatin relaxation, mediated by either: chloroquine, sodium butyrate or hypotonic conditions, the accumulation of Rad51 at DSBs in Trrap deficient cells was rescued (Murr et al., 2006). These results suggested that the Trrap-Tip60 complex functions to acetylate histones in the vicinity of a DSB, and that this remodelling is essential for the recruitment of repair proteins at the site of a lesion. In recent years several papers have demonstrated the importance of KAP-1 phosphorylation (pKAP-1) in response to DSBs to implement dynamic and localized chromatin changes necessary for DSB repair (Goodarzi et al., 2008; Ziv et al., 2006). KAP-1 is a heterochromatin associated building protein that is phosphorylated by ATM at S824 (Goodarzi et al., 2008) (see 3.1.4.1 for further discussion on KAP-1). The importance of KAP-1 mobility for HC associated repair was first demonstrated by Ziv *et al* (2006) when MNase accessibility was found to increase following KAP-1 knockdown. Later Goodarzi et al (2008) demonstrated that the requirement for ATM in DSB repair could be overcome following HC mediated relaxation via KAP-1 knockdown or expression of a phosphomimetic KAP-1^{S824D}, while the expression of a non-phosphorylatable KAP-1 conferred a constitutive HC DSB repair defect similar to that of A-T cells. The authors proposed that ATM dependent phosphorylation of KAP-1 functions to perturb heterochromatin at the site of a DSB. A later publication from the same laboratory established that the mediator proteins 53BP1, RNF8 and MDC1 promote KAP-1 phosphorylation and assist in DSB repair at heterochromatin (Noon et al., 2010). At early time points after IR, pKAP-1

immunostaining appears pan-nuclear. This reflects the wide spread untethered activity of ATM at early time points after IR. At later time points when ATM activity is tethered by mediator proteins such as MDC1 and 53BP1, localized KAP-1 phosphorylation occurs, and these foci locate to slow repairing DSBs at regions of heterochromatin. Cells missing 53BP1 displayed largely normal pKAP-1 induction (pan-nuclear staining), but due to an inability to concentrate ATM they failed to form pKAP-1 IRIF overlapping with HC DSBs (Noon et al., 2010). The authors proposed that IRIF foci concentrate ATM activity at a DSB to promote localized alterations in regions of chromatin otherwise inhibitory to repair. Collectively these findings are consistent with the notion that the HC superstructure is a barrier to DSB repair and the importance of ATM phosphorylation in increasing the global accessibility of chromatin after DNA damage. In this chapter I will focus on whether heterochromatin influences DDR signalling. This is important because heterochromatin levels can vary between cell types and also there are patients with disordered heterochromatin.

1.30.2 The impact of chromatin on DDR signalling

One of the earliest detectable chromatin modifications to occur following DSB induction is the phosphorylation of H2AX on S139 (Rogakou et al., 1998). H2AX is a member of the H2A histone family, which is one of five histone families that package and organize DNA into chromatin (see 1.15 for further discussion on chromatin). The importance of H2AX is not yet fully understood. $H2AX^{-/-}$ mice have a subtle DSB repair defect, are subject to increased genomic instability and male H2AX knockout mice are infertile; however, cell cycle checkpoints remain intact although they are impaired at low doses (Celeste et al., 2002). From these results it was concluded that H2AX is not required for the initial recognition of a DSB, but for the focal accumulation of repair proteins to the site of lesion (Celeste et al., 2002). In humans, the H2AX gene (H2AXFX), which maps to chromosome 11 at position 11q23, is a region frequently mutated or deleted in a large number of human cancers (Ghiassi-nejad et al., 2002). During DSB repair, phosphorylated H2AX (γH2AX) acts as a binding platform for the recruitment and retention of DSB signalling factors to the site of the lesion (as described in section 1.6). Damage induced phosphorylation of H2AX can spread over megabases of chromatin regions flanking the DSB. Local concentrations of γH2AX foci can be visualized at interphase cells by

immunofluorescence microscopy. γH2AX foci have been reported to be unevenly distributed throughout the nucleus and to form at the site of a DSB in a non-symmetrical fashion in both yeast (Cowell et al., 2007; Kim et al., 2007; Shroff et al., 2004) and mammals (Berkovich et al., 2007; Meier et al., 2007; Savic et al., 2009). γH2AX foci are excluded from nuclear regions enriched for heterochromatic markers HP1 and H3K9Me3 following IR in MCF7 cells (Cowell et al., 2007). However, the treatment of S phase cells with HU lead to efficient H2AX phosphorylation at both euchromatin and heterochromatin, suggesting that ongoing replication partially relieves the heterochromatic barrier (Cowell et al., 2007). In human fibroblast cells, using immunoFISH techniques, Falk et al (2008), reported γH2AX induction following IR to be under-represented in the silenced chromatin of chromosome 18, in comparison to the gene rich uncondensed chromatin of chromosome 19. Following analysis of confocal microscopy images, the higher sensitivity of these regions to DNA damage was also observed to be accompanied by more efficient repair. Similar findings have been observed in the budding yeast Saccharomyces cerevisae, using an HO-inducible DSB system. The Haber laboratory used chromatin immunoprecipitation (ChIP) analysis to examine the spreading of phosphorylated H2AX along chromatin. Upon induction of a single DSB they could detect approximately 50 kilo bases (kb) of phosphorylated H2AX at either side of the HO induced break site. However, when the HO inducible break was situated in the vicinity of the heterochromatic, silenced HML and HMR loci, γH2AX expansion was inhibited (Kim et al., 2007). In primary mouse fibroblasts a similar phenomenon was observed when cells were treated with the HDAC inhibitor trichostatin A (TSA), a drug which relaxes chromatin. Following relaxation, the total amount of H2AX phosphorylated at the site of a neocarzinostatin (NCS) induced DSB was found to increase (Kim et al., 2007). As well as these effects of HC, the impact of global chromatin relaxation has also been assessed in mouse embryonic stem cells expressing half the wild type complement of the linker histone H1 (Murga et al., 2007). Histone H1 depletion resulted in enhanced radioresistance and hyperactive checkpoint responses compared to WT or H1 complemented stem cells. γH2AX and Chk1 phosphorylation at Ser345 was also found to be hyperactive in H1 depleted cells. This result was recapitulated following treatment with TSA (Murga et al., 2007). Collectively these findings suggest that processing of DSBs at heterochromatin might differ from that at euchromatin and that chromatin structure has a significant impact on damage response signalling. In this chapter I sought to determine what impact reduced heterochromatin content would have on the expansion of IR induced γH2AX foci particularly at HC associated DSBs.

1.30.3 Model systems to analyze IR induced signalling in the context of reduced chromatin organization.

Although numerous properties of HC differ, the molecular components constituting HC formation are largely shared by all. Chemical modifications on chromatin such as acetylation, methylation, phosphorylation, ubiquitination and SUMOylation are important in the epigenetic control of gene transcription (see 1.17 for further discussion). DNA modifications carried out by enzymes such as DNA methyltransferase (DNMTs) modify chromatin by addition or removal of these modifications. Other proteins bind and integrate with nucleosomes to form a higher order chromatin superstructure which is silenced from transcription. Such examples include the KRuppel Associated Box (KRAB) Associated Protein 1 (KAP-1) and Methyl CpG binding Protein 2 (MeCP2). Similarly, Lamin A which is a structural component of the lamina membrane, co-ordinates chromosomal location and silencing mediated partly through histone deacetylases (HDACs) (Han et al., 2008). Loss of these modifying enzymes or heterochromatin scaffolding proteins results in reduced higher order chromatin organization. Cells deficient in these proteins are ideal candidates for analyzing the effect of chromatin superstructure on ATM dependent DSB induced signalling. Similarly, patient cell lines with mutations in these proteins offer a similar advantage.

1.30.3.1 KAP-1

The transcription co-repressor KAP-1 is a critical heterochromatin building factor. KAP-1 mediates DNA binding via association with a kruppel associated box (KRAB) domain. KRAB is a repression domain encoded by many transcription factors which contains a conserved amino terminal motif that contains multiple DNA binding Cys2-His2 zinc fingers (Bellefroid et al., 1991). The C-terminus of KAP-1 contains a PHD finger and bromodomain, which typically are known as methyl-lysine or acetyl-lysine binding domains, respectively. The PHD-bromodomain of KAP-1 acts to control site specific KAP-1 SUMOylation (Li et al., 2007; Zeng et al., 2008). KAP-1 SUMOylated residues serve as a recruitment platform for the nucleosome-remodelling and histone deacetylation (NuRD) chromatin remodelling complex (Ivanov et al., 2007). NuRD

mediates remodelling through the removal of acetyl residues via HDAC1/2. A second SUMOylated KAP-1 site interacts with SET domain, bifurcated 1 (SETDB1) histone methyltransferase via SUMO interacting motifs (Ivanov et al., 2007), and modifies chromatin via addition of methyl groups to histone tails (Figure 3.1)

1.30.3.2 DNMTs

Transcriptional silencing and HC formation can be mediated by the removal of methyl residues from histone tails. This is typically carried out by DNA methyltransferases (DNMTs). Human cells encode for 4 different DNMT's, which are DNMT1, DNMT2, DNMT3A and DNMT3B. DNMT3B is a maintenance methyltransferase and predominantly methylates hemimethylated CpG dinucleotides in the mammalian genome. DNMT2 has strong sequence similarity with methyltransferases of both prokaryotes and eukaryotes, and has been shown to target small transfer RNA (Goll et al., 2006). DNMT3A and DNMT3B can methylate hemimethylated and unmethylated DNA and are described as de novo methyltransferases (Goll and Bestor, 2005). DNMT3B deficient mice are embryonic lethal, whereas DNMT3A deficient mice develop and appear normal at birth, implying that despite the similarities in function, the specific targets of each of the DNMT's differs (Chen et al., 2003). DNMT3B knockout mice have marked demethylation or pericentric satellite repeats, which is a similar characteristic of Immunodeficiency Centromeric instability facial anomalies (ICF) syndrome patients (Hata et al., 2002).

1.30.3.3 ICF syndrome

ICF (Immunodeficiency Centromeric instability Facial anomalies) syndrome is an autosomal recessive syndrome characterized by severe immunodeficiency and instability at pericentric heterochromatin. Typical ICF patients have mutations in the de novo DNA methyltransferase 3B (DNMT3B) (Figure 3.2B). Loss of DNMT3B results in hypomethylation at constitutive heterochromatin, in particular at satellite regions on chromosomes 1, 9 and 16. Due to hypomethylation at these chromosomal locations gross chromosomal rearrangements, whole

arm deletions, chromosome breaks and multi-radial chromosome junctions can occur (Ehrlich, 2003).

1.30.3.4 MeCP2

Methylation at CpG dinucleotides is one of the most abundant epigenetic modifications in mammalian genomes and plays an essential part in the control of gene expression. CpG islands are GC-rich regions of DNA stretching for an average of ~1kb and are coincident with the promoters of ~60% of human RNA pol transcribed genes. However methylation at these regions promotes the binding of the methyl binding domain (MBD) protein MeCP2. MeCP2 is a 5-methyl cytosine binding protein that acts as a transcriptional repressor through recruitment of transcriptional co-repressors such as Sin3A and HDAC's (Figure 3.3). Four functional domains comprise MeCP2: a MBD which binds methyl residues, a transcriptional repressor domain (TRD) which is responsible for recruiting silencing factors such as HDACs, a NLS and a large C-terminal domain (Figure 3.3). MeCP2 is expressed in all tissues, with highest levels of expression in the brain, lung and spleen and lower in the heart and kidney (Shahbazian et al., 2002). The broad spectrum of HC accessory factors capable of interacting with MeCP2 means that MeCP2 contributes to a broad range of HC structures in the mammalian cell. For example HP1γ relocalization during myogenic differentiation correlates with the presence of MeCP2 (Agarwal et al., 2007). HP1γ and MeCP2 directly interact via the TRD of MeCP2, arguing that they co-operate in the formation of repressive sub-nuclear compartments involved in epigenetic silencing. MeCP2 also interacts with the inner membrane protein Lamin B receptor (LBR), and this interaction has been suggested to contribute to heterochromatin formation at the nuclear periphery.

1.30.3.5 Rett syndrome

Rett syndrome is an X-linked progressive neurological disorder (Rett, 1966) caused by mutations in the MECP2 gene. Affected individuals develop normally until 6-18 months of age, thereafter regression of acquired skills begins. Individuals loose speech, develop microcephaly,

mental retardation and stereotypical hand movements (typically continuous clasping of hands) (Moog et al., 2003). Rett syndrome is the most common neurological disorder to affect females, with a penetrance in Europe of 1:15,000 (Hagberg et al., 1985). Approximately 1% of the total reported cases of Rett syndrome are inherited; the vast majority of cases are sporadic (Schanen et al., 1997). Almost all MeCP2 mutations are de novo, except for cases were the mutation has been inherited from a healthy or mildly affected mother, which either had gonadal mosacism or favourable X chromosome inactivation (XCI). Around 60% of MeCP2 mutations are caused by a C>T transition at 8 CpG dinucleotides (R106, R133, R158, R168, R255, R270, R294 and R306), located in the third and fourth exon (Matijevic et al., 2009) (Figure 3.2A). Frequently, nonsense, frameshift and splicing mutations occur after the MBD which result in premature termination and a truncated protein product. Although deletions occur frequently, identical deletions are rare. (Shahbazian and Zoghbi, 2001), suggest that truncated proteins still bind methylated DNA but cannot interact with the Sin3A co-repressor.

1.30.3.6 HGPS

Hutchinson-Gilford progeria syndrome (HGPS) is the most severe of the premature aging progeriod syndromes. Affected individuals have a mean life span of 13 years. It is an extremely rare condition with only 150 documented cases of HGPS worldwide. Affected individuals develop normally at birth, but prematurely display characteristics associated with aging, such as alopecia, severe lipodystropy, scleroderma and varied skin hyper-pigmentation (Kudlow et al., 2007). HGPS in the majority of cases is caused by aberrant splicing of LMNA, a gene that encodes A-type nuclear lamins. A type lamins belong to a family of intermediate filament proteins that are the main components of the nuclear lamina (proteinacious meshwork that underlies the inner nuclear membrane). All A type lamins are encoded by a single LMNA locus through alternative splicing. The Lamin A protein is synthesized as a precursor protein called prelamin A (Rusinol and Sinensky, 2006) (Figure 3.4). The C-terminal of prelamin A undergoes farnesylation. Farnesylation is the addition of a 15-carbon isoprenoid farnesyl group to a four amino acid CAAX motif at the C-terminus of a protein. Farnesylated prelamin A undergoes two cleavage events, one of which removes the farnesyl. Hence, mature lamin A contains no farnesyl (Pendas et al., 2002). The most frequent HGPS associated mutation Gly608Gly, is a

silent base substitution that activates a cryptic spice donor in exon 11 of LMNA. The resulting mutant protein is called progerin. Progerin retains it's C-terminal, and lacks the recognition sequence for the second cleavage, and therefore remains farnesylated (Dahl et al., 2006). The mutant protein localizes to the nuclear periphery, and cells from HGPS patients typically have irregular nuclear morphology. HGPS patient cells also show relocalization or decreased expression of heterochromatin protein-1 (HP1) (Scaffidi and Misteli, 2005).

1.30.4 The crosstalk between ATM and ATR in G2/M checkpoint activation

Despite structural similarities and stimulation by similar genotoxic stresses the target specificities and development requirements between Chk1 and Chk2 kinases differ. Chk1 is essential for mammalian development and viability (Takai et al., 2000), whereas Chk2 deficient mice are viable, fertile and only show tumour susceptibility when exposed to carcinogens (Hirao et al., 2000; Takai et al., 2002). Chk1 deficient mice have early embryonic lethality, making studies in knockout mice difficult. However RNAi mediated knockdown of Chk1 in human cells has revealed an essential role for Chk1 in control of Cdc25A protein turnover, supporting a role for Chk1 in S and intra-S phase checkpoints (see 1.10.3 for a further discussion on the S phase checkpoint). A-T patients and ATM knockout mice are sensitive to IR induced DSBs and are defective in activating checkpoint arrest. However, damage responses to UV and replication associated damage, which activates ATR, are normal in A-T cells. ATR dependent signalling is triggered by a range of DNA damaging agents including IR, UV light, interstrand crosslinking agents such as cis-platin, and replication inhibitors such as hydroxyurea. All of these agents pose the potential to induced replication fork stalling. The strict model of ATM to Chk2 and ATR to Chk1 mediated signalling has been expanded by evidence of cross-talk between these kinases. An overlapping role for ATM in the activation of Chk1 in response to IR was established after Chk1 phosphorylation at Ser317, which occurs normally after replication associated DNA damage, was compromised in ATM defective cells (Gatei et al., 2003). RPA focus formation after IR in ATM and Nbs1 deficient cells is also severely impaired (Jazayeri et al., 2006). ATLD ($Mre11^{-/-}$) cells (which lack the nuclease component of the MRN complex) also have defective Chk1 phosphorylation after IR (Jazayeri et al., 2006). From this data it was proposed that after IR, ssDNA regions which are required for

ATR activation are generated via DNA end resection in a process that is regulated by ATM. ATM dependent Chk1 phosphorylation is inhibited by the CDK inhibitor roscovitine (Jazayeri et al., 2006). CDK phosphorylation regulates the activity of CtIP, a nuclease that has recently been established to regulate DSB repair pathway choice between HR and NHEJ (see 4.1.3 for further discussion). Furthermore ATM dependent CtIP phosphorylation at Ser664 and Ser745 regulates CtIP mediated resection. Therefore ATM has been proposed to promote resection via activation of CtIP. Thus Chk1 can contribute to G2/M checkpoint arrest via signalling from replication associated DNA damage in S phase (via ATR) or from resected DSBs in G2 (via ATM – ATR). Chk2 is activated at non-resected DSBs in G2 via ATM. Both Chk2 and Chk1 can contribute to G2/M checkpoint arrest (Figure 3.5).

1.30.5 Sensitivity of the G2/M checkpoint

Although ATM is sensitively activated by low numbers of DSBs (and likely by a single DSB), it is now evident that G2/M checkpoint arrest is less sensitive. It was first made apparent that the level of ATM activation does not directly correlate with the activation of Chk2 in 2004 when Buscemi et al reported that a phosphorylation dependent band shift of Chk2 was only observed after IR doses above 1 Gy, despite ATM phosphorylation being apparent after doses as little as 0.25 Gy IR (Bakkenist and Kastan, 2003; Buscemi et al., 2004). In accordance with this, the incorporation of radiolabelled isotopes during DNA synthesis was only inhibited after IR doses above 1 Gy (inducing roughly 19 DSBs). The authors concluded that the ATM dependent Chk2 pathway is only activated when ≥19 DSBs are present (Buscemi et al., 2004). This mechanism of checkpoint insensitivity was suggested to enable DSB repair to occur in the presence of less than ~ 19 DSBs without the activation of a Chk2 dependent checkpoint. The G2/M checkpoint can be activated by DSBs that are either generated in S phase and progress into G2 or DSBs induced directly in G2 phase. To study checkpoint induction and release following IR in G2, Deckbar et al (2006) irradiated cells 4 hours after pulse labelling with BrdU (a time at which cells were shown to progress into G2) and cell cycle progression was analysed by FACS. Checkpoint deficient cells, such as A-T, continuously progressed into mitosis. Wildtype cells initiated and sustained a checkpoint arrest for 4 hours after 1 Gy before progressing into mitosis. Checkpoint release in Artemis cells occurred later than compared to wildtype cells, which the authors concluded was likely reflective of their repair defect. To

evaluate whether DSB repair was completed upon G2/M checkpoint release, chromosome aberrations in mitotic cells were analysed in cells after checkpoint release. Unexpectedly the number of chromosome breaks in released wildtype and Artemis cells was similar despite the longer checkpoint arrest observed in Artemis cells. These results lead to the proposal of a threshold number of DSBs being required to initiate and sustain G2/M checkpoint arrest. Using premature chromosome condensation (PCC) analysis, wildtype and Artemis cells were both found to have 3-4 PCC breaks at the time of checkpoint release. Using PFGE, previous studies have established that 3-6 DSBs equate to 1 PCC break (Cornforth & Bedford, 1993). Given that 1 PCC break represents between 3-6 DSBs, the sensitivity of the G2/M checkpoint was proposed to be 10-25 DSBs (Deckbar et al., 2007). This was further supported by γH2AX foci analysis showing that ~20 DSBs remained after checkpoint release and that the duration of G2/M checkpoint maintenance extended with increasing dose. Therefore G2/M checkpoint arrest is only sustained when the damage level remains above the threshold and the number of DSBs remaining directly influences the duration of arrest. The identification of a G2/M checkpoint threshold helped to explain the exaggerated sensitivity of G2 phase cells to low doses IR (Marples et al., 2004). Low dose hypersensitivity describes a phenomenon by which cells die from excessive sensitivity to small doses of IR. From survival experiments it became apparent that the dose of IR required to change from low-dose hyper-radiosensitivity to an increased radioresistant response corresponded to the activation point of the G2/M checkpoint (Marples et al., 2004). Since a certain number of DSBs are required to generate enough signalling to initiate arrest, doses of IR which fail to introduce enough DSBs to reach the threshold and activate a checkpoint arrest pose a threat to genomic stability or cell survival. Since DSBs arise endogenously following metabolic processes and replication stress, which if repaired correctly have no effect on survival, having a DSB threshold prevents unnecessary activation of the checkpoint.

1.30.6 Aims of this chapter

The impact of HC on the DSB damage responses is important to evaluate, not least because the HC content can differ between tissues and cell types. Additionally, human syndromes with disordered heterochromatin structure have been reported. These syndromes include Rett Syndrome, which harbours mutations in MeCP2, a methyl CpG-binding protein, Immunodeficiency with Centromere instability and Facial anomalies (ICF), Syndrome which is mutated in the DNA methyl transferase, DNMT3B and Hutchinson

Gilford Progeria Syndrome (HGPS), which has mutations in Lamin A and displays progressive HC loss (Shumaker et al., 2006). Previous studies have shown that global chromatin compaction caused by histone H1 limits the strength of damage response signalling (Murga et al., 2007). Conversely, more recently transcription has been shown to restrict γH2AX expansion (Iacovoni et al., 2010). Interestingly, in addition to being inhibitory to DSB repair, studies have shown that HC also restricts the expansion of γH2AX, since they do not expand within chromocentres but rather on their periphery and HDAC inhibition leads to wider γH2AX foci (Cowell et al., 2007; Goodarzi et al., 2008; Kim et al., 2007). However, whether this impacts upon ATM signalling since foci can expand on the chromocentre periphery and whether ATM-dependent modifications overcome any barrier to signalling as they do for DSB repair has not been examined. Here, I investigate how HC influences damage response signalling focusing on the impact of disordered heterochromatin found in human patients.

1.31 Results

1.31.1 The speed and size of IR induced γH2AX foci at heterochromatin regions is enhanced following KAP-1 knockdown.

Previous publications have established that the heterochromatic building factor KAP-1 is phosphorylated by ATM at Ser824 in response to DSB induction (Ziv et al., 2006). This phosphorylation event alters KAP-1 association with nuclease resistant chromatin and has been proposed to induce nucleasomal remodelling to facilitate repair at otherwise inaccessible DSBs (Goodarzi et al., 2008; Ziv et al., 2006). As discussed in detail previously (see section 3.1.2), γH2AX signalling has been demonstrated to be DNA sequence independent (Kim et al., 2007), but in contrast, global chromatin compaction influences γH2AX foci formation (Kim et al., 2007; Murga et al., 2007). In consideration of this data, I sought to determine whether KAP-1 enriched chromatin impacts upon IR-induced γH2AX foci expansion at the site of heterochromatin DSBs (HC-DSBs) as it does for DSB repair (Goodarzi et al., 2008). To analyze IR-induced signalling at HC regions, I utilized murine NIH3T3 cells, which have chromocentres that correspond to pericentric and centromeric HC that can be readily identified as densely

staining DAPI regions (Goodarzi et al., 2008; Guenatri et al., 2004). I initially verified that the DAPI dense regions were enriched for the heterochromatic marker Histone H3 trimethylated at lys9 (H3K9me3) (Figure 3.6). NIH3T3 cells were treated with or without KAP-1 siRNA for 48 hours, followed by irradiation with 3 Gy IR. 30 minutes post IR, cells were fixed and immunostained. It was important to select for G0/G1 phase cells only, because in G2 phase, DAPI regions become more diffuse and stain positively for KAP-1, as well as for both HC and EC markers, (H3K9me3 and H3K9Ac respectively) (Goodarzi et al., 2010). To select for G0/G1 phase cells, cells were stained for pSer10 histone H3, a mitotic marker which also allows identification of G2 phase cells within an asynchronous population. G1 phase cells are selected by negative or weak pSer10 histone H3 staining. γH2AX and chromocentre overlap was quantified in G1 cells following KAP-1 knockdown using high resolution deconvolved z stacked images (Figure 3.7). I observed more than a 3-fold increase in γH2AX foci expansion at DAPI dense regions compared to control siRNA transfected cells. In order to analyze the volume of interior γH2AX signal expansion at the chromocentres, 3D models of representative high resolution deconvolved z stacked images were generated. The volume of interior γH2AX signal at the HC periphery was quantified using Hygens co-localization software (Figure 3.8, MeCP2 will be discussed in 3.2.2). By this method, the volume of γH2AX expansion into heterochromatin was also found to be at least 3 fold greater following KAP-1 knockdown. From these results I concluded that KAP-1 enriched heterochromatin acts as a barrier to IR induced γH2AX foci expansion. Having established that KAP-1 enriched chromatin impacts on the size of IR induced γH2AX foci expansion at the site of a HC-DSB, I next sought to determine whether KAP-1 knockdown affects the intensity of γH2AX foci following IR at both euchromatin and heterochromatin DSBs. NIH3T3 cells were treated with control and KAP-1 siRNA using the conditions described above. 30 minutes post 3 Gy IR cells were fixed and immunostained for γH2AX, pSer10 histone H3 and DAPI. γH2AX and DAPI signal intensity was analyzed using ImageJ software (Figure 3.9). For control siRNA treated cells, 20% of DSBs induced after 3 Gy IR were found to locate at heterochromatic regions and the median γH2AX signal intensity was 50 a.u.. For KAP-1 knockdown cells, there was an increase in the number of DSBs located or overlapping with regions of heterochromatin. The γH2AX signal intensity for these breaks also increased with a median signal intensity of ~60 a.u.. Representative images used for analysis are shown in figure 3.9A. Importantly, the same number of DSBs were induced under each siRNA condition. Therefore differences in γH2AX signal intensity between control and KAP-1 siRNA treatment could not be accounted for by a difference in DSB induction. Considering that γH2AX foci expansion at HC regions increased following KAP-1 knockdown, I next analyzed what effect reduced chromatin organization had on the kinetics of DDR protein recruitment to

the site of a DSB. NIH3T3 cells were treated with control or KAP-1 siRNA for 48 hours. At indicated time-points post 1 Gy IR cells were fixed and immunostained for γH2AX, pSer10 histone H3 and DAPI. The number of γH2AX foci overlapping/juxtaposing or non-overlapping with chromocentres were scored as HC and EC, respectively. As expected the formation of HC associated DSBs was slower than EC associated DSBs. Consistent with the notion that heterochromatin acts as a barrier to repair, the rate of γH2AX foci formation at heterochromatin was faster following KAP-1 knockdown (Figure 3.10). Collectively, these results demonstrate that depletion of the HC factor KAP-1, enhances the speed and signal expansion of γH2AX foci at HC regions.

1.31.2 MeCP2 and DNMT3B knockdown cells show increased signal expansion and faster γH2AX foci formation in NIH 3T3 cells.

DNA methylation is an important epigenetic modification. In particular methylation events on CpG islands regulate gene silencing through chromatin compaction. An important methyltransferase involved in DNA methylation is DNMT3B. DNMT3B is a de novo methyltransferase that is important for embryonic development, imprinting, heterochromatin formation and female inactivate X chromosome silencing (see 3.1.3.2 for further discussion on DNMT3B). MeCP2 is a methyl CpG binding protein which binds methylated promoter regions and is associated with transcriptional silencing (see 3.1.3.4 for further discussion on MeCP2). To consider whether loss of methylation dependent chromatin compaction affects signal expansion, NIH3T3 cells were treated with either DNMT3B or MeCP2 siRNA, irradiated with 3 Gy IR and examined as described previously. Regions of γH2AX and chromocentre overlap were determined using high resolution deconvolved z stacked images (Figure 3.12, 3.13). First I established whether loss of MeCP2 or DNMt3B affected the size or number of chromocentres per cell (KAP-1 knockdown was also included in this analysis) (Figure 3.11). In knockdown cells a small reduction in the number of chromocentres was observed. The size of chromocentres only significantly changed in MeCP2 knockdown cells. To account for these changes, γH2AX and DAPI overlap was calculated per chromocentre rather than per cell. Image analysis of γH2AX and DAPI overlap per chromocentre revealed almost a 3 fold increase in γH2AX foci expansion following DNMT3B or MeCP2 siRNA (Figure 3.12, 3.13). Additionally, three

dimensional image analysis revealed a greater volume of overlap between γH2AX and HC with DNMT3B or MeCP2 knockdown compared to control cells (Figure 3.8). Similar to the results obtained in KAP-1 knockdown cells, DNMT3B and MeCP2 knockdown also enhanced the rate of γH2AX foci formation at HC regions (Figure 3.14). I subsequently analyzed whether γH2AX foci signal intensity increased following MeCP2 and DNMT3B knockdown. NIH 3T3 cells were treated as described previously. MeCP2 and DNMT3B siRNA caused a statistically significant increase in γH2AX signal intensity with the effect being greater on the foci associated with higher density DAPI regions (Figure 3.15). In somewhat distinction to the findings following KAP-1 loss, the impact, particularly following MeCP2 siRNA, was also upon regions of intermediate DAPI density possibly due to the role of methylation as a transcriptional repressor at CGIs at both constitutive and facultative HC. In contrast, KAP-1 is primarily enriched within constitutive HC and conferred a more specific enrichment at heterochromatin. Here I have demonstrated that reduced heterochromatin organization induced by MeCP2 or DNMT3B knockdown enhances the size of IR induced γH2AX expansion at regions of heterochromatin. Furthermore, knockdown of these heterochromatin associated factors also enhances the signal intensity of γH2AX in response to IR. Therefore MeCP2 and DNMT3B dependent chromatin organization also creates a barrier to IR induced γH2AX expansion at heterochromatin regions.

1.31.3 IR induced ATM signalling is hyperactivated in Rett syndrome patient cells and MeCP2 knockdown cells

γH2AX acts as a docking site for the recruitment of several different DNA repair factors, one of which is the ATM binding protein complex, MRN . MRN mediated binding of ATM tethers ATM at the site of the break and aids to maintain ATM in an active state (Chapman and Jackson, 2008). ATM is also the main PIKK responsible for γH2AX phosphorylation in response to IR (Stiff et al., 2004). Therefore, in the context of reduced higher order chromatin structure, where the γH2AX response is enhanced, ATM activation would also be expected to be enhanced. Following my observation of enhanced γH2AX foci expansion and signal intensity in KAP-1, DNMT3B and MeCP2 knockdown cells, I next examined ATM activation in these cellular contexts. First I analyzed cells derived from Rett syndrome patents, which have mutations in

MeCP2. MeCP2 is a protein involved in transcriptional regulation and loss of this protein could potentially result in the up regulation of proteins involved in the DDR. Therefore, first I confirmed that Rett cell lines have normal levels of damage response protein expression and ATM dependent phosphorylation without DNA damage. For this and subsequent analysis I used three different Rett syndrome cell lines. This was to confirm that any differences observed between the Rett syndrome and wild type cells was a true phenotype observed with MeCP2 loss and not another patient specific mutation. Cycling populations of 48BR (WT) and Rett syndrome patient (GM16548, GM11272, GM11272) primary fibroblast cells were harvested for whole cell protein extraction (as described in materials and methods). Extracts were resolved on an SDS denaturing PAGE gel and membranes were immunoblotted with indicated antibodies. The Rett syndrome cell lines analyzed had normal levels of damage response protein expression for the selected proteins analyzed (Figure 3.16A). To analyze IR induced ATM activation, cycling 48BR and Rett syndrome patient (GM16548, GM11272, GM11272) cells were irradiated with either 0 or 0.5 Gy IR and harvested for whole cell extracts 30 minutes later. 60 μg of each protein sample was resolved on an SDS denaturing PAGE gel and immunoblotted with the indicated antibodies. Low dose IR was used because at higher doses, such as 3 Gy IR, the DDR signalling responses appears saturated by western blotting analysis and any difference between WT and Rett syndrome cells might not be detectable. Strikingly, ATM activation as monitored by Ser1981 phosphorylation (pSer1981 ATM), was 2-3 fold greater in the Rett cells compared to 48BR primary cells following 0.5 Gy IR (Figure 3.17). However the pSer1981 ATM signal obtained varied between each Rett syndrome cell line. ATM is activated at DSBs in G1 and G2 phase cells and replication dependent DSBs in S phase. Since G2 phase cells contain double the amount of DNA compared to G1 phase cells, the magnitude of ATM activation could differ. Further S phase cells activate ATM at IR induced DSBs as well as replication associated DSBs. Therefore differences in cell cycle distribution could impact upon the magnitude of ATM signalling. To confirm that the increased ATM activity observed in the Rett syndrome cells was a consequence of enhanced DDR signalling generated per DSB and not a consequence of a different cell cycle kinetics compared to control cells, cell cycle profiles were established for each cell line using FACS. For cell cycle profile analysis, cycling and contact inhibited G1 arrested 48BR and Rett syndrome (GM16548, GM11271, GM11272) primary fibroblast cells were prepared for FACS analysis (as described in materials and methods). The percentage of cells arrested at G1 was similar between WT and Rett syndrome (GM11271 & GM11272) primary fibroblast cells (Figure 3.16B). Analysis of cycling cell populations revealed that the S phase cell population of Rett syndrome (GM11271 & GM11272) primary fibroblast cells was roughly double that observed in 48BR cells. However,

the S phase population contributed a relatively small fraction (<9%) of the total cell population. The S phase cell population in cycling Rett syndrome (GM16548) primary fibroblast cells however was almost four times greater than WT cells (Figure 3.16B). In consideration of cell cycle profile analysis I selected Rett syndrome (GM11271 & GM11272) primary fibroblast cell lines for subsequent western blotting analysis. However, since Rett syndrome (GM16548) primary fibroblast cells was found to have the greatest S phase population but the weakest ATM pS1981 activation, variation in pS1981 ATM activation could not be accounted for simply by differences in cell cycle distribution. Therefore, the hyperactivity in pS1981 ATM activation observed in the Rett syndrome cell lines compared to WT cells was unlikely to be a consequence of replication dependent repair. I next examined ATM activation in G1 arrested 48BR and Rett syndrome (GM11271) primary fibroblast cells. 48BR and Rett syndrome (GM11271) fibroblast cells were grown in dishes for more than 10 days until completely confluent. Cells were irradiated with either 0, 0.5 or 3 Gy IR and harvested at indicated time points post IR. Whole cell protein extracts were prepared and immunoblotted for the indicated antibodies. Consistent with the results observed in the cycling cell populations, G1 arrested populations also showed enhanced pS1981 ATM and pThr68 Chk2 activation after 0.5 and 3 Gy IR (Figure 3.17B). However, the increase in ATM activity in G1 arrested cell populations was not as dramatic as that observed in cycling cell populations. To further substantiate my findings from western blot analysis, I next analysed pS1981 ATM activation by IF since this allows G1 and G2 phase cells to be identified within an asynchronous population using the cell cycle marker, CENP-F. pS1981 ATM antibody specificity was confirmed previously in Noon et al, 2010. 48BR and Rett syndrome (GM11272) primary fibroblast cells were irradiated with 0, 0.5 or 3 Gy IR. 30 minutes post IR, cells were fixed and immunostained for pS1981 ATM, CENP-F and DAPI. Pan nuclear pS1981 ATM signal intensity in G1 (CENP-F negative) or G2 (CENP-F positive) cells was analyzed using ImageJ software. Consistent with the results obtained by Western Blotting, IR induced pan nuclear pSer1981 ATM signal intensity showed >2 fold increase in the Rett patient cells compared to control cells in G1 phase (Figure 3.18). In G2 phase there was only a modest increase in pSer1981 signalling between WT and Rett syndrome cells (Figure 3.18). I next analyzed whether MeCP2 knockdown in 48BR primary cells would result in an enhanced ATM signalling response. 48BR primary cells were treated with either control or MeCP2 siRNA for 48 hours. Cells were irradiated with 0, 0.5 or 3 Gy IR. 30 minutes post IR cells were fixed and immunostained for pS1981 ATM, CENP-F and DAPI. Pan nuclear pS1981 ATM signal intensity in G1 and G2 phase cells was analyzed using ImageJ software. Strikingly, following MeCP2 knockdown, pS1981 ATM signal intensity in G1 and G2 phase was enhanced more than 2 fold following 0.5 and 3 Gy IR (Figure 3.19). This data

suggests that the disordered chromatin present in Rett syndrome leads to enhanced ATM activation after IR.

1.31.4 ATM activation is hyperactive in ICF syndrome patient cells

To further analyze the effect of reduced higher order chromatin structure on DDR signalling, I next analyzed pSer1981 ATM in Immunodeficiency Centromeric instability and Facial anomalies (ICF) syndrome cells. ICF syndrome is caused by mutations in DNMT3B and since previously I observed greater signal expansion following DNMT3B knockdown, ICF syndrome cells are ideal candidates to analyze ATM signalling in the context of reduced chromatin organization. Contact inhibited G1 arrested 1BR and ICF hTERT fibroblast cells were irradiated with either 0 or 0.5 Gy IR. 30 minutes post IR, whole cell extracts were prepared and immunostained with the indicated antibodies. Conversely, ICF syndrome patient cells have been reported to have high levels of endogenous ATM activation even in the absence of DNA damage (Goldstine et al., 2006). Indeed, when the ICF syndrome hTERT immortalized fibroblasts western blots were overexposed, the 0 hour pS1981 ATM signal was as pronounced as that observed in the 1BR hTERT fibroblast cells after 0.5 Gy IR (Figure 3.20). Despite this, IR induced pS1981 ATM activation was also observed to be hyperactive in the ICF hTERT fibroblast cells compared to control cells (Figure 3.20). Taken together, these results demonstrate that greater signal expansion in cell lines with disordered or reduced chromatin formation, leads to an increase in ATM signalling which is greater than control cells.

1.31.5 Rett syndrome patient cells and MeCP2 knockdown cells exhibit a hyperactive IR induced G/M checkpoint arrest

The presence of hyperactive ATM activation in the context of reduced chromatin organization, led me to evaluate what impact this had on checkpoint initiation. It has previously been

reported that G2/M checkpoint arrest is not activated following exposure to low doses of IR (Krempler et al., 2007). Here an IR dose above 0.5 Gy IR (inducing roughly 15-20 DSBs in G2) was required to initiate and sustain checkpoint arrest. Since it is known that ATM and ATR activate Chk2 and Chk1 respectively, to initiate G2/M checkpoint arrest, if ATM dependent DSB induced signalling is enhanced in the context of reduced heterochromatin, it would be anticipated that the G2/M checkpoint arrest would be initiated at lower IR doses in chromatin defective cells compared to wild type cells. To analyze the sensitivity of G2/M checkpoint arrest Rett syndrome cell lines (GM16548, GM11271, & GM11272) were irradiated with the indicated low IR doses. One hour following IR cells were fixed and stained for the mitotic marker pSer10-histone H3, which is a distinctive marker for highly condensed metaphase chromosomes (Hans and Dimitrov, 2001). Strikingly, G2/M checkpoint initiation was observed at doses as low as 0.125 Gy IR in the Rett syndrome cell lines, where only 30% of the mitotic population (as identified by pSer10-histone H3) were in mitosis, compared to 80% in the control cells (Figure 3.21A). This dramatic difference in the percentage of cells entering mitosis between the Rett and WT populations was observed until 1 Gy IR. This is likely because 1 Gy IR, which induces roughly 40 DSBs in G2, generates a DDR signal sufficient to activate checkpoint arrest. To confirm that this dramatic difference in G2/M checkpoint sensitivity was not a phenotype only observed when comparing the Rett syndrome cell lines to 48BR primary cells, another primary fibroblast was analyzed in conjunction with the Rett syndrome cell lines. Here, 1BR primary fibroblast and Rett syndrome cell lines (GM16548, GM11271, & GM11272) were treated and harvested as before. Consistent with the result observed when analysing 48BR primary cells, 1BR primary cells were also less sensitive to low doses IR in comparison to the Rett syndrome cell lines (Figure 3.21A). MeCP2 knockdown in the Rett syndrome cell lines did not show an additive affect (Figure 3.21B). Since NIH3T3 cells were previously exploited to visualize γH2AX foci expansion at heterochromatic regions in the context of reduced chromatin organization, I next analyzed whether MeCP2 knockdown in these cells affected G2/M checkpoint sensitivity. NIH3T3 mouse cells were transfected with MeCP2 siRNA for 48 hours and irradiated with the indicated doses of IR. One hour post IR, cells were fixed and stained for pSer10-histone H3. Similar to Rett syndrome patient cells, MeCP2 siRNA transfected cells also initiated G2/M arrest at IR doses as low as 0.125 Gy (Figure 3.22A). Collectively, reduced MeCP2 levels results in a hypersensitive G2/M checkpoint arrest.

1.31.6 ICF syndrome cells and DNMT3B knockdown cells exhibit a hyperactive IR induced G2/M checkpoint arrest

G2/M checkpoint initiation was next analyzed in ICF syndrome cells. Because of the slow growing nature of ICF fibroblast cell lines, G2/M checkpoint initiation was analyzed using a lymphoblastiod cell line derived from ICF syndrome patient (GM08714). ICF syndrome LBLs were irradiated with the indicated IR doses and 1 hour later harvested by cytospinning. Cells were fixed and stained for pSer10-histone H3. Again, the sensitivity of the G/M checkpoint was monitored by the presence of cells in mitosis as identified by pSer10-histone H3. Similar to my previous observation using MeCP2 deficient cells, ICF patient cells also exhibited a hypersensitive G2/M checkpoint compared to WT cells (Figure 3.23). After IR with 0.125 Gy, the ICF mitotic index was reduced to 40% of that of untreated cells, whereas the mitotic index of wildtype cells remained at 98% of that of untreated cells (Figure 3.23A). Similar analysis of an hTERT immortalized ICF syndrome fibroblast also revealed a hypersensitive checkpoint arrest (Figure 3.23B). ICF (PT3) hTERT cells were grown on cover-slips for 48 hours, irradiated with the indicated doses of IR and one hour later fixed and stained for pSer10-histone H3 (Figure 3.23B). G2/M sensitivity was monitored by the percentage of cells in mitosis as identified by pSer10-histone H3. Consistent with the observation made with ICF syndrome patient GM08714, ICF syndrome hTERT line PT3 also initiated G2/M arrest at lower doses IR compared to WT cells. DNMT3B siRNA transfection in NIH3T3 cells gave a similar result (Figure 3.22B). Despite having less than the required number of DSBs necessary to satisfy arrest in wildtype cells, Rett and ICF syndrome cells and MeCP2 and DNMT3B knockdown cells are able to initiate G2/M arrest at low doses IR. This could suggest that chromatin defective cells lines generate more DDR signalling per DSB compared to WT cells, suggesting that the barrier imposed by heterochromatin to repair also impacts on the strength of the DDR signalling response. To further investigate ATM signalling in the context of reduced heterochromatin, G2/M checkpoint initiation was analyzed in a further syndrome with disordered chromatin organization. HGPS cells have mutations in the LMNA gene which encodes an intermediate filament protein that provides a scaffold for protein complexes regulating nuclear structure and function (see 3.1.3.6 for further discussion on HGPS). HGPS cells were irradiated with the indicated dose of IR. One hour following IR, cells were fixed and immunostained for the mitotic marker, pSer10 H3 (Figure 3.23C). As observed with Rett syndrome and ICF syndrome patient

cells, HGPS cells also responded hyperactively to low doses IR and initiated a G2/M checkpoint at IR doses as low as 0.25 Gy IR.

1.32 Discussion

1.32.1 Heterochromatin acts as a barrier to IR induced γH2AX signal expansion

The possibility of higher order chromatin structure acting as a barrier to γH2AX expansion was first reported by Kim et al (2007) in yeast. The authors showed that γH2AX expansion was inhibited at an HO induced DSB at the silenced HML and HMR loci. Treatment of human cancer cells with the HDAC inhibitor, TSA, demonstrated that IR induced γH2AX foci can increase in size (Kim et al., 2007). Previous studies have demonstrated that depletion of the linker histone H1 in murine ES cells increases γH2AX and 53BP1 signal intensity per nucleus following IR (Murga et al., 2007). Furthermore, the signal intensity per γH2AX foci is enhanced in H1 depleted cells compared to control (Murga et al., 2007). The reverse side of the coin, also provides examples, where the loss or inhibition of chromatin remodelling complexes reduces the magnitude of the IR induced DDR signalling cascade. For example, SWI/SNF depleted cells have reduced IR induced signalling and fail to initiate a G2/M checkpoint response following lower doses IR (Park et al., 2006). Loss of the chromatin remodeller SWI/SNF reduces the size of γH2AX foci (Park et al., 2006). Therefore reduced chromatin remodelling at the site of the DSB also inhibits γH2AX expansion. Here I have demonstrated that heterochromatic relaxation mediated by KAP-1, MeCP2 or DNMT3B knockdown enables IR induced γH2AX foci to expand at least three times more at heterochromatic regions compared to control cells. Like that observed in H1 depleted ES cells, γH2AX signal intensity per foci are also enhanced following KAP-1, MeCP2 or DNMT3B knockdown. In addition, the kinetics of γH2AX foci formation at heterochromatin occurs faster following KAP-1, MeCP2 or DNMT3B knockdown. The impact of KAP-1 siRNA was predominantly observed at DSBs with the highest DAPI-density consistent with KAP-1 being predominantly localised at highly compacted HC; the impact for MeCP2 was broader, possibly reflecting the presence of methylated CpGs in a wider range of compacted regions (although predominantly in HC-DNA). It is possible that higher order chromatin

structure may appear refractory to γH2AX expansion if the H2AX histone variant was of low abundance in heterochromatin. This would mean a heterochromatin associated DSB would not generate sufficient focal phospho-H2AX to generate a detectable γH2AX foci by immunofluorescence. However exposure of S phase cells, where heterochromatin structure is less condensed to enable replication, to HU, leads to abundant γH2AX foci at both euchromatin and heterochromatin (Cowell et al., 2007). From these experiments I postulate that KAP-1, MeCP2 and DNMT3B enriched higher order chromatin acts as a restrictive barrier to the expansion of IR induced γH2AX. Also, KAP-1, MeCP2 and DNMT3B enriched chromatin impedes the rate of DDR factor recruitment to the site of a lesion. Here one could envision that sufficient relaxation at the site of a DSB must first be initiated to expose local H2AX C-terminal tails, which, following phosphorylation by ATM, can bind MRN/MDC1. MRN then recruits and tethers ATM at the site of a break. This process stimulates an ATM auto-activation loop, whereby ATM is tethered at the break site to phosphorylate more H2AX and downstream DDR proteins. Hence if the chromatin structure around a DSB is already relaxed or partially relaxed, this above mentioned activation loop could happen more rapidly. Interestingly, despite observing an increase in γH2AX signal intensity for DSBs induced in both EC and HC, the most dramatic effect was observed at HC associated DSBs. This could possibly be explained by recent publications which describe transcriptionally active regions as being refractory to γH2AX expansion. Iacovoni et al, 2010, reported that following γH2AX profiling analysis by ChIP, RNA polymerase and γH2AX never overlap. Similarly, RNA polymerase has been described to function in chromosome decondensation immediately after transcription (Shanbhag et al., 2010).

Analysis of pS1981 ATM activation in Rett syndrome cells by western blot and IF, revealed that ATM activation is increased at least two fold in the Rett syndrome cells compared to control cells. Despite all three Rett syndrome patient cells analyzed displaying enhanced ATM activation compared to control cells in response to IR, the magnitude of ATM activation varied. Since the MeCP2 gene is located on the X chromosome, skewed X chromosome inactivation may account for differences in MeCP2 expression between the Rett syndrome patients. Alternatively the location of the patients MeCP2 gene mutation may affect residual function. For example, a mutation in the transcriptional repressor domain (TRD) of the MeCP2 gene may enable the MeCP2 gene product to still functionally bind di-methylated CpG islands but not recruit co-repressors such as Sin3A or HDACs (Yusufzai and Wolffe, 2000). Whereas, a mutation in the methyl binding domain of the MeCP2 gene may prevent it from binding methylated DNA altogether. In this scenario a redundant DNA methyl binding protein

could possibly bind and functionally replace MeCP2. In this circumstance the impact of ATM signalling would be expected to be less dramatic since the chromatin architecture would be in a conformation resembling that which would contain a functional MeCP2 protein. Kudo et al, demonstrated that when mutants in the MeCP2 methyl binding domain (MBD) were transfected into cells, the mutant MeCP2 protein was unable to localize to heterochromatin and repress a reporter (Kudo et al., 2001). However, in the case where MeCP2 can bind CpG islands but not recruit silencing factors, the MBD would be blocked to other redundant factors, and the higher order silencing normally initiated by a functional MeCP2 would not result, hence a more open chromatin conformation would remain. Alternatively the promoter regions controlling MeCP2 expression may be less active or the MeCP2 transcript may be less stable. For example, deletions within the C-terminus of MeCP2, which are common mutations in classic RTT, significantly decrease protein stability (Yusufzai and Wolffe, 2000). In addition, MeCP2 mutants have been shown to offer varying levels of protection from MNase digestion depending on the type of mutation (Nikitina et al., 2007).

1.32.2 The impact of higher order chromatin structure on checkpoint response signalling

In all mammalian cells DSBs produce a damage response signalling cascade irrespective of their genomic or chromatic location that may be sufficient to initiate a checkpoint response. The effect that chromatin compaction exerts on damage response signalling is an emerging field. Previously Murga et al (2007) reported hyperactive checkpoint response after low doses IR in ES cells with reduced linker histone H1 levels. Linker histone loss will affect both EC and HC. Here, I have focussed on the effect of HC superstructure on DDR signalling. A number of lines of evidence presented here would imply that higher order chromatin structure does indeed dampen the IR induced DDR. I have shown that pS1981 ATM activation is hyperactive in G0/G1 and cycling cell populations of MeCP2 deficient Rett syndrome cells. In addition ICF (DNMT3B) syndrome cells display hyperactive ATM activation following low doses IR. γH2AX acts as a scaffold to recruit MDC1, MRN and 53BP1, which together serve to retain ATM at the DSB. Thus, it might be anticipated that foci size correlates with the magnitude of the downstream response. Yet, cells lacking γH2AX show efficient DDR signalling and checkpoint arrest except after low IR doses (Fernandez-Capetillo et al., 2002). I next analysed what impact enhanced

signalling has on checkpoint arrest in chromatin deficient cells. G2/M checkpoint sensitivity has been demonstrated to require at least 20 DSBs to initiate arrest (Deckbar et al., 2007). Therefore at low doses IR which produces less than 20 DSBs, G2/M checkpoint arrest would not be expected. Strikingly Rett syndrome, ICF syndrome, and HGPS cell lines exhibited a hypersensitive G2/M checkpoint arrest following low doses IR. The dramatic sensitivity of the G2/M checkpoint observed was unexpected as roughly only 25% of the genome is organised into heterochromatin (Goodarzi et al., 2008). Therefore after an IR dose of 0.25 Gy which induces ≤ 10 DSBs in G2, only ~ 3 of these DSBs would be expected to reside within heterochromatin. Therefore only 3 DSBs would be expected to contribute to the dramatic sensitivity observed. This might be possible if heterochromatin associated γH2AX foci were able to expand without any chromatin associated barriers. Since Rett and ICF syndrome cells still stain positively for heterochromatin associated markers such as TriMeK9 H3, it appears that heterochromatin structure is not completely abolished in these cells. It is more likely that other genomic regions such as facultative heterochromatin are also disorganized in Rett and ICF syndrome cells. Therefore a larger fraction of DSBs, not solely constitutive heterochromatin associated DSBs, are likely to contribute to IR induced G2/M checkpoint signalling. However I cannot fully exclude the possibility that KAP-1, MeCP2 or DNMT3B may contribute to γH2AX or ATM dependent signalling by regulating the expression of an as yet unidentified DSB repair protein.

Analysis of ATM activation in G1 phase ICF syndrome cells revealed that pSer1981 ATM activation is hyperactive in these cells compared to WT cells after IR. However, ATM activation at 0 hours in the absence of IR in the ICF syndrome cells was as pronounced as that observed in wildtype cells after 0.5 Gy IR. Endogenous ATM activation in ICF syndrome cells has previously been reported by Goldstine et al (2006). Downstream ATM targets, such as p53, NBS1 and SMC1 were not phosphorylated in ICF syndrome cells despite ATM activation (Goldstine et al., 2006). Endogenous ATM activation could not be accounted for by inefficient repair given that ICF syndrome cells subjected to IR produce normal numbers of γH2AX and repair with wildtype kinetics. ATM activation has also been reported in the absence of DSBs following treatments that induce chromatin defects, such as chloroquine treatment (Bakkenist and Kastan, 2003; Kitagawa et al., 2004). However, most chromatin disordered cells do not display endogenous ATM activation. ATM displays little phosphorylation on pS1981 in Rubinstein-Taybi syndrome (RSTS) patients, Facioscapulohumeral muscular dystrophy (FSHD) patients (Goldstine et al., 2006) and importantly Rett syndrome patient cells in the absence of DNA damage. RSTS is caused by de novo mutations in the CREB binding gene, CBP (Bartsch et

al., 2005). CBP regulates the expression of the histone methyltransferase Suv39H1/2 which is responsible for hypermethylating histone H3 at lysine 9 (TrimeK9 H3)(Lee et al., 2008). TriMeK9 H3 promotes chromosome condensation and induces gene silencing (Lee et al., 2008). FSHD is caused by mutations at the sub-telomeric region of chromosome 4 (Wijmenga et al., 1990). The disease is caused by molecular rearrangements that cause copy number variations of a 3.3 Kb tandem repeated microsatellite called D4Z4 (Wijmenga et al., 1992). D4Z4 units are normally heavily methylated, however FSHD patients have been shown to harbour euchromatin associated modifications, such as H3K4 diMe, at these units (Jiang et al., 2003; Zeng et al., 2009). TriMeK9 H3 modifications are also reduced in FSHD patients making chromatin organization in these cells less organized (Zeng et al., 2009). DNMT3B is responsible for maintaining large pericentric heterochromatin regions on chromosome 1, 9 and 16; therefore it is possible that large genomic disorganization is sufficient to active ATM surveillance mechanisms. Alternatively, endogenous ATM activation may be a consequence of chromosomal DNA instabilities reported for ICF syndrome cells which frequently arise after spindle mis-regulation at the disordered centromeric chromatin (Tuck-Muller et al., 2000).

The data presented here strongly suggests that higher order chromatin structure dampens the IR induced signalling at each heterochromatic associated DSB. Interestingly, Bao *et al*, reported that CD133 glioma stem cells activate a robust DNA damage response (Bao et al., 2006). Stem cells are an undifferentiated cell type characterized by their potential to self-renew indefinitely and to differentiate into any cell type. Abundant histone modifications typically found in stem cells are those which are associated with transcriptional activity such as H3 and H4 hyperacetylation as well as global hypermethylation H3-K9 (Kimura et al., 2004). Repressive heterochromatic marks such as H3-triMeK9, H3-MeK27, H3diMeK20 and H4-triMeK20 are greatly reduced in stem cells (Martens et al., 2005). The chromatin disordered cell line analyzed here, which have reduced higher order chromatin structure, are characteristically more stem cell like. This is potentially interesting when considering whether altered chromatin compaction could be exploited in the treatment of cancer cells to enhance their radiosensitivity to IR. Indeed, chromatin altering cancer therapeutics such as HDAC inhibitors, are at present in clinical use and trials. The most potent HDAC inhibitors are the hydroxamic acid derivatives, like SAHA, which have recently been approved for the therapy of T-cell lymphomas (Santini et al., 2007). Other classes of HDAC inhibitors include short chain fatty acids (SCFA) such as valproic acid, benzamides, epoxyketones and non-epoxyketone containing cyclic tetrapeptides, all of which function to increase the sensitivity of cells to IR

(Santini et al., 2007). MeCP2 and DNMT3B open an avenue for other drug developments which target these chromatin architecture proteins.

Chapter 4: Analysis of G2/M checkpoint maintenance and DSB repair in cell lines derived from patients with disordered chromatin

Analysis of G2/M checkpoint maintenance and DSB repair in cell lines derived from patients with disordered chromatin.

1.33 Introduction

1.33.1 Fast and slow repair component of DSB repair

The two major pathways of DSB repair are homologous recombination (HR) and Non homologous end joining (NHEJ). HR leads to accurate repair of the DSB by using a sister chromosome as a homologous template to re-replicate faithfully the damaged bases which require replacement. NHEJ is considered less accurate. Here the broken end is modified and ligated with no regard of homology. As a result insertions and deletions can be generated (Leiber, 2008). Given the different mechanisms underlying NHEJ and HR, it would seem plausible that the kinetics of repair would differ between the two mechanisms. Indeed, Mao et al (2008) found that NHEJ was completed within 30 minutes after DSB induction, whereas HR was not completed until at least 7 hours after DSB induction. To monitor DSB repair fluorescent reporter constructs where chromosomally integrated into human fibroblasts. Following I-SceI endonuclease cutting, ligation was monitored by the reconstruction of fluorescent GFP. Interestingly the efficiency of repair varied between cell lines carrying identical constructs, which the authors speculated might be a consequence of the chromosomal location of the integrated construct (Mao et al., 2008). In G1 phase, since there is no sister homologue to mediate HR repair, all DSBs are repaired by NHEJ (Beucher et al., 2009). Despite the utilisation of a single DSB repair process, there is still a fast and slow component to repair (Goodarzi et al., 2008). The fast component requires the core NHEJ factors Ku70/80, DNA-PKcs, Ligase IV, XLF and XRCC4; the slow component additionally requires ATM and Artemis. It has recently been established that the slow component

of repair in G1 represents DSBs which reside within regions of HC (Goodarzi et al., 2008). At HC DSBs ATM phosphorylates KAP-1 to mediate nucleosomal remodelling which likely facilitates access to repair proteins (Goodarzi et al., 2008; Ziv et al., 2006). Given that Artemis cleaves DNA hairpin intermediates during V(D)J recombination, the dependency on Artemis suggests a requirement for end processing (Ma et al., 2002). Thus, a working model is that HC DSBs, which are refractory to DSB repair, undergo limited end processing prior to re-joining. Given the highly repetitive nature of DNA associated at HC, damaged termini may form secondary structures or hairpins that require processing prior to ligation. In G2, HR is the slow component that involves Rad51, Rad54, BRCA2, ATM and Artemis (Figure 4.1). Beucher et al (2009) observed that following KAP-1 knockdown in G2 phase cells, the requirement for ATM in DSB repair was relieved. This suggested that HR repair in G2 is associated with regions of heterochromatin (Beucher et al., 2009).

1.33.2 Repair of heterochromatin associated DSBs by HR

In mammalian cells, ATM and the endonuclease Artemis have been shown to be required for repair of a subset of DSBs in G1 (Riballo et al., 2004). Beucher et al (2009), later demonstrated that ATM and Artemis are also required for a similar sized subset in G2. ATM inhibition and Artemis knockdown resulted in a repair defect that was epistatic with Brca2, Rad52 and Rad54 after IR in G2. BrdU repair incorporation after IR was also dependent on ATM and Artemis in G2. However ATM and Artemis cells do not show sensitivity to crosslinking agents like HR mutants, and spontaneous SCEs and I-Sce-I induced HR can occur without Artemis both implying that ATM and Artemis are not core HR factors (Beucher et al., 2009). Since the fast component of DSB repair (repair occurring within 2 hours of irradiation) is unaffected in HSC62 (Brca2- deficient) cells both in G1 and G2, Beucher et al (2009), suggests that HR specifically represents the slow component of DSB repair in G2. Following previous reports that knockdown

of the heterochromatic building factor KAP-1 alleviates the requirement for ATM in repair of the slow component of DSB repair in G1 (Goodarzi et al., 2008), KAP-1 knockdown was subsequently tested in G2 and again found to overcome the requirement for ATM in DSB repair. This suggested that the slow repairing DSB fraction in G2, which is repaired by HR, represents those breaks which reside within regions of HC. The authors proposed that certain types of breaks dependent on location or nature may undergo resection.

1.33.3 ATR and Chk1 activation at resected DSBs

In G2 phase around 20% of DSBs undergo ATM dependent resection which represents the slow component of DSB repair in G2 (Beucher et al., 2009). Resected 3' single stranded (ss) DNA overhangs (ssDNA) are rapidly bound by RPA which leads to ATR recruitment and Chk1 activation at the site of the lesion (Jazayeri et al., 2006; Wyman and Kanaar, 2006) (see 3.1.4 for further discussion). The C-terminal binding protein (CtIP) is essential to generate RPA coated ssDNA ends (Sartori et al., 2007). CtIP physically interacts with the MRN complex (Sartori et al., 2007) and is recruited with BRCA1 to control G2/M checkpoint arrest. ATM dependent phosphorylation of CtIP promotes CtIP relocation to MRN bound DSBs. Recently Kaidi et al (2010) identified a further step which is required to initiate CtIP dependent resection. Here the authors found that impaired RPA foci formation reduced HR repair and caused sensitization to CPT following the depletion of the lysine deacetylase (KDAC) sirtuin1 (SIRT1). A model was proposed whereby CtIP is constitutively acetylated in undamaged cells, and that following replicative stress CtIP is deacetylated by SIRT6 to allow the initiation of resection. However CtIP is still phosphorylated and recruited to damage sites in SIRT6 depleted cells following DNA damage (Kaidi et al., 2010). Generation of a constitutively deacetylated CtIP rescued SIRT6 loss, which lead to the proposal that SIRT6 promotes the process of resection rather than CtIP recruitment (Kaidi et al., 2010). RPA coated

ssDNA recruits and activates ATR/ATRIP/TopBP1 complexes and subsequently Chk1 (Paulsen and Cimprich, 2007). In short, these studies demonstrate that in G2 phase, ATM is activated at unresected DSBs, which, if not repaired by NHEJ undergo resection in an ATM dependent manner to allow the activation of ATR. Hence there appears to be a hand over from ATM to ATR signaling as resection ensues.

1.33.4 Checkpoint maintenance

Following IR, ATM activates the G2/M checkpoint within one hour due to DSBs generated in G2 (Beamish et al., 1994). At later times post IR, G2/M arrest is ATR dependent due to ATR activation at resected DSB in S phase (Wang et al., 2003; Wang and Qin, 2003). As mentioned in section 4.1.2, ATR can also regulate a replication independent checkpoint in G2 which is dependent on ATM (Jazayeri et al., 2006). Here ATM functions upstream of ATR to initiate resection by phosphorylating the endonuclease CtIP. Therefore the G2/M checkpoint can be initiated by three mechanisms; ATM to Chk2 signalling at DSBs or ATM – ATR to Chk1 signalling at resected DSBs in G2 phase, or ATR to Chk1 signalling at replication associated damage in S phase. Since the majority of NHEJ will be completed after late time points after IR, the maintenance of G2/M checkpoint arrest is highly dependent on resected DSBs (Shibata et al., 2010). However, unrepaired non-resected DSBs will also sustain ATM to Chk2 signalling at later times (Shibata et al., 2010). Despite the fact that only 15% of DSBs undergoing resection in G2 at late time points after IR, the slow repairing component of repair represents DSBs which undergo resection. Therefore the majority of DSBs that signal at late time points after IR are resected DSBs since the majority of NHEJ will already be completed. Hence the maintenance of G2/M checkpoint arrest is mainly dependent on Chk1 in repair proficient cells. Shibata et al (2010) demonstrated a critical role of Chk1 in maintaining G2/M arrest by showing that in Chk1 depleted cells or in ATR-SS hTERT cells (which are mutated in ATR) there is premature release

from G2/M checkpoint arrest. APH was added during these experiments to prevent S phase cells from entering G2 during analysis. Thus, these findings provided evidence that Chk1 dependent signalling from resected DSBs in irradiated G2 rather than S phase contribute to maintain G2/M checkpoint arrest.

1.33.5 The role of the mediator proteins in maintaining G2/M checkpoint arrest

The mediator proteins 53BP1 and MDC1 are dispensable for G2/M checkpoint arrest, except after low doses IR (Fernandez-Capetillo et al., 2002; Lou et al., 2006). However both are required for maintenance of checkpoint arrest (Shibata et al., 2010). Despite the subtle roles of 53BP1 and MDC1 in DSB repair, MEFs lacking 53BP1 or MDC1 have increased genomic instability (Fernandez-Capetillo et al., 2002; Peng and Chen, 2003). This could be attributed to their role in maintaining and tethering active ATM at DSBs (Noon et al., 2010) and subsequently prolonging Chk1 and Chk2 activation (Shibata et al., 2010). Shibata *et al* (2010) found that 53BP1 deficient cells fail to activate Chk1 normally after IR and have a diminished ability to sustain ATM to Chk2 signalling. Similarly, the BRCA1 deficient human carcinoma cell line HCC1987 is unable to activate a G2/M checkpoint even after 6 Gy IR (Xu et al., 2002). BRCA1 is also required for ATM and ATR dependent phosphorylation of p53, c-Jun, Nbs1 and Chk2 following exposure to IR or UV and for ATM phosphorylation of CtIP (Foray et al., 2003).

1.33.6 Checkpoint recovery

In budding yeast one DSB is sufficient to activate the G2/M checkpoint (Pellicioli et al., 2001). Mec1 (ATR homolog) has a more prominent role than Tel1 (ATM homolog) in

activating the downstream target kinases, Chk1 and Rad53 (Chk2 homolog) (Harrison and Haber, 2006). In yeast the G2/M checkpoint can be resolved by two distinct phenomena known as checkpoint recovery or checkpoint adaptation. Recovery of the checkpoint occurs when DSB repair has been completed. Adaptation describes restart of the cell cycle despite incomplete DSB repair.

Following completion of DNA damage, cells exit the G2/M arrest and enter mitosis, a phenomenon known as checkpoint recovery. In mammalian cells, checkpoint recovery primarily involves the ubiquitin mediated proteasome degradation of the checkpoint mediator claspin and the mitosis inhibiting kinase WEE1 (Mailand et al., 2006). After DNA damage, Claspin initiates G2/M checkpoint arrest by associating with replication forks where it interacts with the kinase domain of Chk1 (Lee et al., 2005). This interaction promotes Chk1 phosphorylation by ATR and enhances Chk1 autophosphorylation (Lee et al., 2005). To initiate G2/M checkpoint release, Claspin is degraded in a ubiquitin ligase SCF-dependent manner (Mailand et al., 2006). The adaptor protein β-TrCP links Claspin and WEE1 with the SCF ubiquitin ligase complex (Mailand et al., 2006). The interaction of Claspin with $SCF^{\beta TrCP}$ is dependent on the protein kinase, PIK1, phosphorylation of Claspin (Mailand et al., 2006). Disruption of Claspin removes Chk1 from the DSB and prevents Chk1 mediated inhibitory phosphorylation of Cdc25A; similarly WEE1 degradation eliminates a direct inhibition on cdk1 activity (Bartek et al., 2007). Hence both mechanisms converge on re-activating cyclin-CDK complexes to enable entry into mitosis. Interestingly, $SCF^{\beta TrCP}$ acts as a regulatory ubiquitin switch where it functions both in checkpoint initiation and recovery. During checkpoint initiation $SCF^{\beta TrCP}$ promotes Cdc25C degradation (see 1.10.4 for further discussion).

1.33.7 Checkpoint adaptation

Checkpoint adaptation occurs when cells divide following long checkpoint arrest despite the presence of irreparable DNA lesions. Adaptation was initially believed to be

restricted to single celled organisms such as yeast. However Syljuasen, 2006, reported the occurrence of checkpoint adaptation in human cells (Syljuasen, 2007). U20S cells exposed to 6 Gy IR were found to maintain a checkpoint arrest for up to 12 hours. However, at late times cells began to divide. At this dose clonogenic survival is only 4% and chromosome segregation is defective (Sandell et al., 1993), implying that DSBs may remain unrepaired. To test this, γH2AX foci were analyzed in mitotic cells released from the checkpoint. Indeed γH2AX foci were significantly increased in irradiated cells. However it is important to note that despite the fact that U2OS cells express p53 and Rb, they lack p16. Therefore checkpoint function in these cells may not represent a wildtype phenotype. In yeast we know that cells are released as a consequence of checkpoint adaptation. Whereas in mammalian cells, cells are released when less than 20 DSBs remain (as discussed in detail in chapter 3) (Deckbar et al., 2007). Therefore checkpoint arrest in mammalian cells is dependent on dose rather than time.

1.33.8 Aims of this chapter

The maintenance of IR induced G2/M checkpoint arrest is known to require around 15-20 DSBs (Deckbar et al., 2007). At late time points after IR, the maintenance of arrest is heavily dependent on slow repairing resected DSBs since the majority of fast repairing NHEJ will have been completed (Shibata et al., 2010). Repair deficient cell lines such as Artemis or XLF maintain checkpoint arrest for longer than WT cells, implying a communication mechanism between the repair and checkpoint machinery – i.e. that the checkpoint machinery can sense the status of DSB repair. In chapter 3, I showed that cells with reduced HC organization are able to initiate a G2/M checkpoint at low IR doses, which in WT cells is insufficient to generate enough signalling to elicit arrest. This increase in damage response signaling was attributable to increased γH2AX expansion at HC associated DSBs and consequently hyperactive ATM activation. Based on the findings presented in chapter 3, in this chapter, I further explore how

disordered chromatin impacts upon the response to DNA damage. Firstly, I examine its impact on DSB repair and particularly on the repair of HC-DSBs by asking whether the need for ATM is diminished in the disordered HC syndromes. Next I wished to address whether amplified ATM dependent signaling in the context of reduced higher order chromatin structure would affect the duration of G2/M checkpoint arrest.

1.34 Results

1.34.1 Rett syndrome cell lines repair with normal DSB kinetics in G1 and G2.

For sustained ATM activation, the initially activated ATM must be maintained in an active state at a DSB or ATM must be continuously recruited and activated at the DSB site. Sustained ATM activation is observed most markedly in cells with impaired NHEJ such as XLF or DNA-PKi treated cells (Shibata et al., 2010). Therefore, it was important to establish that DSB repair was normal in the chromatin disordered syndrome cells to rule out the possibility that prolonged ATM activation occurs as a consequence of incomplete or failed DSB repair. Firstly I monitored γH2AX foci disappearance in primary Rett fibroblasts after IR. Contact inhibited G1 arrested or cycling 48BR (WT) and Rett syndrome (GM16548, GM11271, & GM11272) cell lines were irradiating with 3 Gy IR. Cells were fixed at the indicated time points post IR and immunostained for γH2AX, CENP-F and DAPI. γH2AX foci were scored in G1 (CENP-F negative) and G2 (CENP-F positive) phase cells. Importantly, both wild type and Rett syndrome cell lines repaired DSBs with normal kinetics (Figure 4.2A, Figure 4.3). DSB repair was also monitored as described above in the ICF hTERT fibroblast line. Again, γH2AX foci disappeared with normal repair kinetics in the ICF (PT3) hTERT fibroblasts (Brunton et al., manuscript submitted). Therefore hyperactive ATM signalling as a consequence of slower or incomplete DSB repair could be ruled out.

1.34.2 MeCP2 knockdown alleviates the requirement for ATM in DSB repair although this is not observed in Rett Syndrome cell lines.

A previous publication from our laboratory established a role for ATM in initiating nucleasomal remodelling at HC-DSBs via its phosphorylation of the heterochromatic building factor KAP-1 (Goodarzi et al., 2008). In addition knockdown of heterochromatin building proteins including HDAC1 and 2 and HP1, was shown to alleviate the requirement for ATM in DSB repair. It was postulated that ATM dependent DSBs in G1 are those which reside within heterochromatin. In consideration of this data, I tested whether Rett syndrome cell lines, which have a more relaxed chromatin configuration, would also overcome the requirement for ATM in DSB repair. Contact inhibited G1 arrested 48BR (WT) and Rett syndrome (GM16548, GM11271 & GM11272) cell lines were treated with or without ATMi 30 minutes prior to irradiating with 3 Gy IR. Cells were fixed at the indicated time points and immunostained for γH2AX, CENP-F and DAPI. γH2AX foci were scored in G1 (CENP-F negative) phase cells. ATMi treatment had no effect on DSB repair at early time points (< 2 hours) after IR in both 48BR and Rett syndrome cell lines consistent with previous findings (Figure 4.2A). However at late time points (> 8 hour) after IR, ATMi treated 48BR and Rett syndrome cells manifested a repair defect. After 24 hours recovery following 3 Gy IR, ATMi treated 48BR and Rett syndrome cells manifest a repair defect of ~ 8-10 DSBs. This was distinct to the findings observed following knock down of the heterochromatic building factors, KAP-1, HDAC1/2 or HP1, where there ceased to be a requirement for ATM for DSB repair (Goodarzi et al., 2008). This was somewhat surprising but suggested that MeCP2 loss in the patient cells does not sufficiently relax the chromatin structure to overcome ATM's role in HC-DSB repair. Therefore it was possible that the residual MeCP2 expressed in the patient cells promotes sufficient chromatin compaction to necessitate a requirement for ATM for HC-DSB repair. To test this, 48BR and Rett syndrome (GM16548, GM11271 & GM11272) cell lines were treated with either control or MeCP2 siRNA for 48 hours and then exposed to 3 Gy IR. 30 minutes prior to irradiation, cells were treated with or without ATMi. Cells were fixed at the indicated time points and immunostained for γH2AX, CENP-F and DAPI. γH2AX foci were counted

in G1 (CENP-F negative) cells. Consistent with the data observed in KAP-1 knockdown cells, cells knocked-down for MeCP2 no longer required ATM for HC-DSB repair (Figure 4.2B). This suggested that MeCP2 enriched chromatin does pose a barrier to DSB repair. However the MeCP2 mutations in the Rett syndrome cell lines do not sufficiently change heterochromatin to overcome this barrier. Similarly, ICF hTERT cell were unable to overcome the requirement for ATM in DSB repair, whilst DNMT3B knockdown in wildtype and ICF (PT3) hTERT cells did alleviate the heterochromatin associated barrier to DSB repair (Brunton et al., manuscript submitted).

1.34.3 Chromatin disordered cells exhibit a prolonged G2/M checkpoint arrest

After confirming that DSB repair was normal in the Rett syndrome cells, I next analyzed checkpoint maintenance in these cells. Based on previous analysis, checkpoint arrest is released when DDR signalling decreases as DSB repair ensues (Deckbar et al., 2007). Therefore a hyperactive checkpoint signalling response would be expected to manifest as prolonged checkpoint arrest. To examine checkpoint maintenance in irradiated G2 phase cells only, the replicative polymerase inhibitor aphidicolin (APH) was added immediately after IR. 48BR and Rett syndrome (GM11272) cells were irradiated with 2 Gy IR. Cells were harvested at the indicated time points and immunostained for the mitotic specific marker, pS10 histone H3 and DAPI. pS10 histone H3 positive mitotic cells were scored and expressed as a percentage of the mitotic population present in unirradiated cells (Figure 4.4A). Four hours post 1 Gy IR, both 48BR and Rett syndrome cells began to release from the G2/M checkpoint. However, Rett syndrome patient (GM11272) cells lagged behind wild type cells release from the checkpoint, with only 40% of the mitotic population cycling in the Rett syndrome cells compared to 80% in control cells at 10 hours after IR demonstrating a prolonged maintenance of checkpoint arrest. To confirm that prolonged G2/M checkpoint maintenance is a consequence of reduced MeCP2 levels, MeCP2 was transiently knocked down in 1BR

hTERT cells. 1BR hTERT cells were treated with either control or MeCP2 siRNA for 48 hours. Following transfection, cells were irradiated with 2 Gy IR and harvested at the indicated time points. Cells were immunostained as before. Consistent with the result observed in Rett syndrome (GM11272) cells, MeCP2 knockdown cells also maintained G2/M checkpoint arrest longer than control cells (Figure 4.4B). To further establish the effect that heterochromatin relaxation has on checkpoint maintenance, HGPS, ICF and Rett syndrome lymphoblastoid cells were treated as above, harvested by cytospinning and the mitotic index scored. Strikingly, cell lines from patients with impaired HC displayed prolonged G2/M checkpoint arrest up to 8 hours after 2 Gy IR whereas control cells are released by 6 hours (Figure 4.5).

1.34.4 Chk1 phosphorylation is hyperactive in Rett syndrome and MeCP2 knockdown cells

Chk2 and Chk1 both function to maintain checkpoint arrest, and loss of either kinase results in premature checkpoint release (Shibata et al., 2010). However, after high doses IR, either kinase alone can function to initiate checkpoint arrest. This is most likely because after a high dose there is a sufficient threshold signal generated by either kinase to activate checkpoint arrest. However, as DSB repair ensues and the number of DSBs diminishes, the combined function of both kinases is required – Chk2 being activated at non-resected DSBs and Chk1 being activated at the resected DSBs (Shibata et al., 2010). DSB repair in G2 phase, like G1, has two components of repair one with fast kinetics involving the core NHEJ machinery (see 4.1.1 for further discussion) and the other occurring with slow kinetics involving ATM and Artemis and the HR proteins (Beucher et al., 2009). It is these slowly repaired DSBs that undergo resection. Thus, although only 15-20% of total DSBs undergo resection in G2, at late time points after IR the majority of DSBs that remain are those which have undergone resection since the majority of DSB repair by NHEJ is completed (fast component). Thus, Chk1 has a greater role in maintaining checkpoint arrest than Chk2 (Beucher et

al., 2009). In summary, the mechanisms that serve to maintain arrest represent either ATR dependent activation of Chk1 at resected DSBs or sustained ATM to Chk2 signalling at un-repaired DSBs; with the former begin the most significant.

Given that DSB repair is normal in Rett syndrome and MeCP2 knock down cells (Figure 4.1) prolonged checkpoint maintenance as a consequence of sustained ATM to Chk2 signalling could be ruled out although initial checkpoint arrest is dependent on ATM-Chk2 signalling. I next wished to establish whether loss of MeCP2 activity affects resection to ATR/Chk1 signalling in irradiated G2 cells. To test this, pan nuclear Chk1 phosphorylation at Ser345 (pSer345) was analysed by IF in 48BR and Rett syndrome patient (GM11272) cells. Cells were irradiated with 10 Gy IR. 1 hour post irradiation cells were fixed and immunostained for pSer345 Chk1, DAPI and the G2 marker CENP-F. Pan nuclear pSer345 Chk1 signal intensity in G2 phase (CENP-F positive) cells was analyzed using ImageJ software. Higher doses of IR were used to enable detection of Chk1 pSer345 induction. Strikingly, Rett syndrome (GM11272) cells activated pSer345 almost 2 fold greater than control cells (Figure 4.6). Given that Chk1 can be activated by ATR at stalled or collapsed replication forks independently of ATM, and despite previously adding aphidicolin to prevent S phase cells entering G2 phase and contributing to signalling, it was important to confirm that hyperactive Chk1 activation in G2 was dependent on ATM mediated resected DSBs. To test this, 48BR (WT) and Rett syndrome (GM11272) cells were treated with or without ATMi 30 minutes prior to irradiating with 10 Gy IR. One hour post IR, cell were fixed and immunostained for pSer345 Chk1 and DAPI. Following ATMi treatment, Chk1 activation was dramatically reduced in both control and Rett syndrome 3 cells (Figure 4.6). This suggested that the majority of Chk1 activation observed was ATM dependent in G2 cells. To further consolidate that this result was a consequence of MeCP2 loss, 48BR (WT) cells were treated with either control or MeCP2 siRNA for 48 hours. Cells were irradiated with either 6 or 10 Gy IR and fixed and immunostained 1 hr later. As observed in the Rett syndrome cells, after 6 Gy IR, Chk1 pSer345 induction was almost 3 fold greater in MeCP2 knockdown cells. Similarly, following 10 Gy IR, Chk1 pSer345 activation was 2 fold greater in MeCP2 knockdown cells (Figure 4.7).

1.34.5 RPA foci signal intensity is enhanced in Rett syndrome cells.

Chk1 is activated at RPA coated resected DSBs in G2 by ATR. Therefore hyperactive Chk1 activation is likely to be indicative of enhanced resection. Having established that Chk1 activation is hyperactive in MeCP2 and Rett syndrome cells, I next analysed RPA foci in these cells. To exclude S phase cells from analysis, 48BR (WT) and Rett syndrome (GM11272) cells were treated with aphidicolin directly after IR. 30 minutes post 3 Gy IR, cell were fixed and immunostained for RPA, 53BP1 and DAPI. 53BP1 was used as a biomarker for DSBs. Signal intensity of RPA foci co-localizing with 53BP1 was quantified using ImageJ software. Consistent with the observation of hyperactive Chk1 activation, RPA foci signal intensity was also enhanced in Rett syndrome cells (Figure 4.8). This might suggest that Rett syndrome cells undergo larger scale ATM dependent resection. This is particularly interesting following reports that HR repair in G2 phase is associated with DSBs that reside within regions of heterochromatin (see 4.1.2 for further discussion).

1.34.6 Rett syndrome cells have normal survival after IR.

Having established that Rett syndrome cells initiate a hypersensitive G2/M checkpoint arrest i.e. they initiate arrest at a radiation dose which in wildtype cells is below the threshold number of DSBs required to initiate arrest (Figure 3.20), and maintain G2/M checkpoint arrest longer than wildtype cells despite having normal DSB repair (Figure 4.3), I next analysed whether hyperactive ATM dependent Chk2 and Chk1 signalling impacts upon Rett syndrome cell survival. Following IR, radiosensitivity was assessed by colony survival analysis. 48BR and Rett syndrome cells were trypsinized, irradiated with the indicated doses IR and plated onto feeder cells prepared 24 hours earlier. Cells were left to form colonies for 3 weeks. At all doses of IR, Rett syndrome cells show a modest resistance but the significance of this result requires further investigation (Figure 4.9).

1.35 Discussion

1.35.1 Chromatin disorganization prolongs G2/M checkpoint arrest

The maintenance of G2/M checkpoint arrest following IR is dependent on Chk2 signalling at non-resected DSBs, or Chk1 signalling at resected DSBs in G2 or collapsed replication forks in S phase (Shibata et al., 2010). A threshold of DDR signalling that accumulates from at least 15-25 DSBs is required to satisfy and maintain checkpoint arrest (Deckbar et al., 2007). In this chapter I have established that cell lines with reduced higher order chromatin organization show prolonged G2/M checkpoint arrest despite having normal DSB repair. Therefore late repairing DSBs which remain in a cell with reduced HC superstructure generate enough damage response signalling to sustain checkpoint arrest. Additionally, MeCP2 knockdown, like KAP-1 knockdown, overcomes the barrier to ATM dependent DSB repair. This further consolidates the notion that ATM dependent DSBs are those which reside within HC (Goodarzi et al., 2008).

1.35.2 Heterochromatin and homologous recombination

In G2 phase cells at late time points after IR the fast component of DSB repair, namely NHEJ, is completed, and the majority of DSBs still signalling to maintain arrest are those dependent on HR (Beucher et al., 2009; Shibata et al., 2010). In this chapter I analysed whether prolonged checkpoint arrest was dependent on HR. Indeed I did not observe a significant change in Chk2 phosphorylation at later time points after IR, although ATM/Chk2 signalling was enhanced at initial time points. Importantly, Chk1 phosphorylation was found to be hyperactive in G2 phase cells and this hyperactivity was dependent on ATM, demonstrating that Chk1 activation is dependent on DSB end resection. Additionally RPA signal intensity per foci was also enhanced in Rett

syndrome cells. In conclusion HC superstructure appears to act as a barrier to ATM dependent resection in G2, and removing this barrier by MeCP2 knockdown increases the magnitude of resection. It is still unclear whether loss of MeCP2 causes a longer length of DNA resection per DSB only by RPA foci analysis. However, importantly, this result suggests that relaxed HC superstructure following MeCP2 siRNA enhanced the number of RPA at DSB, which lead to a larger range of scaffold for ATR-Chk1 activation. Interestingly, Beucher et al (2009) reported that the dependency for ATM in the slow repair component of DSB repair in G2 could be overcome with KAP-1 knockdown. This suggested that HR repair in G2 occurs at regions of heterochromatin. Here I have shown that by removing the HC associated barrier resection at HC DSBs is enhanced.

It is interesting to speculate that a more accurate DSB repair mechanism such as HR would have a greater precedence to repair HC associated DSBs given the highly repetitive nature of DNA at these regions. Additionally resection mediated remodelling events such as those observed in yeast may be required to facilitate the access of repair proteins to HC associated DSBs. For example, in yeast, histone loss following DNA damage is tightly coupled to the rate of resection. Strains lacking the Arp8 chromatin remodeling subunit, Ino80, have defective resection (Shimada et al., 2008). Consistent with this, chromatin disassembly is strongly reduced in strains lacking the nuclease, Mre11 (Shimada et al., 2008). Srs2 helicase mutant strains are also defective in checkpoint recovery, but deletion of Rad51 alleviates this defect (Vaze et al., 2002). Harrison and Haber proposed that the presence of Rad51 filaments promoted continuous DNA damage checkpoint signaling even after completion of repair (Harrison and Haber, 2006). In addition, displacement of repair factors following chromatin remodeling has also been shown to be sufficient to inactive the checkpoint (Soutoglou and Misteli, 2008). The observation that RPA foci signal intensity was enhanced in Rett syndrome cells suggests that a higher dependency on HR repair prolongs G2/M checkpoint arrest. If resection does function to remodel nucleosomes then complete HC relaxation would be expected to overcome the requirement for resection. Given that Rett syndrome cells still require ATM to complete DSB repair, and only after all MeCP2 expression has been abolished in these cells by siRNA is the requirement for ATM in DSB repair overcome suggest that the MeCP2 expressed in the

patient cells is still sufficient to maintain a barrier to a subcomponent of DSB repair. Hence G2 phase DSBs in Rett syndrome cells may still pose a barrier to repair which requires resection mediated remodelling. However, given the relaxed but not abolished HC superstructure of Rett syndrome cells, resection may progress with reduced HC restrictive barriers. Hence the dependency on resection may be dictated by how efficiently the HC superstructure is relaxed. It would be of interest in future experiments to establish whether loss of other HC associated factors also increase or reduce the magnitude of resection.

In this chapter I focused my attention on Rett syndrome cells because I observed the most dramatic impact in these cells and because they grew with similar kinetics to wildtype cells and had a low number of endogenous γH2AX foci. Rett syndrome cells showed a prolonged G2/M checkpoint arrest despite having normal DSB repair. Therefore lower numbers of γH2AX foci are sufficient to maintain checkpoint arrest in these cells. This data further consolidates the notion that more DDR signaling is generated per DSB in cells with reduced HC organization.

1.35.3 Signalling the end of DSB repair

Studies in yeast have suggested that chromatin reassembly, rather than the completion of DSB repair, is the signal to end DDR signaling and facilitate checkpoint release. Given that chromatin organization is perturbed in Rett, ICF and HPGS cell lines, reassembly of chromatin structure after DSB repair may be prolonged and subsequently checkpoint arrest maintained for longer. Kim and Haber tested whether loss of histone chaperones Asf1 and CAF-1 would affect recovery of the checkpoint after DNA damage. Chromatin assembly factor (CAF-1) and anti-silencing function 1 (Asf1) are involved in replication-coupled nucleosome assembly via interactions with histone H3 and H4. Kim & Haber reported that DSB repair in asf1 and cac1 double mutant yeast strains was normal. However mutants maintained G2/M arrest and

Rad53 phosphorylation almost 4 hours longer than WT strains. In addition, asf1 mutants lacking H3 H4 binding sites failed to suppress the G2/M checkpoint. The authors concluded that chromatin assembly is required for the termination of the damage induced G2/M checkpoint (Kim and Haber, 2009). The relevance of this to higher eukaryotes is less understood, but Asf1 proteins are highly conserved, and human Asf1 can functionally replace the yeast Asf1 protein (Tamburini and Tyler, 2005). CAF-1 also exists in mammalian cells and is recruited to sites of UV lesions (Green et al., 2005) where is associates with histone H3.1 (Tagami et al., 2004). Following NER mediated repair of UV lesions, CAF-1 mediates the deposition of histone H3 and H4 (Polo et al., 2006). It is interesting to speculate whether the process of chromatin reassembly, rather than DSB repair completion, signals the end of repair.

It is still unclear after DNA repair if nucleosomes are reassembled using pre-existing histones or replaced with new histones. Histone modifying enzymes can be recruited to specific histone modifications which can allow spreading of these modifications to neighboring histones (Jenuwein, 2001; Jenuwein and Allis, 2001). Partial histone recycling may enable maintenance of epigenetic information by a semiconservative mechanism which is similar to the mechanism employed for DNA replication. Chromatin disordered cell lines could potentially have an epigenetic code which is less organized making the process of histone recycling during repair less efficient and as a consequence checkpoint arrest prolonged.

Recently, γH2AX has been shown to inhibit neural stem cell (NSC) proliferation (Fernando et al., 2011). NCSs reside in particular regions of the brain and self-renew to generate neurons throughout life. The largest region of neurogenesis in the brain is known as the subventricular zone (SVZ) (Lim and Alvarez-Buylla, 1999). γH2AX phosphorylation at the SVZ slows NCS division, limits differentiation and reduces NCS niche size (Fernando et al., 2011). Therefore hyperactive and prolonged H2AX signaling in the SVZ would be expected to deplete NCS numbers and hence affect normal brain development. It is interesting to speculate whether the hyperactive signaling observed in Rett syndrome fibroblasts also occurs in neurons in response to replicative or

oxidative damage, and whether this signaling affects NCS differentiation. The Rett syndrome phenotype might be established later in development if the SVZ layer is depleted. Hence, early brain development is normal, but due to hyperactive ATM and hence gH2AX expansion, the SVZ layer is depleted due to either senescence or slow cycling. Therefore no NCS are available to acquire or maintain new skills such as speech.

Chapter 5: DSBs dependent on Artemis for repair reside within regions of heterochromatin

DSBs dependent on Artemis for repair reside within regions of heterochromatin

1.36 Introduction

1.36.1 RS-SCID

The Artemis gene was first identified in a small population of Athabascan-speaking Native Americans. Athabascan-type severe combined immunodeficiency (SCIDA) is characterised by a

failure to develop lymph nodes and a general failure to thrive (Moshous et al., 2001). A subset of SCID patients display sensitivity to ionizing radiation and are described as RS-SCID (radiation sensitive - severe combined immunodeficiency). In the majority of cases, patients are mutant for Artemis and are phenotypically characterised as T cell-negative (T-), B cell-negative (B-), natural killer cell-positive (NK+) (Moshous et al., 2001). The immunodeficient phenotype of these patients relates to the role of Artemis during V(D)J recombination a process which generates antibody diversity (see section 5.1.4 for details). The radiosensitivity experienced by these patients is a consequence of Artemis being required for the repair of a subset of DSBs. The nature of these lesions that are dependent on Artemis for repair is unknown.

1.36.2 Gene location and family

The Artemis gene encodes 685 amino acids with 14 exons and is located on chromosome 10. Sequence analysis revealed the murine protein to be 78 % identical to the human Artemis sequence (Moshous et al., 2001). Artemis, along with SNM1 (sensitive to nitrogen mustard 1), CPSF (cleavage and polyadenylation specificity factor), Pso2 and Apollo form a subgroup from the metallo-β-lactamase family which is characterised by the presence of a β-CASP (CPSF-Artemis-Snml-Pso2) domain (Callebaut et al., 2002). Conserved residues between family members are predicted to be positioned in the vicinity of the catalytic centre formed by the metal binding residues (Callebaut et al., 2002).

1.36.3 The Artemis endonuclease

Artemis is a mammalian endonuclease that functions during V(D)J recombination and a subset of DSB repair. Nucleases can be grouped into two main families either exo or endo – nucleases. Exonucleases are typically sequence independent. Endonucleases can be further divided into those which are sequence independent (i.e. restriction enzymes) or structure specific. The nuclease activity of Artemis is conferred by a β-lactamase (aa1-135) and β-CASP (aa155-385) domains within its N-terminus (Ma et al., 2005a). On association with DNA-PK, Artemis cleaves 5’ and 3’ overhangs and nicks DNA hairpins (Ma et al., 2005b). Using varying radiolabelled DNA

substrates Artemis was found to have activity on a wide range of DNA structures including 3' flaps, pseudo Y structures, stem loop structures, symmetrical bubbles, heterologous loops and gapped DNA (Ma et al., 2005b). Y structures and nicked DNA were not cleaved by the Artemis DNA-PK complex. All of the substrates for endonuclelytic action by Artemis and DNA-PK had ss to ds DNA transitions. Un-cleaved substrates included blunt duplex DNA, nicked DNA, perfect Y structures and perfect ss DNA. Therefore unlike some endonucleases which are structure and sequence specific, Artemis on association with DNA-PK is functional on a wide range of end substrates.

In response to DSBs, Artemis is rapidly phosphorylated by ATM (Poinsignon et al., 2004; Riballo et al., 2004). However, the functional relevance of this phosphorylation event remains unclear. Artemis contains 10 ST/Q PIKK target phosphorylation sites, 8 of which are contained within its C-terminus (Goodarzi et al., 2006). Artemis cDNA mutated for 7 of these sites is still able to complement the radiosensitivity of Artemis defective cells (Poinsignon et al., 2004). Expression of WT or Artemis protein mutated for all potential C-terminal PIKK phosphorylation sites (referred to as 9A) in a Artemis defective (CJ179) hTERT cell line was still able to restore mutant Artemis cells to a WT phenotype, as monitored by 53BP1 foci disappearance after 10 Gy IR (Goodarzi et al., 2006). This suggested that Artemis activity was not dependent on phosphorylation at these PIKK target sites. Further mutation of all 10 PIKK target SQ sites found the same phenotype as the 9A mutant. Therefore loss of every SQ/TQ site in Artemis did not compromise Artemis's function in vivo (Goodarzi et al., 2006). In addition, Artemis MEFs transfected with V(D)J coding joint substrate plasmids, Rag1 and Rag2 and WT or 9A mutants were still capable of cleaving the hairpin substrate. Therefore Artemis phosphorylation by ATM is dispensable for its nuclease activity in both DSB repair and V(D)J recombination (Goodarzi et al., 2006). DNA-PK defective cells, like Artemis cells, have a DSB repair defect after IR and are V(D)J recombination compromised (Le Deist et al., 2004). DNA-PKcs undergoes autophosphorylation within two distinct regions known as the ABCDE and PQR clusters (Merkle et al., 2002). Phosphorylation site mutants for the ABCDE cluster fail to rescue the DSB repair or V(D)J recombination defect of DNA-PK mutants. Goodarzi et al (2006) subsequently established that DNA-PK autophosphorylation is a prerequisite for Artemis activity. Different in vivo experiments which incubated either: Artemis, DNA-PK (unphosphorylated) and Wortmannin or Artemis, DNA-PK (phosphorylated) and PIKK inhibitor Wortmannin found Artemis was still functional in the presence of Wortmannin if DNA-PK had already undergone autophosphoryltion (Goodarzi et al., 2006). Additionally incubating Artemis and DNA-PK with non-hydrolysable ATPγS, no ATP or PIKK inhibitor Wortmannin were unable to support Artemis

activity on radiolablled DNA overhangs. This suggested that DNA-PK autophosphorylation was required for Artemis nuclease activity. At relevant salt concentrations Ku is also required for Artemis endonuclease activity (Goodarzi et al., 2006). DNA-PK but not Ku dissociates from blunt DNA after autophosphorylation. However, if DNA overhangs persist, DNA-PK remains stably associated with DNA even after autophosphorylation (Goodarzi et al., 2006). The addition of Artemis removed DNA-PK from the DNA end (Goodarzi et al., 2006). This was established in vivo by adding Ku + DNA-PK or Ku, DNA-PK + Artemis. Immunoprecipitation for Ku and immunoblotting for bound proteins established that only when Artemis was present did DNA-PK dissociate from Ku. The authors then tested whether DNA-PK autophosphorylation site mutants could support Artemis activity. In this scenario, no Artemis cleavage was found. The authors concluded that autophosphorylation at DNA-PK ABCDE cluster is required for Artemis nuclease activity. A model was suggested in which DNA-PK autophosphorylation may alter the holoenzyme conformation which facilitates exposure of ss to ds DNA junction to enable Artemis cleavage (Goodarzi et al., 2006). Therefore ATM dependent Artemis phosphorylation is dispensable for Artemis activation.

1.36.4 Artemis and DSB repair

Around 10% of DSBs remain unjoined for up to 14 days in CJ179 (Art) primary cells after 80 Gy when monitored by Pulse Field Gel Analysis (PFGA) (Riballo et al., 2004). This phenotype is identical to A-T cells. A-T and Artemis cells both loose γH2AX foci with similar kinetics as WT cells up to 4 hours after IR. At later time points (> 8 hours up to 14 days) A-T and Artemis cells have persistent γH2AX foci. This defect can be rescued following over-expression with Artemis cDNA. A mutant (D37N) Artemis cDNA with disrupted overhang endonucleolytic and hairpin cleavage activities (Pannicke et al., 2004) fails to rescue the DSB defect of CJ179 (Art) cells. This demonstrated that the function of Artemis in DSB repair requires its endonuclease activity. Since mutations in core NHEJ factors results in a marked DSB repair defect at early time points after IR (Kuhne et al., 2004), ATM and Artemis are not considered core components of NHEJ, but rather are required for the repair of a subset of DSBs at later time points (Riballo et al., 2004).

The addition of ATM inhibitor (ATMi) to CJ179 (Art) cells was shown to have no additive effect on γH2AX foci loss after 2 Gy IR, which suggested that ATM and Artemis function in the same repair pathway (Riballo et al., 2004). Previously the dependency for ATM and Artemis in DSB repair was proposed to be a consequence of end complexity since an increased reliance for these proteins was observed for repair of lesions generated by densely ionizing α particles (Riballo et al., 2004). In this model ATM was thought to phosphorylate and activate Artemis. However as mentioned earlier, ATM dependent Artemis phosphorylation is dispensable for Artemis activity (Goodarzi et al., 2006). Further analysis of damage complexity and ATM dependency using varying damage inducing agents such as neocarzinostatin (NCS) which produces defined DSB possessing phosphoglycolate or 3'-phospho termini refractory to ligation, and carbon K which induces clustered DSBs both generated a DSB repair fraction dependent on ATM which was similar to X-rays. Therefore the DSB repair fraction dependent on ATM did not exceed 20-25%. Therefore ATM dependency is not a consequence of increased damage complexity (Goodarzi et al., 2008). This finding necessitated a re-think for the role of ATM and Artemis in DSB repair. Using NIH 3T3 cell which have easily identifiable regions of heterochromatin, at 30 minutes after 0.25 – 2 Gy IR, the percentage of heterochromatin associated DSBs is roughly 25%, which is consistent with stochastic DSB induction (Goodarzi et al., 2008). By contrast, the percentage of heterochromatin associated DSBs at 24 hours after 1 – 3 Gy IR with ATMi is roughly 60 – 70% (Goodarzi et al., 2008). Analysis of ATM dependent repair in Klinefeter syndrome cell lines, which have an XXXY genotype and consequently more silenced heterochromatin, found a greater number of persisting DSBs in the Klinefelter syndrome cells after ATMi than control cells (Goodarzi et al., 2008). Similarly analysis of γH2AX foci in ATMi treated HGPS cells which have reduced chromatin organization found only half the number of foci remaining after 24-48 hours after IR compared to ATMi treated WT cells. This suggested that ATM dependent DSBs reside within or are located at regions of heterochromatin (Goodarzi et al., 2008).

KAP-1 phosphorylation has been shown to correlate with global chromatin relaxation as measured by micrococcal nuclease digestion of genomic DNA (Ziv et al., 2006). Increased nucleosome compaction, as caused by heterochromatin formation, is more resistant to salt solublization and MNase digestion (Yoda and Ando, 2004). KAP-1, HP1 and HDAC1 are found in greatest abundance in fractions most resistant to nuclease digestion. IR induced DNA damage induces a reduction of KAP-1 in the most nuclease resistant chromatin fractions. A small fraction of KAP-1 remains chromatin bound even after 80 Gy IR (Goodarzi et al., 2008). The reduction of KAP-1 in nuclease resistant chromatin fractions was reversed within several hours,

mirroring the loss of γH2AX and indicative of a dynamic equilibrium with repair. KAP-1 release from chromatin enriched protein fractions does not occur with ATMi treatment (Goodarzi et al., 2008). This suggested that ATM dependent phosphorylation of KAP-1 was required to mediate nucleasomal relaxation. Further experiments established that heterochromatin relaxation mediated by either: KAP-1, HDAC1/2 or HP1 knockdown overcomes the requirement for ATM in DSB repair. Given that ATM and Artemis have epistatic repair defects following exposure to IR, in this chapter I wish to address whether the dependency for Artemis in DSB repair could also be overcome following heterochromatin relaxation.

1.36.5 Aims of this chapter

Both ATM and Artemis have epistatic repair defects and are required for the repair of a subset of DSBs that are repaired with slow kinetics in G1 (Riballo et al., 2004). ATM functions at this subfraction to mediate nucleasomal remodelling via phosphorylation of the heterochromatin building factor KAP-1, thereby facilitating access to other wise inaccessible DSBs (Goodarzi et al., 2008). Based on these findings, I wished to address in this chapter whether Artemis also functions like ATM to mediate or participate in nucleasomal remodelling. Firstly, I examine whether Artemis dependent DSBs localize to regions of heterochromatin. I further examined whether these DSBs are enriched for heterochromatin associated markers such as phosphorylated KAP-1 and Tri-Me K9 Histone H3. Following DSB induction KAP-1 dissociates from nuclease resistant chromatin enriched protein fractions, and the reestablishment of KAP-1 at these fractions directly correlates with DSB repair (Goodarzi et al., 2008). I next wished to address whether Artemis dependent DSBs would prolong the duration that KAP-1 remained dissociated from heterochromatin enriched fractions. Following siRNA mediated heterochromatin relaxation the requirement for ATM in DSB repair can be alleviated (Goodarzi et al., 2008). Finally I addressed whether heterochromatin relaxation could alleviate the requirement for Artemis in DSB repair.

1.37 Results

1.37.1 DSBs dependent on Artemis for repair are visibly associated with DAPI dense chromocenters.

The heterochromatic content of the human genome is known to be in the range of 10-25% (Miklos and John, 1979). This percentage correlates with the DSB repair fraction that is dependent upon Artemis for repair. It has recently been reported by Goodarzi et al (2008) that DSBs dependent upon ATM signalling localize to regions of heterochromatin. To determine whether Artemis dependent breaks localize to regions of heterochromatin, I examined, by immunoflorescence, whether γH2AX foci that persist in Artemis siRNA transfected cells localize with regions of heterochromatin. I utilized contact inhibited G1 phase NIH3T3 mouse cells to rule out any complication posed by cell division or replication. These cells also offer the advantage of having easily identifiable heterochromatic regions following dense DAPI staining (Guenatri et al., 2004), thus enabling regions of heterochromatin to be imaged under the microscope. NIH 3T3 cells were treated with either control, Artemis oligo A and B, or 53BP1 siRNA for 48 hours as a control for HC-DSB repair deficiency. Since specific antibodies against the mouse Artemis protein are unavailable to confirm successful knockdown, cells were selected on the basis of those which maintained a DSB repair fraction of 10-20% 24 hours after recovery following 3 Gy IR (Figure 5.1). The estimated transfection efficiency was monitored using 53BP1 knockdown by immunoflorescence alongside the system employed to transfect the Artemis siRNA. γH2AX foci were scored in non-expressing cells (Figure 5.1). Like ATM inhibited cells, γH2AX foci persisting in the presence of Artemis siRNA localized to regions of heterochromatin. To quantify these findings, I enumerated the total number of γH2AX foci and the total number of those foci that localized to regions of heterochromatin (Figure 5.2). Strikingly, more than 70% of unrepaired IR induced DSBs were found to be visibly associated with regions of heterochromatin in Artemis defective cells (Figure 5.2).

1.37.2 Late repairing Artemis dependent γH2AX foci co-localize with pKAP-1 foci

Unrepaired DNA DSBs that reside within heterochromatin signal to ATM. This signalling event maintains the phosphorylation of KAP-1 until the completion of repair (Goodarzi et al., 2008).

Therefore, I postulated that DSBs dependent on Artemis that localize with regions of heterochromatin should also localize with pKAP-1 foci. To investigate this, 1BR (WT) and Artemis primary fibroblasts were irradiated with 3 Gy IR, fixed and immunostained at the indicated time points post IR for pKAP-1, γH2AX and DAPI. As expected, increased γH2AX foci in Artemis defective human cells highly contain pKAP-1 signal at DSBs (Figure 5.3).

1.37.3 Artemis dependent DSBs are enriched for the heterochromatic marker Tri-Me K9 Histone H3.

Finally, I utilized a method other than microscopy to observe the correlation between heterochromatin and Artemis dependent repair. I reasoned that if Artemis dependent DSBs reside at regions of heterochromatin then γH2AX containing nucleosomes should be enriched for heterochromatin associated modifications such as Tri-Me K9 histone H3. To test this, I immunoprecipitated for γH2AX containing nucleosomes after IR in CJ179 (Art) primary cells and blotted for Tri-Me K9 Histone H3. First Artemis defective CJ hTERT cells were irradiated with either 10 Gy IR with a recovery time of 30 minutes (early time point) or 80 Gy with a 48 hour recovery (late time point). The early time point should represent stochastic DSB's distributed evenly throughout euchromatin and heterochromatin. At this time point there is enough time for repair foci to form but no actual repair to proceed. The late time point should represent only those DSBs dependent on Artemis for repair. Isolated protein samples were sonicated for 1 minute and DNA was extracted and resolved on a DNA agarose gel to ensure the same range of polynucleosomes were isolated for each sample (Figure 5.4). Following IR, I used γH2AX antibodies to immunoprecipitate (IP) nucleosomes which localize with DSBs and blotted for γH2AX and the heterochromatic marker Tri-Me K9 Histone H3 (Figure 5.4). Using these conditions similar amounts of γH2AX were IP'd for early and late time points. Where equivalent levels of γH2AX were IP'd, late repairing Artemis dependent DSBs were associated with roughly four times more histone H3 K9 trimethylation than cells with stochastically incurred DSBs (Figure 5.4). This data strongly suggested that Artemis plays a role in repair of DSBs associated with heterochromatin. Wildtype cells were not used during this analysis because at late time points after IR, all DSBs are repaired.

1.37.4 KAP-1 remains dissociated from chromatin enriched fractions following IR for longer in Artemis defective cells.

As mentioned in the introduction, global chromatin relaxation has been shown to correlate with KAP-1 phosphorylation (Ziv et al., 2006). KAP-1 retention at micrococcal nuclease (MNase) resistant chromatin enriched protein fractions is reduced following IR, and the reestablishment of KAP-1 in these fractions directly correlates with DSB repair (Goodarzi et al., 2008). Here I want to address what affect Artemis deficiency has on IR induced KAP-1 dynamics at heterochromatin enriched chromatin fractions. If Artemis dependent DSBs reside at heterochromatin, then one would expect ATM signalling from these breaks to maintain KAP-1 phosphorylation (pKAP-1) and subsequently prolong the duration that nucleosomes remain in a dynamic configuration. Therefore chromatin enriched fractions in Artemis defective cells would be expected to have less KAP-1 associated at later times after IR compared to WT cells. To test this, Artemis and WT MEFs were irradiated with 40 Gy IR and harvested 2 hours later. Protein extracts were subjected to increasing concentrations of salt and nuclease treatments to separate extracts into fractions of increasingly compacted chromatin. Under conditions of no IR, KAP-1 and HDAC1 protein levels were similar between WT and Artemis MEFs. Importantly, KAP-1 was only soluble in the chromatin enriched C3 protein fractions. Similarly HDAC1 was only found in increasingly compacted chromatin fractions (C2 and C3). Importantly the same volume of histones were collected between WT and Artemis MEFs for each fraction as monitored by Histone H3 (Figure 5.5). Strikingly, 8 hours after 40 Gy IR, KAP-1 remained dissociated from nuclease resistant fractions prepared from Artemis MEFs, whereas WT cells had re-established WT levels of KAP-1 association (Figure 5.5). This result suggested that Artemis dependent DSBs are located at KAP-1 enriched heterochromatin and that delayed DSB repair dependent on Artemis prolongs chromatin relaxation.

1.37.5 KAP-1 knockdown does not relieve the dependency for Artemis in DSB repair.

ATM is known to phosphorylate the heterochromatic building factor, KAP-1. Following reports that phosphorylation of KAP-1 by ATM results in global chromatin relaxation (Goodarzi et al., 2008; Ziv et al., 2006), it has been postulated that this relaxation may facilitate access to DSB's that would otherwise remain inaccessible. Artemis and ATM deficiency cause epistatic repair defects and both function in the slow repair component of NHEJ. Therefore, it is possible that Artemis, like ATM, may play a role in chromatin relaxation. To test this, I examined whether Artemis-dependent repair was alleviated by KAP-1 knockdown using the siRNA in 48BR (WT) and CJ (Art) hTERT human cells. To confirm successful knockdown, cells were stained for KAP-1 and γH2AX (Figure 5.6). Following KAP-1 knockdown (Figure 5.7), the Artemis-dependent repair fraction was not alleviated. This suggested that Artemis, unlike ATM, does not play a direct role in heterochromatic modulation that is associated with KAP-1 phosphorylation. To confirm functionally successful siRNA mediated knockdown of KAP-1, 48BR (WT) and CJ (Art) hTERT cells were transfected with KAP-1 siRNA and treated with ATMi inhibitor (ATMi) 30 minutes before IR. The ATM-dependent repair defect of A-T cells is known to be relieved by siRNA mediated knockdown of KAP-1 (Goodarzi et al., 2008). Therefore, if siRNA mediated knockdown of KAP-1 is successful, hTERT cells treated with ATMi and KAP-1 siRNA should show a phenotype similar to cells transfected with KAP-1 siRNA only. If, however, KAP-1 siRNA mediated knockdown is unsuccessful, 48BR (WT) hTERT cells will have a repair defect which is phenotypically similar to A-T cells i.e. a 10-20% DSB repair fraction that remains un-repaired after 24 hours post IR. Following KAP-1 siRNA transfection in combination with ATMi, both 48BR (WT) and CJ (Art) hTERT cells showed a phenotype which was comparable to cells treated with KAP-1 siRNA only (Figure 5.7). 48BR (WT) hTERT cells showed no increased repair fraction after 24 hours following 3 Gy IR compared to untreated cells. Therefore it can be concluded that siRNA mediated knock down of KAP-1 was successful.

1.37.6 KAP-1 or HDAC1 and HDAC2 knockdown also does not alleviate the DSB repair defect of Artemis defective mouse embryonic fibroblasts (MEFs).

To confirm our findings obtained with KAP-1 siRNA in human cells, I repeated these experiments in mouse embryonic fibroblasts (MEFs). Knockdown was verified by immunofluorescence (Figure 5.8), and γH2AX foci were scored specifically in KAP-1 depleted cells. As expected, the Artemis dependent DSB repair defect was not alleviated following KAP-1 knockdown in Artemis defective mouse cells. To further consolidate this result, the histone deacetylases 1 and 2 (HDAC1 and HDAC2) were also knocked down. Histone deacetylases are a class of enzymes that remove acetyl groups from histone tails. Removal of these acetyl groups re-establishes the binding between the negative DNA phosphate backbone and positive histone tails, and is often associated with transcriptional silencing. HDAC1 and HDAC2 also act as a component of NuRD chromatin remodelling complex and a subunit of which interacts with KAP-1 to initiate transcriptional silencing (Feng and Zhang, 2003). γH2AX foci were scored specifically in cells successfully knocked down for HDAC1 and HDAC2 (Figure 5.9).The Artemis dependent repair fraction persisted following knockdown, therefore, heterochromatic relaxation, via knockdown of HDAC1 and HDAC2, was also unable to relieve the repair defect associated with Artemis defective cells.

1.38 Discussion

1.38.1 The role of Artemis in ATM dependent DSB repair

ATM and Artemis are required for a subset of DSB repair that occurs with slow kinetics by NHEJ in G0/G1 phase (Riballo et al., 2004). In this chapter, I focused on addressing the role of Artemis in ATM dependent DSB repair following IR. I demonstrate that DSBs that persist in the absence of Artemis localize to dense DAPI staining chromocenters and that Artemis dependent repair foci localize with heterochromatin associated repair foci, such as pKAP-1 foci. Moreover, Artemis dependent DSBs were found to be associated with roughly 4 times more histone H3 K9 trimethylation (a heterochromatic marker) than repair fractions with stochastically incurred DSBs. Additionally, KAP-1 remains dissociated from chromatin enriched fractions for longer in Artemis defective cells compared to WT. These results suggest that Artemis dependent DSBs in

G1 reside at HC regions, and incomplete repair of these DSBs promotes the dissociation of KAP-1 and presumably HC relaxation at these DSBs for longer. However, unlike ATM deficient cells, perturbing the heterochromatin structure through KAP-1 or HDAC1/2 knockdown does not alleviate the dependency of Artemis in DSB repair.

The data thus far suggests that Artemis is unlikely to function like ATM to induce heterochromatic relaxation, and is likely to function downstream of this process. Given that Artemis is known to function during V(D)J recombination to remove hair-pin intermediate structures, and DSBs dependent on Artemis for repair do appear to associate with heterochromatin, I therefore propose that the repetitive nature of heterochromatic DNA may have a higher dependency on Artemis for repair to relive secondary structures or hairpins that form at damaged termini. Given that Artemis can cleave a variety of end substrates (Ma et al., 2002) it is possible that other nucleases which are more substrate specific cannot recognise these complex structures as substrates. Therefore heterochromatin associated DSBs could possibly have a specificity for Artemis over other nucleases. A related endonuclease known as Apollo, functions at repetitive telomeric DNA to generate a protective 3' ss overhang at leading strand telomeres after replication to prevent NHEJ of telomere ends. It is possible that Artemis endonuclease activity functions at other repetitive regions elsewhere in the genome. Repair of DSBs by HR in G2 requires the known HR proteins, BRCA2, Rad51 and Rad54, and also Artemis and ATM (Beucher et al., 2009). The dependency for ATM in G2 is relieved by KAP-1 knockdown, suggesting that repair by HR in G2 is associated with HC DSBs. The requirement for Artemis is reliant on it's nuclease function. However not all HR associated repair is dependent on Artemis, because spontaneous SCEs and I-Sce1 induced HR repair do not require Artemis, therefore resection can occur without Artemis. These results suggest that Artemis is required for early steps of HR repair to function as an endonuclease possibly during processing which is necessary to enable resection of IR induced DSBs. Highly repetitious DNA sequences, such as centromeric satellite repeats, have been shown to from hairpins (Oritz-Lombardia et al., 1998). Additionally, repeating DNA units in disease genes, such as those found in Alzheimer's disease, are also capable of forming hairpins (Gacy et al., 1995). A model has been proposed that Artemis is required to remove secondary structures which arise as HC DSBs that might be refractory to resection in G2. I propose that in G1, Artemis carries out a similar function to remove structures refractory to DSB repair by NHEJ. Future approaches to address Artemis's function in DSB repair will likely be based on identifying the end structure or lesion which is dependent on Artemis processing.

Chapter 6: Analysis of G2/M checkpoint arrest after heavy ion irradiation

Heavy ions

1.39 Introduction

Charged particle radiotherapy using protons and heavier ions was first proposed for clinical application by Robert Wilson in 1946 (Wilson, 1946). In the early 1950s, the clinical use of proton and helium ion beams was first initiated at the Lawrence Berkeley National Laboratory in the United States. In Japan, the decision was made in 1984 to build the Heavy Ion Medical Accelerator in Chiba (HIMAC) at the National Institute of Radiological Sciences (NIRS). The accelerator complex was completed by the end of 1993. A year later clinical studies with carbon ions for cancer therapy were initiated, and to date more than 5196 patients have been treated with Carbon ions (Okada et al., 2010). Currently the availability of heavy ion radiotherapy (RT) is limited. Worldwide only 3 facilities offer Carbon ion RT: two hospital based facilities in Japan, the HIMAC and the Hyogo Ion Beam Medical Center (HIBMC), and a physic research facility at Gesellschaft fur Schrrerionedforschung Institute (GSI), Darmstadt in Germany. At the HIMAC a number of studies are ongoing using RT treatments of tumors of the head and neck, prostate, lung, liver as well as sarcomas of soft tissue and bone carcinomas. Patients are treated in 3 different treatment rooms, which are equipped with a vertical beam line, a horizontal beam line and the third with a vertical and a horizontal beam line.

Exposure to heavy ions also occurs naturally during space exploration. Space travel encompasses exposure to a broad spectrum of radiation ranging from infrared rays to galactic cosmic rays (GCR). GCR are composed of protons (85%), alpha particles (14%) and highly energized protons and iron nuclei (Simpson & Shapiro, 1983). Developments of efficient

countermeasures are key issues for manned space exploration. Therefore a better understanding of how cells respond to heavy ion irradiation is important for both radiotherapy and space exploration. In this chapter I will focus on how the G2/M checkpoint responds following irradiation with Carbon and Iron (Fe) ions. Also I will establish how many heavy ions induced DSBs are required to maintain G2/M checkpoint arrest.

1.39.1 Linear energy transfer (LET)

Various types of ionizing radiation exist such as those produced by radioactive decay (such as γ rays), particle accelerators (such as X-rays and Carbon ions) and those found in cosmic rays (such as Fe ions). When radiation is absorbed in biological material, ionizations and excitations occur that are not distributed at random but are localized along the tracks travelled by the individual charged particles in a pattern that depends on the type of radiation. X-rays are fast moving electrons with very small mass and are said to be sparsely ionizing. Densely ionizing radiations such as Carbon and Fe ions have a greater biological effectiveness than sparsely ionizing X-rays or γ rays. Because heavy ions are densely ionizing they are described as having a high linear energy transfer (LET). LET is the energy transferred per unit length of a track, and is a measure of the energy transferred to material as an ionizing particle travels through it. LET is measured in Kiloelectron volt per micrometer (KeV/µm) of unit of density material (see table 6.1 for X-ray, Carbon ions and Fe ions LET values). Therefore high LET ionizing radiations deposit energy in high density pockets along its trajectory track. Complex DSBs are those described as having damaged bases or sugars at damaged end termini or with multiple damaged sites in close proximity (Goodarzi et al., 2008; Riballo et al., 2004). Simple DSBS are those with directly ligatable damaged ends which are sparsely distributed. Heavy ions can produce a complex mixture of both low and high complexity DNA damage. The complexity of DNA damage has been shown to increase with increasing LET values (Anderson et al., 2010) (See 6.1.4 for further discussion on clustered DNA damage). Moreover the generation of small DNA fragments induced after IR also increases with increasing LET (Lobrich et al., 1996). In addition to the direct track of ionization from a high LET particle, δ rays also emanate from the

main track. δ rays produce simpler DNA damage similar to X-rays (Cucinotta et al., 1998). High LET produces more complex irreparable DSBs, and as a result a greater biological consequence than compared to X-rays.

1.39.2 Relative biological effectiveness (RBE)

Absorbed dose is a measurement of the energy absorbed per unit mass of tissue, and is expressed in units of Gy or Rad. Despite giving the same dose, equal doses of different types of radiation do not produce equal biological effect. For example 1Gy of Fe ions produces greater biological effect than 1 Gy of X-rays. The difference lies in the energy deposition, whether it is sparsely as for X-ray or densely as for heavy ions. Consequently, heavy ions have high relative biological effectiveness (RBE). High LET produces more complex slowly repairing and possibly irreparable DSBs, which result in a greater biological consequence in comparison to X-rays. Analysis of chromosome break rejoining by premature chromosome condensation (PCC) analysis showed that rejoining decreases with increasing complexity (Kawata et al., 2001a; Kawata et al., 2001b; Kawata et al., 2001c) again likely contributing to the high RBE of heavy ion irradiation. For radiation with optimal LET of 100 KeV/μm, the average separation between ionizing events is similar to the diameter of the DNA double helix (2 nm). At this dose, the IR track can most sufficiently produce DSBs in a single track. RBE depends on the radiation quality (LET), radiation dose, dose rate and the biological system or end point.

1.39.3 Braggs peak

The advancement in Carbon ion radiotherapy was not only a consequence of their greater RBE but also because unlike X-rays, Carbon ions do not deposit their maximum energy on contact with skin. Instead Carbon ions are capable of penetrating through tissue to deposit their maximum radiation dose to a given point in the body. This is because charged particles slow

down as they travel through a material as a result of electromagnetic interactions (forces that cause the interactions between electrically charged particles). The slower they move, the more efficient they are at ionizing atoms in their path and the more likely they are to interact with atomic nuclei. This means that the highest radiation dose is delivered at the point in the body at which they stop - the so-called Bragg peak - while the dose elsewhere is low (Figure 6.1). Carbon ions have a sharp Bragg peak (a pronounced rise in energy deposition of radiation during its travel through matter); with a steep dose fall off downstream. This is particularly useful because tissue surrounding the tumor will not be hit by radiation. Before treating a patient, radiation oncologists identify the precise location of the tumour by imaging it. This is often done using modern imaging techniques such as - X-ray computed tomography (CT), magnetic resonance imaging (MRI) or positron emission tomography (PET). The energy of the Carbon ion beam is then adjusted to match the tumour depth. Moreover the Bragg peak can be modulated into a plateau that deposits a high dose of radiation throughout the depth of the tumour, known as a spread out Bragg peak (SOBP). A SOBP is normally achieved by magnetics which scatter the beam to a defined field. Because the human body has effective repair mechanisms, it can tolerate some collateral damage. And since cancer cells often divide more rapidly than healthy cells and so are particularly vulnerable to DNA damage – targeted DNA damage at the tumor is often successful in destroying the tumor.

1.39.4 Clustered DNA damage

Clustered DNA damage was first described by Ward as locally multiple damaged sites (LMDS) which describes several closely spaced damages within a short DNA segment (Ward, 1981). Clustered DNA lesions were proposed to account for the increased lethality induced by IR, which cannot be fully explained by the amount of DSBs formed. IR induces DNA damage by direct ionization and through generation of hydroxyl radicals that attack DNA. Two or more DNA lesions of the same or different nature may be produced in close proximity to each other on opposite DNA strands. To establish the complexity of DNA damage that is produced after heavy ion IR, Michael Huels and colleagues at the University of Sherbrooke decided to look into this issue in more detail. They fired low-energy ions onto a film of biomolecules in an ultrahigh vacuum and analyzed the ions that desorb from the film with a mass spectrometer.

The results showed that the initial damage caused by the ions at their track ends is significantly more complex, clustered and lethal than that induced by X- or gamma-rays (Deng et al., 2006). Severe damage can be caused by energies as low as 0.25 eV per nucleon -- which is very low when compared with the energy of a typical heavy-ion beam. Using the Monte Carlo algorithm Semenenko & Stewart, established that Low LET radiations can create clusters with as many as 10 lesions (Semenenko and Stewart, 2004), and ~30% of DSBs after low energy electrons are expected to contain clustered DSBs (Nikjoo et al., 1997). High LET is capable of producing damage with up to 25 lesions per cluster(Semenenko and Stewart, 2004), and ~70% of DSBs after high LET particles are expected to be clustered (Nikjoo et al., 1997). Local clustered DNA damage is expected to be more prone to misrepair, and therefore could account for the higher RBE associated with increasing LET values.

1.39.5 Heavy ions

High LET radiations are a critical component of space travel and are increasingly being used as an alternative for radiotherapy during cancer treatment. Heavy ions can be forced to deliver a much greater dose to the tumor while sparing normal tissue (Halperin, 2006). Newer than protons on the particle-therapy scene is ion therapy. Heavy ions, such as carbon, have a higher RBE than protons and are thought to provide more effective treatment for certain, deep-seated tumours that are often "radioresistant". This is because the rate at which a charged particle loses energy in a material - which is quantified by its linear energy transfer (LET) - increases with the mass of the particle.

1.39.6 Aims of this chapter

Previous analysis of DSB repair after heavy ion irradiation has been monitored by PCC in G1 which showed slower rejoining following irradiation with heavy ions compared to X-rays

(Okayasu et al., 2006). Recently high resolution microscopy has been used to analyze γH2AX foci after vertical Fe ion irradiation, which is a more sensitive DSB assay able to monitor DSB repair in individual cells and at physiologically relevant doses (Nakajima et al., manuscript submitted). However vertical irradiation can be problematic as not all underlying γH2AX foci in a track can be identified, therefore there is potential to underestimate the number of γH2AX induced. To overcome this issue, in this chapter I have analyzed DSB repair after horizontal Fe ion irradiation. After horizontal irradiation it is possible to identify all DSBs in a track by using γH2AX as a biomarker for DSB repair.

DSB complexity increases with radiation ionization density (Anderson et al., 2010). Therefore heavy ion irradiation is expected to produce DSBs with various complexities and clustering. The speed of repair after heavy ion irradiation has been shown to be determined by cluster complexity (Nakajima et al., manuscript submitted). The rate of repair has also been shown to directly influence the duration of checkpoint arrest (Shibata et al., 2010). Given that heavy ion irradiation induces complex clustered DNA damage, in this chapter I wished to address whether heavy ion induced DNA damage would maintain a prolonged G2/M checkpoint arrest. Additionally I wanted to establish how many clustered DSBs would be required to maintain G2/M checkpoint arrest.

1.40 Results

1.40.1 Fe ion induced DSBs are repaired with slower kinetics than X-ray induced DSBs.

Heavy ion irradiation is known to induce DSBs that are more complex and clustered in comparison to X-ray. This is because heavy ions have a higher LET in comparison to X-rays, meaning the rate of energy loss along a heavy ion ionizing trajectory is denser than compared to lower LET sources such as X-rays. The nature of heavy ion induced DSB repair is largely unknown. Given that the DNA damage induced after heavy ion irradiation is more complex than that after X-ray, it is unknown whether the rate of repair is slower after heavy ion irradiation when using γH2AX as a monitor for DSB repair. To address this question I first selected a method of radiation which was optimal for γH2AX analysis. At the NIRS HIMAC facility, there are two directional methods available for administering heavy ion irradiation,

these being either horizontal or vertical (Figure 6.2). Vertical irradiation is problematic as underlying foci in an ionizing track can be missed when scoring foci, therefore an underestimation of the number of γH2AX in a track is possible. However, irradiating at low doses vertically ensures all cells are hit with the ion beam. Horizontal irradiation is problematic at lower doses IR because not all the cells in a sample are hit with the beam, and the variation in damaged induced between hit cells is large. However, irradiating horizontally enables all foci to be visualized in a track, which allows for a more accurate quantification of the number of DSBs induced. Taking these points into consideration, horizontal irradiation was selected because as mentioned above, all DSB foci can be visualized. To analyze γH2AX foci after horizontal Fe IR, 1BR hTERT cells were irradiated with either 1 Gy X-ray or 1Gy horizontal Fe ion IR, fixed at indicated time points after IR, and immunostained for γH2AX, CENP-F (G2 phase marker) and DAPI. γH2AX foci were counted in G1 phase cells. Because of the variation in damage induced between cells after horizontal Fe ion IR (Figure 6.3), to quantify DSB repair foci numbers were normalized to the 1 hour time point. As expected, DSB repair after Fe ion irradiation was greatly reduced in comparison to X-ray (Figure 6.4), with ~65% of DSBs still remaining 8 hours after Fe ion IR. At the equivalent time point after X-ray only ~10% of DSBs remained unrepaired. 24 hours post irradiation, more than 95% of DSBs had been repaired after X-ray, whereas only ~55% after Fe ion IR. I next analyzed DSB repair in G2 phase cells under the conditions described above. In G2 phase, very little repair was observed after Fe ion IR, with ~70% of DSBs remaining unrepaired up until 24 hours (Figure 6.5). In G2 phase, both NHEJ and HR can function to repair DSBs. NHEJ repairs DSBs with faster kinetics compared to HR (Beucher et al., 2009; Shibata et al., 2010). Therefore the slower repair kinetics observed after Fe ion IR in G2 is likely because complex lesions such as those produced after heavy ion irradiation are being repaired by HR (Shibata et al., 2011).

1.40.2 Heavy ion irradiation initiates G2/M checkpoint arrest at lower doses IR in comparison to X-ray.

As discussed in chapter 3, while ATM is a very sensitive DSB response kinase, its role in G2/M checkpoint activation requires a minimum number of DSBs i.e. 15-25 DSBs are required to initiate and maintain checkpoint arrest (Deckbar et al., 2007). Since heavy ion irradiation

induces DNA damage which is clustered and complex, I wished to determine whether lower doses of heavy ion IR could initiate a G2/M checkpoint arrest in comparison to X-ray. 1BR hTERT or 48BR primary cells were irradiated with either X-ray, Fe ion (horizontal or vertical) or Carbon ion irradiation at various doses of IR. Prior to IR cells were treated with aphidicolin, a replication polymerase inhibitor which prevents S phase cells progressing into G2 phase during analysis. One hour after treatment, cells were fixed and immunostained for serine 10 phosphorylated histone H3 (pH3). pH3 is a biomarker for mitosis, which can be used to identify mitotic cells from an asynchronous population (Ajiro et al., 1996). The number of mitotic cells were counted and normalized to the unirradiated control. Irradiating cells with 0.25 Gy X-ray (which is roughly 10 DSBs in G2) resulted in ~30% of the cycling 1BR hTERT cell population arresting in G2 (Figure 6.6). An equivalent dose after Carbon ion irradiation resulted in ~55% of cycling 48BR primary cells arresting in G2. The same dose after both horizontal and vertical Fe ion irradiation resulted in roughly 90% of the cycling 1BR hTERT cell population arresting in G2, with only 10% of cells still progressing into mitosis. Of note, quantification of the mitotic population after horizontal Fe IR was calculated to take into consideration non-hit cells. Similarly, after 0.5 Gy IR, ~95% of cells were arrested after heavy ion irradiation, but only 50% after X-ray. These results demonstrate that heavy ion induced DNA damage can initiate a G2/M checkpoint arrest at lower doses IR compared to X-ray. A mentioned in the introduction, equal doses of different types of radiation do not produce equal biological effect. Therefore high LET ionizing radiations would be expected to produce greater biological effect than lower LET ionizing radiations at equivalent doses.

1.40.3 Heavy ion induced DNA damage maintains a prolonged G2/M checkpoint arrest.

1.40.3.1 Horizontal Fe ion irradiation

Having demonstrated that after Fe ion irradiation DSB repair is extremely slow in comparison to X-ray in G2 (Figure 6.5), I next wanted to address what impact slow repair kinetics had on G2/M checkpoint maintenance. Additionally I wanted to establish how many Fe ion induced DSBs were required to maintain G2/M checkpoint arrest. To test this, 1BR hTERT cells were

irradiated with either 1 Gy X-ray or 1 Gy horizontal Fe ion irradiation. Prior to IR, cells were treated with aphidicolin, a DNA polymerase inhibitor, which prevents S phase cells progressing into G2. Every subsequent 24 hours after IR, aphidicolin was re-added to the samples. Cells were harvested at indicated time points after IR and immunostained for pH3, CENP-F, γH2AX and DAPI. This enabled me to monitor both mitotic index and the number of DSBs remaining at each time point. As mentioned earlier, horizontal irradiation doesn't hit all cells and the variation in DNA damage between each cell is large. Therefore when scoring mitotic cells after horizontal IR, it was not possible to distinguish between non-hit cycling mitotic cells and hit mitotic cells that were released from the G2/M checkpoint. Since non-hit cells remained cycling, full checkpoint arrest was not observed after horizontal Fe ion IR (Figure 6.7). To establish how many Fe ion induced DSBs/clusters are required to maintain checkpoint arrest I scored γH2AX foci in mitotic cells rather than G2 phase cells. This was because if a mitotic cell contained γH2AX foci at later time points after IR I could be sure that this cell was a hit G2 phase cell now released into mitosis. After 16 hours recovery following 1 Gy horizontal Fe IR, mitotic cells containing γH2AX foci had on average 7 γH2AX clustered foci (Figure 6.7 & 6.10). This resulted indicated that ≥7 clustered γH2AX foci induced after Fe ion irradiation are required to maintain G2/M checkpoint arrest. Analysis of the G2 phase cell population indicated that after Fe ion irradiation depletion of G2 phase cells is slower than after X-ray (Figure 6.7). This result implies that DSB repair is slower after Fe ion irradiation as previously shown (Figure 6.4 & Figure 6.5).

1.40.3.2 Vertical Fe ion irradiation

To establish whether cells maintain a prolonged checkpoint arrest after heavy ion irradiation, I next irradiated vertically with Fe ion. 1BR hTERT cells were irradiated with 1 Gy X-ray or vertical Fe ion IR. Prior to irradiation, cells were treated with aphidicolin to prevent S phase cells progressing into G2. Cells were fixed at indicated time points after IR and immunostained for pH3, CENP-F, γH2AX and DAPI. After vertical Fe ion IR, all cells are hit. Therefore, a full checkpoint arrest was observed (Figure 6.8C). Cells irradiated with X-rays began to release from the G2/M checkpoint 4 hours after IR, with around ~30% of cells reentering mitosis. Fe ion irradiated cells were still completely arrested at the G2/M checkpoint 4 hours after IR. A

full checkpoint release was observed 8 hours after X-ray, implying that the DSB induced DDR signaling was below the threshold of 15-25 DSBs. Fe ion irradiated cells emerged from the G2/M checkpoint 16 hours post IR; however at this time point only ~30% of cells had started to recycle. This result implied that Fe ion induced DSBs maintain a prolonged checkpoint arrest. It was also important to establish that at later time points after IR there are still sufficient G2 phase cells remaining to enter mitosis. Scoring CENP-F positive staining cells (G2 phase marker) revealed that the G2 phase population was only marginally reduced after Fe ion irradiation compared to X-ray irradiation. This result implied that after Fe ion irradiation some of the DNA damage is irreparable and some cells remain permanently arrested (>16 hours). To establish how many Fe ions IR induced DSBs were required to maintain arrest, γH2AX foci clusters were scored in mitotic cells at 16 and 24 hours after IR. At 16 hours after IR, mitotic cells contained on average ≥ 6 clustered γH2AX foci (Figure 6.8 & 6.10). This resulted implied that at least 7 clustered γH2AX foci are required to maintain G2/M checkpoint arrest after Fe ion irradiation.

1.40.3.3 Carbon ion irradiation

I next analyzed G2/M checkpoint arrest after Carbon ion irradiation. 1BR hTERT cells were irradiated with 1 Gy X-ray or 1 Gy Carbon ions. Prior to irradiation cells were treated with aphidicolin to prevent S phase cells progressing into G2 during analysis. Cells were fixed at indicated time points post IR and immunostained for pH3, CENP-F, γH2AX and DAPI. Carbon ion irradiated cells remained completely arrested 4 hours after IR, whereas 30% of cells irradiated with X-rays had already started to recycle at this time point (Figure 6.9). A staggered checkpoint release was observed between 8 and 24 hours after Carbon ion irradiation, whereas X-ray irradiated cells were observed to have a sharp peak in checkpoint released cells at 8 hours post IR. This staggered release after Carbon ions could reflect different lesions with varying complexity repairing at different rates. Around 60% of cells irradiated with Carbon ions were able to reenter mitosis which was distinct to only 30% of cells after Fe ion irradiation. Carbon ions have a lower LET value compared to Fe ions (See table 6.1). Consequently the DNA damage produced after Carbon ions is less complex and expected to be easier to repair. This might explain why cells are able to release from the G2/M checkpoint after carbon ions but less so after Fe ions. To establish how irradiated cells were progressing through the cell cycle,

G1 (CENP-F negative), S (pan-nuclear γH2AX) and G2 (CENP-F positive) cells were scored. From this analysis it appeared that cells released from the G2/M checkpoint progressed through G1 phase slowly (Figure 6.9). Despite NHEJ being a fast repair pathway, slower repair kinetics have been observed if the DNA damage is clustered (Nakajima et al., manuscript submitted). To establish how many clustered DSBs were required to maintain G2/M checkpoint arrest after Carbon IR, γH2AX foci were scored in mitotic cells at 16 and 24 hours post IR. 16 hours after IR, mitotic cells contained around 6-7 clustered γH2AX foci (Figure 6.9 & 6.10). This result implied that at least 7 Carbon ion clustered γH2AX foci are required to maintain G2/M checkpoint arrest.

1.41 Discussion

Analysis of DSB repair after heavy ion irradiation has predominantly been monitored by PCC analysis, a technique which involves the fusion of mitotic cells with interphase cells. Fusion induces the immediate condensation of the interphase chromatin into discrete chromosomes resembling compacted mitotic chromosomes. However this technique is limiting because physiologically relevant doses of IR cannot be used. Here I have employed a more sensitive DSB biomarker, γH2AX, to monitor DSB repair in both G1 and G2 phase of the cell cycle and at physiologically relevant doses of IR. As expected the rate of DSB repair was greatly reduced after Fe ion IR compared to X-rays in both G1 and G2 (Figure 6.4 & 6.5). Interestingly repair of heavy ion induced DSBs in G2 phase was extremely reduced with as little as 10% repair 24 hours post IR (Figure 6.5). Given that in G2 phase both NHEJ and HR can function to repair DSBs and that HR is a slower repair mechanism (Beucher et al., 2009; Shibata et al., 2010), I propose that complex clustered DSBs induced by Fe ions are predominantly repaired by HR in G2. In line with this, >80% of G2 phase heavy ion induced DSBs have been observed to co-localize with RPA foci (Jeggo laboratory, unpublished finding). It would be of interest to establish whether there is an absolute requirement for heavy ion induced DSBs to be repaired by HR in G2 by using a HR deficient cell line. However heavy ion induced DSBs in G1 have recently been shown to be predominantly repaired by NHEJ (Nakajima *et al*, manuscript submitted). Therefore if heavy ion induced DSBs do not produce end termini which are sufficiently single stranded to mediate RPA binding without the necessity of resection; it is

likely that G2 phase heavy ion induced DSBs could be repaired by NHEJ in G2, but this requires further consolidation.

The activation of ATM has been shown not to strictly correlate with the phosphorylation of Chk2 (Buscemi et al., 2004). Fewer DSBs are required to activate ATM than Chk2, which was indicative of a threshold of DDR signaling being required to initiate G2/M checkpoint arrest. Later it was shown that a threshold of between 15-25 DSBs is required to initiate and sustain G2/M checkpoint arrest (Deckbar et al., 2007). Given that heavy ion irradiation produces DSBs with increased end complexity and clustering, I wished to address whether these complex clustered DSBs would either generate more DDR signaling than a typical X-ray induced γH2AX foci or whether the clustering of foci would impede DDR signaling. Analysis of cells arresting at the G2/M checkpoint following IR with low doses of heavy ions revealed that cells were able to checkpoint arrest at doses as low as 0.25 Gy, whereas after X-rays, cells do not respond until doses of at least 0.5 Gy (Figure 6.6). This result indicated that heavy ion induced DSBs are able to signal sufficiently to activate a full DDR which is capable of activating a full checkpoint arrest. Therefore DSBs in close proximity (clusters) can still proficiently signal to the checkpoint machinery and fewer clustered γH2AX foci are required to initiate checkpoint arrest than compared to individual foci.

Maintenance of checkpoint arrest is directly correlated with the rate of DSB repair (Shibata et al., 2010). Therefore a greater persistence of a fraction of DSBs after exposure to high LET radiation would be expected to maintain a prolonged G2/M checkpoint arrest. Indeed analysis of G2/M checkpoint release showed that after heavy ion IR, irradiated cells were arrested for at least a further 2 hours compared to X-rays (Figure 6.7, 6.8, & 6.9). After Fe ion irradiation only ~30% of cells enter mitosis before 8 hours, whereas 100% of cells enter after X-ray (Figure 6.8). The difference in checkpoint release between Fe ions and X-rays could be explained by the different LET values between the two types of IR. The high LET value of Fe ions means DSBs induced are highly clustered and are likely to be difficult to repair. It has been suggested that clustered DSBs could be resistant to processing by glycosylases or endonucleases, as shown for synthetic oligonucleotides containing clusters of specific compositions or configurations (Lomax et al., 2004). Repair resistant clusters could persist for a substantial time after IR (Tsao et al., 2007). The greater persistence of a fraction of DSBs after exposure to high LET radiation is likely related to their increased complexity. Carbon ion irradiated cells also maintained checkpoint arrest for a further 2 hours more than cells irradiated with X-rays. When cells were released 8 hours after IR with Carbon ions, up to 60%

of cells were capable of reentering mitosis, which contrasted to only 30% of cells after Fe ions. This result likely reflects differences in energy deposition (LET) between Carbon and Fe ions. Fe ions deposit nearly twice as much energy per unit track compared to Carbon ions. Therefore DSBs induced after Fe ions would be expected to be more complex and clustered than Carbon ion induced DSBs. Therefore repair of Fe ion induced DSBs would be expected to be less efficient compared to Carbon and therefore checkpoint arrest maintained for longer. As mentioned previously, 15-25 DSBs are required to maintain checkpoint arrest after low LET radiations such as γ rays or X-rays. After higher LET radiation around 7 clustered DSBs were required to maintain G2/M checkpoint arrest (Figure 6.7, 6.8, & 6.9). On average each clustered DSB contains ~5 γH2AX foci 16 hours after IR with heavy ions. Therefore 7 clustered DSBs at 16 hours after IR would be expected to contain 35 single γH2AX foci. Therefore in consideration of individual foci, single γH2AX foci are able to activate the DDR more sufficiently than compared to clustered foci to maintain G2/M checkpoint arrest. Clinically this is very important because cells still manifesting up to 7 clustered DSBs can be released from the G2/M checkpoint and progress into mitosis. In conclusion, heavy ion induced DSBs are repaired with slow kinetics which is related to their increased complexity. These DSBs maintain a prolonged G2/M checkpoint arrest and some cells with irreparable DSBs remain arrest for more than 96 hours after IR. Therefore the duration of G2/M checkpoint arrest increases with increasing LET values.

1.41.1 Implications for heavy ion radiotherapy

Late effects of high LET are arguably a health risk for both space exploration and cancer patients undergoing heavy ion radiotherapy. Unrepaired DNA lesions such as those observed in response to Fe ions, would presumably result in persistent DNA damage signaling culminating in senescence and apoptosis, both processes constituting both bone fide barriers to carcinogenesis (Bartkova et al., 2006). One interesting point is whether cells in senescence evade cell death by remaining arrested, then at later times after IR re-enter G1 phase and begin recycling. This is of particular importance when considering whether senescent cancer cells can re-enter the cell cycle after radiotherapy. A recycling cancer stem cell which evaded death would then be able to repopulate a cancer tumor cell population thereby re-establishing

the cancer. Also a senescent cell population has the ability to alter its microenvironment through paracrine signaling (Ewald et al., 2008). These secretions can alter and adapt neighboring cells inducing them to divide. This has the potential to stimulate un-regulated cell growth and ultimately cancer. Therefore cells manifesting irreparable heavy ion induced clustered DSBs, have the potential to enter senescence and at a later time induce cellular changes which could lead to cancer.

Chapter 7: Discussion

Discussion

1.42 Major aims

Whilst the majority of DSB repair is ATM dependent, a subset of slow repairing DSBs, representing those located at regions of heterochromatin require ATM and the mediator proteins (Goodarzi et al., 2008; Riballo et al., 2004). Heterochromatin poses a barrier to DSB repair which is now known to be relieved by ATM dependent phosphorylation of the heterochromatin building factor KAP-1 (Goodarzi et al., 2008). This process requires the tethering of ATM at the DSB via a 53BP1-dependent process to achieve localized and concentrated KAP-1 phosphorylation (Noon et al., 2010). Chromatin configuration has been demonstrated to also affect the magnitude of DDR signalling. Previous studies have shown that an overall reduction in chromatin structure following depletion of the linker histone H1 enhances the strength of the DDR (Murga et al., 2007). However the effect of HC superstructure specifically on DDR signalling has yet to be investigated. This is of particular importance because human syndromes exist which have disordered heterochromatin. One major aim of my thesis was to investigate how HC influences damage response signalling focussing on the impact of disordered HC found in human syndromes.

The fraction of DSBs that remain unrepaired in the absence of ATM also require the endonuclease Artemis. This initial model proposed that a requirement for Artemis correlated with damage end complexity (Riballo et al., 2004). However, induction of more complex DSBs such as those after Carbon-K X-rays did not increase the dependency for Artemis in DSB repair (Goodarzi et al., 2008). My next aim was to establish whether like ATM, Artemis dependent DSBs are those which reside within HC.

Arrest of the cell cycle at the G2/M checkpoint following DNA damage infliction is a fundamental endpoint for ATM signalling. A threshold of ATM signalling has been defined whereby 10-25 DSBs are required to initiate and sustain checkpoint arrest (Deckbar et al., 2007). From the results obtained in chapter 3 and 4 it became apparent that under conditions where the cellular HC content was reduced, the DDR amalgamating from each DSB was enhanced and consequently the G2/M checkpoint could be arrested when less than the

previously established threshold of DSBs were present. My next aim was to establish what affect increased damage complexity has on G2/M checkpoint arrest. To address this question cells were irradiated with Carbon and Iron heavy ions at the NIRS in Chiba, Japan.

1.43 The impact of higher order chromatin structure on ATM signalling and G2/M checkpoint arrest.

1.43.1 Major conclusions

- Reducing the HC content of a cell by knocking down either: KAP-1, DNMT3B or MeCP2 enhances the rate and size of IR induced γH2AX foci formation at regions of HC.
- ATM signalling is hyperactive in cells deficient for MeCP2 and DNMT3B after IR.
- MeCP2 and DNMT3B deficient cells are capable of initiating a G2/M checkpoint arrest after low doses of IR, which in wildtype cells are insufficient to meet the threshold of DDR signalling normally required to initiate checkpoint arrest.
- Despite responding to DSBs hyperactively, MeCP2 and DNMT3B deficient cells repair DSBs with normal kinetics.
- Like KAP-1 mediated HC relaxation, MeCP2 and DNMT3B knockdown can overcome the requirement for ATM in DSB repair.
- Cells deficient for HC associated factors: MeCP2, DNMT3B or Lamin A, maintain a prolonged G2/M checkpoint arrest.
- Chk1 phosphorylation is hyperactive in MeCP2 deficient cells.
- The signal intensity for RPA foci is enhanced in MeCP2 deficient cells.

1.43.2 ATM dependent DDR in the context of reduced HC organization

1.43.3 γH2AX foci expansion and DDR signalling

In chapters 3 and 4, I demonstrated that by reducing the HC content of a cell the IR induced ATM dependent response to a DSB can be amplified, resulting in greater encroachment of

γH2AX foci into HC regions, faster γH2AX foci formation at HC associated DSBs and a hypersensitive and prolonged G2/M checkpoint arrest. I have shown that HC relaxation also results in increased ATM, Chk2 and Chk1 activation, indicating that by relieving the HC superstructure, IR induced signalling can be enhanced. Importantly DSB repair as monitored by γH2AX foci analysis was normal in HC relaxed cells. Therefore amplified DDR signalling could be not be accounted for by defective DSB repair. In a HC relieved cell one could envision that firstly γH2AX is phosphorylated by ATM. MRN is recruited to γH2AX. Nbs1 binds and 53BP1 indirectly tethers ATM (Noon et al., 2010) at the site of a DSB, resulting in an auto-activatory loop of recruitment and tethering. γH2AX expansion can then spread over megabases at HC regions. As a result, ATM can phosphorylate and activate more Chk2 at the site of a DSB. Therefore, increased foci expansion would lead to increased amounts of pATM localized at DSBs and in turn elevated levels of pChk2. This leads to a more efficient G2/M checkpoint arrest. This can also be applied to checkpoint maintenance, where ATM at the site of a DSB maintains Chk2 phosphorylation. Therefore HC relaxation not only facilitates repair (Riballo et al., 2004), but also assists optimal signalling from these breaks to enhance foci expansion (Figure 7.1).

Loss of HDAC 1 and 2 has previously been demonstrated to result in a hyperactive response to IR induced DSBs (Miller et al., 2010). γH2AX signalling is also enhanced as monitored by western blot in HDAC inhibited cells. Chk1, Chk2 and p53 are likewise increased and sustained for longer in HDAC1 and 2 depleted cells. However, analysis of DSB repair in these cells either by monitoring rejoining of a linearized plasmid or by the neutral comet assay revealed that DSB repair, particularly NHEJ, was reduced in HDAC1 and 2 knockdown cells (Miller et al., 2010). GFP-Ku70 and GFP-Art localized to sites of microirradiation for longer in HDAC inhibited cells (Miller et al., 2010). However this result could fit with chromatin remodelling signalling the end of DSB repair rather than the completion of repair (Polo et al., 2006). Another difference between the results observed with MeCP2 loss and HDAC1/2 loss is that HDAC1/2 cells have a reduced survival rate after IR (Miller et al., 2010), whereas MeCP2 deficient Rett syndrome cells have normal survival after IR. Given that survival after IR is reflective of DSB repair capacity, it is likely that MeCP2, unlike HDAC1/2, does not have a direct role in DSB repair.

CHD4 (Chromodomain helicase DNA-binding protein 4) is an ATPase chromatin remodelling protein that complexes with the NuRD complex and is involved in chromatin remodelling. Knockdown of CHD4 results in an increase of γH2AX as monitored by WB and a

prolonged checkpoint arrest after IR (Polo et al., 2010). CHD4 knockdown cells accumulate p21 in unstressed conditions. IR induced p21 induction was p53 dependent, and was more robust and occurred earlier in CHD4 cells (Larsen et al., 2010). Importantly Rett cells express normal p53 levels, therefore hyperactive checkpoint responses in Rett syndrome cells is unlikely to be a result of endogenously active p53. Larsen *et* al, 2010, reported an increased level of DSBs in CHD4 deficient cells immediately after IR when monitoring damage by PFGE. The authors suggest that HC relaxation following CHD4 loss may result in a chromatin configuration which is more susceptible to IR. Analysis of DSBs by γH2AX foci analysis in KAP-1, MeCP2 and DNMT3B knockdown cells revealed that γH2AX foci form with faster kinetics in these cells but that the number of DSBs induced was similar between knockdown and control cells. Discrepancies between these results may perhaps be a consequence of different assays being used to monitor DSB induction. Here, I have used γH2AX analysis, which is a more sensitive assay compared to PFGE that can be used at lower and more physiologically relevant doses of IR. Nonetheless, CHD4 loss might have a greater impact on chromatin configuration than compared to KAP-1, MeCP2 or DNMT3B loss, and therefore could make chromatin more amenable to DNA damage.

DNA damage complexity and chromatin complexity affect speed of DSB repair, and slowly repairing DSBs undergo resection in G2 (Shibata et al., 2011). After exposure to X-rays, in both G1 and G2 phase, DSB repair proceeds with a fast and slow component. The fast component in G1 represents DSBs which reside within EC regions being repaired by core NHEJ factors. The slow component in G1 represents DSBs that reside within HC which require ATM, Artemis and the mediator proteins, in addition to the core NHEJ factors. In G2, fast repairing DSBs are repaired by NHEJ, and slow component represents repair of HC associated DSBs by HR, which requires resection (Beucher et al., 2009; Shibata et al., 2010). In G2 phase cells, knockdown of CIP does not affect DSB repair kinetics at 0.5 and 2 hours after IR. However DSB repair kinetics at later time points after IR (between 4 and 8 hours) is, surprisingly, accelerated in comparison to control cells (Shibata et al., 2011). This result suggested that by eliminating resection DSB repair is channelled through the faster NHEJ pathway (Shibata et al., 2011). Thus, by preventing resection, which normally occurs at HC regions, repair can be accelerated. From this result, it might be expected that the requirement for resection would be removed in a HC reduced cell because DSBs would be expected to be more accessible and hence faster to repair. Importantly, in the Rett syndrome cells in G2 phase, I observed an enhanced RPA response. This suggests that at HC, even if the time dependent barrier is removed, DSBs at these regions

still undergo resection, suggesting that the same component of the HC barrier remains. Further analysis is required to understand the impact of chromatin structure on resection

It is unclear whether the overall density of compaction or some fine detail of histone positioning is inhibitory to repair and signalling. Other NuRD complex components such as CHD4/Mi-2β and HDAC1/2 have been observed to be recruited to laser track induced lesions at early times (< 15 minutes) and promote re-joining of rapidly repairing lesions. Therefore the remodelling capabilities of these factors are not solely required for the repair of slow repairing HC associated DSBs (Murga et al., 2007; Polo et al., 2006; Riballo et al., 2004). It is possible to speculate that non HC regions may require tightening or additionally nucleosomes may require modification before repair can occur at some or all EC DSBs. Nucleosomes have been shown to act as a barrier to Ku sliding on DNA (Roberts and Ramsden, 2007). It has been suggested that HDAC1 and 2 may restrain unproductive Ku sliding to promote NHEJ (Miller et al., 2010). Therefore a certain chromatin configuration may be required for DSB repair not solely a relaxed one.

1.43.4 The effect of HC protein loss on gene transcription

The impact of heterochromatin relaxation on transcription remains unclear. p53 cell cycle regulation and apoptosis have been shown to be regulated by KAP-1 SUMOylation (Li et al., 2007). KAP-1 SUMOylation is important for recruitment of silencing complex NuRD and the SETDB1 HMT (Ivanov et al., 2007). ATM mediated phosphorylation of KAP-1 on Ser824 is able to inhibit KAP-1 SUMOylation. SUMOylated KAP-1 decreases H3-K9 and H3-K14 Ac and increases H3-K9 methylation at the p21 promoter. KAP-1 binding motifs have been found at a number of genes including gadd45α, bax, puma and noxa (Elkon et al., 2003; Zheng et al., 2000), which are involved in cell cycle regulation and apoptosis. However the on-going requirement for 53BP1 and ATM for HC DSB repair (Noon et al., 2010) suggests that the HC superstructure is not completely abolished and HC associated markers such as tri-methylation remain relatively unchanged Furthermore gross changes to the HC superstructure, KAP-1 mobility or in vivo association with nucleosomes are not evident after IR (Goodarzi et al., 2008; Noon et al., 2010; Ziv et al., 2006). Although these studies do not preclude a highly localized effect below the threshold of detection by these techniques, it seems unlikely that KAP-1

containing HC becomes completely dismantled after ATM phosphorylation. It is more likely that KAP-1 dependent remodelling is sufficient for DSB repair but not adequate to invoke expression of KAP-1 dependent genes. Transcriptional regulation of proteins involved in cell cycle progression, such as p21, by KAP-1 might offer an evolutionary advantage to survival, given that KAP-1 associated DSBs take longer to repair, and therefore require longer checkpoint arrest. Hence, KAP-1 dissociation from a DSB might dictate the length of checkpoint arrest.

The role of DNMT3B in transcriptional regulation is also unclear as previous studies have failed to separate the function of DNMT3B from DNMT31. Previously, depletion of DNMT1 and 3B has been shown to increase transcription of cyclin B2 (Tschop and Engeland, 2007). Cyclin B acts as a central regulator during the G2/M transition of the cell cycle. The down regulation of cell cycle regulators CDC25C and CDK2 after DNA damage in DNMT1-null or DNMT1 or 3B null cells is diminished (Le Gac et al., 2006). Zebularine, a drug that selectively traps and depletes nuclear DNMT1 and 3B, relieves p53 mediated repression of endogenous CDC25C and CDK2 (Le Gac et al., 2006). These results suggest that DNMT3B and or DNMT31 have a regulatory role in turning the G2/M checkpoint off. IP experiments have shown that DNMT1, p53 H3K9me2 and HDAC1 are associated at the CDC25C and CDK2 promoters (Tschop and Engeland, 2007). Therefore it is likely that DNMT31, rather than DNMT3B has a more central role in regulating this promoter. Further work is required to determine the impact of KAP-1, MeCP2 and DNMT3B loss on protein expression profiles.

1.43.5 Implications

Rett syndrome is an X-linked neurological disorder which results from mutations in the MeCP2 gene. Patients typically develop normally until two years of age, thereafter learned skills such as speech and purposeful hand-movements begin to regress. The neurological defects associated with Rett syndrome likely reflect disordered expression of neuronal specific genes as a consequence of MeCP2 loss. MeCP2 controls expression of several genes involved in neuron maturation including brain derived neurotrophic factor (BDNF) (Chen et al., 2003). BDNF is essential for neural plasticity, learning and memory. Following membrane depolarization, calcium ions influx resulting in MeCP2 phosphorylation and release from BDNF

promoter region. As a consequence, BDNF expression is transcriptionally up-regulated (Chen et al., 2003). MeCP2 also functions to regulate distal-less homeobox 5 (DLX5) expression. DLX5 is an important imprinted gene that regulates the production of enzymes that synthesize GABA (γ-aminobutyric acid). GABA is a mammalian neurotransmitter which controls neuron excitability and muscle contraction (Watanabe et al., 2002). DLX5 expression was found to be five times greater in MeCP2 null mice. Similarly, DLX5 imprinting in Rett syndrome lymphocytes is lost (Horike, 2005; Horike et al., 2005). Rett syndrome patients have no increased incidence of cancer. This could possibly be attributable to hypersensitive DNA damage detection which enables G2/M checkpoint arrest to be initiated when less than 20 DSBs are present. Excessive signalling during brain development in response to oxidative stress could potentially interfere with normal brain development. Irregular chromatin organization could account for some of the brain defects associated with Rett and ICF syndrome.

ICF syndrome is a rare autosomal recessive disease characterized by facial dysmorphism, immunodeficiency and irregular centromeric satellite DNA at chromosomes 1, 9 and 16. Immunodeficiency associated with ICF syndrome results after translocations involving chromosome 14, 15 and/or 16 which encode for the human immunoglobin V(D)J segments. In particular translocations often involve chromosome 16 which is disorganized at the centromeric regions in ICF patients as a result of DNMT3B loss. ICF syndrome patients have an increased incidence of cancer, which could be attributable to DNMT3B being involved in centromere chromatin organization, consequently ICF patients have irregular centromeres which makes chromosomal segregation during mitosis prone to error. This leads to genomic instability and chromosomal fragmentation eventually leading to cancer.

1.44The role of Artemis in DSB repair

1.44.1 Major conclusions

- DSBs dependent on Artemis for repair are visibly associated with DAPI dense chromocentres and co-localize with HC associated repair foci such as pKAP-1 foci.
- Artemis dependent breaks reside at regions of HC enriched for TriMeK9 histone H3.
- The dissociation of KAP-1 from chromatin following IR is prolonged in Artemis deficient cells.

- The dependency for Artemis in DSB repair cannot be overcome by KAP-1 or HDAC1/2 knockdown.

1.44.2 Artemis dependent DSBs reside within regions of heterochromatin

ATM and Artemis are required for the repair of a subset of IR induced DSBs (Goodarzi et al., 2008; Riballo et al., 2004). This subcomponent of DSB repair is repaired with slow kinetics and earlier studies suggested that DSB complexity determines the speed of repair. However this model was not consolidated by further studies examining the repair of DSBs with varying end complexities. For example the repair of DSBs induced by neocarzinostatin (NCS), a drug which produces a homogeneous population of relatively simple DSBs, were repaired with similar kinetics as IR induced DSBs (Goodarzi et al., 2008). This advocated for an alternative model and, given that ATM dependent DSBs have been shown to reside with HC (Goodarzi et al., 2008), it was proposed that chromatin complexity rather than damage complexity might influence DSB repair kinetics. In chapter 5, I demonstrated that DSBs persisting in Artemis deficient cells also localize to regions of HC. However in contrast to ATM, loss of Artemis has no effect on the induction or localization of pKAP-1. Depletion of HC associated factors such as KAP-1 or HDAC 1/2 did not rescue the Artemis dependent DSB repair defect, suggesting that Artemis does not function like ATM to mediate HC relaxation and is likely to function downstream of this process. This model is consistent with Artemis functioning as an endonuclease on DSB termini. Given that heterochromatic DNA is often highly repetitious with complex secondary structures (Yunis et al., 1971), it is conceivable that Artemis which functions to remove hairpins during V(D)J recombination, may also operate at HC to remove complex secondary structures which are refractory to repair. However the precise role of Artemis in DSB repair is still unclear and requires further investigation.

KAP-1 phosphorylation has been demonstrated to increase the accessibility of MNase digestibility, and this accessibility is dependent on ATM (Ziv et al., 2006). I have demonstrated that in Artemis defective cells KAP-1 remains dissociated from HC enriched chromatin fractions for longer after IR. This result suggests that chromatin surrounding an Artemis dependent DSB remains relaxed for longer. Therefore despite Artemis and ATM harbouring an identical repair defect, the nature of the chromatin alterations surrounding these DSBs is distinct. What affect prolonged relaxation at Artemis dependent DSBs has on transcription is unclear, but KAP-1 has

been suggested to function as a transcriptional repressor for some HC associated genes (Li et al., 2007).

The examination of Artemis's function is clinically valuable since patients display severe combined immunodeficiency (SCID) (Moshous et al., 2001). Despite this phenotype patients can survive into adulthood following bone marrow transplantation (Neven et al., 2009).

1.45Heavy ion irradiation and checkpoint arrest

1.45.1 Major conclusions

- Heavy ion induced DSBs are repaired with slower kinetics than X-ray induced DSBs, particularly in G2 phase.
- Single heavy ion tracks can induce a G2/M checkpoint arrest.
- Heavy ion induced DSBs maintain a prolonged G2/M checkpoint arrest.
- DDR signalling from 7 heavy ion induced DSBs/clusters is sufficient to maintain G2/M checkpoint arrest.

In chapter 6, I have demonstrated that DSB repair after heavy ion irradiation is extremely slowed, in particular in G2 phase, where as little as 10% DSB repair is observed 24 hours after IR. In G2 phase two pathways of DSB repair exist, one with fast kinetics involving NHEJ the other with slow kinetics involving HR proteins, ATM and Artemis (Beucher et al., 2009; Shibata et al., 2010). The slower repair kinetics in G2 after heavy ion IR would suggest that complex clustered lesions are repaired by HR in G2. After X-rays, a threshold of 15-25 DSBs is required to initiate and sustain G2/M checkpoint arrest (Deckbar et al., 2007). Heavy ion induced DNA damage produces DSBs that are in close proximity (clusters). I have shown that signalling from these clusters is sufficient to initiate a G2/M checkpoint arrest. High resolution imaging after vertical IR suggests that a single cluster/track is sufficient to induce checkpoint arrest (Nakajima et al., manuscript submitted). Therefore clustered DSBs are able to proficiently signal to the checkpoint machinery and fewer clustered γH2AX foci are required compared to individual foci to satisfy arrest. The duration of DSB repair dictates the length of checkpoint arrest (Shibata et al., 2010). As expected, after heavy ion irradiation G2/M checkpoint arrest

was maintained for at least a further 4 hours compared to X-ray treated cells. Cells released from the checkpoint were found to still manifest ~7 clustered γH2AX foci. Therefore cells can enter mitosis while harbouring DNA damage induced after heavy ion irradiation.

Previously nearly 100% of carbon ion induced DSBs have been shown co-localize with RPA, whereas only 20-30% of X-ray induced DSBs undergo resection (Shibata et al., 2011). The speed of DSB repair correlates with DSB end resection (Shibata *et al*, 2011). As mentioned earlier, in G2 phase CtIP KD cells, normal repair kinetics are observed 0.5 and 2 hours after IR, but at later times after IR (between 4 and 8 hours) DSB repair proceeds with faster repair kinetics compared to control cells (Shibata et al., 2011). This result suggested that by preventing resection DSB repair is channelled through the faster NHEJ pathway. However BRCA2 siRNA treated cells still maintain a DSB repair defect. CtIP knockdown alleviates the BRCA2 dependent repair defect in G2. Therefore in the absence of resection all DSBs can be repaired by NHEJ. Given that HR is associated with the repair of complex DSBs which normally require resection to mediate end ligation (Shibata et al., 2011); it would be of interest to establish whether repair of heavy ion induced DSBs was still possible in BRCA2 and CtIP knockdown cells.

1.46Final summary

To facilitate repair of DSBs residing at regions of HC, ATM is required to mediate relaxation by phosphorylating the C-terminus of KAP-1 at Ser824 (Goodarzi et al., 2008). This posed the question as to whether HC also acts as a barrier to IR induced γH2AX expansion particularly at HC associated DSBs. The work presented here has demonstrated that by reducing the HC content of a cell by removing KAP-1, MeCP2 or DNMT3B, the expansion of γH2AX can be enhanced. DDR signalling including ATM and Chk2 is also heightened in these cellular contexts, which is reflected in a hypersensitive and prolonged G2/M checkpoint arrest. Therefore HC relaxation not only facilitates repair of HC associated DSBs, but also assists in optimal signalling from these breaks. Artemis and ATM are both required for repair of a subset of slow repairing DSBs in G1. Here I have demonstrated that like ATM, Artemis is required for repair of HC associated DSBs. However, unlike ATM, Artemis is likely to function downstream of the process of HC relaxation. In G1, chromatin complexity rather than damage complexity confers a

slowing on DSB repair kinetics. In G2, both NHEJ and HR can repair DSBs. Slow repairing DSBs in G2 represent those which reside within HC being repaired by HR. I have presented work here which demonstrates that heavy ion induced DSBs are repaired with extremely slow kinetics, particularly in G2 phase, suggesting that complex DSBs are also repaired by HR despite not necessarily being HC associated. Heavy ion induced DSBs are produced in close proximity and produce clustered γH2AX foci. I have demonstrated that the DDR signalling emanating from these clusters is sufficient to mediate checkpoint arrest at lower doses IR compared to X-ray. Importantly cells can enter mitosis still manifesting up to 7 clustered heavy ion induced γH2AX foci.

Overall G2/M checkpoint arrest can be initiated and prolonged at lower dose IR when either the chromatin content of a cell is reduced or when the clustering of damage increases (i.e. the rate of repair prolonged as a result of increased damage complexity). In relation to DSB repair, the kinetics γH2AX formation can be enhanced in HC reduced cells, and the duration of DNA repair prolonged with increasing damage complexity.

References

Agarwal, N., Hardt, T., Brero, A., Nowak, D., Rothbauer, U., Becker, A., Leonhardt, H., and Cardoso, M.C. (2007). MeCP2 interacts with HP1 and modulates its heterochromatin association during myogenic differentiation. Nucleic acids research *35*, 5402-5408.

Agrawal, A., and Schatz, D.G. (1997). RAG1 and RAG2 form a stable postcleavage synaptic complex with DNA containing signal ends in V(D)J recombination. Cell *89*, 43-53.

Ahn, J., and Prives, C. (2002). Checkpoint kinase 2 (Chk2) monomers or dimers phosphorylate Cdc25C after DNA damage regardless of threonine 68 phosphorylation. J Biol Chem *277*, 48418-48426.

Ahn, J., Urist, M., and Prives, C. (2004). The Chk2 protein kinase. DNA Repair (Amst) *3*, 1039-1047.

Ahn, J.Y., Li, X., Davis, H.L., and Canman, C.E. (2002). Phosphorylation of threonine 68 promotes oligomerization and autophosphorylation of the Chk2 protein kinase via the forkhead-associated domain. J Biol Chem *277*, 19389-19395.

Ahn, J.Y., Schwarz, J.K., Piwnica-Worms, H., and Canman, C.E. (2000). Threonine 68 phosphorylation by ataxia telangiectasia mutated is required for efficient activation of Chk2 in response to ionizing radiation. Cancer Res *60*, 5934-5936.

Ajiro, K., Yoda, K., Utsumi, K., and Nishikawa, Y. (1996). Alteration of cell cycle-dependent histone phosphorylations by okadaic acid. Induction of mitosis-specific H3 phosphorylation and chromatin condensation in mammalian interphase cells. The Journal of biological chemistry *271*, 13197-13201.

Alderton, G.K., Joenje, H., Varon, R., Borglum, A.D., Jeggo, P.A., and O'Driscoll, M. (2004). Seckel syndrome exhibits cellular features demonstrating defects in the ATR-signalling pathway. Hum Mol Genet *13*, 3127-3138.

Ali, A., Zhang, J., Bao, S., Liu, I., Otterness, D., Dean, N.M., Abraham, R.T., and Wang, X.F. (2004). Requirement of protein phosphatase 5 in DNA-damage-induced ATM activation. Genes Dev *18*, 249-254.

Allen, C., Halbrook, J., and Nickoloff, J.A. (2003). Interactive competition between homologous recombination and non-homologous end joining. Mol Cancer Res *1*, 913-920.

Anderson, J.A., Harper, J.V., Cucinotta, F.A., and O'Neill, P. (2010). Participation of DNA-PKcs in DSB repair after exposure to high- and low-LET radiation. Radiat Res *174*, 195-205.

Ayoub, N., Jeyasekharan, A.D., Bernal, J.A., and Venkitaraman, A.R. (2008). HP1-beta mobilization promotes chromatin changes that initiate the DNA damage response. Nature *453*, 682-686.

Bakkenist, C.J., and Kastan, M.B. (2003). DNA damage activates ATM through intermolecular autophosphorylation and dimer dissociation. Nature *421*, 499-506.

Banin, S., Moyal, L., Shieh, S., Taya, Y., Anderson, C.W., Chessa, L., Smorodinsky, N.I., Prives, C., Reiss, Y., Shiloh, Y.*, et al.* (1998). Enhanced phosphorylation of p53 by ATM in response to DNA damage. Science *281*, 1674-1677.

Bao, S., Wu, Q., McLendon, R.E., Hao, Y., Shi, Q., Hjelmeland, A.B., Dewhirst, M.W., Bigner, D.D., and Rich, J.N. (2006). Glioma stem cells promote radioresistance by preferential activation of the DNA damage response. Nature *444*, 756-760.

Bartek, J., Bartkova, J., and Lukas, J. (2007). DNA damage signalling guards against activated oncogenes and tumour progression. Oncogene *26*, 7773-7779.

Bartkova, J., Rezaei, N., Liontos, M., Karakaidos, P., Kletsas, D., Issaeva, N., Vassiliou, L.V., Kolettas, E., Niforou, K., Zoumpourlis, V.C.*, et al.* (2006). Oncogene-induced

senescence is part of the tumorigenesis barrier imposed by DNA damage checkpoints. Nature *444*, 633-637.

Beamish, H., Khanna, K.K., and Lavin, M.F. (1994). Ionizing radiation and cell cycle progression in ataxia telangiectasia. Radiat Res *138*, S130-133.

Bekker-Jensen, S., and Mailand, N. (2010). Assembly and function of DNA double-strand break repair foci in mammalian cells. DNA Repair (Amst) *9*, 1219-1228.

Bellefroid, E.J., Poncelet, D.A., Lecocq, P.J., Revelant, O., and Martial, J.A. (1991). The evolutionarily conserved Kruppel-associated box domain defines a subfamily of eukaryotic multifingered proteins. Proc Natl Acad Sci U S A *88*, 3608-3612.

Bennardo, N., Cheng, A., Huang, N., and Stark, J.M. (2008). Alternative-NHEJ is a mechanistically distinct pathway of mammalian chromosome break repair. PLoS Genet *4*, e1000110.

Berkovich, E., Monnat, R.J., Jr., and Kastan, M.B. (2007). Roles of ATM and NBS1 in chromatin structure modulation and DNA double-strand break repair. Nat Cell Biol *9*, 683-690.

Beucher, A., Birraux, J., Tchouandong, L., Barton, O., Shibata, A., Conrad, S., Goodarzi, A.A., Krempler, A., Jeggo, P.A., and Lobrich, M. (2009). ATM and Artemis promote homologous recombination of radiation-induced DNA double-strand breaks in G2. Embo J *28*, 3413-3427.

Bianchi, M.E., and Agresti, A. (2005). HMG proteins: dynamic players in gene regulation and differentiation. Curr Opin Genet Dev *15*, 496-506.

Biton, S., Barzilai, A., and Shiloh, Y. (2008). The neurological phenotype of ataxia-telangiectasia: solving a persistent puzzle. DNA Repair (Amst) *7*, 1028-1038.

Black, B.E., and Bassett, E.A. (2008). The histone variant CENP-A and centromere

specification. Curr Opin Cell Biol *20*, 91-100.

Boisvert, F.M., Rhie, A., Richard, S., and Doherty, A.J. (2005). The GAR motif of 53BP1 is arginine methylated by PRMT1 and is necessary for 53BP1 DNA binding activity. Cell Cycle *4*, 1834-1841.

Bonner, W.M., Redon, C.E., Dickey, J.S., Nakamura, A.J., Sedelnikova, O.A., Solier, S., and Pommier, Y. (2008). GammaH2AX and cancer. Nat Rev Cancer *8*, 957-967.

Booher, R.N., Holman, P.S., and Fattaey, A. (1997). Human Myt1 is a cell cycle-regulated kinase that inhibits Cdc2 but not Cdk2 activity. J Biol Chem *272*, 22300-22306.

Boutros, R., and Byrne, J.A. (2005). D53 (TPD52L1) is a cell cycle-regulated protein maximally expressed at the G2-M transition in breast cancer cells. Exp Cell Res *310*, 152-165.

Boyd, S.D., Tsai, K.Y., and Jacks, T. (2000). An intact HDM2 RING-finger domain is required for nuclear exclusion of p53. Nat Cell Biol *2*, 563-568.

Bunting, S.F., Callen, E., Wong, N., Chen, H.T., Polato, F., Gunn, A., Bothmer, A., Feldhahn, N., Fernandez-Capetillo, O., Cao, L.*, et al.* (2010). 53BP1 inhibits homologous recombination in Brca1-deficient cells by blocking resection of DNA breaks. Cell *141*, 243-254.

Burnett, G., and Kennedy, E.P. (1954). The enzymatic phosphorylation of proteins. J Biol Chem *211*, 969-980.

Buscemi, G., Perego, P., Carenini, N., Nakanishi, M., Chessa, L., Chen, J., Khanna, K., and Delia, D. (2004). Activation of ATM and Chk2 kinases in relation to the amount of DNA strand breaks. Oncogene *23*, 7691-7700.

Busino, L., Donzelli, M., Chiesa, M., Guardavaccaro, D., Ganoth, D., Dorrello, N.V., Hershko, A., Pagano, M., and Draetta, G.F. (2003). Degradation of Cdc25A by beta-TrCP

during S phase and in response to DNA damage. Nature *426*, 87-91.

Callebaut, I., and Mornon, J.P. (1997). From BRCA1 to RAP1: a widespread BRCT module closely associated with DNA repair. FEBS Lett *400*, 25-30.

Callebaut, I., Moshous, D., Mornon, J.P., and de Villartay, J.P. (2002). Metallo-beta-lactamase fold within nucleic acids processing enzymes: the beta-CASP family. Nucleic acids research *30*, 3592-3601.

Campisi, J. (2005). Aging, tumor suppression and cancer: high wire-act! Mech Ageing Dev *126*, 51-58.

Canman, C.E., Lim, D.S., Cimprich, K.A., Taya, Y., Tamai, K., Sakaguchi, K., Appella, E., Kastan, M.B., and Siliciano, J.D. (1998). Activation of the ATM kinase by ionizing radiation and phosphorylation of p53. Science *281*, 1677-1679.

Carson, C.T., Schwartz, R.A., Stracker, T.H., Lilley, C.E., Lee, D.V., and Weitzman, M.D. (2003). The Mre11 complex is required for ATM activation and the G2/M checkpoint. EMBO J *22*, 6610-6620.

Castilla, L.H., Couch, F.J., Erdos, M.R., Hoskins, K.F., Calzone, K., Garber, J.E., Boyd, J., Lubin, M.B., Deshano, M.L., Brody, L.C*., et al.* (1994). Mutations in the BRCA1 gene in families with early-onset breast and ovarian cancer. Nat Genet *8*, 387-391.

Celeste, A., Petersen, S., Romanienko, P.J., Fernandez-Capetillo, O., Chen, H.T., Sedelnikova, O.A., Reina-San-Martin, B., Coppola, V., Meffre, E., Difilippantonio, M.J*., et al.* (2002). Genomic instability in mice lacking histone H2AX. Science *296*, 922-927.

Chan, D.W., Chen, B.P., Prithivirajsingh, S., Kurimasa, A., Story, M.D., Qin, J., and Chen, D.J. (2002). Autophosphorylation of the DNA-dependent protein kinase catalytic subunit is required for rejoining of DNA double-strand breaks. Genes Dev *16*, 2333-2338.

Chapman, J.R., and Jackson, S.P. (2008). Phospho-dependent interactions between NBS1 and MDC1 mediate chromatin retention of the MRN complex at sites of DNA damage. EMBO Rep *9*, 795-801.

Charier, G., Couprie, J., Alpha-Bazin, B., Meyer, V., Quemeneur, E., Guerois, R., Callebaut, I., Gilquin, B., and Zinn-Justin, S. (2004). The Tudor tandem of 53BP1: a new structural motif involved in DNA and RG-rich peptide binding. Structure *12*, 1551-1562.

Chen, H.Z., Tsai, S.Y., and Leone, G. (2009). Emerging roles of E2Fs in cancer: an exit from cell cycle control. Nat Rev Cancer *9*, 785-797.

Chen, M., Cortay, J.C., Logan, I.R., Sapountzi, V., Robson, C.N., and Gerlier, D. (2005). Inhibition of ubiquitination and stabilization of human ubiquitin E3 ligase PIRH2 by measles virus phosphoprotein. J Virol *79*, 11824-11836.

Chen, T., Ueda, Y., Dodge, J.E., Wang, Z., and Li, E. (2003). Establishment and maintenance of genomic methylation patterns in mouse embryonic stem cells by Dnmt3a and Dnmt3b. Molecular and cellular biology *23*, 5594-5605.

Chen, W.G., Chang, Q., Lin, Y., Meissner, A., West, A.E., Griffith, E.C., Jaenisch, R., and Greenberg, M.E. (2003). Derepression of BDNF transcription involves calcium-dependent phosphorylation of MeCP2. Science *302*, 885-889.

Ciccia, A., and Elledge, S.J. (2010). The DNA damage response: making it safe to play with knives. Mol Cell *40*, 179-204.

Cimprich, K.A., and Cortez, D. (2008). ATR: an essential regulator of genome integrity. Nat Rev Mol Cell Biol *9*, 616-627.

Clapperton, J.A., Manke, I.A., Lowery, D.M., Ho, T., Haire, L.F., Yaffe, M.B., and Smerdon, S.J. (2004). Structure and mechanism of BRCA1 BRCT domain recognition of phosphorylated BACH1 with implications for cancer. Nat Struct Mol Biol *11*, 512-518.

Cortez, D., Glick, G., and Elledge, S.J. (2004). Minichromosome maintenance proteins are direct targets of the ATM and ATR checkpoint kinases. Proc Natl Acad Sci U S A *101*, 10078-10083.

Cortez, D., Guntuku, S., Qin, J., and Elledge, S.J. (2001). ATR and ATRIP: partners in checkpoint signaling. Science *294*, 1713-1716.

Costantini, S., Woodbine, L., Andreoli, L., Jeggo, P.A., and Vindigni, A. (2007). Interaction of the Ku heterodimer with the DNA ligase IV/Xrcc4 complex and its regulation by DNA-PK. DNA Repair (Amst) *6*, 712-722.

Cowell, I.G., Sunter, N.J., Singh, P.B., Austin, C.A., Durkacz, B.W., and Tilby, M.J. (2007). gammaH2AX foci form preferentially in euchromatin after ionising-radiation. PLoS One *2*, e1057.

Craig, J.M. (2005). Heterochromatin--many flavours, common themes. Bioessays *27*, 17-28.

Cucinotta, F.A., Wilson, J.W., Tripathi, R.K., and Townsend, L.W. (1998). Microscopic fragmentation model for galactic cosmic ray studies. Adv Space Res *22*, 533-537.

Cui, X., Yu, Y., Gupta, S., Cho, Y.M., Lees-Miller, S.P., and Meek, K. (2005). Autophosphorylation of DNA-dependent protein kinase regulates DNA end processing and may also alter double-strand break repair pathway choice. Mol Cell Biol *25*, 10842-10852.

Dahl, K.N., Scaffidi, P., Islam, M.F., Yodh, A.G., Wilson, K.L., and Misteli, T. (2006). Distinct structural and mechanical properties of the nuclear lamina in Hutchinson-Gilford progeria syndrome. Proc Natl Acad Sci U S A *103*, 10271-10276.

Dalal, S.N., Yaffe, M.B., and DeCaprio, J.A. (2004). 14-3-3 family members act coordinately to regulate mitotic progression. Cell Cycle *3*, 672-677.

de Lange, T. (2004). T-loops and the origin of telomeres. Nat Rev Mol Cell Biol *5*, 323-

329.

de Ruijter, A.J., van Gennip, A.H., Caron, H.N., Kemp, S., and van Kuilenburg, A.B. (2003). Histone deacetylases (HDACs): characterization of the classical HDAC family. Biochem J *370*, 737-749.

Deckbar, D., Birraux, J., Krempler, A., Tchouandong, L., Beucher, A., Walker, S., Stiff, T., Jeggo, P., and Lobrich, M. (2007). Chromosome breakage after G2 checkpoint release. J Cell Biol *176*, 749-755.

Deng, Z., Bald, I., Illenberger, E., and Huels, M.A. (2006). Reactive scattering damage to DNA components by hyperthermal secondary ions. Phys Rev Lett *96*, 243203.

Dewey, W.C., Ling, C.C., and Meyn, R.E. (1995). Radiation-induced apoptosis: relevance to radiotherapy. Int J Radiat Oncol Biol Phys *33*, 781-796.

Difilippantonio, S., Gapud, E., Wong, N., Huang, C.Y., Mahowald, G., Chen, H.T., Kruhlak, M.J., Callen, E., Livak, F., Nussenzweig, M.C*., et al.* (2008). 53BP1 facilitates long-range DNA end-joining during V(D)J recombination. Nature *456*, 529-533.

Din, S., Brill, S.J., Fairman, M.P., and Stillman, B. (1990). Cell-cycle-regulated phosphorylation of DNA replication factor A from human and yeast cells. Genes Dev *4*, 968-977.

DiTullio, R.A., Jr., Mochan, T.A., Venere, M., Bartkova, J., Sehested, M., Bartek, J., and Halazonetis, T.D. (2002). 53BP1 functions in an ATM-dependent checkpoint pathway that is constitutively activated in human cancer. Nat Cell Biol *4*, 998-1002.

Downs, J.A., Allard, S., Jobin-Robitaille, O., Javaheri, A., Auger, A., Bouchard, N., Kron, S.J., Jackson, S.P., and Cote, J. (2004). Binding of chromatin-modifying activities to phosphorylated histone H2A at DNA damage sites. Molecular cell *16*, 979-990.

Duchaud, E., Ridet, A., Stoppa-Lyonnet, D., Janin, N., Moustacchi, E., and Rosselli, F. (1996). Deregulated apoptosis in ataxia telangiectasia: association with clinical

stigmata and radiosensitivity. Cancer Res *56*, 1400-1404.

Ehrlich, M. (2003). The ICF syndrome, a DNA methyltransferase 3B deficiency and immunodeficiency disease. Clin Immunol *109*, 17-28.

Elkon, R., Linhart, C., Sharan, R., Shamir, R., and Shiloh, Y. (2003). Genome-wide in silico identification of transcriptional regulators controlling the cell cycle in human cells. Genome Res *13*, 773-780.

Elledge, S.J. (1996). Cell cycle checkpoints: preventing an identity crisis. Science *274*, 1664-1672.

Eriksson, M., Brown, W.T., Gordon, L.B., Glynn, M.W., Singer, J., Scott, L., Erdos, M.R., Robbins, C.M., Moses, T.Y., Berglund, P.*, et al.* (2003). Recurrent de novo point mutations in lamin A cause Hutchinson-Gilford progeria syndrome. Nature *423*, 293-298.

Esashi, F., Christ, N., Gannon, J., Liu, Y., Hunt, T., Jasin, M., and West, S.C. (2005). CDK-dependent phosphorylation of BRCA2 as a regulatory mechanism for recombinational repair. Nature *434*, 598-604.

Falck, J., Coates, J., and Jackson, S.P. (2005). Conserved modes of recruitment of ATM, ATR and DNA-PKcs to sites of DNA damage. Nature *434*, 605-611.

Feng, Q., and Zhang, Y. (2003). The NuRD complex: linking histone modification to nucleosome remodeling. Curr Top Microbiol Immunol *274*, 269-290.

Fernandez-Capetillo, O., Chen, H.T., Celeste, A., Ward, I., Romanienko, P.J., Morales, J.C., Naka, K., Xia, Z., Camerini-Otero, R.D., Motoyama, N.*, et al.* (2002). DNA damage-induced G2-M checkpoint activation by histone H2AX and 53BP1. Nat Cell Biol *4*, 993-997.

Fernet, M., Megnin-Chanet, F., Hall, J., and Favaudon, V. (2010). Control of the G2/M

checkpoints after exposure to low doses of ionising radiation: implications for hyper-radiosensitivity. DNA Repair (Amst) *9*, 48-57.

FitzGerald, J.E., Grenon, M., and Lowndes, N.F. (2009). 53BP1: function and mechanisms of focal recruitment. Biochem Soc Trans *37*, 897-904.

Foray, N., Marot, D., Gabriel, A., Randrianarison, V., Carr, A.M., Perricaudet, M., Ashworth, A., and Jeggo, P. (2003). A subset of ATM- and ATR-dependent phosphorylation events requires the BRCA1 protein. Embo J *22*, 2860-2871.

Gabant, G., Lorphelin, A., Nozerand, N., Marchetti, C., Bellanger, L., Dedieu, A., Quemeneur, E., and Alpha-Bazin, B. (2008). Autophosphorylated residues involved in the regulation of human chk2 in vitro. J Mol Biol *380*, 489-503.

Galanty, Y., Belotserkovskaya, R., Coates, J., Polo, S., Miller, K.M., and Jackson, S.P. (2009). Mammalian SUMO E3-ligases PIAS1 and PIAS4 promote responses to DNA double-strand breaks. Nature *462*, 935-939.

Garcia-Cao, M., O'Sullivan, R., Peters, A.H., Jenuwein, T., and Blasco, M.A. (2004). Epigenetic regulation of telomere length in mammalian cells by the Suv39h1 and Suv39h2 histone methyltransferases. Nature genetics *36*, 94-99.

Gatei, M., Sloper, K., Sorensen, C., Syljuasen, R., Falck, J., Hobson, K., Savage, K., Lukas, J., Zhou, B.B., Bartek, J.*, et al.* (2003). Ataxia-telangiectasia-mutated (ATM) and NBS1-dependent phosphorylation of Chk1 on Ser-317 in response to ionizing radiation. The Journal of biological chemistry *278*, 14806-14811.

Gellert, M. (1997). Recent advances in understanding V(D)J recombination. Adv Immunol *64*, 39-64.

Ghiassi-nejad, M., Mortazavi, S.M., Cameron, J.R., Niroomand-rad, A., and Karam, P.A. (2002). Very high background radiation areas of Ramsar, Iran: preliminary biological studies. Health Phys *82*, 87-93.

Goldstine, J.V., Nahas, S., Gamo, K., Gartler, S.M., Hansen, R.S., Roelfsema, J.H., Gatti, R.A., and Marahrens, Y. (2006). Constitutive phosphorylation of ATM in lymphoblastoid cell lines from patients with ICF syndrome without downstream kinase activity. DNA Repair (Amst) *5*, 432-443.

Goll, M.G., and Bestor, T.H. (2005). Eukaryotic cytosine methyltransferases. Annual review of biochemistry *74*, 481-514.

Goll, M.G., Kirpekar, F., Maggert, K.A., Yoder, J.A., Hsieh, C.L., Zhang, X., Golic, K.G., Jacobsen, S.E., and Bestor, T.H. (2006). Methylation of tRNAAsp by the DNA methyltransferase homolog Dnmt2. Science *311*, 395-398.

Goodarzi, A.A., Jeggo, P., and Lobrich, M. (2010). The influence of heterochromatin on DNA double strand break repair: Getting the strong, silent type to relax. DNA Repair (Amst) *9*, 1273-1282.

Goodarzi, A.A., Jonnalagadda, J.C., Douglas, P., Young, D., Ye, R., Moorhead, G.B., Lees-Miller, S.P., and Khanna, K.K. (2004). Autophosphorylation of ataxia-telangiectasia mutated is regulated by protein phosphatase 2A. EMBO J *23*, 4451-4461.

Goodarzi, A.A., Noon, A.T., Deckbar, D., Ziv, Y., Shiloh, Y., Lobrich, M., and Jeggo, P.A. (2008). ATM signaling facilitates repair of DNA double-strand breaks associated with heterochromatin. Molecular cell *31*, 167-177.

Goodarzi, A.A., Yu, Y., Riballo, E., Douglas, P., Walker, S.A., Ye, R., Harer, C., Marchetti, C., Morrice, N., Jeggo, P.A*., et al.* (2006). DNA-PK autophosphorylation facilitates Artemis endonuclease activity. Embo J *25*, 3880-3889.

Gorbunova, V., Seluanov, A., and Pereira-Smith, O.M. (2002). Expression of human telomerase (hTERT) does not prevent stress-induced senescence in normal human fibroblasts but protects the cells from stress-induced apoptosis and necrosis. J Biol Chem *277*, 38540-38549.

Gottlieb, T.M., and Jackson, S.P. (1993). The DNA-dependent protein kinase: requirement for DNA ends and association with Ku antigen. Cell *72*, 131-142.

Grawunder, U., Zimmer, D., Fugmann, S., Schwarz, K., and Lieber, M.R. (1998).

DNA ligase IV is essential for V(D)J recombination and DNA double-strand break repair in human precursor lymphocytes. Molecular cell *2*, 477-484.

Green, E.M., Antczak, A.J., Bailey, A.O., Franco, A.A., Wu, K.J., Yates, J.R., 3rd, and Kaufman, P.D. (2005). Replication-independent histone deposition by the HIR complex and Asf1. Current biology : CB *15*, 2044-2049.

Guenatri, M., Bailly, D., Maison, C., and Almouzni, G. (2004). Mouse centric and pericentric satellite repeats form distinct functional heterochromatin. J Cell Biol *166*, 493-505.

Hagberg, B., Goutieres, F., Hanefeld, F., Rett, A., and Wilson, J. (1985). Rett syndrome: criteria for inclusion and exclusion. Brain Dev *7*, 372-373.

Hakem, R. (2008). DNA-damage repair; the good, the bad, and the ugly. EMBO J *27*, 589-605.

Halperin, E.C. (2006). Particle therapy and treatment of cancer. Lancet Oncol *7*, 676-685.

Han, X., Feng, X., Rattner, J.B., Smith, H., Bose, P., Suzuki, K., Soliman, M.A., Scott, M.S., Burke, B.E., and Riabowol, K. (2008). Tethering by lamin A stabilizes and targets the ING1 tumour suppressor. Nat Cell Biol *10*, 1333-1340.

Hanks, S.K., and Hunter, T. (1995). Protein kinases 6. The eukaryotic protein kinase superfamily: kinase (catalytic) domain structure and classification. FASEB J *9*, 576-596.

Hans, F., and Dimitrov, S. (2001). Histone H3 phosphorylation and cell division. Oncogene *20*, 3021-3027.

Harrison, J.C., and Haber, J.E. (2006). Surviving the breakup: the DNA damage checkpoint. Annu Rev Genet *40*, 209-235.

Hartlerode, A.J., and Scully, R. (2009). Mechanisms of double-strand break repair in somatic mammalian cells. Biochem J *423*, 157-168.

Hartwell, L.H., and Kastan, M.B. (1994). Cell cycle control and cancer. Science *266*, 1821-1828.

Hata, K., Okano, M., Lei, H., and Li, E. (2002). Dnmt3L cooperates with the Dnmt3 family of de novo DNA methyltransferases to establish maternal imprints in mice. Development *129*, 1983-1993.

Hay, R.T. (2005). SUMO: a history of modification. Mol Cell *18*, 1-12.

Hayflick, L., and Moorhead, P.S. (1961). The serial cultivation of human diploid cell strains. Exp Cell Res *25*, 585-621.

Hendry, J.H., Potten, C.S., and Merritt, A. (1995). Apoptosis induced by high- and low-LET radiations. Radiat Environ Biophys *34*, 59-62.

Herbig, U., Ferreira, M., Condel, L., Carey, D., and Sedivy, J.M. (2006). Cellular senescence in aging primates. Science *311*, 1257.

Hiom, K., and Gellert, M. (1997). A stable RAG1-RAG2-DNA complex that is active in V(D)J cleavage. Cell *88*, 65-72.

Hirao, A., Kong, Y.Y., Matsuoka, S., Wakeham, A., Ruland, J., Yoshida, H., Liu, D., Elledge, S.J., and Mak, T.W. (2000). DNA damage-induced activation of p53 by the checkpoint kinase Chk2. Science *287*, 1824-1827.

Hoeijmakers, J.H. (2009). DNA damage, aging, and cancer. N Engl J Med *361*, 1475-1485.

Horike, S. (2005). [How the methyl-CpG binding protein-related epigenetic disease turns on the genes that produce its symptoms]. Tanpakushitsu Kakusan Koso *50*, 978-984.

Horike, S., Cai, S., Miyano, M., Cheng, J.F., and Kohwi-Shigematsu, T. (2005). Loss of silent-chromatin looping and impaired imprinting of DLX5 in Rett syndrome. Nature genetics *37*, 31-40.

Huang, B., Eberstadt, M., Olejniczak, E.T., Meadows, R.P., and Fesik, S.W. (1996). NMR structure and mutagenesis of the Fas (APO-1/CD95) death domain. Nature *384*, 638-641.

Huen, M.S., Grant, R., Manke, I., Minn, K., Yu, X., Yaffe, M.B., and Chen, J. (2007). RNF8 transduces the DNA-damage signal via histone ubiquitylation and checkpoint protein assembly. Cell *131*, 901-914.

Huen, M.S., Sy, S.M., and Chen, J. (2010). BRCA1 and its toolbox for the maintenance of genome integrity. Nat Rev Mol Cell Biol *11*, 138-148.

Huertas, P., and Jackson, S.P. (2009). Human CtIP mediates cell cycle control of DNA end resection and double strand break repair. J Biol Chem *284*, 9558-9565.

Iacovoni, J.S., Caron, P., Lassadi, I., Nicolas, E., Massip, L., Trouche, D., and Legube, G. (2010). High-resolution profiling of gammaH2AX around DNA double strand breaks in the mammalian genome. Embo J *29*, 1446-1457.

Ivanov, A.V., Peng, H., Yurchenko, V., Yap, K.L., Negorev, D.G., Schultz, D.C., Psulkowski, E., Fredericks, W.J., White, D.E., Maul, G.G*., et al.* (2007). PHD domain-mediated E3 ligase activity directs intramolecular sumoylation of an adjacent bromodomain required for gene silencing. Molecular cell *28*, 823-837.

Jackson, S.P., and Bartek, J. (2009). The DNA-damage response in human biology and disease. Nature *461*, 1071-1078.

Janzen, V., Forkert, R., Fleming, H.E., Saito, Y., Waring, M.T., Dombkowski, D.M., Cheng, T., DePinho, R.A., Sharpless, N.E., and Scadden, D.T. (2006). Stem-cell ageing modified by the cyclin-dependent kinase inhibitor p16INK4a. Nature *443*, 421-426.

Jazayeri, A., Balestrini, A., Garner, E., Haber, J.E., and Costanzo, V. (2008).

Mre11-Rad50-Nbs1-dependent processing of DNA breaks generates oligonucleotides that stimulate ATM activity. EMBO J *27*, 1953-1962.

Jazayeri, A., Falck, J., Lukas, C., Bartek, J., Smith, G.C., Lukas, J., and Jackson, S.P. (2006). ATM- and cell cycle-dependent regulation of ATR in response to DNA double-strand breaks. Nat Cell Biol *8*, 37-45.

Jenuwein, T. (2001). Re-SET-ting heterochromatin by histone methyltransferases. Trends in cell biology *11*, 266-273.

Jenuwein, T., and Allis, C.D. (2001). Translating the histone code. Science *293*, 1074-1080.

Jowsey, P., Morrice, N.A., Hastie, C.J., McLauchlan, H., Toth, R., and Rouse, J. (2007). Characterisation of the sites of DNA damage-induced 53BP1 phosphorylation catalysed by ATM and ATR. DNA Repair (Amst) *6*, 1536-1544.

Kaidi, A., Weinert, B.T., Choudhary, C., and Jackson, S.P. (2010). Human SIRT6 promotes DNA end resection through CtIP deacetylation. Science *329*, 1348-1353.

Kaneda, M., Okano, M., Hata, K., Sado, T., Tsujimoto, N., Li, E., and Sasaki, H. (2004). Essential role for de novo DNA methyltransferase Dnmt3a in paternal and maternal imprinting. Nature *429*, 900-903.

Kass, E.M., Ahn, J., Tanaka, T., Freed-Pastor, W.A., Keezer, S., and Prives, C. (2007). Stability of checkpoint kinase 2 is regulated via phosphorylation at serine 456. J Biol Chem *282*, 30311-30321.

Kastan, M.B., Zhan, Q., el-Deiry, W.S., Carrier, F., Jacks, T., Walsh, W.V., Plunkett, B.S., Vogelstein, B., and Fornace, A.J., Jr. (1992). A mammalian cell cycle checkpoint pathway utilizing p53 and GADD45 is defective in ataxia-telangiectasia. Cell *71*, 587-597.

Katsuragi, Y., and Sagata, N. (2004). Regulation of Chk1 kinase by autoinhibition and ATR-mediated phosphorylation. Mol Biol Cell *15*, 1680-1689.

Katyal, S., and McKinnon, P.J. (2008). DNA strand breaks, neurodegeneration and aging in the brain. Mech Ageing Dev *129*, 483-491.

Kawata, T., Durante, M., Furusawa, Y., George, K., Ito, H., Wu, H., and Cucinotta, F.A. (2001). G2-chromosome aberrations induced by high-LET radiations. Adv Space Res *27*, 383-391.

Kawata, T., Durante, M., Furusawa, Y., George, K., Takai, N., Wu, H., and Cucinotta, F.A. (2001). Dose--response of initial G2-chromatid breaks induced in normal human fibroblasts by heavy ions. Int J Radiat Biol *77*, 165-174.

Kawata, T., Durante, M., George, K., Furusawa, Y., Gotoh, E., Takai, N., Wu, H., and Cucinotta, F.A. (2001). Kinetics of chromatid break repair in G2-human fibroblasts exposed to low- and high-LET radiations. Phys Med *17 Suppl 1*, 226-228.

Keeney, S., and Neale, M.J. (2006). Initiation of meiotic recombination by formation of DNA double-strand breaks: mechanism and regulation. Biochem Soc Trans *34*, 523-525.

Kellum, R. (2003). HP1 complexes and heterochromatin assembly. Curr Top Microbiol Immunol *274*, 53-77.

Kerzendorfer, C., and O'Driscoll, M. (2009). Human DNA damage response and repair deficiency syndromes: linking genomic instability and cell cycle checkpoint proficiency. DNA Repair (Amst) *8*, 1139-1152.

Khanna, K.K., Lavin, M.F., Jackson, S.P., and Mulhern, T.D. (2001). ATM, a central controller of cellular responses to DNA damage. Cell Death Differ *8*, 1052-1065.

Kim, J.A., and Haber, J.E. (2009). Chromatin assembly factors Asf1 and CAF-1 have overlapping roles in deactivating the DNA damage checkpoint when DNA repair is complete. Proc Natl Acad Sci U S A *106*, 1151-1156.

Kim, J.A., Kruhlak, M., Dotiwala, F., Nussenzweig, A., and Haber, J.E. (2007). Heterochromatin is refractory to gamma-H2AX modification in yeast and mammals. J Cell Biol *178*, 209-218.

Kim, K.K., Soonpaa, M.H., Daud, A.I., Koh, G.Y., Kim, J.S., and Field, L.J. (1994). Tumor suppressor gene expression during normal and pathologic myocardial growth. J Biol Chem *269*, 22607-22613.

Kim, Y.C., Gerlitz, G., Furusawa, T., Catez, F., Nussenzweig, A., Oh, K.S., Kraemer, K.H., Shiloh, Y., and Bustin, M. (2009). Activation of ATM depends on chromatin interactions occurring before induction of DNA damage. Nat Cell Biol *11*, 92-96.

Kimura, H., Tada, M., Nakatsuji, N., and Tada, T. (2004). Histone code modifications on pluripotential nuclei of reprogrammed somatic cells. Molecular and cellular biology *24*, 5710-5720.

Kitagawa, R., Bakkenist, C.J., McKinnon, P.J., and Kastan, M.B. (2004). Phosphorylation of SMC1 is a critical downstream event in the ATM-NBS1-BRCA1 pathway. Genes Dev *18*, 1423-1438.

Kiyono, T., Foster, S.A., Koop, J.I., McDougall, J.K., Galloway, D.A., and Klingelhutz, A.J. (1998). Both Rb/p16INK4a inactivation and telomerase activity are required to immortalize human epithelial cells. Nature *396*, 84-88.

Knighton, D.R., Zheng, J.H., Ten Eyck, L.F., Ashford, V.A., Xuong, N.H., Taylor, S.S., and Sowadski, J.M. (1991). Crystal structure of the catalytic subunit of cyclic adenosine monophosphate-dependent protein kinase. Science *253*, 407-414.

Kramer, A., Mailand, N., Lukas, C., Syljuasen, R.G., Wilkinson, C.J., Nigg, E.A., Bartek, J., and Lukas, J. (2004). Centrosome-associated Chk1 prevents premature activation of cyclin-B-Cdk1 kinase. Nat Cell Biol *6*, 884-891.

Krempler, A., Deckbar, D., Jeggo, P.A., and Lobrich, M. (2007). An imperfect G2M checkpoint contributes to chromosome instability following irradiation of S and G2 phase cells. Cell cycle *6*, 1682-1686.

Kruger, W., Peterson, C.L., Sil, A., Coburn, C., Arents, G., Moudrianakis, E.N., and Herskowitz, I. (1995). Amino acid substitutions in the structured domains of histones H3 and H4 partially relieve the requirement of the yeast SWI/SNF complex for transcription. Genes Dev *9*, 2770-2779.

Kudlow, B.A., Kennedy, B.K., and Monnat, R.J., Jr. (2007). Werner and Hutchinson-Gilford progeria syndromes: mechanistic basis of human progeroid diseases. Nat Rev Mol Cell Biol *8*, 394-404.

Kudo, S., Nomura, Y., Segawa, M., Fujita, N., Nakao, M., Dragich, J., Schanen, C., and Tamura, M. (2001). Functional analyses of MeCP2 mutations associated with Rett syndrome using transient expression systems. Brain Dev *23 Suppl 1*, S165-173.

Kuhne, M., Riballo, E., Rief, N., Rothkamm, K., Jeggo, P.A., and Lobrich, M. (2004). A double-strand break repair defect in ATM-deficient cells contributes to radiosensitivity. Cancer research *64*, 500-508.

Kumagai, A., and Dunphy, W.G. (2003). Repeated phosphopeptide motifs in Claspin mediate the regulated binding of Chk1. Nat Cell Biol *5*, 161-165.

Lane, D.P. (1992). Cancer. p53, guardian of the genome. Nature *358*, 15-16.

Larsen, D.H., Poinsignon, C., Gudjonsson, T., Dinant, C., Payne, M.R., Hari, F.J., Danielsen, J.M., Menard, P., Sand, J.C., Stucki, M.*, et al.* (2010). The chromatin-remodeling factor CHD4 coordinates signaling and repair after DNA damage. J Cell Biol *190*, 731-740.

Lavin, M.F. (1999). ATM: the product of the gene mutated in ataxia-telangiectasia. Int J

Biochem Cell Biol *31*, 735-740.

Lavin, M.F. (2008). Ataxia-telangiectasia: from a rare disorder to a paradigm for cell signalling and cancer. Nat Rev Mol Cell Biol *9*, 759-769.

Le Deist, F., Poinsignon, C., Moshous, D., Fischer, A., and de Villartay, J.P. (2004). Artemis sheds new light on V(D)J recombination. Immunol Rev *200*, 142-155.

Le Gac, G., Esteve, P.O., Ferec, C., and Pradhan, S. (2006). DNA damage-induced down-regulation of human Cdc25C and Cdc2 is mediated by cooperation between p53 and maintenance DNA (cytosine-5) methyltransferase 1. The Journal of biological chemistry *281*, 24161-24170.

Lee, H.S., Park, J.H., Kim, S.J., Kwon, S.J., and Kwon, J. (2010). A cooperative activation loop among SWI/SNF, gamma-H2AX and H3 acetylation for DNA double-strand break repair. EMBO J *29*, 1434-1445.

Lee, J., Gold, D.A., Shevchenko, A., and Dunphy, W.G. (2005). Roles of replication fork-interacting and Chk1-activating domains from Claspin in a DNA replication checkpoint response. Molecular biology of the cell *16*, 5269-5282.

Lee, J., Kumagai, A., and Dunphy, W.G. (2007). The Rad9-Hus1-Rad1 checkpoint clamp regulates interaction of TopBP1 with ATR. J Biol Chem *282*, 28036-28044.

Lee, J.H., and Paull, T.T. (2005). ATM activation by DNA double-strand breaks through the Mre11-Rad50-Nbs1 complex. Science *308*, 551-554.

Lee, J.H., Xu, B., Lee, C.H., Ahn, J.Y., Song, M.S., Lee, H., Canman, C.E., Lee, J.S., Kastan, M.B., and Lim, D.S. (2003). Distinct functions of Nijmegen breakage syndrome in ataxia telangiectasia mutated-dependent responses to DNA damage. Mol Cancer Res *1*, 674-681.

Leuschner, P.J., Ameres, S.L., Kueng, S., and Martinez, J. (2006). Cleavage of the siRNA passenger strand during RISC assembly in human cells. EMBO Rep *7*, 314-320.

Li, B., Gogol, M., Carey, M., Lee, D., Seidel, C., and Workman, J.L. (2007). Combined action of PHD and chromo domains directs the Rpd3S HDAC to transcribed chromatin. Science *316*, 1050-1054.

Li, S., Ting, N.S., Zheng, L., Chen, P.L., Ziv, Y., Shiloh, Y., Lee, E.Y., and Lee, W.H. (2000). Functional link of BRCA1 and ataxia telangiectasia gene product in DNA damage response. Nature *406*, 210-215.

Li, X., Lee, Y.K., Jeng, J.C., Yen, Y., Schultz, D.C., Shih, H.M., and Ann, D.K. (2007). Role for KAP1 serine 824 phosphorylation and sumoylation/desumoylation switch in regulating KAP1-mediated transcriptional repression. The Journal of biological chemistry *282*, 36177-36189.

Lim, D.S., Vogel, H., Willerford, D.M., Sands, A.T., Platt, K.A., and Hasty, P. (2000). Analysis of ku80-mutant mice and cells with deficient levels of p53. Mol Cell Biol *20*, 3772-3780.

Lindahl, T., and Barnes, D.E. (2000). Repair of endogenous DNA damage. Cold Spring Harb Symp Quant Biol *65*, 127-133.

Liu, V.F., and Weaver, D.T. (1993). The ionizing radiation-induced replication protein A phosphorylation response differs between ataxia-telangiectasia and normal human cells. Molecular and Cellular Biology *13*, 7222-7231.

Lo, K.W., Kan, H.M., Chan, L.N., Xu, W.G., Wang, K.P., Wu, Z., Sheng, M., and Zhang, M. (2005). The 8-kDa dynein light chain binds to p53-binding protein 1 and mediates DNA damage-induced p53 nuclear accumulation. J Biol Chem *280*, 8172-8179.

Lobrich, M., Cooper, P.K., and Rydberg, B. (1996). Non-random distribution of DNA double-strand breaks induced by particle irradiation. Int J Radiat Biol *70*, 493-503.

Lomax, M.E., Cunniffe, S., and O'Neill, P. (2004). Efficiency of repair of an abasic site within DNA clustered damage sites by mammalian cell nuclear extracts. Biochemistry *43*, 11017-11026.

Lou, Z., Minter-Dykhouse, K., Franco, S., Gostissa, M., Rivera, M.A., Celeste, A., Manis, J.P., van Deursen, J., Nussenzweig, A., Paull, T.T*., et al.* (2006). MDC1 maintains genomic stability by participating in the amplification of ATM-dependent DNA damage signals. Molecular cell *21*, 187-200.

Lovejoy, C.A., and Cortez, D. (2009). Common mechanisms of PIKK regulation. DNA Repair (Amst) *8*, 1004-1008.

Lovly, C.M., Yan, L., Ryan, C.E., Takada, S., and Piwnica-Worms, H. (2008). Regulation of Chk2 ubiquitination and signaling through autophosphorylation of serine 379. Mol Cell Biol *28*, 5874-5885.

Lowe, S.W., Ruley, H.E., Jacks, T., and Housman, D.E. (1993). p53-dependent apoptosis modulates the cytotoxicity of anticancer agents. Cell *74*, 957-967.

Loyola, A., Huang, J.Y., LeRoy, G., Hu, S., Wang, Y.H., Donnelly, R.J., Lane, W.S., Lee, S.C., and Reinberg, D. (2003). Functional analysis of the subunits of the chromatin assembly factor RSF. Molecular and cellular biology *23*, 6759-6768.

Lu, B., Jan, L., and Jan, Y.N. (2000). Control of cell divisions in the nervous system: symmetry and asymmetry. Annu Rev Neurosci *23*, 531-556.

Lu, C., Zhu, F., Cho, Y.Y., Tang, F., Zykova, T., Ma, W.Y., Bode, A.M., and Dong, Z. (2006). Cell apoptosis: requirement of H2AX in DNA ladder formation, but not for the activation of caspase-3. Mol Cell *23*, 121-132.

Lukas, C., Bartkova, J., Latella, L., Falck, J., Mailand, N., Schroeder, T., Sehested, M., Lukas, J., and Bartek, J. (2001). DNA damage-activated kinase Chk2 is independent of proliferation or differentiation yet correlates with tissue biology. Cancer Res *61*, 4990-4993.

Lukas, C., Melander, F., Stucki, M., Falck, J., Bekker-Jensen, S., Goldberg, M., Lerenthal,

Y., Jackson, S.P., Bartek, J., and Lukas, J. (2004). Mdc1 couples DNA double-strand break recognition by Nbs1 with its H2AX-dependent chromatin retention. EMBO J *23*, 2674-2683.

Lusser, A., and Kadonaga, J.T. (2003). Chromatin remodeling by ATP-dependent molecular machines. Bioessays *25*, 1192-1200.

Ma, Y., Pannicke, U., Lu, H., Niewolik, D., Schwarz, K., and Lieber, M.R. (2005). The DNA-dependent protein kinase catalytic subunit phosphorylation sites in human Artemis. The Journal of biological chemistry *280*, 33839-33846.

Ma, Y., Pannicke, U., Schwarz, K., and Lieber, M.R. (2002). Hairpin opening and overhang processing by an Artemis/DNA-dependent protein kinase complex in nonhomologous end joining and V(D)J recombination. Cell *108*, 781-794.

Ma, Y., Schwarz, K., and Lieber, M.R. (2005). The Artemis:DNA-PKcs endonuclease cleaves DNA loops, flaps, and gaps. DNA Repair (Amst) *4*, 845-851.

Mailand, N., Bekker-Jensen, S., Bartek, J., and Lukas, J. (2006). Destruction of Claspin by SCFbetaTrCP restrains Chk1 activation and facilitates recovery from genotoxic stress. Molecular cell *23*, 307-318.

Mailand, N., Bekker-Jensen, S., Faustrup, H., Melander, F., Bartek, J., Lukas, C., and Lukas, J. (2007). RNF8 ubiquitylates histones at DNA double-strand breaks and promotes assembly of repair proteins. Cell *131*, 887-900.

Mailand, N., Podtelejnikov, A.V., Groth, A., Mann, M., Bartek, J., and Lukas, J. (2002). Regulation of G(2)/M events by Cdc25A through phosphorylation-dependent modulation of its stability. EMBO J *21*, 5911-5920.

Manis, J.P., Morales, J.C., Xia, Z., Kutok, J.L., Alt, F.W., and Carpenter, P.B. (2004). 53BP1 links DNA damage-response pathways to immunoglobulin heavy chain class-switch recombination. Nat Immunol *5*, 481-487.

Manke, I.A., Lowery, D.M., Nguyen, A., and Yaffe, M.B. (2003). BRCT repeats as phosphopeptide-binding modules involved in protein targeting. Science *302*, 636-639.

Mao, Z., Bozzella, M., Seluanov, A., and Gorbunova, V. (2008). Comparison of nonhomologous end joining and homologous recombination in human cells. DNA Repair (Amst) *7*, 1765-1771.

Marmorstein, R. (2001). Protein modules that manipulate histone tails for chromatin regulation. Nat Rev Mol Cell Biol *2*, 422-432.

Marples, B., Wouters, B.G., Collis, S.J., Chalmers, A.J., and Joiner, M.C. (2004). Low-dose hyper-radiosensitivity: a consequence of ineffective cell cycle arrest of radiation-damaged G2-phase cells. Radiat Res *161*, 247-255.

Martens, J.H., O'Sullivan, R.J., Braunschweig, U., Opravil, S., Radolf, M., Steinlein, P., and Jenuwein, T. (2005). The profile of repeat-associated histone lysine methylation states in the mouse epigenome. Embo J *24*, 800-812.

Matic, I., Macek, B., Hilger, M., Walther, T.C., and Mann, M. (2008). Phosphorylation of SUMO-1 occurs in vivo and is conserved through evolution. J Proteome Res *7*, 4050-4057.

Matijevic, T., Knezevic, J., Slavica, M., and Pavelic, J. (2009). Rett syndrome: from the gene to the disease. Eur Neurol *61*, 3-10.

Matranga, C., Tomari, Y., Shin, C., Bartel, D.P., and Zamore, P.D. (2005). Passenger-strand cleavage facilitates assembly of siRNA into Ago2-containing RNAi enzyme complexes. Cell *123*, 607-620.

Matsuoka, S., Ballif, B.A., Smogorzewska, A., McDonald, E.R., 3rd, Hurov, K.E., Luo, J., Bakalarski, C.E., Zhao, Z., Solimini, N., Lerenthal, Y.*, et al.* (2007). ATM and ATR substrate analysis reveals extensive protein networks responsive to DNA damage.

Science *316*, 1160-1166.

Matsuoka, S., Rotman, G., Ogawa, A., Shiloh, Y., Tamai, K., and Elledge, S.J. (2000). Ataxia telangiectasia-mutated phosphorylates Chk2 in vivo and in vitro. Proc Natl Acad Sci U S A *97*, 10389-10394.

Maya, R., Balass, M., Kim, S.T., Shkedy, D., Leal, J.F., Shifman, O., Moas, M., Buschmann, T., Ronai, Z., Shiloh, Y.*, et al.* (2001). ATM-dependent phosphorylation of Mdm2 on serine 395: role in p53 activation by DNA damage. Genes Dev *15*, 1067-1077.

McVey, M., and Lee, S.E. (2008). MMEJ repair of double-strand breaks (director's cut): deleted sequences and alternative endings. Trends Genet *24*, 529-538.

Meier, A., Fiegler, H., Munoz, P., Ellis, P., Rigler, D., Langford, C., Blasco, M.A., Carter, N., and Jackson, S.P. (2007). Spreading of mammalian DNA-damage response factors studied by ChIP-chip at damaged telomeres. Embo J *26*, 2707-2718.

Merkle, D., Douglas, P., Moorhead, G.B., Leonenko, Z., Yu, Y., Cramb, D., Bazett-Jones, D.P., and Lees-Miller, S.P. (2002). The DNA-dependent protein kinase interacts with DNA to form a protein-DNA complex that is disrupted by phosphorylation. Biochemistry *41*, 12706-12714.

Metzler-Guillemain, C., Luciani, J., Depetris, D., Guichaoua, M.R., and Mattei, M.G. (2003). HP1beta and HP1gamma, but not HP1alpha, decorate the entire XY body during human male meiosis. Chromosome Res *11*, 73-81.

Meza, J.E., Brzovic, P.S., King, M.C., and Klevit, R.E. (1999). Mapping the functional domains of BRCA1. Interaction of the ring finger domains of BRCA1 and BARD1. J Biol Chem *274*, 5659-5665.

Miklos, G.L., and John, B. (1979). Heterochromatin and satellite DNA in man: properties and prospects. Am J Hum Genet *31*, 264-280.

Miller, K.M., Tjeertes, J.V., Coates, J., Legube, G., Polo, S.E., Britton, S., and Jackson, S.P. (2010). Human HDAC1 and HDAC2 function in the DNA-damage response to promote DNA nonhomologous end-joining. Nature structural & molecular biology *17*, 1144-1151.

Miyazaki, T., Bressan, D.A., Shinohara, M., Haber, J.E., and Shinohara, A. (2004). In vivo assembly and disassembly of Rad51 and Rad52 complexes during double-strand break repair. EMBO J *23*, 939-949.

Mohammad, D.H., and Yaffe, M.B. (2009). 14-3-3 proteins, FHA domains and BRCT domains in the DNA damage response. DNA Repair (Amst) *8*, 1009-1017.

Moog, U., Smeets, E.E., van Roozendaal, K.E., Schoenmakers, S., Herbergs, J., Schoonbrood-Lenssen, A.M., and Schrander-Stumpel, C.T. (2003).Neurodevelopmental disorders in males related to the gene causing Rett syndrome in females (MECP2). Eur J Paediatr Neurol *7*, 5-12.

Morgan, D.O. (1995). Principles of CDK regulation. Nature *374*, 131-134.

Moshous, D., Callebaut, I., de Chasseval, R., Corneo, B., Cavazzana-Calvo, M., Le Deist, F., Tezcan, I., Sanal, O., Bertrand, Y., Philippe, N.*, et al.* (2001). Artemis, a novel DNA double-strand break repair/V(D)J recombination protein, is mutated in human severe combined immune deficiency. Cell *105*, 177-186.

Murayama, A., Ohmori, K., Fujimura, A., Minami, H., Yasuzawa-Tanaka, K., Kuroda, T., Oie, S., Daitoku, H., Okuwaki, M., Nagata, K.*, et al.* (2008). Epigenetic control of rDNA loci in response to intracellular energy status. Cell *133*, 627-639.

Murga, M., Bunting, S., Montana, M.F., Soria, R., Mulero, F., Canamero, M., Lee, Y., McKinnon, P.J., Nussenzweig, A., and Fernandez-Capetillo, O. (2009). A mouse model of ATR-Seckel shows embryonic replicative stress and accelerated aging. Nat Genet *41*, 891-898.

Murga, M., Jaco, I., Fan, Y., Soria, R., Martinez-Pastor, B., Cuadrado, M., Yang, S.M.,

Blasco, M.A., Skoultchi, A.I., and Fernandez-Capetillo, O. (2007). Global chromatin compaction limits the strength of the DNA damage response. J Cell Biol *178*, 1101-1108.

Murr, R., Loizou, J.I., Yang, Y.G., Cuenin, C., Li, H., Wang, Z.Q., and Herceg, Z. (2006). Histone acetylation by Trrap-Tip60 modulates loading of repair proteins and repair of DNA double-strand breaks. Nat Cell Biol *8*, 91-99.

Muslin, A.J., Tanner, J.W., Allen, P.M., and Shaw, A.S. (1996). Interaction of 14-3-3 with signaling proteins is mediated by the recognition of phosphoserine. Cell *84*, 889-897.

Naka, K., Tachibana, A., Ikeda, K., and Motoyama, N. (2004). Stress-induced premature senescence in hTERT-expressing ataxia telangiectasia fibroblasts. J Biol Chem *279*, 2030-2037.

Nakada, D., Matsumoto, K., and K., S. (2003). ATM-related Tel1 associates with double-strand breaks through an Xrs2-dependent mechanism. Genes and Development *17*, 1957-1962.

Nakada, S., Tai, I., Panier, S., Al-Hakim, A., Iemura, S., Juang, Y.C., O'Donnell, L., Kumakubo, A., Munro, M., Sicheri, F.*, et al.* (2010). Non-canonical inhibition of DNA damage-dependent ubiquitination by OTUB1. Nature *466*, 941-946.

Neven, B., Leroy, S., Decaluwe, H., Le Deist, F., Picard, C., Moshous, D., Mahlaoui, N., Debre, M., Casanova, J.L., Dal Cortivo, L.*, et al.* (2009). Long-term outcome after hematopoietic stem cell transplantation of a single-center cohort of 90 patients with severe combined immunodeficiency. Blood *113*, 4114-4124.

Nielsen, P.R., Nietlispach, D., Mott, H.R., Callaghan, J., Bannister, A., Kouzarides, T., Murzin, A.G., Murzina, N.V., and Laue, E.D. (2002). Structure of the HP1 chromodomain bound to histone H3 methylated at lysine 9. Nature *416*, 103-107.

Niida, H., Katsuno, Y., Banerjee, B., Hande, M.P., and Nakanishi, M. (2007). Specific role of Chk1 phosphorylations in cell survival and checkpoint activation. Mol Cell Biol *27*,

2572-2581.

Nikitina, T., Ghosh, R.P., Horowitz-Scherer, R.A., Hansen, J.C., Grigoryev, S.A., and Woodcock, C.L. (2007). MeCP2-chromatin interactions include the formation of chromatosome-like structures and are altered in mutations causing Rett syndrome. The Journal of biological chemistry *282*, 28237-28245.

Nikjoo, H., O'Neill, P., Goodhead, D.T., and Terrissol, M. (1997). Computational modelling of low-energy electron-induced DNA damage by early physical and chemical events. Int J Radiat Biol *71*, 467-483.

Noon, A.T., Shibata, A., Rief, N., Lobrich, M., Stewart, G.S., Jeggo, P.A., and Goodarzi, A.A. (2010). 53BP1-dependent robust localized KAP-1 phosphorylation is essential for heterochromatic DNA double-strand break repair. Nat Cell Biol *12*, 177-184.

O'Driscoll, M., and Jeggo, P.A. (2008). The role of the DNA damage response pathways in brain development and microcephaly: insight from human disorders. DNA Repair (Amst) *7*, 1039-1050.

O'Driscoll, M., Ruiz-Perez, V.L., Woods, C.G., Jeggo, P.A., and Goodship, J.A. (2003). A splicing mutation affecting expression of ataxia-telangiectasia and Rad3-related protein (ATR) results in Seckel syndrome. Nature Genetics *33*, 497-501.

Okada, T., Kamada, T., Tsuji, H., Mizoe, J.E., Baba, M., Kato, S., Yamada, S., Sugahara, S., Yasuda, S., Yamamoto, N.*, et al.* (2010). Carbon ion radiotherapy: clinical experiences at National Institute of Radiological Science (NIRS). Journal of Radiation Research *51*, 355-364.

Okayasu, R., Okada, M., Okabe, A., Noguchi, M., Takakura, K., and Takahashi, S. (2006). Repair of DNA damage induced by accelerated heavy ions in mammalian cells proficient and deficient in the non-homologous end-joining pathway. Radiat Res *165*, 59-67.

Palmer, D.K., O'Day, K., Trong, H.L., Charbonneau, H., and Margolis, R.L. (1991).

Purification of the centromere-specific protein CENP-A and demonstration that it is a distinctive histone. Proc Natl Acad Sci U S A *88*, 3734-3738.

Pannicke, U., Ma, Y., Hopfner, K.P., Niewolik, D., Lieber, M.R., and Schwarz, K. (2004). Functional and biochemical dissection of the structure-specific nuclease ARTEMIS. Embo J *23*, 1987-1997.

Park, J.H., Park, E.J., Lee, H.S., Kim, S.J., Hur, S.K., Imbalzano, A.N., and Kwon, J. (2006). Mammalian SWI/SNF complexes facilitate DNA double-strand break repair by promoting gamma-H2AX induction. Embo J *25*, 3986-3997.

Paull, T.T., and Gellert, M. (1998). The 3' to 5' exonuclease activity of Mre 11 facilitates repair of DNA double-strand breaks. Mol Cell *1*, 969-979.

Paulsen, R.D., and Cimprich, K.A. (2007). The ATR pathway: fine-tuning the fork. DNA Repair (Amst) *6*, 953-966.

Pazin, M.J., and Kadonaga, J.T. (1997). SWI2/SNF2 and related proteins: ATP-driven motors that disrupt protein-DNA interactions? Cell *88*, 737-740.

Pellegrini, M., Celeste, A., Difilippantonio, S., Guo, R., Wang, W., Feigenbaum, L., and Nussenzweig, A. (2006). Autophosphorylation at serine 1987 is dispensable for murine Atm activation in vivo. Nature *443*, 222-225.

Pellicioli, A., Lee, S.E., Lucca, C., Foiani, M., and Haber, J.E. (2001). Regulation of Saccharomyces Rad53 checkpoint kinase during adaptation from DNA damage-induced G2/M arrest. Molecular cell *7*, 293-300.

Pendas, A.M., Zhou, Z., Cadinanos, J., Freije, J.M., Wang, J., Hultenby, K., Astudillo, A., Wernerson, A., Rodriguez, F., Tryggvason, K.*, et al.* (2002). Defective prelamin A processing and muscular and adipocyte alterations in Zmpste24 metalloproteinase-deficient mice. Nature genetics *31*, 94-99.

Peng, A., and Chen, P.L. (2003). NFBD1, like 53BP1, is an early and redundant transducer mediating Chk2 phosphorylation in response to DNA damage. The Journal of biological chemistry *278*, 8873-8876.

Peters, A.H., O'Carroll, D., Scherthan, H., Mechtler, K., Sauer, S., Schofer, C., Weipoltshammer, K., Pagani, M., Lachner, M., Kohlmaier, A.*, et al.* (2001). Loss of the Suv39h histone methyltransferases impairs mammalian heterochromatin and genome stability. Cell *107*, 323-337.

Poinsignon, C., de Chasseval, R., Soubeyrand, S., Moshous, D., Fischer, A., Hache, R.J., and de Villartay, J.P. (2004). Phosphorylation of Artemis following irradiation-induced DNA damage. Eur J Immunol *34*, 3146-3155.

Polo, S.E., Kaidi, A., Baskcomb, L., Galanty, Y., and Jackson, S.P. (2010). Regulation of DNA-damage responses and cell-cycle progression by the chromatin remodelling factor CHD4. Embo J *29*, 3130-3139.

Polo, S.E., Roche, D., and Almouzni, G. (2006). New histone incorporation marks sites of UV repair in human cells. Cell *127*, 481-493.

Postow, L., Ghenoiu, C., Woo, E.M., Krutchinsky, A.N., Chait, B.T., and Funabiki, H. (2008). Ku80 removal from DNA through double strand break-induced ubiquitylation. J Cell Biol *182*, 467-479.

Preuss, S., and Pikaard, C.S. (2007). rRNA gene silencing and nucleolar dominance: insights into a chromosome-scale epigenetic on/off switch. Biochim Biophys Acta *1769*, 383-392.

Quennet, V., Beucher, A., Barton, O., Takeda, S., and Lobrich, M. (2010). CtIP and MRN promote non-homologous end-joining of etoposide-induced DNA double-strand breaks in G1. Nucleic Acids Res.

Reid, L.J., Shakya, R., Modi, A.P., Lokshin, M., Cheng, J.T., Jasin, M., Baer, R., and Ludwig, T. (2008). E3 ligase activity of BRCA1 is not essential for mammalian cell

viability or homology-directed repair of double-strand DNA breaks. Proc Natl Acad Sci U S A *105*, 20876-20881.

Rett, A. (1966). [On a unusual brain atrophy syndrome in hyperammonemia in childhood]. Wien Med Wochenschr *116*, 723-726.

Riballo, E., Kuhne, M., Rief, N., Doherty, A., Smith, G.C., Recio, M.J., Reis, C., Dahm, K., Fricke, A., Krempler, A.*, et al.* (2004). A pathway of double-strand break rejoining dependent upon ATM, Artemis, and proteins locating to gamma-H2AX foci. Molecular cell *16*, 715-724.

Riballo, E., Woodbine, L., Stiff, T., Walker, S.A., Goodarzi, A.A., and Jeggo, P.A. (2009). XLF-Cernunnos promotes DNA ligase IV-XRCC4 re-adenylation following ligation. Nucleic Acids Res *37*, 482-492.

Richards, E.J., and Elgin, S.C. (2002). Epigenetic codes for heterochromatin formation and silencing: rounding up the usual suspects. Cell *108*, 489-500.

Roberts, S.A., and Ramsden, D.A. (2007). Loading of the nonhomologous end joining factor, Ku, on protein-occluded DNA ends. The Journal of biological chemistry *282*, 10605-10613.

Rogakou, E.P., Nieves-Neira, W., Boon, C., Pommier, Y., and Bonner, W.M. (2000). Initiation of DNA fragmentation during apoptosis induces phosphorylation of H2AX histone at serine 139. J Biol Chem *275*, 9390-9395.

Rogakou, E.P., Pilch, D.R., Orr, A.H., Ivanova, V.S., and Bonner, W.M. (1998). DNA double-stranded breaks induce histone H2AX phosphorylation on serine 139. The Journal of biological chemistry *273*, 5858-5868.

Ross, G.M. (1999). Induction of cell death by radiotherapy. Endocr Relat Cancer *6*, 41-44.

Roth, D.B., and Wilson, J.H. (1986). Nonhomologous recombination in mammalian cells: role for short sequence homologies in the joining reaction. Molecular and Cellular Biology *6*, 4295-4304.

Rouse, J., and Jackson, S.P. (2000). LCD1: an essential gene involved in checkpoint control and regulation of the MEC1 signalling pathway in Saccharomyces cerevisiae. EMBO J *19*, 5801-5812.

Rusinol, A.E., and Sinensky, M.S. (2006). Farnesylated lamins, progeroid syndromes and farnesyl transferase inhibitors. J Cell Sci *119*, 3265-3272.

Saitoh, H., and Hinchey, J. (2000). Functional heterogeneity of small ubiquitin-related protein modifiers SUMO-1 versus SUMO-2/3. J Biol Chem *275*, 6252-6258.

Sanchez, Y., Wong, C., Thoma, R.S., Richman, R., Wu, Z., Piwnica-Worms, H., and Elledge, S.J. (1997). Conservation of the Chk1 checkpoint pathway in mammals: linkage of DNA damage to Cdk regulation through Cdc25. Science *277*, 1497-1501.

Sartori, A.A., Lukas, C., Coates, J., Mistrik, M., Fu, S., Bartek, J., Baer, R., Lukas, J., and Jackson, S.P. (2007). Human CtIP promotes DNA end resection. Nature *450*, 509-514.

Savic, V., Yin, B., Maas, N.L., Bredemeyer, A.L., Carpenter, A.C., Helmink, B.A., Yang-Iott, K.S., Sleckman, B.P., and Bassing, C.H. (2009). Formation of dynamic gamma-H2AX domains along broken DNA strands is distinctly regulated by ATM and MDC1 and dependent upon H2AX densities in chromatin. Molecular cell *34*, 298-310.

Savitsky, K., Bar-Shira, A., Gilad, S., Rotman, G., Ziv, Y., Vanagaite, L., Tagle, D.A., Smith, S., Uziel, T., Sfez, S*., et al.* (1995). A single ataxia telangiectasia gene with a product similar to PI-3 kinase. Science *268*, 1749-1753.

Scaffidi, P., and Misteli, T. (2005). Reversal of the cellular phenotype in the premature aging disease Hutchinson-Gilford progeria syndrome. Nat Med *11*, 440-445.

Schanen, N.C., Dahle, E.J., Capozzoli, F., Holm, V.A., Zoghbi, H.Y., and Francke, U. (1997). A new Rett syndrome family consistent with X-linked inheritance expands the X chromosome exclusion map. Am J Hum Genet *61*, 634-641.

Schreiber, V., Dantzer, F., Ame, J.C., and de Murcia, G. (2006). Poly(ADP-ribose): novel functions for an old molecule. Nat Rev Mol Cell Biol *7*, 517-528.

Scorah, J., Dong, M.Q., Yates, J.R., 3rd, Scott, M., Gillespie, D., and McGowan, C.H. (2008). A conserved proliferating cell nuclear antigen-interacting protein sequence in Chk1 is required for checkpoint function. J Biol Chem *283*, 17250-17259.

Semenenko, V.A., and Stewart, R.D. (2004). A fast Monte Carlo algorithm to simulate the spectrum of DNA damages formed by ionizing radiation. Radiat Res *161*, 451-457.

Serrano, M., and Blasco, M.A. (2001). Putting the stress on senescence. Curr Opin Cell Biol *13*, 748-753.

Shahbazian, M.D., Antalffy, B., Armstrong, D.L., and Zoghbi, H.Y. (2002). Insight into Rett syndrome: MeCP2 levels display tissue- and cell-specific differences and correlate with neuronal maturation. Human molecular genetics *11*, 115-124.

Shahbazian, M.D., and Zoghbi, H.Y. (2001). Molecular genetics of Rett syndrome and clinical spectrum of MECP2 mutations. Curr Opin Neurol *14*, 171-176.

Shanbhag, N.M., Rafalska-Metcalf, I.U., Balane-Bolivar, C., Janicki, S.M., and Greenberg, R.A. (2010). ATM-dependent chromatin changes silence transcription in cis to DNA double-strand breaks. Cell *141*, 970-981.

Shibata, A., Barton, O., Noon, A.T., Dahm, K., Deckbar, D., Goodarzi, A.A., Lobrich, M., and Jeggo, P.A. (2010). Role of ATM and the damage response mediator proteins 53BP1 and MDC1 in the maintenance of G(2)/M checkpoint arrest. Molecular and cellular biology *30*, 3371-3383.

Shibata, A., Conrad, S., Birraux, J., Geuting, V., Barton, O., Ismail, A., Kakarougkas, A.,

Meek, K., Taucher-Scholz, G., Lobrich, M.*, et al.* (2011). Factors determining DNA double-strand break repair pathway choice in G2 phase. Embo J.

Shieh, S.Y., Ahn, J., Tamai, K., Taya, Y., and Prives, C. (2000). The human homologs of checkpoint kinases Chk1 and Cds1 (Chk2) phosphorylate p53 at multiple DNA damage-inducible sites. Genes Dev *14*, 289-300.

Shiloh, Y. (2003). ATM and related protein kinases: safeguarding genome integrity. Nat Rev Cancer *3*, 155-168.

Shimada, K., Oma, Y., Schleker, T., Kugou, K., Ohta, K., Harata, M., and Gasser, S.M. (2008). Ino80 chromatin remodeling complex promotes recovery of stalled replication forks. Current biology : CB *18*, 566-575.

Shimada, M., Niida, H., Zineldeen, D.H., Tagami, H., Tanaka, M., Saito, H., and Nakanishi, M. (2008). Chk1 is a histone H3 threonine 11 kinase that regulates DNA damage-induced transcriptional repression. Cell *132*, 221-232.

Shroff, R., Arbel-Eden, A., Pilch, D., Ira, G., Bonner, W.M., Petrini, J.H., Haber, J.E., and Lichten, M. (2004). Distribution and dynamics of chromatin modification induced by a defined DNA double-strand break. Current biology : CB *14*, 1703-1711.

Shull, E.R., Lee, Y., Nakane, H., Stracker, T.H., Zhao, J., Russell, H.R., Petrini, J.H., and McKinnon, P.J. (2009). Differential DNA damage signaling accounts for distinct neural apoptotic responses in ATLD and NBS. Genes Dev *23*, 171-180.

Shumaker, D.K., Dechat, T., Kohlmaier, A., Adam, S.A., Bozovsky, M.R., Erdos, M.R., Eriksson, M., Goldman, A.E., Khuon, S., Collins, F.S.*, et al.* (2006). Mutant nuclear lamin A leads to progressive alterations of epigenetic control in premature aging. Proc Natl Acad Sci U S A *103*, 8703-8708.

Siliciano, J.D., Canman, C.E., Taya, Y., Sakaguchi, K., Appella, E., and Kastan, M.B. (1997). DNA damage induces phosphorylation of the amino terminus of p53. Genes Dev *11*, 3471-3481.

Sims, R.J., 3rd, Nishioka, K., and Reinberg, D. (2003). Histone lysine methylation: a signature for chromatin function. Trends Genet *19*, 629-639.

Simsek, D., and Jasin, M. (2010). Alternative end-joining is suppressed by the canonical NHEJ component Xrcc4-ligase IV during chromosomal translocation formation. Nat Struct Mol Biol *17*, 410-416.

Singleton, B.K., Torres-Arzayus, M.I., Rottinghaus, S.T., Taccioli, G.E., and Jeggo, P.A. (1999). The C terminus of Ku80 activates the DNA-dependent protein kinase catalytic subunit. Molecular and Cellular Biology *19*, 3267-3277.

Smith, G.C., Cary, R.B., N.D., L., Hann, B.C., Teo, S.H., Chen, D.J., and Jackson, S.P. (1999). Purification and DNA binding properties of the ataxia-telangiectasia gene product ATM. Proc Natl Acad Sci U S A *96*, 11134-11139.

Smits, V.A., Reaper, P.M., and Jackson, S.P. (2006). Rapid PIKK-dependent release of Chk1 from chromatin promotes the DNA-damage checkpoint response. Curr Biol *16*, 150-159.

Sobacchi, C., Marrella, V., Rucci, F., Vezzoni, P., and Villa, A. (2006). RAG-dependent primary immunodeficiencies. Hum Mutat *27*, 1174-1184.

Sorensen, C.S., Syljuasen, R.G., Falck, J., Schroeder, T., Ronnstrand, L., Khanna, K.K., Zhou, B.B., Bartek, J., and Lukas, J. (2003). Chk1 regulates the S phase checkpoint by coupling the physiological turnover and ionizing radiation-induced accelerated proteolysis of Cdc25A. Cancer Cell *3*, 247-258.

Soutoglou, E., and Misteli, T. (2008). Activation of the cellular DNA damage response in the absence of DNA lesions. Science *320*, 1507-1510.

Stagni, V., di Bari, M.G., Cursi, S., Condo, I., Cencioni, M.T., Testi, R., Lerenthal, Y., Cundari, E., and Barila, D. (2008). ATM kinase activity modulates Fas sensitivity through

the regulation of FLIP in lymphoid cells. Blood *111*, 829-837.

Stavnezer, J., Guikema, J.E., and Schrader, C.E. (2008). Mechanism and regulation of class switch recombination. Annu Rev Immunol *26*, 261-292.

Stearns, T. (2001). Centrosome duplication. a centriolar pas de deux. Cell *105*, 417-420.

Stewart, G.S., Panier, S., Townsend, K., Al-Hakim, A.K., Kolas, N.K., Miller, E.S., Nakada, S., Ylanko, J., Olivarius, S., Mendez, M.*, et al.* (2009). The RIDDLE syndrome protein mediates a ubiquitin-dependent signaling cascade at sites of DNA damage. Cell *136*, 420-434.

Stewart, G.S., Wang, B., Bignell, C.R., Taylor, A.M., and Elledge, S.J. (2003). MDC1 is a mediator of the mammalian DNA damage checkpoint. Nature *421*, 961-966.

Stiff, T., O'Driscoll, M., Rief, N., Iwabuchi, K., Lobrich, M., and Jeggo, P.A. (2004). ATM and DNA-PK function redundantly to phosphorylate H2AX after exposure to ionizing radiation. Cancer Res *64*, 2390-2396.

Stommel, J.M., Marchenko, N.D., Jimenez, G.S., Moll, U.M., Hope, T.J., and Wahl, G.M. (1999). A leucine-rich nuclear export signal in the p53 tetramerization domain: regulation of subcellular localization and p53 activity by NES masking. EMBO J *18*, 1660-1672.

Strahl, B.D., and Allis, C.D. (2000). The language of covalent histone modifications. Nature *403*, 41-45.

Sullivan, T., Escalante-Alcalde, D., Bhatt, H., Anver, M., Bhat, N., Nagashima, K., Stewart, C.L., and Burke, B. (1999). Loss of A-type lamin expression compromises nuclear envelope integrity leading to muscular dystrophy. J Cell Biol *147*, 913-920.

Sun, Y., Jiang, X., Chen, S., Fernandes, N., and Price, B.D. (2005). A role for the Tip60 histone acetyltransferase in the acetylation and activation of ATM. Proc Natl Acad Sci U

S A *102*, 13182-13187.

Sun, Y., Jiang, X., Xu, Y., Ayrapetov, M.K., Moreau, L.A., Whetstine, J.R., and Price, B.D. (2009). Histone H3 methylation links DNA damage detection to activation of the tumour suppressor Tip60. Nat Cell Biol *11*, 1376-1382.

Sun, Y., Xu, Y., Roy, K., and Price, B.D. (2007). DNA damage-induced acetylation of lysine 3016 of ATM activates ATM kinase activity. Mol Cell Biol *27*, 8502-8509.

Suto, R.K., Clarkson, M.J., Tremethick, D.J., and Luger, K. (2000). Crystal structure of a nucleosome core particle containing the variant histone H2A.Z. Nat Struct Biol *7*, 1121-1124.

Syljuasen, R.G. (2007). Checkpoint adaptation in human cells. Oncogene *26*, 5833-5839.

Tafani, M., Cohn, J.A., Karpinich, N.O., Rothman, R.J., Russo, M.A., and Farber, J.L. (2002). Regulation of intracellular pH mediates Bax activation in HeLa cells treated with staurosporine or tumor necrosis factor-alpha. J Biol Chem *277*, 49569-49576.

Tagami, H., Ray-Gallet, D., Almouzni, G., and Nakatani, Y. (2004). Histone H3.1 and H3.3 complexes mediate nucleosome assembly pathways dependent or independent of DNA synthesis. Cell *116*, 51-61.

Takahashi, K., and Kaneko, I. (1985). Changes in nuclease sensitivity of mammalian cells after irradiation with 60Co gamma-rays. Int J Radiat Biol Relat Stud Phys Chem Med *48*, 389-395.

Takai, H., Naka, K., Okada, Y., Watanabe, M., Harada, N., Saito, S., Anderson, C.W., Appella, E., Nakanishi, M., Suzuki, H.*, et al.* (2002). Chk2-deficient mice exhibit radioresistance and defective p53-mediated transcription. Embo J *21*, 5195-5205.

Takai, H., Tominaga, K., Motoyama, N., Minamishima, Y.A., Nagahama, H., Tsukiyama, T., Ikeda, K., Nakayama, K., and Nakanishi, M. (2000). Aberrant cell cycle checkpoint

function and early embryonic death in Chk1(-/-) mice. Genes Dev *14*, 1439-1447.

Takai, H., Tominaga, K., Motoyama, N., Minamishima, Y.A., Nagahama, H., Tsukiyama, T., Ikeda, K., Nakayama, K., and Nakanishi, M. (2000). Aberrant cell cycle checkpoint function and early embryonic death in Chk1(-/-) mice. Genes Dev *14*, 1439-1447.

Takisawa, H., Mimura, S., and Kubota, Y. (2000). Eukaryotic DNA replication: from pre-replication complex to initiation complex. Curr Opin Cell Biol *12*, 690-696.

Tamburini, B.A., and Tyler, J.K. (2005). Localized histone acetylation and deacetylation triggered by the homologous recombination pathway of double-strand DNA repair. Molecular and cellular biology *25*, 4903-4913.

Terada, Y., Tatsuka, M., Jinno, S., and Okayama, H. (1995). Requirement for tyrosine phosphorylation of Cdk4 in G1 arrest induced by ultraviolet irradiation. Nature *376*, 358-362.

Tsao, D., Kalogerinis, P., Tabrizi, I., Dingfelder, M., Stewart, R.D., and Georgakilas, A.G. (2007). Induction and processing of oxidative clustered DNA lesions in 56Fe-ion-irradiated human monocytes. Radiat Res *168*, 87-97.

Tschop, K., and Engeland, K. (2007). Cell cycle-dependent transcription of cyclin B2 is influenced by DNA methylation but is independent of methylation in the CDE and CHR elements. Febs J *274*, 5235-5249.

Tsukuda, T., Fleming, A.B., Nickoloff, J.A., and Osley, M.A. (2005). Chromatin remodelling at a DNA double-strand break site in Saccharomyces cerevisiae. Nature *438*, 379-383.

Tuck-Muller, C.M., Narayan, A., Tsien, F., Smeets, D.F., Sawyer, J., Fiala, E.S., Sohn, O.S., and Ehrlich, M. (2000). DNA hypomethylation and unusual chromosome instability in cell lines from ICF syndrome patients. Cytogenet Cell Genet *89*, 121-128.

Uziel, T., Lerenthal, Y., Moyal, L., Andegeko, Y., Mittelman, L., and Shiloh, Y. (2003). Requirement of the MRN complex for ATM activation by DNA damage. EMBO Journal *22*, 5612-5621.

Varela, I., Cadinanos, J., Pendas, A.M., Gutierrez-Fernandez, A., Folgueras, A.R., Sanchez, L.M., Zhou, Z., Rodriguez, F.J., Stewart, C.L., Vega, J.A*., et al.* (2005). Accelerated ageing in mice deficient in Zmpste24 protease is linked to p53 signalling activation. Nature *437*, 564-568.

Vaze, M.B., Pellicioli, A., Lee, S.E., Ira, G., Liberi, G., Arbel-Eden, A., Foiani, M., and Haber, J.E. (2002). Recovery from checkpoint-mediated arrest after repair of a double-strand break requires Srs2 helicase. Molecular cell *10*, 373-385.

Vogel, H., Lim, D.S., Karsenty, G., Finegold, M., and Hasty, P. (1999). Deletion of Ku86 causes early onset of senescence in mice. Proc Natl Acad Sci U S A *96*, 10770-10775.

Wang, B., Matsuoka, S., Carpenter, P.B., and Elledge, S.J. (2002). 53BP1, a mediator of the DNA damage checkpoint. Science *298*, 1435-1438.

Wang, M., Wu, W., Rosidi, B., Zhang, L., Wang, H., and Iliakis, G. (2006). PARP-1 and Ku compete for repair of DNA double strand breaks by distinct NHEJ pathways. Nucleic Acids Res *34*, 6170-6182.

Wang, X., Khadpe, J., Hu, B., Iliakis, G., and Wang, Y. (2003). An overactivated ATR/CHK1 pathway is responsible for the prolonged G2 accumulation in irradiated AT cells. The Journal of biological chemistry *278*, 30869-30874.

Wang, X., Zou, L., Lu, T., Bao, S., Hurov, K.E., Hittelman, W.N., Elledge, S.J., and Li, L. (2006). Rad17 phosphorylation is required for claspin recruitment and Chk1 activation in response to replication stress. Mol Cell *23*, 331-341.

Wang, Y., and Qin, J. (2003). MSH2 and ATR form a signaling module and regulate two branches of the damage response to DNA methylation. Proc Natl Acad Sci U S A *100*, 15387-15392.

Ward, I.M., and Chen, J. (2001). Histone H2AX is phosphorylated in an ATR-dependent manner in response to replicational stress. J Biol Chem *276*, 47759-47762.

Ward, I.M., Reina-San-Martin, B., Olaru, A., Minn, K., Tamada, K., Lau, J.S., Cascalho, M., Chen, L., Nussenzweig, A., Livak, F.*, et al.* (2004). 53BP1 is required for class switch recombination. J Cell Biol *165*, 459-464.

Ward, J.F. (1981). Some biochemical consequences of the spatial distribution of ionizing radiation-produced free radicals. Radiat Res *86*, 185-195.

Watanabe, K., Iwabuchi, K., Sun, J., Tsuji, Y., Tani, T., Tokunaga, K., Date, T., Hashimoto, M., Yamaizumi, M., and Tateishi, S. (2009). RAD18 promotes DNA double-strand break repair during G1 phase through chromatin retention of 53BP1. Nucleic Acids Res *37*, 2176-2193.

Watanabe, M., Maemura, K., Kanbara, K., Tamayama, T., and Hayasaki, H. (2002). GABA and GABA receptors in the central nervous system and other organs. Int Rev Cytol *213*, 1-47.

Weissman, L., de Souza-Pinto, N.C., Stevnsner, T., and Bohr, V.A. (2007). DNA repair, mitochondria, and neurodegeneration. Neuroscience *145*, 1318-1329.

West, S.C. (2003). Molecular views of recombination proteins and their control. Nat Rev Mol Cell Biol *4*, 435-445.

Williams, R.S., and Tainer, J.A. (2007). Learning our ABCs: Rad50 directs MRN repair functions via adenylate kinase activity from the conserved ATP binding cassette. Mol Cell *25*, 789-791.

Williams, R.S., Williams, J.S., and Tainer, J.A. (2007). Mre11-Rad50-Nbs1 is a keystone complex connecting DNA repair machinery, double-strand break signaling, and the chromatin template. Biochem Cell Biol *85*, 509-520.

Wilson, C.W. (1946). Energy absorption and integral dose in x-ray and radium therapy; a review. Radiology *47*, 263-278.

Wold, M.S. (1997). Replication protein A: a heterotrimeric, single-stranded DNA-binding protein required for eukaryotic DNA metabolism. Annu Rev Biochem *66*, 61-92.

Wolter, K.G., Hsu, Y.T., Smith, C.L., Nechushtan, A., Xi, X.G., and Youle, R.J. (1997). Movement of Bax from the cytosol to mitochondria during apoptosis. J Cell Biol *139*, 1281-1292.

Wu, L.C., Wang, Z.W., Tsan, J.T., Spillman, M.A., Phung, A., Xu, X.L., Yang, M.C., Hwang, L.Y., Bowcock, A.M., and Baer, R. (1996). Identification of a RING protein that can interact in vivo with the BRCA1 gene product. Nat Genet *14*, 430-440.

Wyman, C., and Kanaar, R. (2006). DNA double-strand break repair: all's well that ends well. Annu Rev Genet *40*, 363-383.

Xia, B., Sheng, Q., Nakanishi, K., Ohashi, A., Wu, J., Christ, N., Liu, X., Jasin, M., Couch, F.J., and Livingston, D.M. (2006). Control of BRCA2 cellular and clinical functions by a nuclear partner, PALB2. Mol Cell *22*, 719-729.

Xie, G., Habbersett, R.C., Jia, Y., Peterson, S.R., Lehnert, B.E., Bradbury, E.M., and D'Anna, J.A. (1998). Requirements for p53 and the ATM gene product in the regulation of G1/S and S phase checkpoints. Oncogene *16*, 721-736.

Xu, B., Kim, S.T., Lim, D.S., and Kastan, M.B. (2002). Two Molecularly Distinct G2/M Checkpoints Are Induced by Ionizing Irradiation. Molecular and cellular biology *22*, 1049-1059.

Xu, X., Tsvetkov, L.M., and Stern, D.F. (2002). Chk2 activation and phosphorylation-dependent oligomerization. Mol Cell Biol *22*, 4419-4432.

Yang, S., Jeong, J.H., Brown, A.L., Lee, C.H., Pandolfi, P.P., Chung, J.H., and Kim, M.K.

(2006). Promyelocytic leukemia activates Chk2 by mediating Chk2 autophosphorylation. J Biol Chem *281*, 26645-26654.

Yang, X.H., and Zou, L. (2006). Recruitment of ATR-ATRIP, Rad17, and 9-1-1 complexes to DNA damage. Methods Enzymol *409*, 118-131.

Yang, Z., Kodama, S., Suzuki, K., and Watanabe, M. (1998). Telomerase activity, telomere length, and chromosome aberrations in the extension of life span of human embryo cells induced by low-dose X-rays. J Radiat Res (Tokyo) *39*, 35-51.

Yarden, R.I., Pardo-Reoyo, S., Sgagias, M., Cowan, K.H., and Brody, L.C. (2002). BRCA1 regulates the G2/M checkpoint by activating Chk1 kinase upon DNA damage. Nat Genet *30*, 285-289.

Yoda, K., and Ando, S. (2004). Immunological analysis and purification of centromere complex. Methods in enzymology *375*, 270-277.

You, Z., and Bailis, J.M. (2010). DNA damage and decisions: CtIP coordinates DNA repair and cell cycle checkpoints. Trends Cell Biol *20*, 402-409.

Yu, J.S., Chen, W.J., Ni, M.H., Chan, W.H., and Yang, S.D. (1998). Identification of the regulatory autophosphorylation site of autophosphorylation-dependent protein kinase (auto-kinase). Evidence that auto-kinase belongs to a member of the p21-activated kinase family. Biochem J *334 (Pt 1)*, 121-131.

Yu, X., and Chen, J. (2004). DNA damage-induced cell cycle checkpoint control requires CtIP, a phosphorylation-dependent binding partner of BRCA1 C-terminal domains. Mol Cell Biol *24*, 9478-9486.

Yu, X., Chini, C.C., He, M., Mer, G., and Chen, J. (2003). The BRCT domain is a phospho-protein binding domain. Science *302*, 639-642.

Yunis, J.J., Roldan, L., Yasmineh, W.G., and Lee, J.C. (1971). Staining of satellite DNA in

metaphase chromosomes. Nature *231*, 532-533.

Yusufzai, T.M., and Wolffe, A.P. (2000). Functional consequences of Rett syndrome mutations on human MeCP2. Nucleic acids research *28*, 4172-4179.

Zeng, L., Yap, K.L., Ivanov, A.V., Wang, X., Mujtaba, S., Plotnikova, O., Rauscher, F.J., 3rd, and Zhou, M.M. (2008). Structural insights into human KAP1 PHD finger-bromodomain and its role in gene silencing. Nature structural & molecular biology *15*, 626-633.

Zhang, X., Morera, S., Bates, P.A., Whitehead, P.C., Coffer, A.I., Hainbucher, K., Nash, R.A., Sternberg, M.J., Lindahl, T., and Freemont, P.S. (1998). Structure of an XRCC1 BRCT domain: a new protein-protein interaction module. EMBO J *17*, 6404-6411.

Zhang, Y., and Rowley, J.D. (2006). Chromatin structural elements and chromosomal translocations in leukemia. DNA Repair (Amst) *5*, 1282-1297.

Zhang, Y., and Xiong, Y. (2001). A p53 amino-terminal nuclear export signal inhibited by DNA damage-induced phosphorylation. Science *292*, 1910-1915.

Zheng, L., Pan, H., Li, S., Flesken-Nikitin, A., Chen, P.L., Boyer, T.G., and Lee, W.H. (2000). Sequence-specific transcriptional corepressor function for BRCA1 through a novel zinc finger protein, ZBRK1. Molecular cell *6*, 757-768.

Zhu, J., Woods, D., McMahon, M., and Bishop, J.M. (1998). Senescence of human fibroblasts induced by oncogenic Raf. Genes Dev *12*, 2997-3007.

Ziv, Y., Bielopolski, D., Galanty, Y., Lukas, C., Taya, Y., Schultz, D.C., Lukas, J., Bekker-Jensen, S., Bartek, J., and Shiloh, Y. (2006). Chromatin relaxation in response to DNA double-strand breaks is modulated by a novel ATM- and KAP-1 dependent pathway. Nat Cell Biol *8*, 870-876.

Zou, L., and Elledge, S.J. (2003). Sensing DNA damage through ATRIP recognition of

RPA-ssDNA complexes. Science *300*, 1542-1548.

Appendix

Analysis of human syndromes with disordered chromatin reveals the impact of heterochromatin on the efficacy of ATM-dependent G2/M checkpoint arrest.

Holly Brunton[1], Aaron A. Goodarzi[1], Angela T. Noon[1], Amruta Shrikhande[1], R. Scott Hansen[2], Penny A. Jeggo[1*] and Atsushi Shibata[1*]

[1]Genome Damage and Stability Centre, University of Sussex,

[2]Departments of Medicine and Genome Sciences, University of Washington, Seattle, WA 98195, USA

Running Title: Disordered heterochromatin enhances ATM signalling

***Corresponding authors:**

A. Shibata as303@sussex.ac.uk

Tel: 0044 1273 678482

Fax: 0044 1273 678121

P. A. Jeggo p.a.jeggo@sussex.ac.uk

Tel: 0044 1273 678482

Fax: 0044 1273 678121

Abstract

Heterochromatin (HC) poses a barrier to γH2AX foci expansion and DNA double strand break (DSB) repair, the latter being relieved by ATM-dependent KAP-1 phosphorylation. Using high resolution imaging, we show that the HC superstructure markedly restricts ATM signalling to cell cycle checkpoint proteins. The impact of HC is greater than anticipated from the percentage of HC-DNA and, in distinction to DSB repair, ATM only partly overcomes the constraints posed by HC. Importantly, we examine ATM signalling in human syndromes with disordered HC. Following depletion of MeCP2 and DNMT3B, proteins defective in Rett and Immunodeficiency with Centromere instability and Facial anomalies (ICF) Syndromes, respectively, we demonstrate enhanced γH2AX signal expansion at HC-chromocentres in mouse NIH3T3 cells, which have visible HC-chromocentres. Previous studies have shown that the G2/M checkpoint is inefficient requiring multiple DSBs to initiate arrest. MeCP2 and DNMT3B depletion leads to hypersensitive radiation-induced G2/M checkpoint arrest despite normal DSB repair. Cell lines from Rett, ICF and Hutchinson Guildford Progeria Syndrome patients similarly showed hyperactivated ATM signalling, hypersensitive and prolonged G2/M checkpoint arrest. Collectively, these findings reveal that heterochromatin contributes to the previously described inefficient G2/M checkpoint arrest and demonstrate how the signalling response can be uncoupled from DSB repair.

Introduction

The DNA damage response (DDR) to the presence of DNA double strand breaks (DSBs) encompasses pathways of DSB repair and a signal transduction response that includes the activation of cell cycle checkpoint arrest and/or apoptosis. ATM-dependent signalling is the most significant signal transduction pathway activated by DSBs (19). An early step in the signalling pathway is the phosphorylation of H2AX, a step that can be affected by either ATM or DNA-PKcs. The damage response mediator proteins, MDC1, RNF8, RNF168 and 53BP1, localise to the DSB generating irradiation-induced foci (IRIF) (25-26, 34). The precise function of IRIF remains unclear; cells lacking IRIF activate checkpoint arrest normally except at low doses where IRIF appear to function to amplify the signal. Most DSB repair occurs independently of ATM signalling but, critically, a subset of DSBs requires ATM and IRIF proteins for their repair (15, 28).

Over the past few years, a range of studies have demonstrated that chromatin structure exerts a significant impact on the DDR. For example histone H1 restricts DDR signal amplification and reduced H1 levels confer hypersensitive G2/M checkpoint arrest (23). This study provided initial evidence that the size of γH2AX foci determines the magnitude of the ATM signal and the sensitivity of G2/M checkpoint arrest. Additionally, studies have shown that both transcription and higher order chromatin structure can impact upon the expansion of γH2AX foci (8, 15, 17-18). Of relevance to this work, it has been shown that γH2AX foci expansion is restricted by heterochromatin (HC) and that IRIF expand on the periphery rather than within HC regions (8, 15, 18). Further, despite the expansion of IRIF at the HC periphery, ATM-dependent signalling is required for the repair of HC-DSBs in contrast to DSBs located within euchromatic (EC) regions. Such repair requires ATM-dependent phosphorylation of the HC building factor, Kruppel-associated box (KRAB)-associated protein-1 (KAP-1) (24). Thus, the sub-set of DSBs that specifically require ATM for repair represent HC-DSBs. Interestingly,

recent findings have also shown the HC restricts DSB repair by homologous recombination in Drosophila, although there are differences to the situation in mammalian cells (7). Firstly, HC-DSB repair in Drosophila is predominantly ATR-dependent. Further, the phosphorylation site on KAP-1 does not appear to be conserved in Drosophila. Thus, whilst HC represents a barrier to repair in both organisms, the way of overcoming this may differ to some extent. In mammalian cells, although γH2AX foci do not expand within the centre of densely staining DAPI-chromocentres, they appear to expand normally at their periphery albeit with restricted encroachment into the HC superstructure. Indeed, no difference in the size of γH2AX foci at EC and HC DSBs is apparent or has been reported. Thus, although ATM-dependent KAP-1 phosphorylation is required to enable repair of HC-DSBs, it is unclear whether the HC superstructure actually impacts upon ATM signalling to the checkpoint machinery.

G2/M checkpoint arrest, a crucial endpoint of ATM signalling, co-ordinates DSB formation and repair with cell cycle progression. The G2/M checkpoint has a defined sensitivity and as a consequence is not activated by low radiation doses (10, 13). The same concept also results in the release of cells from checkpoint arrest prior to completion of DSB repair. The magnitude of ATM signalling and the impact on the initiation and maintenance of checkpoint arrest is thus responsive to the progress of DSB repair; hence defects that impair DSB repair result in prolonged ATM signalling and checkpoint arrest. The recent analysis of factors that influence chromatin modifications such as HDAC1/2 and CHD4 have shown that they can impact upon both DSB repair and signal expansion with enhanced signalling likely being a consequence of impaired DSB repair (22, 27). In the first part of this study, we examine whether HC superstructure modulates the magnitude of ATM signalling to cell cycle checkpoint arrest. In contrast to the situation above where DSB repair is impaired, we examine situations where the rate of DSB repair is unperturbed. We observed that depletion of factors required for the building of the HC superstructure confers enhanced ATM signal expansion at HC-DSBs compared to that arising at EC-DSBs. Unexpectedly, this resulted in hypersensitive and

prolonged G2/M checkpoint arrest. These findings provide the first evidence that HC superstructure exerts a significant impact upon checkpoint arrest independently of any impact on DSB repair, uncoupling checkpoint signalling from repair.

How HC superstructure influences the DDR is important to evaluate, not least because the HC content can differ between tissues and cell types. Further, human syndromes with disordered HC structure have been reported. These syndromes include Rett Syndrome, which harbours mutations in MeCP2, a methyl CpG-binding protein, Immunodeficiency with Centromere instability and Facial anomalies (ICF), Syndrome which is mutated in the DNA methyl transferase, DNMT3B and Hutchinson Gilford Progeria Syndrome (HGPS), which has mutations in Lamin A and displays progressive HC loss (3, 5, 9, 31). The HC superstructure involves a self-reinforcing web of histone and DNA modifications constructed with additional factors or complexes that have chromatin remodelling activity. KAP-1 functions as a scaffold protein and targets the KRAB-ZFP superfamily, thereby co-ordinating histone methylation and the deposition of HP1 (4). Methylation at CpG islands contributes to gene silencing due, in part, to the recruitment of methyl-CpG-binding protein 2 (MeCP2) (33), which interacts with HDAC1/2 and additional co-repressor proteins (1). MeCP2 also directly interacts with HP1 (2).

In the second part of our study, we examine whether disordered HC in patient cells impacts upon ATM signalling to cell cycle checkpoint arrest. Importantly, in these syndromes, the rate of DSB repair is identical to that observed in control, although the requirement for ATM is partly overcome. Strikingly, despite a normal rate of DSB repair in these syndrome cells, we observe hypersensitive and prolonged G2/M checkpoint arrest. Our findings show that HC exerts a substantial impact on the magnitude of ATM signalling and contributes to the previously described inefficient G2/M checkpoint response.

Materials and methods

Cell culture, drug treatment and irradiation

48BR (wild type) and GM16548, GM11271 and GM11272 (Rett/MeCP2) primary human fibroblasts, 1BR hTERT and PT3 (ICF/DNMT3B) hTERT cells were cultured in DMEM with 15% FCS. GM02188 (wild type), GM16548 (Rett/MeCP2), GM08714 (ICF/DNMT3B) and AG10801 (HGPS/Lamin A) are lymphoblastoid cell lines (LBLs) and were cultured in RPMI with 10% FCS. NIH 3T3, MEFs and A549 cells were cultured in MEM with 10% FCS. All culture medium are supplemented with L-glutamine, penicillin and streptomycin. 10 μM ATM inhibitor (Calbiochem) and 2.5 μM Chk1/Chk2 inhibitor, SB218078 (Tocris Bioscience, USA), were added

30 min before IR. Cells were irradiated in medium using either a ^{137}Cs gamma-source (dose rate, 7.5 Gy/min) or 250 kV X-rays delivered at 12 mA (dose rate, 0.5 Gy/min).

siRNA knockdown and MeCP2 expression

siRNA transfection of 48BR, 1BR hTERT, A549 and NIH 3T3 cells was undertaken using Metafectene Pro (Biotex, Germany) or Hiperfect (Qiagen, Hilden, Germany) according to the manufacture's instructions. Scramble control, mouse MeCP2 and mouse DNMT3B were from Dharmacon SMART pool siRNA. Two distinct human MeCP2 and DNMT3B siRNA oligonucleotides were obtained from Invitrogen. The sequence of human and mouse KAP-1 siRNA is as described previously (15). siRNA knockdown was carried out in suspended cells after trypsinization. After 24 hr, cells were trypsinized and retransfected with siRNA. Cells were incubated for 48 hr after the second transfection prior to analysis. The MeCP2 expressing vector (pEGFP-MeCP2) was kindly provided by Dr. Adrian Bird. Wild type (WT) EGFP-MeCP2 was expressed in Rett LBL cells using GeneJuice (Novagen, MERCK, Germany) according to the manufacture's instructions. To express WT MeCP2 in MeCP2 siRNA cells, three mutations within the siRNA target sequence were introduced in MeCP2 cDNA using QuikChange^{TM} Site-Directed Mutagenesis Kit (Invitrogen). pEGFP-MeCP2 plasmid was transfected into cells for 6 hours, 24 hours after siRNA knock down of 1BR hTERT cells. Following incubation at 37 ^{o}C for 16-24 hour, cells were irradiated and analysed.

Immunofluorescence and immunoblotting

Immunofluorescence and immunoblotting were performed using antibodies against γH2AX (Upstate Technology, UK), 53BP1 (Bethyl Laboratories, Montgomery, USA), p-histone H3 (p-H3)

Ser10 (Upstate Biotechnology, Buckingham, UK), Chk2 pThr68 (Cell signalling technology, Beverly, MA, USA), Chk2 (Abcam, Cambridge, UK or Cell signalling technology, Beverly, MA, USA), KAP-1 (Abcam, Cambridge, UK), Ku70 (Sata Cruz, CA, USA), ATM pSer1981 (Epitomics, CA, USA), ATM (Cell signalling technology, Beverly, MA, USA), ATR (Santa Cruz, CA, USA), Chk1 (Cell signalling technology, Beverly, MA, USA), p53 (Santa Cruz, CA, USA), Ku80 (polyclonal rabbit antibody), Actin (Abcam, Cambridge, UK) and CENP-F (Abcam, Cambridge, UK). For immunofluorescence, cover-slips were visualized using the Zeiss Axioplan microscope and simple PCI software. An Applied Precision® DeltaVision® RT Olympus IX70 deconvolution microscope and softWoRx® Suite software was used for high resolution and three dimensional imaging of deconvolved z-stacks.

Analysis of signal intensity by ImageJ and softWoRx® Suite software

The signal intensity of FITC and DAPI per γH2AX focus was quantified with ImageJ in Fig. 2C and 4C. In the pChk2 and pATM signal intensity analyses in Fig. 3C and 6D, the untreated nuclear intensity was subtracted from the IR induced nuclear signal intensity. The images were taken by the Zeiss Axioplan microscope with identical exposure time. The size of γH2AX foci at chromocentre in Fig. 2E and 4E was quantified with ImageJ after deconvolution with softWoRx® Suite software. Quantitative measurements of γH2AX and DAPI overlap were obtained and visualized as a red signal using softWoRx® Suite software. The size of overlapping regions per cell was quantified by ImageJ. The number of chromocentres was analysed and showed similar between cell lines (data not shown). The size of overlap per chromocentre was normalized following these analyses. The volume of the interior signal was visualized and measured by Huygens Professional, Scientific Volume Imaging. Similar to the analysis of overlap, the volume per chromocentre was normalized to the number of chromocentres (Fig. 2F and 4F).

γH2AX foci and G2/M checkpoint analysis

DSB repair was monitored by disappearance of γH2AX foci (21). G1 and G2 phase cells were identified using the cell cycle marker, anti-CENPF in human cells and anti-p-H3 Ser10 in mouse cells, respectively (6). S phase cells show a mild CENPF signal whereas G2 cells shows substantially greater signal. M phase cells are identified by their morphological changes, i.e. condensed chromatin by DAPI. For DSB repair in cycling cells and maintenance of G2/M checkpoint analysis, 4 μM aphidicolin (APH) was added immediately after IR to block entry of irradiated S phase cells into G2 during analysis. Replication in the presence of APH induces extensive γH2AX signalling, which helps the identification of S phase cells during γH2AX foci analysis. APH does not impact upon DSB repair and signalling in G1 and G2 phase (6, 21, 30). For initiation of G2/M checkpoint analysis, cells were fixed 1 or 2 h after IR, and stained for p-H3 Ser10 and DAPI. p-H3 Ser10 positive and condensed chromatin cells were counted as mitotic index. >400 cells were scored per condition.

Trimethylated K9 of histone H3 IP

After IR, $5x10^6$ LBL cells were washed with PBS and then with low-salt buffer (LSB) [10 mM HEPES [pH 7.4], 25 mM KCl, 10 mM NaCl, 1 mM $MgCl_2$, 0.1 mM EDTA]. Pelleted cells were resuspended in LSB + phosphatase and a protease inhibitor cocktail (Sigma-Aldrich, UK) and snap frozen in liquid nitrogen. Cells were quick thawed and immediately centrifuged for 10 min at 10,000 rpm. The pellet was resuspended and treated with 100 U/ml MNase in nuclease buffer [10 mM HEPES [pH 7.9], 10 mM KCl, 1.0 mM $CaCl_2$, 1.5 mM $MgCl_2$, 0.34 M sucrose, 10% glycerol, 1 mM DTT, 0.1% [v/v] Triton X-100]. After incubation at 37 ^oC for 45 min, an equal volume of solubilization buffer [nuclease buffer + 2% [v/v] NP-40, 2% [v/v] Triton X-100, 600

mM NaCl] was added. Samples were then briefly sonicated and centrifuged at 10,000 rpm for 10 min. The resulting supernatant, containing solubilized nucleosomes (50 μg) was incubated with 2 μg of ChIP grade α-TriMe K9 histone H3 monoclonal antibody (Abcam, Cambridge, UK) overnight at 4 ^{o}C. Immunocomplexes were pulled down by adding protein G and A-sepharose (1:1) for 30 min at 4 ^{o}C. Samples were boiled for 3 min before electrophoresis in SDS-PAGE.

Pulsed-field gel electrophoresis (PFGE)

Cells were exposed to 20 Gy IR and trypsinised at the times indicated, then washed twice with PBS and embedded in 0.75% low melting agarose gel plugs (SeaPlaque agarose, Cambrex Bioproducts) at a concentration of 0.75×10^5 cells/plug. Plugs were placed in buffer containing 20 μg/ml proteinase K, 0.5 M EDTA, and 1% sarkosyl (pH 9.0) and incubated at 50°C for 24 hours in the dark. Plugs were washed with 50 mM EDTA at room temperature for 1 hour and stored at 4°C. PFGE was carried out using a CHEF Mapper (Bio-Rad), with a cooling module (Model 1000 Mini Chiller, Bio-Rad) in 1% agarose gels (Pulsed Field Certified Agarose, Bio-Rad) in 0.5 × TBE. The forward and reverse voltage gradients were 5.4 V/cm and 3.6 V/cm, respectively for 5 to 60 seconds for a total of 20 h at 14°C. After PFGE, gels were stained with ethidium bromide and photographed under UV transillumination. The signal intensity of the smear was quantified by ImageJ at each time point and normalized to the intensity at 15 min after IR.

Results

KAP-1 depletion enhances the expansion of HC-associated γH2AX foci

Previous studies have shown that γH2AX foci do not expand into HC regions and that HC can restrict DSB repair (8, 15, 18). siRNA mediated depletion of KAP-1, which is a HC building factor, does not affect the rate of DSB repair in control cells but bypasses the requirement for ATM (15). Here, we examined how depletion of KAP-1 and other HC factors impact upon γH2AX signal expansion at HC-DSBs. Firstly, we compared the kinetics of IR-induced γH2AX foci formation at HC and EC regions using NIH3T3 cells, which have readily visualised dense DAPI staining chromocentres that correspond to pericentromeric and centromeric HC (15-16). We defined γH2AX foci that overlap/juxtapose or do not overlap with chromocentres as HC and EC associated foci, respectively (Fig. 1A). To directly compare the speed of foci formation at EC versus HC-DSBs, we enumerated γH2AX foci up to 20 min post IR when foci numbers become maximal (Fig. 1B-D). Significantly, we show that the kinetics of γH2AX formation is dose independent and occurs more rapidly at EC than at HC-DSBs (Fig. 1E).

We next examined whether loss of KAP-1 temporally affects the appearance of γH2AX foci formation after IR. Although KAP-1 siRNA does not significantly change the size or structure of chromocentres (data not shown), it specifically enhances the rate of foci formation at HC-DSBs (Fig. 2A and B). To assess the size of γH2AX foci, we monitored the signal intensity at foci of different DAPI signal intensity following control or KAP-1 siRNA at 30 min post IR, a time when maximal foci numbers have been reached. We arbitrarily defined regions of high and low DAPI signal as representing HC or EC regions. Although an inexact definition, it allows the impact of chromatin compaction to be assessed. Initially, we carried out a two-dimensional analysis of the size of individual foci. In control cells, the foci size at 30 min post IR was independent of DAPI signal intensity. Thus, despite their slower rate of formation, foci at

HC-DSBs reach a similar size to those at EC-DSBs by 30 mins. KAP-1 siRNA significantly increased the γH2AX signal intensity at DAPI regions of higher density relative to those of lower density, where no significant impact of KAP-1 siRNA was observed (Fig. 2C). Surprisingly, the signal intensity at regions of high DAPI signal following KAP-1 depletion was greater than in the regions of lower DAPI signal and greater than observed in control cells (see discussion for possible explanations). This suggests that ATM signalling either does not fully relieve the barrier posed by HC to foci expansion or does so inefficiently. To engineer loss of ATM signalling specifically at HC-DSBs, we examined the impact of 53BP1 knockdown, since we have previously shown that 53BP1 increases the retention of ATM at DSBs specifically promoting pKAP-1 foci formation at KAP-1-rich HC-DSBs; it does not impair pan-nuclear pKAP-1 since 53BP1 only slightly reduces overall ATM signalling (24). Significantly, 53BP1 siRNA resulted in a greater decrease in size of γH2AX foci at HC compared to EC regions (Fig. 2C). This suggests that ATM-dependent pKAP-1 accumulation at HC-DSBs enhances γH2AX foci size but does not fully overcome the barrier posed by the HC superstructure. In contrast, ATM inhibitor (ATMi) treatment reduced γH2AX foci size irrespective of DAPI density (Fig. 2C).

Thus, global HC relaxation following KAP-1 knockdown provides a greater level of foci expansion than observed in control cells despite ATM activation. This is likely because in control cells pKAP-1 formation around a DSB only causes HC relaxation in the DSB vicinity whereas KAP-1 knockdown causes more extensive HC relaxation.

To assess further the impact of HC on γH2AX foci expansion, we quantified the magnitude of γH2AX-chromocentre overlap using high resolution deconvolved z-stacked images in KAP-1 depleted cells (this also represents a two dimensional analysis) (Fig. 2D) (N.B. we did not perform this analysis in 53BP1 siRNA or ATMi treated cells because of the tiny size of the foci at HC regions). We observed a > 3 fold increase in the magnitude of γH2AX foci-chromocentre overlap following KAP-1 siRNA (Fig. 2E). To examine whether this represents

expansion of foci on the surface of chromocentres or into the HC interior, we measured the volume of γH2AX signal within the HC interior using three dimensional modelling software (Fig. 2F). Strikingly, we observed substantially greater γH2AX-DAPI overlap within the interior of chromocentres following KAP-1 siRNA. Collectively, these findings show that HC confers a substantial barrier to both the speed of formation and expansion of γH2AX foci and ATM signalling partly but not fully overcomes this barrier. Despite this, γH2AX foci formed at HC and EC regions are similar size largely due to the expansion of HC-foci into the neighbouring EC region.

Depletion of KAP-1 enhances ATM signalling and G2/M checkpoint sensitivity.

We next examined whether the enhanced γH2AX foci expansion at chromocentres which we observe following KAP-1 siRNA correlates with enhanced checkpoint signalling and arrest. To monitor checkpoint signalling, we examined IR-induced Chk2 phosphorylation (pChk2) by Western blotting and observed increased pChk2 following KAP-1 depletion (Fig. 3A). The ATM dependency of Chk2 activation was confirmed using ATMi (Fig. 3B). By immunofluorescence (IF), KAP-1 depleted cells showed a 2-3 fold increase in pChk2 levels compared to control after IR (Fig. 3C). We also examined the sensitivity of G2/M checkpoint arrest following KAP-1 siRNA, exploiting our previous findings that checkpoint arrest is not initiated after low IR doses (10). Cells were transfected with control or KAP-1 siRNA in WT or *ATM*$^{-/-}$ MEFs and G2/M checkpoint arrest monitored by scoring phospho-histone H3 Ser10 positive cells 1 hr after IR. G2/M arrest was abolished in *ATM*$^{-/-}$ MEFs irrespective of KAP-1 status (Fig. 3D), confirming that G2/M checkpoint arrest is ATM dependent. Importantly, KAP-1 depleted cells showed hypersensitive checkpoint arrest at lower doses compared to control cells. We consolidated this result in human A549 cells using a different KAP-1 siRNA oligonucleotide ± ATMi addition (Fig. 3E). Similar to the results in MEFs, KAP-1 siRNA treated cells were fully-arrested after low doses,

whereas control cells do not fully activate checkpoint arrest (Fig. 3E). We also observed similar hypersensitive checkpoint arrest following combined HDAC1&2 siRNA (Fig. 3E). Collectively, these results demonstrate that the increased γH2AX signal expansion following KAP-1 siRNA correlates with more sensitive G2/M checkpoint arrest. In contrast, KAP-1 siRNA does not influence the kinetics or extent of DSB repair in control cells but merely overcomes the need for ATM (15). Since KAP-1 siRNA could exert multiple impacts leading to abnormal checkpoint arrest, we next examined whether a similar effect was observed following loss of other factors required for the HC superstructure.

Depletion of MeCP2 and DNMT3B causes faster γH2AX foci formation and increased signal expansion in NIH3T3 cells.

DNA methylation at CpG islands (CGIs) is an important epigenetic modification that regulates gene silencing and chromatin compaction. DNA methylation at CGIs recruits the methyl binding domain (MBD) proteins which recruit additional chromatin remodellers to silence chromatin (35). Here, we focused on changes in methylation-dependent chromatin compaction caused by loss of methyl CpG binding protein 2 (MeCP2) or DNA methyltransferease 3B (DNMT3B), since they represent components mutated in human syndromes (see below). Prior to examining patient cell lines, we examined the impact of siRNA-mediated knockdown since the mutations in patients are likely hypomorphic and may be less impacting.

Firstly, we found that neither depletion of MeCP2 nor DNMT3B by siRNA impacted upon the rate of DSB repair in mouse and human cells (data not shown and see Fig. 5). Next, we used siRNA-treated NIH3T3 cells to examine whether methylation-dependent chromatin compaction affects IR-induced γH2AX foci formation at HC regions. Similar to the results

following KAP-1 siRNA, depletion of either MeCP2 or DNMT3B resulted in more rapid HC γH2AX foci formation after IR (Fig. 4A and B). Moreover, MeCP2 and DNMT3B siRNA caused a statistically significant increase in γH2AX signal intensity with the effect being greater on the foci associated with higher density DAPI regions (Fig. 4C). In somewhat distinction to the findings following KAP-1 loss, the impact, particularly following MeCP2 siRNA, was also upon regions of intermediate DAPI density possibly due to the role of methylation as a transcriptional repressor at CGIs at both constitutive and facultative HC. In contrast, KAP-1 is primarily enriched within constitutive HC. We also analysed the extent of γH2AX and DAPI overlap in high resolution deconvolved z-stacked images (Fig. 4D). Although we observed minor changes in the number of chromocentres in MeCP2 and DNMT3B depleted cells (data not shown), computational analysis of γH2AX and DAPI overlap per chromocentre revealed a ~3 fold increase in γH2AX foci expansion following MeCP2 or DNMT3B siRNA (Fig. 4E). Additionally, three dimensional image analyses revealed a greater volume of overlap between γH2AX and HC within the interior of chromocentres (Fig. 4F). Collectively, these data demonstrate that MeCP2 and DNMT3B dependent chromatin organization also creates a barrier to IR induced γH2AX foci expansion at HC regions since depletion of MeCP2 or DNM3T enhances foci expansion into the HC core.

Loss of MeCP2/DNMT3B alleviates the ATM dependency of DSB repair.

We observed that, despite the impact on ATM signalling (Fig. 4), IR-induced DSBs are repaired with normal kinetics following MeCP2 or DNMT3B siRNA using γH2AX foci analysis and Pulsed-field gel electrophoresis (Fig. 5A and B). We also observed normal DSB repair kinetics after IR in three primary G0/G1 fibroblasts derived from Rett Syndrome patients (Fig. 5C). We previously reported that loss of HC building factors (e.g. KAP-1, HP1 or HDAC1/2) overcomes the requirement for ATM for DSB repair (15). We, therefore, examined whether MeCP2

deficiency in Rett cells alleviates the DSB repair defect conferred by addition of ATMi. Surprisingly, loss of MeCP2 activity in Rett cell lines does not affect DSB repair kinetics in the presence of ATMi (Fig. 5C). In contrast, MeCP2 siRNA, whilst not affecting DSB repair in the absence of ATMi, almost entirely alleviated the DSB repair defect conferred by ATMi addition in WT and Rett cell lines in G1 and G2 phase (Fig. 5D and E). These findings suggest MeCP2 contributes to the barrier that HC poses to DSB repair but that the hypomorphic mutations in MeCP2 patient cells do not sufficiently change the HC superstructure to overcome this barrier. An ICF Syndrome fibroblast cell line also showed normal DSB repair (Fig. 5F). Addition of ATMi also resulted in the DSB repair defect observed in control cells. DNMT3B depletion partly relieved the repair defect conferred by ATMi addition in control and ICF Syndrome cells, although the magnitude was smaller than that observed following MeCP2 depletion (Fig. 5F).

Cell lines from Rett and ICF Syndrome patients exhibit hyperactive IR-induced ATM signalling.

Since human fibroblasts do not display the well defined chromocentres present in MEFs, we could not readily examine γH2AX signal expansion at HC-DSBs in patient cells. We instead examined downstream events that might be influenced by enhanced γH2AX foci expansion and examined the IR-induced activation of two ATM-dependent phosphorylation events (i.e. ATM autophosphorylation (pATM) and pChk2). To avoid difficulties due to cell cycle stage (e.g. S phase cells have different chromatin superstructure compared to G0/G1 phase cells), we examined contact inhibited primary cells. Although several Rett Syndrome cell lines were available to us, only one line (GM11272) met the criterion of having sufficiently good growth and undergoing contact inhibition to permit this analysis (data not shown). First, we confirmed that Rett cell lines have normal levels of damage response protein expression and ATM dependent phosphorylation without DNA damage (Fig. 6A and B). Following exposure to 0.5 and 3 Gy IR, we observed enhanced levels of pATM and pChk2 in GM11272 (Rett) cells

compared to 48BR (WT) fibroblasts (Fig. 6C), despite similar numbers of γH2AX foci (Fig. 5C). To substantiate these findings in cycling cells (excluding S phase cells), we quantified pATM levels in G1 or G2 phase GM11272 (Rett) cells and in MeCP2 siRNA treated cells using IF and cell cycle markers. Consistent with the results obtained following immunoblotting, GM11272 (Rett) cells and MeCP2 siRNA treated cells showed a >2 fold increase in pATM in both G1 and G2 phase compared to 48BR (WT) cells (Fig. 6D-E and MeCP2 siRNA data is not shown). We further consolidated the notion that ATM signal expansion is enhanced at HC-DSBs in Rett Syndrome cells using a co-immunoprecipitation (IP) procedure. Following IP using, α-TriMe K9 histone H3 antibody to immunoprecipitate HC-DNA regions and immunoblotting using γH2AX antibody, we observed that the γH2AX signal in the HC-enriched fraction was substantially greater in Rett compared to control cells (Fig. 6F). Direct immunoblotting with γH2AX antibody showed that the signal was only 2 fold enhanced in Rett Syndrome compared to control cells (Fig. 6G). These findings are consistent with our IF analysis in NIH3T3 cells (Fig. 4) and demonstrate that loss of MeCP2 specifically enhances the encroachment of ATM signalling into HC regions.

Additionally, we examined *DNMT3B*-mutated ICF Syndrome cells for their ability to activate ATM signalling after IR. Although ICF cells have a higher endogenous level of pATM consistent with a previous finding (14), we observed substantially greater pATM levels after IR in ICF compared to control cells (Fig. 6H). Taken together with the previous section, our results suggest that the disordered chromatin present in Rett and ICF Syndromes leads to enhanced ATM activation after IR.

Rett Syndrome and other disorders with disorganised chromatin show hypersensitive and prolonged G2/M checkpoint arrest.

To investigate whether increased ATM activation has a functional impact, we examined the efficacy of G2/M checkpoint arrest after IR. Consistent with previous findings, we observed that WT fibroblasts do not fully activate G2/M checkpoint arrest after low doses (Fig. 7A). In striking contrast, three different Rett Syndrome primary fibroblast lines showed hypersensitive arrest 1 hr after IR (Fig. 7A). Full checkpoint arrest was observed in both WT and Rett cells after 3 Gy since a signal sufficient to activate checkpoint arrest is likely achieved. Addition of a Chk1/Chk2 inhibitor abolished G2/M checkpoint arrest in control and Rett cells (Fig. 7B), demonstrating that hypersensitive checkpoint arrest in Rett cells is dependent on ATM-Chk1/Chk2 signalling. Similar analysis of an hTERT immortalised ICF Syndrome cell line also revealed hypersensitive checkpoint arrest, which was also abolished by addition of a Chk1/Chk2 inhibitor (Fig. 7C). Further, MeCP2 and DNMT3B siRNA in 1BR (WT) hTERT cells gave a similar result and MeCP2 siRNA in Rett cells did not show any additivity (Fig. 7D and data not shown). Similar results were also obtained using a lymphoblastoid cell line (LBL) derived from HGPS, another disorder impacting on the HC superstructure (Fig. 7E). The control LBL showed more sensitive arrest compared to the fibroblast cell lines but nonetheless enhanced sensitivity was observed in the HGPS LBL.

Finally, we also examined the maintenance of G2/M checkpoint arrest. We reasoned that, based on our previous analysis, checkpoint arrest is released when DDR signalling decreases as DSB repair ensues (10). Thus, we predicted that hyperactive checkpoint signalling might manifest as prolonged checkpoint arrest despite a normal rate of DSB repair. Strikingly, cell lines from the patients with impaired HC displayed prolonged G2/M checkpoint arrest up to 8 hr after 2 Gy IR (a dose which fully activates checkpoint arrest in all cells), whereas control cells are released by 6 hr (Fig. 7F). Addition of a Chk1/Chk2 inhibitor at 30 min post IR, when cells have initiated checkpoint arrest (30), resulted in immediate release from checkpoint arrest in all cell lines, demonstrating that the enhanced arrest observed in HC disordered patient cells represents hyperactivation of an ATM-Chk1/Chk2 dependent pathway (Fig. 7F).

Taken together, our findings demonstrate that loss of methylation dependent HC compaction in Rett and ICF Syndrome leads to increased signal expansion at HC-DSBs, enhanced ATM activation and hypersensitive G2/M arrest and maintenance.

MeCP2 expression restores normal G2/M checkpoint signalling and arrest in MeCP2 defective cells.

To consolidate that the hypersensitive G2/M checkpoint response in MeCP2 depleted cells is due to loss of MeCP2 activity, we examined whether the effect could be complemented by expression of siRNA resistant MeCP2 cDNA. Whilst MeCP2 expression in control cells did not affect G2/M checkpoint sensitivity, MeCP2 expression in MeCP2 depleted cells restores normal G2/M checkpoint sensitivity (Fig. 8A). A similar, though less marked impact, was also observed when MeCP2 cDNA was expressed in Rett Syndrome LBLs (Fig. 8B). The less significant complementation could be due to the reduced transfection efficiency in LBLs compared to hTERT cells or could be the consequence of a dominant negative impact of the mutant protein. Further, MeCP2 expression restored the requirement for ATM for DSB repair to MeCP2 siRNA treated cells (Fig. 8C).

Discussion

Previous studies have shown that histone H1 restricts DNA damage response (DDR) signalling and that reduced H1 levels confer hypersensitive G2/M checkpoint arrest (23). Here, we focus on the impact of HC superstructure on the DDR since the magnitude of HC can substantially differ between cell types and because patients with disordered HC have been described (3, 5, 9). Previous studies have demonstrated that HC restricts γH2AX expansion and DSB repair (8, 15, 18). ATM signalling overcomes the barrier posed by HC to DSB repair (Goodarzi et al., 2008). However, the downstream consequences that HC poses to γH2AX expansion have not been previously examined. Given that only 15-20 % of DNA is heterochromatic and that, although γH2AX foci only expand on the periphery of HC regions, they rapidly become similar in size to γH2AX foci at EC regions, it might have been anticipated that any impact would be modest. In fact, the impact of HC on DDR signalling is marked and only partly relieved by ATM signalling.

In control cells (with functional ATM), we observe faster formation of γH2AX foci at EC versus HC-DSBs, consistent with previous findings that γH2AX foci rarely form within the core HC region but rather expand on the periphery (8, 15, 18). These previous studies have shown limited overlap between γH2AX foci and HC, consistent with the notion that ATM confers localised HC relaxation in the DSB vicinity sufficient to enable HC-DSB repair. Interestingly, by 30 min post IR, the size of foci at EC and HC regions is similar.

Depletion of KAP-1, MeCP2 or DNMT3B enhanced the speed and size but not the number of γH2AX foci. For analysis, we divided the DAPI-signal intensity into a low and high category, broadly distinguishing EC- and HC-DSBs, respectively. However, it has to be appreciated that there is a range of heterochromatinisation and this represents a somewhat crude division. KAP-1 siRNA impacted primarily at DSBs with the highest DAPI-density consistent with KAP-1 being predominantly localised at highly compacted HC; the impact for MeCP2 was broader, possibly reflecting the presence of methylated CpGs in a wider range of

compacted regions (although predominantly in HC-DNA). Surprisingly, under these conditions γH2AX foci size at HC-DSBs became even larger than EC-DSBs. One possibility is that dynamic but distinct chromatin changes occur at EC versus HC regions. At HC-DSBs, it is necessary to achieve relaxation since HC is a barrier to repair, whilst there may be processes that actually restrict γH2AX foci expansion at EC-DSBs. For example, several recent studies have reported that CHD4, a global chromatin remodelling component associated with HDAC activity, is recruited to DSBs after IR (20, 27, 32). Additionally, recent studies have suggested that transcription is silenced at transcriptionally active DSBs and/or restricts γH2AX foci expansion (17, 29). These dynamic changes may tend to diminish signalling at EC-DSBs but enhance it at HC-DSBs. Our analysis of cells lacking 53BP1, which promotes concentrated pKAP-1 at HC-DSBs but does not affect pan-nuclear pKAP-1 (24), shows specific restriction in the expansion of HC-DSBs strongly suggesting that one function of ATM is to enhance signalling from HC-DSBs (ATM may, however, additionally perturb expansion at EC-DSBs). Thus, the end result of perturbed HC superstructure when ATM signalling is active may be elevated signal expansion at HC-DSBs relative to EC-DSBs. Our analysis of the overlap between γH2AX foci and regions of high DAPI-density by two and three dimensional modelling was particularly informative. These findings show that knockdown of HC components (KAP-1, MeCP2 and DNMT3B) enhances γH2AX foci expansion into the HC core to a greater extent than observed in control cells, consistent with the notion that ATM signalling only relaxes HC in the DSB vicinity and that most γH2AX foci expansion occurs into the neighbouring EC region (15). Thus, ATM only minimally and locally overcomes the barrier posed by HC to γH2AX foci expansion. Hence γH2AX expansion following depletion of core HC factors is greater and progresses further into the HC core than in control cells.

γH2AX acts as a scaffold to recruit MDC1, MRN and 53BP1, which together aid ATM retention at the DSB (25). Thus, it might be anticipated that foci size correlates with the

magnitude of the downstream response. Yet cells lacking γH2AX show efficient DDR signalling and checkpoint arrest except at low IR doses (12). We, therefore, examined checkpoint signalling at early times after low doses and observed enhanced ATM signalling following KAP-1 or MeCP2 depletion most evident from 10 to 60 min post IR. Previously, we reported that the G2/M checkpoint is insensitive and is not activated by low IR doses (10). Strikingly, we observed that depletion of KAP-1, MeCP2 or DNMT3B by siRNA permits hyperactivation of checkpoint arrest at low doses that fail to arrest control cells. Thus, the impact of HC provides one explanation for the lack of sensitivity of the G2/M checkpoint. Our findings described above are consistent with a recent report that HC can be induced by oncogenic stress and that such HC formation can restrict activation of the DNA damage response and, most importantly, signalling to apoptosis (11). This important finding consolidates our results and shows that HC arising in a distinct manner can exert a similar dampening impact on the damage response.

A major focus of our work is the examination of disorders with aberrant HC. We focused on Rett Syndrome partly because we observed the most dramatic impact in these cells and because they grew well, had low endogenous γH2AX foci numbers and DDR signalling. Rett Syndrome cells show an ~ two fold increase in ATM phosphorylation, hypersensitive checkpoint activation and prolonged checkpoint maintenance, all features consolidated using siRNA-mediated depletion of MeCP2. We did not examine downstream steps of ATM signalling (e.g. Chk2 phosphorylation) in ICF or HGPS cells due to difficulties in obtaining sufficient G0/G1 cells. However, the checkpoint analysis verified hypersensitive arrest and prolonged G2/M checkpoint activation, consistent with enhanced IR-induced ATM activation. A previous study reported elevated endogenous pATM in ICF LCLs without obvious changes in the response to IR (14). However, different methodologies were used and the subtle response to low doses was not examined. Collectively, these findings provide a clinical relevance to our work and show that disorders with impaired HC structure can display enhanced DDR signalling.

A range of studies have shown that the sensitivity and duration of checkpoint arrest reflects the status of DSB repair. Changes to chromatin structure including epigenetic histone modifications have been shown to influence checkpoint arrest via an impact on DSB repair (22, 27). Here, we observed normal DSB repair. Thus, our findings provide a novel example of prolonged checkpoint arrest despite normal DSB repair and demonstrate that the checkpoint response can be markedly affected by the level and degree of HC compaction. We identify syndromes with disordered HC as displaying an abnormal checkpoint response despite normal DSB repair.

A significant question is whether enhanced DDR signalling impacts clinically. We did not observe any significant change in IR sensitivity in primary Rett Syndrome fibroblasts (data not shown). However, in primary fibroblasts survival is likely determined predominantly by DSB repair, which was normal in Rett Syndrome cells. Prolonged arrest may simply lead to delayed cell cycling without a significant impact on survival. However, the response may depend upon cell type; for example in cells that activate apoptosis (which does not occur following IR in primary fibroblasts) elevated signalling may enhance cell death. Further, enhanced signalling from uncapped telomeres could manifest as early-onset senescence following telomere erosion. Significantly, premature ageing is a phenotype of syndromes with disordered chromatin. Finally, the magnitude of HC compaction may differ between stem and differentiated cells, potentially influencing the magnitude of ATM signalling. More specific studies are required to address these questions.

In summary, we have shown an unexpectedly large impact on DDR signalling following loss of proteins that impact upon HC superstructure. The results reveal that the HC superstructure is a barrier to DDR signalling that is partly, but not totally, relieved by ATM signalling. We show that HC relaxation conferred by patient mutations or by knockdown of HC proteins has downstream consequences including hyperactive ATM signalling and checkpoint

arrest which cannot be attributed to impaired DSB repair. Thus, the barrier that HC superstructure poses to checkpoint signalling provides one explanation for the insensitivity of G2/M checkpoint arrest.

Acknowledgements

The PAJ laboratory is supported by the Medical Research Council, the Association for International Cancer Research, Department of Health and the Wellcome Research Trust.

References

1. **Adams, J. M., and S. Cory.** 1998. The Bcl-2 protein family: arbiters of cell survival. Science **281:**1322-1326.

2. **Agarwal, N., T. Hardt, A. Brero, D. Nowak, U. Rothbauer, A. Becker, H. Leonhardt, and M. C. Cardoso.** 2007. MeCP2 interacts with HP1 and modulates its heterochromatin association during myogenic differentiation. Nucleic Acids Res **35:**5402-5408.

3. **Amir, R. E., I. B. Van den Veyver, M. Wan, C. Q. Tran, U. Francke, and H. Y. Zoghbi.** 1999. Rett syndrome is caused by mutations in X-linked MECP2, encoding methyl-CpG-binding protein 2. Nat Genet **23:**185-188.

4. **Anstey, A. V., A. Ryan, L. E. Rhodes, C. R. Charman, C. F. Arlett, R. M. Tyrrell, C. R. Taylor, and A. D. Pearse.** 1999. Characterization of photosensitvity in the Smith-Lemli-Opitz syndrome: a new congenital photosensitivity syndrome. British Journal of Dermatology **141:**406-414.

5. **Barber, J. B., W. Burrill, A. R. Spreadborough, E. Levine, C. Warren, A. E. Kiltie, S. A. Roberts, and D. Scott.** 2000. Relationship between in vitro chromosomal radiosensitivity of peripheral blood lymphocytes and the expression of normal tissue damage following radiotherapy for breast cancer [see comments]. Radiother Oncol **55:**179-186.

6. **Beucher, A., J. Birraux, L. Tchouandong, O. Barton, A. Shibata, S. Conrad, A. A. Goodarzi, A. Krempler, P. A. Jeggo, and M. Lobrich.** 2009. ATM and Artemis promote homologous recombination of radiation-induced DNA double-strand breaks in G2. EMBO J **28:**3413-3427.

7. **Chiolo, I., A. Minoda, S. U. Colmenares, A. Polyzos, S. V. Costes, and G. H. Karpen.** 2011. Double-strand breaks in heterochromatin move outside of a dynamic HP1a domain to complete recombinational repair. Cell **144:**732-744.

8. **Cowell, I. G., N. J. Sunter, P. B. Singh, C. A. Austin, B. W. Durkacz, and M. J. Tilby.** 2007. gammaH2AX foci form preferentially in euchromatin after ionising-radiation. PLoS ONE **2:**e1057.

9. **Dechat, T., K. Pfleghaar, K. Sengupta, T. Shimi, D. K. Shumaker, L. Solimando, and R. D. Goldman.** 2008. Nuclear lamins: major factors in the structural organization and function of the nucleus and chromatin. Genes Dev **22:**832-853.

10. **Deckbar, D., J. Birraux, A. Krempler, L. Tchouandong, A. Beucher, S. Walker, T. Stiff, P. A. Jeggo, and M. Lobrich.** 2007. Chromosome breakage after G2 checkpoint release. Journal of Cell Biology **176:**748-755.

11. **Di Micco, R., G. Sulli, M. Dobreva, M. Liontos, O. A. Botrugno, G. Gargiulo, R. dal Zuffo, V. Matti, G. d'Ario, E. Montani, C. Mercurio, W. C. Hahn, V. Gorgoulis, S. Minucci, and F. d'Adda di Fagagna.** 2011. Interplay between oncogene-induced DNA damage response and heterochromatin in senescence and cancer. Nat Cell Biol **13:**292-302.

12. **Fernandez-Capetillo, O., H. T. Chen, A. Celeste, I. Ward, P. J. Romanienko, J. C. Morales, K. Naka, Z. Xia, R. D. Camerini-Otero, N. Motoyama, P. B. Carpenter, W. M. Bonner, J. Chen, and A. Nussenzweig.** 2002. DNA damage-induced G2-M checkpoint activation by histone H2AX and 53BP1. Nat Cell Biol **4:**993-997.

13. **Fernet, M., F. Megnin-Chanet, J. Hall, and V. Favaudon.** 2009. Control of the G2/M checkpoints after exposure to low doses of ionising radiation: Implications for hyper-radiosensitivity. DNA Repair (Amst).

14. **Goldstine, J. V., S. Nahas, K. Gamo, S. M. Gartler, R. S. Hansen, J. H. Roelfsema, R. A. Gatti, and Y. Marahrens.** 2006. Constitutive phosphorylation of ATM in lymphoblastoid cell lines from patients with ICF syndrome without downstream kinase activity. DNA Repair (Amst) **5:**432-443.

15. **Goodarzi, A. A., A. T. Noon, D. Deckbar, Y. Ziv, Y. Shiloh, M. Lobrich, and P. A. Jeggo.** 2008. ATM signaling facilitates repair of DNA double-strand breaks associated with heterochromatin. Mol Cell **31:**167-177.

16. **Guenatri, M., D. Bailly, C. Maison, and G. Almouzni.** 2004. Mouse centric and pericentric satellite repeats form distinct functional heterochromatin. J Cell Biol **166:**493-505.

17. **Iacovoni, J. S., P. Caron, I. Lassadi, E. Nicolas, L. Massip, D. Trouche, and G. Legube.** 2010. High-resolution profiling of gammaH2AX around DNA double strand breaks in the mammalian genome. EMBO J **29:**1446-1457.

18. **Kim, J. A., M. Kruhlak, F. Dotiwala, A. Nussenzweig, and J. E. Haber.** 2007. Heterochromatin is refractory to gamma-H2AX modification in yeast and mammals. J Cell Biol **178:**209-218.

19. **Kurz, E. U., and S. P. Lees-Miller.** 2004. DNA damage-induced activation of ATM and ATM-dependent signaling pathways. DNA Repair (Amst) **3:**889-900.

20. **Larsen, D. H., C. Poinsignon, T. Gudjonsson, C. Dinant, M. R. Payne, F. J. Hari, J. M. Danielsen, P. Menard, J. C. Sand, M. Stucki, C. Lukas, J. Bartek, J. S. Andersen, and J.**

Lukas. 2010. The chromatin-remodeling factor CHD4 coordinates signaling and repair after DNA damage. J Cell Biol **190:**731-740.

21. **Lobrich, M., A. Shibata, A. Beucher, A. Fisher, M. Ensminger, A. A. Goodarzi, O. Barton, and P. A. Jeggo.** 2010. gamma H2AX foci analysis for monitoring DNA double-strand break repair: Strengths, limitations and optimization. Cell Cycle **9:**662-669.

22. **Miller, K. M., J. V. Tjeertes, J. Coates, G. Legube, S. E. Polo, S. Britton, and S. P. Jackson.** 2010. Human HDAC1 and HDAC2 function in the DNA-damage response to promote DNA nonhomologous end-joining. Nat Struct Mol Biol **17:**1144-1151.

23. **Murga, M., I. Jaco, Y. Fan, R. Soria, B. Martinez-Pastor, M. Cuadrado, S. M. Yang, M. A. Blasco, A. I. Skoultchi, and O. Fernandez-Capetillo.** 2007. Global chromatin compaction limits the strength of the DNA damage response. J Cell Biol **178:**1101-1108.

24. **Noon, A. T., A. Shibata, N. Rief, M. Lobrich, G. S. Stewart, P. A. Jeggo, and A. A. Goodarzi.** 2010. 53BP1-dependent robust localized KAP-1 phosphorylation is essential for heterochromatic DNA double-strand break repair. Nat Cell Biol **12:**177-184.

25. **Panier, S., and D. Durocher.** 2009. Regulatory ubiquitylation in response to DNA double-strand breaks. DNA Repair (Amst) **8:**436-443.

26. **Paull, T. T., E. P. Rogakou, V. Yamazaki, C. U. Kirchgessner, M. Gellert, and W. M. Bonner.** 2000. A critical role for histone H2AX in recruitment of repair factors to nuclear foci after DNA damage. Curr Biol **10:**886-895.

27. **Polo, S. E., A. Kaidi, L. Baskcomb, Y. Galanty, and S. P. Jackson.** 2010. Regulation of DNA-damage responses and cell-cycle progression by the chromatin remodelling factor CHD4. EMBO J **29:**3130-3139.

28. **Riballo, E., M. Kuhne, N. Rief, A. Doherty, G. C. Smith, M. J. Recio, C. Reis, K. Dahm, A. Fricke, A. Krempler, A. R. Parker, S. P. Jackson, A. Gennery, P. A. Jeggo, and M. Lobrich.** 2004. A pathway of double-strand break rejoining dependent upon ATM, Artemis, and proteins locating to gamma-H2AX foci. Mol Cell **16:**715-724.

29. **Shanbhag, N. M., I. U. Rafalska-Metcalf, C. Balane-Bolivar, S. M. Janicki, and R. A. Greenberg.** 2010. ATM-dependent chromatin changes silence transcription in cis to DNA double-strand breaks. Cell **141:**970-981.

30. **Shibata, A., O. Barton, A. T. Noon, K. Dahm, D. Deckbar, A. A. Goodarzi, M. Lobrich, and P. A. Jeggo.** 2010. Role of ATM and the damage response mediator proteins 53BP1 and MDC1 in the maintenance of G(2)/M checkpoint arrest. Mol Cell Biol **30:**3371-3383.

31. **Shumaker, D. K., T. Dechat, A. Kohlmaier, S. A. Adam, M. R. Bozovsky, M. R. Erdos, M. Eriksson, A. E. Goldman, S. Khuon, F. S. Collins, T. Jenuwein, and R. D. Goldman.** 2006. Mutant nuclear lamin A leads to progressive alterations of epigenetic control in premature aging. Proc Natl Acad Sci U S A **103:**8703-8708.

32. **Smeenk, G., W. W. Wiegant, H. Vrolijk, A. P. Solari, A. Pastink, and H. van Attikum.** 2010. The NuRD chromatin-remodeling complex regulates signaling and repair of DNA damage. J Cell Biol **190:**741-749.

33. **Todd, S., K. M. Cerosaletti, T. B. Lewis, A. M. Killary, R. J. Leach, R. E. K. Fournier, and S. L. Naylor.** 1992. Physical mapping of human chromosome 2 using microcell hybrids and the polymerase chain reaction.

34. **Uziel, T., Y. Lerenthal, L. Moyal, Y. Andegeko, L. Mittelman, and Y. Shiloh.** 2003. Requirement of the MRN complex for ATM activation by DNA damage. EMBO J. **22:**5612-5621.

35. **Wade, P. A.** 2001. Methyl CpG binding proteins: coupling chromatin architecture to gene regulation. Oncogene **20:**3166-3173.

Figure legends

Figure 1. The rate of γH2AX foci formation at HC and EC regions.

(A) The typical images of γH2AX foci formation after IR in NIH3T3 cells. HC γH2AX (red) represents regions of γH2AX and dense-DAPI chromocentre overlap as determined by softWoRx® Suite software.

(B-D) The rate of total- (B), EC- (C) and HC- (D) γH2AX foci formation were enumerated after 0.25, 0.5 and 1 Gy IR.

(E) γH2AX foci formation is normalized to the 20 min post IR signal. Similar results have been obtained in more than three independent experiments.

Figure 2. Depletion of KAP-1 enhances the speed and expansion of γH2AX signal at HC regions

(A) KAP-1 siRNA increases the speed of HC γH2AX foci formation. KAP-1 siRNA treated NIH3T3 cells were irradiated with 1 Gy. The number of γH2AX foci overlapping/juxtaposing and non-overlapping with chromocentres was enumerated as HC and EC foci.

(B) The rate of γH2AX foci formation shown in (A) was normalized to the number of foci at 20 min. The knockdown efficiency is shown in right panel.

(C) Greater γH2AX signal intensity at higher dense DAPI regions in KAP-1 siRNA treated cells after IR. KAP-1 siRNA treated NIH3T3 cells were irradiated with 3 Gy IR and fixed 30 min later. The signal intensity of γH2AX and DAPI per focus was quantified using ImageJ. Typical images and values are shown in the right panel. Black bars represent the median. Statistical significance was determined using Student's two-tailed *t* test.

(D, E) Increased γH2AX signal expansion at HC regions following KAP-1 siRNA. High resolution deconvolved z-stacked images in KAP-1-depleted NIH3T3 cells are shown in D. γH2AX signal overlap of with dense DAPI (blue+green) was visualized as red signal determined by softWoRx® Suite software computer analysis. The magnitude of overlap of γH2AX per chromocentre was quantitatively measured by ImageJ and shown in E.

(F) Depletion of KAP-1 enhances signal expansion into the HC interior. The γH2AX signal expansion into the HC interior is shown by three dimensional modelling in NIH3T3 cells. The volume of the interior signal per chromocentre was measured by Huygens Professional, Scientific Volume Imaging. The quantification is shown in the right panel. In panel A-F, G1 cells with p-H3 Ser10 negative were analysed. S phase cells, which show extensive γH2AX signal, were excluded. Error bas represent the S.D. from two independent experiments (A, B, E and F). n; the number of chromocentres analysed (E and F).

Figure 3. KAP-1 depletion enhances ATM signalling and G2/M checkpoint sensitivity.

(A) Increased pChk2 is observed following KAP-1 depletion after IR. 1BR (WT) hTERT cells +/- KAP-1 siRNA were exposed to 0.5 Gy IR and harvested at the indicated time points. The quantification of pChk2 bands normalised by total Chk2 is shown in right panel. Similar results have been observed in 2 additional experiments.

(B) IR-induced pChk2 is ATM dependent irrespective of KAP-1 status. 1BR (WT) hTERT cells +/- KAP-1 siRNA were exposed to 3 Gy IR with or without 10 μM ATM inhibitor and harvested 2 hr post IR.

(C) Enhanced pChk2 signal is observed in KAP-1 depleted cells by IF. 1BR (WT) hTERT cells +/- KAP-1 siRNA were fixed and stained with pChk2, CENPF and DAPI, 30 min after IR. The signal

intensity was analysed using ImageJ. G2 phase cells were identified by CENP-F. α-pChk2 antibody specificity was confirmed as in (30). Results represent the mean +/- S.D. from two experiments.

(D) KAP-1 siRNA knockdown causes hypersensitive G2/M checkpoint arrest. WT and *ATM*$^{-/-}$ MEFs were subjected to KAP-1 siRNA. After IR, cells were fixed 1 hr later and stained with α-p-H3 Ser10 and DAPI. The number of p-H3 Ser10^{+} cells were scored and normalized to the non-irradiated control. >400 cells were scored.

(E) KAP-1 and HDAC1&2 depletion increase the sensitivity of G2/M checkpoint arrest. A549 cells were subjected to KAP-1 siRNA with or without ATM inhibitor or HDAC1/2 double siRNA. The % mitotic cells 2 hr after IR were scored as described in (D). Results represent the mean and S.D. from three experiments (D and E).

Figure 4. Depletion of MeCP2 and DNMT3B allows increased γH2AX signal expansion.

(A) Depletion of MeCP2 and DNMT3B increases the speed of HC γH2AX foci formation. MeCP2 and DNMT3B siRNA treated NIH3T3 cells were irradiated with 1 Gy and fixed at the indicated times. γH2AX foci formation was analysed as described in Fig. 2.

(B) The rate of γH2AX foci formation shown in (A) was normalized to foci numbers counted at 20 min. The knockdown efficiencies are shown in right panel.

(C) MeCP2 and DNMT3B depletion with siRNA enhances γH2AX signal intensity at HC regions. NIH3T3 cells subjected to siRNA irradiated with 3 Gy, fixed 30 min later and stained with α-γH2AX and DAPI. The signal intensity of γH2AX and DAPI per focus was quantified using ImageJ. The black bars represent the median. Statistical significance was determined using Student's two-tailed *t* test.

(D, E) Increased γH2AX signal expansion at HC regions following MeCP2 and DNMT3B siRNA. The regions of γH2AX-chromocentre overlap were analysed as described in Fig. 2.

(F) Depletion of MeCP2 and DNMT3B enhances the γH2AX signal expansion into the HC interior in NIH3T3 cells. The γH2AX signal expansion within DAPI chromocentres in MeCP2 and DNMT3B siRNA treated cells was measured as described in Fig. 2. G1 cells with p-H3 Ser10 negative were analysed (A-F). Results represent the mean and S.D. from two experiments (A, B, E and F). n; the number of chromocentres analysed (E and F).

Figure 5. Rett and ICF Syndrome cell lines show a normal rate of DSB repair; MeCP2 and DNMT3B depletion alleviates the DSB repair defect conferred by ATMi treatment.

(A) Depletion of MeCP2 and DNMT3B does not influence DSB repair kinetics in 1BR (WT) hTERT cells. To assess the impact of ATM on DSB repair, ATMi was added 30 min prior to IR. Similar result was observed in MeCP2 and DNMT3 depleted NIH 3T3 cells (data not shown).

(B) DSB repair was analysed by neutral PFGE after 20 Gy IR. P2 (XLF) hTERT cells show a substantial DSB repair defect, whereas MeCP2, DNMT3B siRNA treated 1BR (WT) hTERT cells show normal DSB repair.

(C) Rett primary fibroblasts show normal DSB repair in G1 phase. The hypomorphic MeCP2 mutations in Rett cells do not overcome the DSB repair defect in ATMi treated cells.

(D) Depletion of MeCP2 with siRNA alleviates the DSB repair defect conferred by ATMi treatment in Rett G1 cells. MeCP2 siRNA was undertaken in control and Rett primary fibroblasts.

(E) Depletion of MeCP2 does not affect DSB repair in G2 phase cells but rescues the repair defect conferred by ATMi addition. 1BR (WT) hTERT cells were subjected to MeCP2 siRNA. G2 cells were identified with CENPF.

(F) ICF fibroblast cells show normal DSB repair. Depletion of DNMT3B partly alleviates the DSB repair defect in the presence of ATMi in ICF G1 cells. DSB repair was measured by γH2AX foci analysis after 3 Gy IR (A and C-F). 4 μM Aphidocolin was added immediately after IR to prevent S phase cells progressing into G2 phase and to identify S phase cells because of extensive γH2AX signalling (A, C-F). Error bas represent the S.D. from three independent experiments (A-F).

Figure 6. Rett Syndrome cell lines exhibit enhanced ATM signalling after IR.

(A) Rett fibroblast cells have normal levels of damage response protein expression. Whole cell protein extracts were obtained from exponentially growing 48BR (WT) and GM16548, GM11272 and GM11272 (Rett/MeCP2) primary human fibroblast cells.

(B) Rett fibroblast cells show normal pATM level without DNA damage. As a positive control, 48BR (WT) cells were irradiated with 0.5 and 3 Gy and the signallings were examined at 30 min after IR.

(C) G0/G1 arrested Rett fibroblast cells exhibit increased pATM /pChk2 compared with control fibroblasts. Primary 48BR and Rett cells were synchronized in G0/G1 with contact inhibition for >10 days. G0/G1 arrest was confirmed by FACS (data not shown).

(D) Enhanced IR-induced pATM in G1 and G2 phase cycling Rett fibroblast cells compared to control fibroblasts. Cycling 48BR and Rett fibroblast cells were irradiated with indicated doses. Cells were fixed and stained with pATM, CENPF and DAPI, 30 min after IR. The signal intensity

was analysed using ImageJ. G2 phase cells were identified by CENP-F. S phase cells, which show intermediate CENPF levels, were excluded from analysis. α-pATM antibody specificity was confirmed as in (24). Results represent the mean +/- S.D. from three experiments.

(E) The typical images of pATM signal in cycling 48BR and Rett fibroblast cells are shown (40x).

(F) Enhanced γH2AX signal in an HC enriched fraction in Rett compared to control cells after IR. Lymphoblastoid cell lines (LBLs) were harvested at 30 min after 10 or 20 Gy IR. To enrich for HC-DNA, the nucleosome fraction was subjected to IP using α-TriMe K9 histone H3 antibody.

(G) Enhanced global γH2AX signalling in Rett cells after IR. Levels of total trimethylated K9 of histone H3 were similar between Rett and control LBLs.

(H) ICF fibroblast cells exhibit greater pATM after IR compared to control cells. PT3 (ICF/DNMT3B) cells were arrested in G0/G1 following contact inhibition. >90% of cells were in G1 phase (data not shown). Cells were irradiated with 0.5 Gy, harvested at 1 hr after IR and processed as described above.

Figure 7. Cell lines from Rett, ICF and HGPS patients show hypersensitive IR-induced G2/M checkpoint arrest.

(A) Hyperactive G2/M checkpoint arrest was observed at lower doses in Rett fibroblasts. Two control (48BR and 1BR) and three Rett Syndrome (GM16548, GM11271 and GM11272) primary fibroblast lines were analysed for G2/M checkpoint arrest.

(B) Enhanced initiation of checkpoint sensitivity in Rett fibroblast cells was abolished by adding the Chk1/Chk2 inhibitor. The Chk1/Chk2 inhibitor, SB218078, was added 30 min prior to IR.

(C) ICF fibroblast cells show hypersensitive G2/M checkpoint arrest. 1BR (WT) and PT3 (ICF/DNMT3) hTERT cells were analysed for G2/M checkpoint arrest. The inhibitor was added 30 min prior to IR.

(D) Depletion of MeCP2 and DNMT3B confers hypersensitive G2/M checkpoint arrest. 1BR (WT) hTERT cells were subjected to MeCP2 and DNMT3B siRNA. Two distinct siRNA oligonucleotides, #1 and #2, were used for each MeCP2 and DNMT3B knockdown.

(E) A LBL cell line from an HGPS patient (AG10801) shows hypersensitive G2/M checkpoint arrest.

(F) Prolonged IR-induced G2/M checkpoint maintenance in patient with HC disorder LBLs. The maintenance of G2/M checkpoint arrest was examined in control (GM02188), Rett (GM16548), ICF (GM08714) and HGPS (AG10801) LBLs. LBLs were used for this analysis to allow direct comparison between all patient lines, because efficiently growing HGPS cells were only available as LBLs. Consistent with fibroblast cell lines, patient LBLs showed hypersensitive initial G2/M checkpoint arrest after low dose IR (data not shown). 4 μM Aphidicolin (APH) was added immediately after 2 Gy IR. We have not examined 12 hr time point in the inhibitor treated cells because of cellular toxicity by the drug. Mitotic index was measured using p-H3 Ser10 at 1 hr after irradiation (A-E). Error bas represent the S.D. from three independent experiments (A-F).

Figure 8. MeCP2 expression restores normal G2/M checkpoint signalling and arrest in MeCP2 defective cells.

(A) MeCP2 expression in MeCP2 depleted cells restores normal G2/M checkpoint arrest. siRNA resistant WT MeCP2 was expressed in 1BR (WT) hTERT cells with or without knocking down endogenous MeCP2 proteins.

(B) MeCP2 expression in Rett LBL cells partially rescues the hypersensitive G2/M checkpoint arrest.

(C) MeCP2 expression in MeCP2 depleted cells restored the requirement for ATM for DSB repair to MeCP2 siRNA treated cells. DSB repair in G1 cells was measured by 53BP1 foci analysis after 3 Gy IR. Mitotic index was measured using p-H3 Ser10 at 1 hr after irradiation (A and B). Error bas represent the S.D. from two or three independent experiments (A-C).

gH2AX cluster foci analysis using high resolution decomboluted image after high LET irradiation

Nakako Nakajima, Atsushi Shibata, Ryuichi Okayasu, Penny Jeggo.

Results

Delta vision deconvolution analysis in complex gH2AX cluster foci following exposure to vertical heavy ions irradiation.

gH2AX form foci at the site of DSBs. ATM and DNA-PK is activated by DSB ends and phosphorylate H2AX. To consolidate whether heavy ion induced gH2AX foci formation is depended on DSB, we examined gH2AX foci formation in the presence of ATMi and DNA-PKi(Figure 1A). Consistent with the observations after X-rays (Stiff, Can Res), the treatment with ATMi/DNA-PKi diminished gH2AX foci formation in G0/G1 cells following exposure to heavy ions.

Interestingly, we reproducibly observed greater size of gH2AX foci after heavy ions compare to that after X-rays (Figure 1B). To investigate gH2AX foci structure with

higher resolution microscope imaging, we utilized DeltaVision microscope with deconvolution following exposure to vertical Fe ions irradiation (Figure 1C, top panel). Interestingly, high resolution deconvoluted image analysis revealed that the larger size of gH2AX focus contains multiple gH2AX foci cluster (We named a complex gH2AX foci as gH2AX cluster foci, and individual foci at cluster region as gH2AX foci). Since it is know that heavy ions induce complex DNA damages, we examined gH2AX cluster foci after heavy ion irradiation with different levels of LET, i.e. we irradiated cells with 1 Gy Fe (200 keV/μm), 1 Gy Carbon (70 keV/μm) and 1 Gy X-ray (~0.1 keV/μm). Following exposure to irradiations, gH2AX cluster foci was frequently observed after heavy ions although levels of cluster foci were largely different between heavy ions and X-rays (Figure 1D, quantification is shown in Figure 2).

We next investigated DSB repair using gH2AX cluster foci analysis by Delta Vision deconvolution. Human fibroblast cells are arrested in G0/G1 with contact inhibition and are irradiated, since DNA damages in S phase might be more complicated, and also DSBs in S/G2 phase are repaired by HR as well as NHEJ. To monitor gH2AX foci complexity, we classified complexity of gH2AX cluster according to the number of foci per cluster (Figure 2A). Using this classification, we analyzed rate of DSB repair in 48BR (WT) primary fibroblast cells following exposure to Fe and X-rays. To examine repair rate in each gH2AX cluster foci, we plotted the % of repair. Consistent with the notion that high LET irradiation causes complex DNA damage, we observed highly cluster foci after Fe ions whereas there are a few >4 cluster foci after X-rays (Figure 2B). Interestingly, we observed slower DSB repair in higher complex gH2AX cluster foci (Figure 2B), especially >7 gH2AX foci per cluster, after Fe ions. Similar tendency, i.e. complex gH2AX cluster foci (>3-4 foci per cluster) are repaired slowly, was observed after X-rays although the incidence of highly-complex gH2AX cluster foci is significantly lower than heavy ion irradiation (Figure 2B). To examine whether DSB repair is required for NHEJ following heavy ions as well as X-rays (Ahnesorg, Buck), we carried out gH2AX cluster foci analysis in NHEJ defective, XLF cells. XLF cells show a substantial repair defect in all categories of cluster foci after Fe ions (Figure 2C). The slightly higher XLF dependency was observed after Fe ions compared to X-rays. This is consistent with the observation in our previous work (ref), although the mechanistic insight in this difference is unclear. Thus, our results demonstrate that DSBs, which form a simple gH2AX cluster foci, are repaired with

faster kinetics whereas highly complex gH2AX cluster foci are repaired with slower kinetics. Also, following exposure to heavy ions as well as X-rays, DSBs are predominantly repaired by NHEJ in G0/G1 cells, suggesting that NHEJ is a major DSB repair pathway in G0/G1 irrespective of damage complexity.

***In vivo* track structure analysis using high resolution gH2AX foci following exposure to horizontal Fe irradiation.**

In the analysis following exposure to vertical irradiation (Figure 1-2), we consider that we might underestimate or miss gH2AX foci behind a cluster foci as we discussed above. In Figure 1 and 2, we analyzed structure of gH2AX cluster foci by two dimensional visualizations after stucking z-axis images. This also might misestimate size of expansion in gH2AX cluster foci at the region of the particulate passage. Therefore, we next irradiated primary 48BR (WT) G0/G1 cells with Fe ions horizontally and analysed gH2AX foci with Delta vision deconvolution. After horizontal Fe irradiation, gH2AX foci track on a line, which Fe is passed through nucleus, is shown at 30 min (Figure 3A) (N.B. we measured foci stack structure at 30 min since a track begins to bend >2 hr post irradiation, and chose cell with a single track). To examine the size of gH2AX foci expansion at track, we measured the width of gH2AX cluster foci from edge to edge in track (named as width per track) and the width of cluster foci from edge to edge in cluster (named as width per cluster) at 30 min after Fe ions. The average width of per track at 30 min after Fe ions is shown in Figure 3B. Interestingly, the width per cluster after Fe ions is approximately 5-fold wider than that after X-rays (Figure 3C). It has been proposed that heavy ion irradiation causes penumbra effect around core irradiation region (ref; physics). Therefore, we estimated the energy levels at core and penumbra region following exposure to Fe ions irradiation (200 keV/μm = 418 MeV/n) (Figure 3D). brabrabra…

To assess this estimation in *in vivo* using gH2AX foci analysis, we measured the distance to the gH2AX foci at non-track region. Interestingly, we observed approximately 3 gH2AX foci at non-track region when cell has a single track and the average of the distance is ~3.5 μm from the middle of track (Figure 3E, top). We further

analysed the relationship between the distance and gH2AX foci cluster (Figure 3E, bottom). We next examined the rate of repair at non-track region in primary 48BR (WT) and XLF hTERT cells (Figure 3F and G).

Comparison of gH2AX cluster foci analysis between vertical and horizontal Fe ions irradiation

As we discussed above, since DNA is continuously moving in nuclei, gH2AX cluster foci might change its structure especially at later time points. To compare the consequent differences in damage structure between vertical and horizontal irradiation, we measured the gH2AX cluster foci in 48BR (WT) cells at 24 hr post irradiation. Since, after horizontal Fe ions, we cannot select cell with a single track at later time points due to DNA movement, we compared the percentage of cluster per cell (Figure 4). Surprisingly, similar type of cluster damages was observed after both horizontal and vertical irradiation, suggesting that the fundamental damage structure is similar irrespective of direction of irradiation.

Rate of gH2AX cluster foci disappearance following exposure to Fe ions and X-rays irradiation

To examine the rate of DSB repair with longer time course, we enumerated the number of gH2AX cluster foci by eyes. Consistent with the previous observation and the data from the time course experiments up to 24 hr (Figure 2), the slower DSB repair kinetics was observed after Fe ions compared to X-rays in 48BR (WT) primary cells (Figure 5A). We also examined the rate of DSB repair in XLF hTERT cells. To directly compare the repair kinetics between cell lines with distinct type of damages, we normalized the gH2AX cluster foci disappearance as a percentage of the repair (Figure 5B, the actual number of gH2AX cluster foci in XLF as well as 48BR cells is shown in Figure 5B). The similar percentage of DSB repair defect was observed in XLF cells after Fe ions and X-rays. We further investigated the repair rate in these cell lines after horizontal Fe ions irradiation. Since cells irradiated with horizontal Fe ions show a variable length and number of tracks between individual cells, e.g. diameter and shape

of a cell and direction of ions largely affect length of track, we monitored the rate of foci disappearance only >8 hr after irradiation.

Discussions

We previously reported that analysis of prematurely condensed choromosomes in G1 showed the slower rejoining following exposure to heavy ions than X-rays (Okayasu, Rad. Res., 2006). In this study, we investigated the DSB repair after heavey ions irradiation using gH2AX foci analysis, which is a sensitive DSB assay and able to monitor DSB repair in individual cells using physiological doses. Furthermore, we developed the assay with high resolution microscope with deconvolution, which has a strong advantage to analyse structure and size of gH2AX foci within a cluster.

Novel gH2AX foci analysis within cluster lesion using high resolution microscope with denovolution.

Advantage:

We revealed that greater size of gH2AX focus visualized by conventional microscope is actually including gH2AX cluster foci using Delta Vision microscope denovolution.

Limitations;

The analysis of gH2AX cluster foci after vertical heavy ions irradiation has technical limitations. At 2 hr, slightly greater % of complex cluster foci formation was observed compared to that at 30 min post irradiation. This could be explained by some reasons, i.e. i) smaller foci can not grow until detectable levels up to 30 min post irradiation. ii) Individual foci merge at later time points since DNA is moving in nucleus (Aten JA, science, 2004) and/or due to recruitment of foci at repair centre (I don't believe repair centre model in yeast though). iii) foci behind cluster foci might appear due to DNA

movement and rotation in two dimension analysis after vertical irradiation. We currently cannot entirely verify these possibilities because of technical limitations, i.e. it might be resolved if gH2AX foci were monitored with Live cell imaging analysis with delta vision microscope, however importantly, we observed that the percentage of complex gH2AX cluster foci in repair defective, XLF, cells was not increased up to 24 hr, suggesting that these possibilities are negligible small.

On the other hand, the analysis after horizontal irradiation has other technical limitations when rate of repair is monitored, i.e. there is huge variation between individual cells because of a variable length of diameter. Also, the issue of DNA movement could be happened after horizontal irradiation as well. Further, as shown in Figure 4, we show the similar percentage of cluster distribution between vertical and horizontal irradiation at 24 hr after damage. This might be dependent on type of cell lines. Since the depth of nuclei is ~<4 μm in primary fibroblast cells and the distance between each cluster is ~3 μm, we estimate the number of cluster per track after vertical irradiation is approximately <1-2. Therefore, we probably did not largely underestimate cluster behind cluster foci even after vertical irradiation Thus, we suggest that this cluster analysis is available for both vertical and horizontal irradiation in fibroblast cells.

b) Higher complex gH2AX cluster foci after heavy ions. In contrast, significantly lower percentage of cluster foci after X-ray, but there are a few cluster and it remains.

c) Speed of repair is determined by the cluster complexity.

Thus we propose that our novel gH2AX cluster foci analysis is useful approach to investigation of type of clustering damage.

δ-electron effect

From the analysis after horizontal irradiation, we demonstrate that the main heavy ion particle causes highly gH2AX cluster foci at main track, and also produce less complex foci around the main track by d-electron effect. These analyses suggested the possibility, i.e. after vertical irradiation, the less cluster gH2AX foci might be due to the d-electron effects. However, we cannot distinguish the main track from the other damages after vertical irradiation.

Physics View

Heavy ions, nuclei of atoms, are accelerated until getting a 60-70% of light speed under vacuum after removing electrons. After releasing from the vacuum condition, nuclei of atoms have to be passed in air. In air, our estimations revealed that heavy ions ~<50% iron nuclears are collapsed until they get a target (*can we show this estimation by physics calculations?*), e.g. cells. We cannot distinguish the damage by original Fe particle from other collapsed atoms, nevertheless importantly, we demonstrate that the heavy ions at main track lead to gH2AX cluster foci high-frequently compared to X-rays.

Complex gH2AX cluster foci is repaired by NHEJ with slower kinetics.

In mammalian cells, NHEJ is a major pathway in G1 phase. In this study, we show that highly complex gH2AX cluster foci are repaired with slower kinetics and the substantial repair defect in the absence of XLF. It is known that NHEJ is a faster repair pathway, nevertheless surprisingly, we observed significantly slower repair kinetics if DSBs at damaged region form highly complex gH2AX cluster foci. In our work, we did not find the obvious merge the individual clusters since the similar number of foci was observed in XLF cell up to 24 hr post irradiation. Thus we speculate that DSBs are repaired within the cluster if DSBs are repaired by either contact-first model or break-first model. However importantly, if high complex gH2AX cluster foci are induced at a certain region, it might make it difficult to find the partner end, leading to reducing the speed of repair, and also it increases the frequency of miss-rejoining and translocation.

In addition, the reason why we chose XLF cell lines as a NHEJ defective cell is we previously found a fewer contribution of alternative DSB repair in XLF defective cell lines compared to Ku80-/- and LigaseIV-/- cell lines after X-rays (Loser et al. and data not shown). Although further work will be required to verify a contribution of alternative end joining pathway in DSB repair after heavy ions, our study strongly demonstrate that NHEJ is a major repair pathway in Fe ions induced DSBs.

Does slower repair kinetics affect relative biological effectiveness?

As we discussed, it is likely that complex cluster fraction with slower repair might lead to miss-rejoining and translocation. This might contribute to the higher RBE ratio after heavy ions compare to X-rays. Also, since we show that the significant number of DSBs within cluster foci has not been repaired until 72-96 hr in non-cycling G0/G1 cells even after low dose, 1 Gy, we speculate that a sever chromosomal instability might be occurred in M phase if cells could not be sustained by G2/M checkpoint arrest and released with cluster damage.

Materials and Methods

Cell culture and irradiation

48BR (Wild type) primary and 2BN (XLF-defective) hTERT human fibroblasts were cultured in DMEM supplemented with 15% fetal calf serum, 100 U/ml penicillin and

100 µg/ml streptomycin at 37°C in a humidified mixture of 95% air 5% CO_2. Cells were seeded into Nunc chamber glass slides and grown to confluence for irradiation.

Exposures to carbon (290 MeV/nucleon, LET 70 keV/µm) and iron (500 MeV/nucleon, LET 200 keV/µm) beams were performed at the Heavy Ion Medical Accelerator (HIMAC) facility of the National Institute of Radiological Sciences (NIRS), Chiba, Japan. Chamber slides were set up in vertical or horizontal position with the cell layers perpendicular to the incident horizontal beam. X-ray irradiation was performed at 200 kVp and 20 mA (Shimadzu, TITAN-320). Dose rates were set at 1 Gy/min for heavy ions and 0.5 Gy/min for X-rays. Cells expected to receive about 1 Gy/min of X-rays, because glass slides on which cells reflect X-rays (Lobrich, add ref).

Immunofluorescence staining

Cells were washed in cold PBS and fixed for 10 min in 4% w/v paraformaldehyde at room temperature. Afterwards, the cells were permeabilized for 2 min in 0.2% v/v Triton X-100 in PBS, washed in PBS. Antibodies were diluted with 4% w/v BSA in PBS. Cells were incubated with mouse anti-γ-H2AX antibody (Millipore) for 1 h at 37°C, washed three times in PBS and incubated with FITC-conjugated rabbit anti-mouse IgG antibody (Sigma) for 1 h at room temperature. Slides were washed twice in PBS and once for 5 min in PBS containing DAPI to stain the DNA, mounted using Vectashield.

Sample analysis and image processing

Microscopic images were captured with An Applied Precision Delta Vision RT Lympus IX70 deconvolution microscope and a Zeiss Axioplan microscope. Images taken by Delta Vision were deconvoluted and processed using softWoRx. Evaluation of foci numbers and cluster numbers, measurement of length and width of track was performed with ImageJ v1.35p.

Figure 1. Development of novel gH2AX cluster foci analysis with high resolution deconvoluted image

A) ATMi and DNA-PKi if anyone has done this expt.

B) gH2AX form bigger foci after heavy ions compared to X-rays.

Cells are irradiated 1 Gy vertical Fe and X-rays and fixed at 30 min post irradiation. Cover-slips were visualized using the Zeiss Axioplan microscope and simple PCI software.

C) Visualisation of gH2AX foci after heavy ions using conventional microscope.

48BR (WT) primary human fibroblast cells were fixed at 2 hr after with 1 Gy vertical Fe ions and stained with gH2AX and DAPI. Cover-slips were visualized using the Zeiss Axioplan microscope and simple PCI software. Two typical cells from the field (x 40) shown in left panel are enlarged with 100x magnification in right panel.

D) Visualisation of gH2AX foci using high resolution microscope Delta Vision with deconvolution.

48BR (WT) primary human fibroblast cells shown in panel C were also taken by an Applied Precision® DeltaVision RT Olympus IX70 deconvolution microscope. After z-sectioning, the images were stuck and deconvoluted with softWoRx Suite software.

E) Comparison of gH2AX cluster foci after Fe, Carbon and X-ray irradiation using Delta Vision deconvolution.

48BR (WT) primary human fibroblast cells were irradiated with 1 Gy vertical Fe, 1 Gy vertical Carbon and 1 Gy X-rays and fixed at 2 hr. Typical gH2AX foci cluster was enlarged in right panel. Greater number of gH2AX cluster foci was observed after higher LET heavy ions compare to X-rays. The quantification of Fe ions and X-rays was shown in Figure 2. 48BR primary human fibroblast cells were arrested in G0/G1 for >7 days after 100% confluent (A-D).

Figure 2. gH2AX cluster foci analysis in WT and NHEJ defective, XLF, cells after Fe ions irradiation.

A) Classification of gH2AX cluster foci.

48BR primary human fibroblast cells were irradiated with 1 Gy Fe ions vertically and stained with gH2AX and DAPI. gH2AX cluster foci was visualized with Delta vision microscope. gH2AX cluster foci were categorised as 1-2, 3-4, 5-6 and >7 foci per cluster as shown in left panel. The original images without labelling are shown in right panel.

B) Higher complex gH2AX cluster foci are repaired with slow kinetics.

48BR (WT) primary human fibroblast cells were irradiated with 1 Gy vertical Fe and 1 Gy X-ray. Cells were fixed at 30 min and 24 hr post irradiation and stained with gH2AX and DAPI. To measure % of repair, the number of remaining cluster was normalized with that at 30 min post irradiation. DSB repair with lower complex gH2AX cluster foci (1-2 gH2AX foci per cluster) shows faster kinetics compared to higher complex cluster. *gH2AX cluster foci with 5-6 and >7 foci were not observed at 30 min after X-rays.

C) DSB repair requires NHEJ in G0/G1 cells following exposure to Fe ions as well as X-rays.

48BR (WT) primary human fibroblast and P2 (XLF) hTERT cells were irradiated with 1 Gy vertical Fe and 1 Gy X-rays. gH2AX cluster foci analysis was carried out at 0.5, 2 and 24 hr after irradiation. 48BR primary human fibroblast and XLF (P2) hTERT cells were arrested in G0/G1 for >7 days after 100% confluent (A-C). >100 foci in two independent experiments was analysed (B-C).

Figure 3. Analysis of *in vivo* track structure after horizontal Fe ions irradiation.

A) Typical image of gH2AX foci track after horizontal Fe ions.

Cells were irradiated with 1 Gy Fe ions horizontally. Cells were fixed at 30 min and stained with gH2AX and DAPI.

B) Measurement of width of track after horizontal Fe ions.

48BR (WT) primary human fibroblast cells were irradiated with 1 Gy Fe ions horizontally. Cells were fixed at 30 min and stained with gH2AX and DAPI. The width of gH2AX cluster foci from edge to edge in track was measured using ImageJ software.

C) Measurement of width per cluster after horizontal Fe ions.

The width of cluster foci from edge to edge in cluster in 48BR (WT) cells was measured at 30 min after horizontal Fe ions irradiation. The longest diameter in gH2AX foci was measured at 30 min after 1 Gy X-rays.

D) Physics graph.

E) Distribution of gH2AX cluster foci at non-track region.

48BR (WT) primary human fibroblast cells were irradiated with 1 Gy Fe ions horizontally. Cells were fixed at 30 min and stained with gH2AX and DAPI. The distance of gH2AX foci from the main track is shown in the box and plots. The middle bar indicates the median in the top panel. The relationship between the distance from the main track and the number of gH2AX foci per cluster is shown in the scatter plot in the bottom panel. >100 foci at non-track region were analysed from two independent experiments.

F) The rate of repair in gH2AX foci at non-track region.

gH2AX foci were enumerated in 48BR (WT) primary and XLF hTERT cells following exposure to 1Gy horizontal Fe ions irradiation. Error bars represent the standard error of the mean (SEM) from 2 independent experiments. The quantification was carried out with combining two independent experiments (B-C and E-F). Cell with a single track were chosen for gH2AX track analysis (B-C and E-F).

Figure 4. Comparison of gH2AX foci cluster between horizontal and vertical Fe ions irradiation.

48BR (WT) primary human fibroblast and P2 (XLF) G0/G1 arrested cells were irradiated with 1 Gy Fe ions horizontally and vertically. gH2AX foci were analysed with Delta Vision deconvolution imaging and with categorization as shown in Figure 2. The quantification was performed with combining two independent experiments

Figure 5. Rate of DSB repair after Fe ions irradiation in 48BR and XLF cells.

A) The number of gH2AX cluster foci after Fe ions and X-rays.

gH2AX foci were enumerated in 48BR (WT) primary and XLF hTERT cells following exposure to 1 Gy X-rays, vertical and horizontal 1 Gy Fe ions. *After horizontal Fe ions, the number of gH2AX foci was enumerated from 8 to 96 hr, since it is too difficult to distinguish individual cluster at earlier time points. To verify the similar levels of induction between cell lines after horizontal Fe ions, the track length per cell was measured in 48BR and XLF cells (Supplemental Figure).*

B) Percentage of rate of gH2AX cluster foci disappearance after Fe ions and X-rays.

The number of gH2AX cluster foci, which is obtained in panel A, was normalized with the number at 30 min post irradiation. Error bars represent the standard error of the mean (SEM) from 2 independent experiments (A-B).

Damaging agent	Type of lesion/DNA alteration	Repair mechanism
Endogenous DNA damage		
Depurination	AP site	NER
Alkylation	Base modification	NER
Cytosine deamination	Base transition	BER
Oxidation	8oxoG	BER
dNTP misincorporation during replication	Base transition	BER
Replication fork stalling	SSB DSB	SSB repair HR
Meiosis	DSB	HR
V(D)J recombination	DSB	NHEJ
Exogenous DNA damage		
MMS (Alkylating agent)	Alkylating agent	
MMC	Covalently crosslinks bases	ICL, FA
CPT	Topoisomerase I inhibitor	SSB repair or HR
Etoposide	Topoisomerase II inhibitor	HR
IR	Various DNA lesions	SSB, DSB, plus others
UV	Thymine dimers, 6-4 photo-products, cyclobutane dimers	NER, HR

Table 1.1: DNA lesions generated by endogenous and exogenous sources of DNA damage, and the main repair pathway employed to deal with each lesion type. AP: apurine/apyrimidine, NER: nucleotide excision repair, BER: base excision repair, SSB: single strand break repair, DSB: double strand break repair, HR: homologous recombination, NHEJ: non-homologous end joining, MMS: methyl methanesulfonate, MMC: mitomycin C, CPT: camptothecin, ICL: interstrand crosslink repair, FA: fanconi anaemia pathway, IR: ionizing radiation, UV: ultra violet light.

DDR mechanism	Type of lesion	Repair proteins
Mismatch repair (MMR)	DNA mismatches, insertions and deletions arising from DNA replication	MSH2 (recognises mismatch), MLH1 (binds hemimethylated daughter and nicks DNA) EXO1 (5'-3' exonuclease) Polymerase δ and ε RFC (Replication Factor C, is a 5 subunit complex that binds 3' termini DNA and using ATP loads PCNA) PCNA (Proliferating Cell Nulcear Antigen acts as a processivity factor for DNA pol δ) RPA (Replication Protein A, protects ss DNA ends) Ligase I
Base excision repair (BER)	Abnormal DNA bases, base adducts, Oxidative damage Abortive topoisomerase I damage	DNA glycosylase (recognizes damaged base and removes base to form an AP site (a site that has neither a purine or pyrimidine base), APE1 endonulcease (cleaves at AP site) DNA polymerases β, δ, ε Flap endonulcease FEN1 (long patch repair generates a flap which is removed by FEN1) Ligase I or III
Single strand break repair (SSBR)	Single stranded breaks	PARP-1,2 (recognise SSB and adds poly ADP-ribose chains) DNA glycosylase APE1 endonuclease DNA polymerases β, δ, ε FEN1 (Flap endonulcease) XRCC1 (accessory factor that interacts with PARP2, DNA ligase III & pol β) PNK (Polynucleotide Kinase - transfers a phosphate to the free hyroxyl end of 5' DNA to ready the DNA for ligation) APTX (Apratxin) Ligase I or III
Nucleotide excision repair (NER)	Bulky base adducts UV photo products	RNA polymerase II XPC, DDB1/2 recognise distorted base CSA & CSB bind some lesions during TC-NER TFIIH subunits XPB & XPD (helicases) unwind DNA XPG (3' endonuclease XPF & ERCC1 (generate a 5' nick) Removal of ss DNA with a 25-30 nucleotide gap DNA polymerases δ or ε fill the gap & PCNA RPA Ligase I
Non Homologous End Joining (NHEJ)	DSBs V(D)J recombination CSR	Ku (recognizes end termini) DNA-PKcs (binds and autophosphorylates at DSB inducing end termini exposure to processing enzymes or ligases) Artemis (endonclease that processes ends refractory to ligation) XRCC4, XLF, Ligase IV (ligation complex)
Homologous recombination (HR)	DSBs Stalled replication forks Meiotic recombination Abortive topo II damage DNA cross links	MRN, CtIP (exonucleases that generate ss DNA end termini) RPA RAD51, RAD52(protein filament which invades sister chromatid in search of homologous template) BRCA1/2 FEN1 DNA polymerases
Fanconi anaemia (FA)	DNA cross links	FANC-A,B,C,E,F,G,L&M (core complex which catalyzes the mono-Ub and subsequent activation of FANCD2 & FANC1) FANCD2 & FANC1 (Following Ub these proteins are recruited to chromatin where they interact with BRCA1/2 and channel repair through HR) HR proteins

Table 1.2: DNA repair pathways and components.

Syndrome	Mutated genes	DDR defect	Phenotype
LIG 4 syndrome	LIG4	NHEJ	Radiosensitive Microcephaly Immunodeficiency Delayed growth
Radiation severe – combined immunodeficiency disorder (RS-SCID)	ARTEMIS	NHEJ	Immunodeficiency Radiosensitive
Ataxia telangiectasia (A-T)	ATM	Damage signalling DSB repair	Ataxia Cerebellar degeneration Immunodeficiency
Ataxia telangiectasia like disorder (A-TLD)	MRE11	Damage signalling DSB repair	Ataxia Cerebellar degeneration Immunodeficiency
Nijmegen breakage syndrome (NBS)	NBS1	Damage signalling DSB repair	Microcephaly Growth retardation Immunodeficiency
Nijmegen breakage like disorder (NBSLD)	RAD50	Damage signalling DSB repair	Microcephaly Growth retardation Immunodeficiency
Seckel syndrome (SS)	ATR PCNT	Damage signalling DSB repair	Microcephaly Severe primordial proportionate growth retardation

Table 1.3: Human disorders associated with defective DDR.
LIG 4 syndrome is caused by hypomorphic mutations in the NHEJ ligase, ligase IV (O'Driscoll et al., 2001). LIG 4 patients display severe immunodeficiency due to an inability to repair DSBs induced during V(D)J recombination (Taccioli et al., 1993). LIG 4 patients are also radiosensitive as a consequence of incomplete DSB ligation during NHEJ repair. Like LIG 4 syndrome, RS-SCID patients ,which have mutations in Artemis, are also radiosensitive and immunodeficient, which is reflective of a role of Artemis in NHEJ (Taccioli et al., 1993). A-T is a neurodegenerate disorder caused by mutations in ATM (Chun & Gatti, 2004). Progressive loss of Purkinje neurons in the cerebellum (the region of brain involved in balance and co-ordination) of A-T patients results in ataxia (Borghesani et al., 2000). A-TLD is caused by mutation in the MRN component, MRE11. A-TLD patients show a delayed onset of ataxia compared to A-T patients, with no cancer predisposition (Stewart et al., 1999). Mutations in another component of the MRN complex, NDB1, results in NBS. NBS is characterized by microcephaly and growth retardation (Mutations in RAD50, a further component of the MRN complex, results in NBSLD, which is phenotypically similar to NBS. SS is caused by mutations in ATR or PCNT, and is characterized by proportionate growth retardation, severe microcephaly and skeletal abnormalities (Seckel & Thomas, 1960).

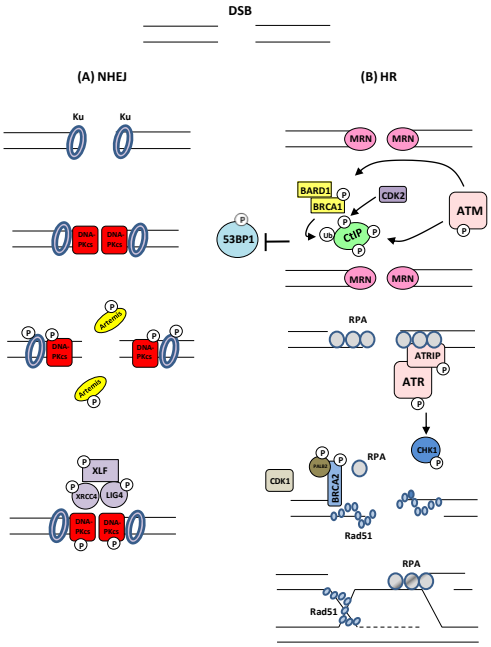

Figure 1.1 : The major DSB repair pathways
(A) NHEJ: The heterodimer Ku rapidly binds DSB ends. Ku promotes repair by NHEJ by recruiting DNA-PKcs. Autophosphorylation of DNA-PKcs at multiple DNA-PKcs amino clusters induces remodelling at the DSB end, which exposes the damage termini for end processing. Ends refractory to direct ligation are processed by the endonuclease Artemis. The ligation complex composed of XRCC4, Ligase 4 and XLF mediate DNA ligation. **(B)** HR: The MRN complex competes with Ku for the DSB end. MRN binding initiates resection together with CtIP to promote HR in S and G2 phase (You & Bailis, 2010. The endonuclease CtIP interacts with BRCA1 and the MRN complex (Huen et al., 2010). BRCA1 ubiquitinates CtIP and facilitates CtIP's association with damage sites (Huen et al., 2010). ATM controls resection by activating CtIP via phosphorylation. 53BP1 has an inhibitory role on resection possibly by blocking end termini (Bunting et al., 2010). Resection generated 3' ssDNA ends are coated with RPA. ATRIP binds RPA and localizes ATR at the site of the DSB. ATR phosphorylates and activates Chk1, which contributes to checkpoint arrest. RPA is displaced from 3' ss ends by BRCA2, and RAD51 filaments are assembled (West, 2003). Rad51 filaments invade the homologous DNA strand in search for a homologous template to use for repair. D loop structures or Holiday junctions formed after strand invasion can be cleaved by a host of nucleases.

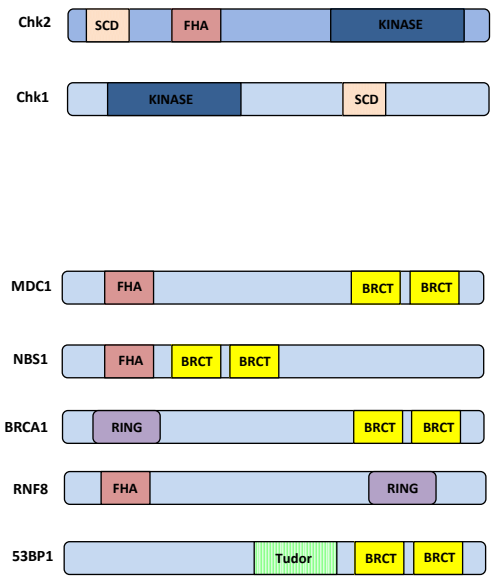

Figure 1.2: Protein domain architecture and phosphomotifs for DDR proteins and checkpoint kinases. Forkhead associated domain (FHA), SQ/TQ clustered (SCD), kinase domain (KINASE), BRCA1 C-terminus domain (BRCT). See 1.4 for details.

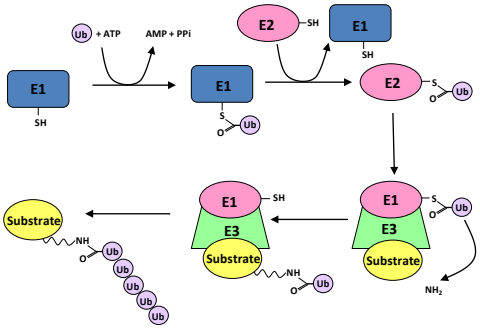

Figure 1.3: The ubiquitination system
Step one in the ubiquitination reaction involves the transfer of ubiquitin to the active site cysteine residue of an E1 ubiquitin ligase, a reaction which requires ATP. In this reaction, the C-terminus of ubiquitin becomes linked to the E1 cysteine sulfhydryl group by a thioester linkage. Step two involves the transfer of ubiquitin from the E1 ubiquitin enzyme to the active site of the E2 ubiquitin conjugating enzyme via a transesterification reaction. Next a E3 ubiquitin enzyme bridges the association of the E2 enzyme with its target substrate. Finally an isopeptide bond is formed between a lysine residue on the target protein and the C-terminal glycine of ubiquitin (reviewed in Hershko & Ciechanover, 1998).

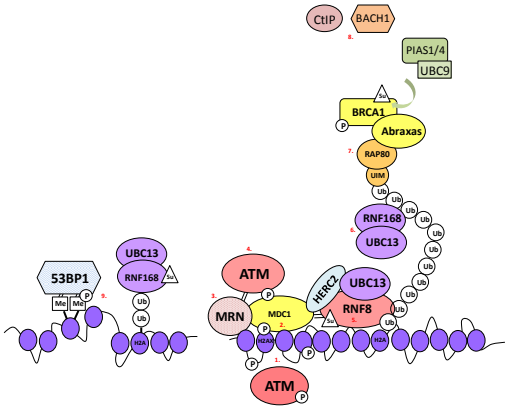

Figure 1.4: ATM dependent signalling events in response to IR.
1. After IR, H2AX is phosphorylated by ATM at Ser139. 2. MDC1 directly binds H2AX via it's BRCT domain. 3. MRN is recruited via association with the FHA and BRCT domains of Nbs1 with MDC1. 4. Nbs1 also interacts with ATM, leading to further recruitment of ATM, which results in an auto-activatory loop. 5. ATM phosphorylates MDC1, which recruits the E3 ubiquitin ligase RNF8 via its FHA domain. HERC2 mediates RNF8 and UBC13 association which promotes further K63 Ub chain synthesis. 6. RNF168-UBC13 recognises RNF8 mediated ubiquitin (Ub) chains. RNF168 acts with UBC13 to amplify the RNF8 dependent histone ubiquitination by targeting H2A histones and promoting further formation of lysine 63 linked Ub conjugates. 7. RAP80 binds K63 ubiquitin chains via a ubiquitin interacting motif (UIM). RAP80 recruits abraxas which interacts with BRCA1 via its BRCT domain. PIAS1/4 on association with UBC9 mediates the SUMOylation of BRCA1, which stimulates BRCA1's Ub ligase activity to further promote Ub chain synthesis. 8. Recruitment of BRCA1 leads to BACH1 recruitment (DNA helicase) and CtIP (exonuclease), both which channel for DSB repair. 9. 53BP1 is subsequently recruited following chromatin ubiquitination. However 53BP1 contains no ubiquitin interacting motifs. It's recruitment is likely dependent on chromatin remodelling events initiated after chromatin ubiquitination which expose residues required for 53BP1 binding. 53BP1 binds methyl residues via it's tudor domain. 53BP1 recruitment channels signalling towards DSB repair.

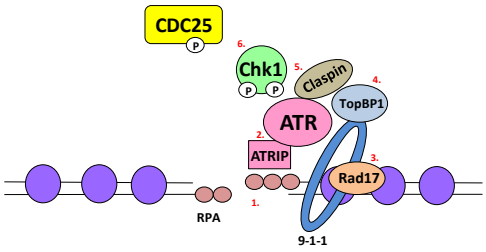

Figure 1.5: ATR dependent Chk1 activation
1. ssDNA is coated by RPA. 2. ATR recognises these regions through ATRIP. 3. Rad17 binds and recruits the Rad9-Rad1-Hus1 (9-1-1) complex (Cortez et al., 2001). 4. The 9-1-1 complex brings TOPBP1 which is required for optimal ATR activation (Kumagou et al., 2006). 5. ATR phosphorylates Chk1 at Ser317 and Ser345 via claspin (Kumagai and Durphy, 2000). 6. Phosphorylated Chk1 is released from chromatin where it can then phosphorylate CDC25 (protein phosphatase) proteins inhibiting their activity and marking them for ubiquitin mediated proteolysis by β-TrCP. Loss of CDC25 activity induces cell cycle checkpoint arrest. ATM and ATR function together in response to DSBs in G2. ATM and the MRN complex are required to initiate resection in G2 to form ssDNA substrate to initiate ATR activation (Jazayer et al., 2006).

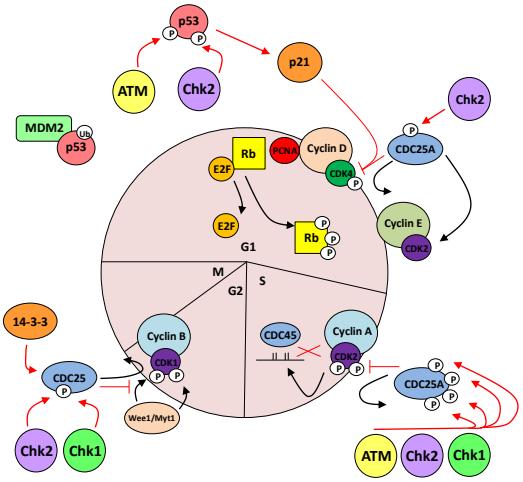

	Function	Phase	Protein
Cyclin dependent kinases (CDKs)	Protein kinases that control cell cycle progression on association with cyclins	G1	Cdk4, Cdk6
		G1/S, S	Cdk2
		G2/M	Cdk1
Cyclins	Proteins that control CDK activity	G1	Cyclin D1, D2, D3 (bind Cdk4 or Cdk6)
		G1/S	Cyclin E (binds Cdk2)
		S	Cyclin A1 & A2 (Bind Cdk2, Cdk1)
		M	Cyclin B1 & B2 (bind Cdk1)

Figure 1.6: The cell cycle checkpoints
G1: In the absence of DNA damage (black arrows), CDC25A removes the inhibitory phosphorylation on CDK4. This enables Rb and E2F to dissociate, allowing E2F to function as a transcription factor, and ready the cell for DNA synthesis. In the presence of DNA damage (red arrows), two distinct pathways function to initiate checkpoint arrest. One pathway involves the phosphorylation p53 and its negative regulator MDM2 by ATM and Chk2, causing p53 stabilization and activation. p53 up-regulates the transcription of the CDK inhibitor p21. p21 inhibits activation of CDK complexes. Without active CDK complexes, the transcription factor E2F remains sequestered by Rb and cell cycle progression is halted. Since this pathway is dependent on transcription it likely takes several hours before fully activated and is likely to be important for maintenance of G1 arrest. The second pathway is dependent on posttranslational modifications such as phosphorylation and is activated more rapidly. During this pathway, Chk2 phosphorylates CDC25A targeting it for degradation. The inhibitory phosphorylation on CDK4 remains, and E2F remains sequestered by Rb, therefore halting cell cycle progression. **S:** In the absence of DNA damage (black arrows), CDC25A removes the inhibitory phosphorylations on CDK2. This enables CDK2/cyclin A to mediate the loading of Ori binding factor CDC45 to origins to initiate DNA synthesis. In response to DNA damage (red arrows), CDC25A is phosphorylated at Ser123, Ser178, Ser276 and Ser292 by ATM, Chk1 or Chk2, marking CDC25A for degradation. Degradation of CDC25A means the inhibitory phosphorylations at Thr14 and Tyr15 on CDK2 remain, which prevents loading of CDC45 to origins and prevents DNA synthesis. **G2/M:** For transition into mitosis (black arrows), the inhibitory phosphorylations at Thr14 and Tyr15 on CDK1 which are carried out by wee1 and Myt kinases must be removed by CDC25. Following removal of these phosphorylations, CDK1 can associate with cyclin B and drive cell cycle progression. In the presence of DNA damage (red arrows), Chk1 and Chk2 phosphorylate CDC25 at Ser216, which induces the binding of 14-3-3 proteins to CDC25 sequestering it in the cytoplasm and inhibiting cell cycle progression.

Complex	Function
Subfamily	INO80
INO80	ATP dependent nucleosome remodeller that restores chromatin architecture after UV damage by removing bulky photo-products (Sarkar et al, 2010). Involved in nucleosomal spacing (Udugama et al, 2010).
Arp5, Arp8 (Actin related proteins)	Form part of the cytoskeleton. Involved in ATP dependent chromatin remodelling
Subfamily	SWRI
Tip60	Acetyltransferase – adds acetyl groups to histones. Has been shown to be important for ATM activation (Sun et al, 2009).
P400	Contains an ATPase chromatin remodelling subunit. Forms complexes with other remodelling complexes.
TTRAP (TRAF & TNF receptor associated protein)	Cation dependent phosphodiesterase. On association with CD40, TNF & TRAFs inhibits nuclear factor kappa β (NFKβ) activation. Structurally similar to APE1 endonulcease and functions in DNA repair (Hu et al, 2000). Also associates with Tip60.
ING3 (Inhibitor of growth family, member 3)	Contains a PHD finger, a common motif often involved in chromatin remodelling
Subfamily	ACF/CHARAC
ACF (Asymmetric crying faces)	ATP dependent chromatin remodeller. Has a role in nucleosome spacing (Racki et al, 2009).
SNF2H	Has helicase and ATPase activity, regulates transcription by altering chromatin structure.
Subfamily	Mi-2/CHD
NuRD (Nucleosome remodelling & histone deactylation)	A complex containing histone deactylation activity and ATP dependent chromatin remodelling (Kunert & Brehm, 2009).
CHD3 (Mi-2α) CHD4 (Mi- 2β) (Chromodomain-helicase-DNA binding)	Contains an ATPase domain followed by two chromodomains (a chromatin binding domain that often binds methylated residues and is often associated with heterochromatin building factors). Important for differentiation and development.
HDAC1 HDAC2 (Histone deacetylase 1/ 2)	Enzymes that remove acetyl groups from lysine residues on histones.
RbAp46 (Rb-associated protein 46)	Component of the histone deacetylase complex that physically interacts with Rb. Also interacts with the NuRD complex. Regulatory subunit that links cell cycle progression, DNA repair and chromatin remodelling.
Subfamily	SWI/SNF
BRG1 (brahma related gene 1)	A protein containing helicase and ATPase activity. Can bind BRCA1 and HP1 (Nielsen et al, 2002). Regulates chromatin structure.

Table 1.4: Chromatin remodelling complexes.

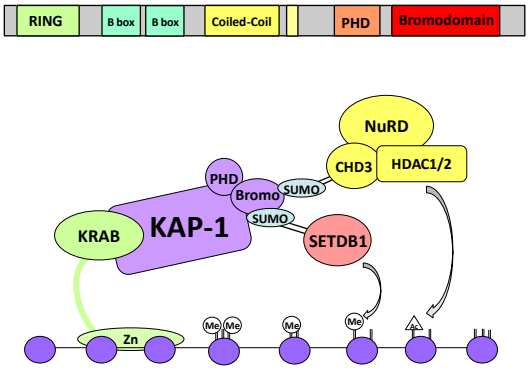

Figure 3.1: KAP-1 and heterochromatin formation
KAP-1 is a HC associated protein that acts as a scaffold for the recruitment of repressor machinery. The associated KRAB-Zinc finger domain facilitates the binding of KAP-1 to DNA. The C-terminus of KAP-1 contains an HP1 interaction domain, a PHD domain and a bromodomain. Bromodomains recognise acetylated lysines on Histone H3 and H4 (Mujtaba et al., 2007). The PHD domain binds the SUMO E3 ligase Ubc9, and directs SUMO conjugation of the bromodomain. SUMOylation at the bromodomain of KAP-1 is recognized by the histone deacetylase complex NuRD via CHD3 and the histone methyltransferase SETDB1. SETDB1 and CHD3 bind the SUMO modified KAP-1 via SUMO interacting motifs (SIMs). These proteins modify chromatin with repressive marks to establish a silenced heterochromatin superstructure. Mutations in either the PHD or bromodomain compromises the association of KAP-1 with CHD3 and SETB1, and relieves transcriptional repression (Ivanov et al., 2007). Repression is relieved by phosphorylation of KAP-1 by ATM. ATM phosphorylates the C-terminus of KAP-1, which impedes the interaction between the SUMOylated bromodomain of KAP-1 and CHD3 (Goodarzi et al., manuscript submitted).

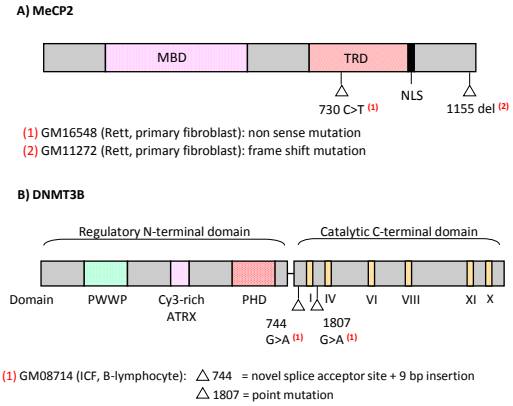

Figure 3.2: Schematic representation of MeCP2 and DNMT3B gene structures.
A: MeCP2: MeCP2 maps to the long arm of the X chromosome on position q28 and undergoes X inactivation. The gene has 4 exons. MeCP2 is an abundant, ubiquitously expressed nuclear protein of 486 aa most frequently encoded by exon 2,3 and 4. A second isoform also exists, MeCP2B, which encodes exon 1,3 and 4. MeCP2 protein contains 4 functional domains: an 85 aa methyl binding domain (MBD), an 104 aa transcriptional repressor domain (TRD) which interacts with the co-repressor Sin3A, a nuclear localization sequence (NLS) for nuclear export and a C-terminal segment which facilitates binding to the nucleosome core (reviewed in Matarazzo et al., 2009). Rett syndrome cell line GM16548 contains a non-sense mutation located in the catalytic domain. Rett syndrome cell line GM11272 contains a deletion at aa 1155 resulting in frame shift mutation. Details on Rett syndrome patient GM11271 mutation are unavailable. **B: DNMT3B:** DNMT3B maps to the long arm of chromosome 20 at position q11.2 (Xie et al., 1999). DNMT3B spans approximately 47 kb and contains 24 exons, 6 of which are alternatively spliced (Xie et al., 1999). DNMT3B is composed of two large regulatory domains. The first being the N-terminal domain which is composed of a chromatin binding PWWP, a zinc finger DNA binding cy3-rich ATRX domain, and also a polybromo homology domain (PHD) like motif. The second domain is the catalytic C-terminal which is composed of 6 motifs (I – X) (reviewed in Ehrlich et al., 2008). ICF syndrome cell line GM08714 is a compound heterozygote. One allele has a G>A transition at 1807, which results in a Ala to Thr substitution at codon 603. The second allele has a G>A substitution which results in generation of a novel splice acceptor site and a 9 bp insertion in the mRNA.

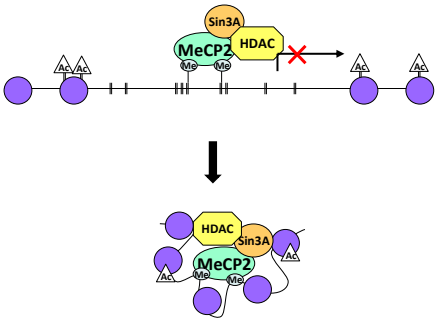

Figure 3.3: MeCP2 and transcriptional silencing
Transcription is suppressed in promoter regions containing methylated CpGs that are bound by MeCP2 (methyl-CpG-binding protein 2). MeCP2 binds methylated DNA and recruits chromatin-remodelling complexes that contain Sin3A (a transcriptional co-repressor) and histone deacetylases (HDACs). This leads to chromatin condensation owing to histone deacetylation, which results in a limited accessibility of the transcriptional machinery to promoter regions. When MeCP2 is not bound to methylated DNA the complex(es) that usually contains MeCP2, SIN3A and/or HDACs are not recruited, and the chromatin remains in a transcriptionally active configuration.

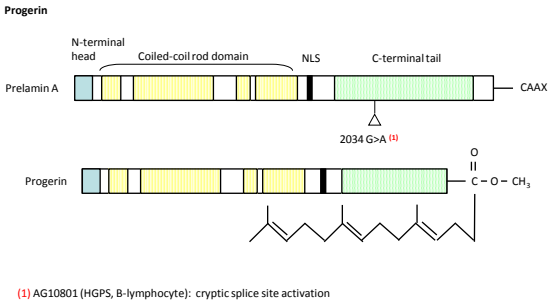

(1) AG10801 (HGPS, B-lymphocyte): cryptic splice site activation

Figure 3.4: A schematic representation of prelamin A maturation into progerin. Lamin A is synthesized as a 664 aa precursor protein called prelamin A. Prelamin A contains a C-terminal CAAX aa motif that undergoes farnesylation. Mature lamin A contains no farnesyl modification. Progerin, the mutant form of prelamin A, retains the C-terminal CAAX motif either due to aberrant splicing as a consequence of splice site loss through mutation or mutations in Zmpste24, which is the endopeptiase encoding gene which encodes the protease responsible for farnesyl production (reviewed in Kudlow et al., 2007). HGPS cell line AG10801 contains a de novo single base substitution G>A change at nucleotide 2034, which results in a change in exon 11 of the lamin A gene. This substitution creates a cryptic splice site which results in skipping 150 bp of the LMNA mRNA leading to deletion of 50 amino acids from the protein (Erikson et al., 2003).

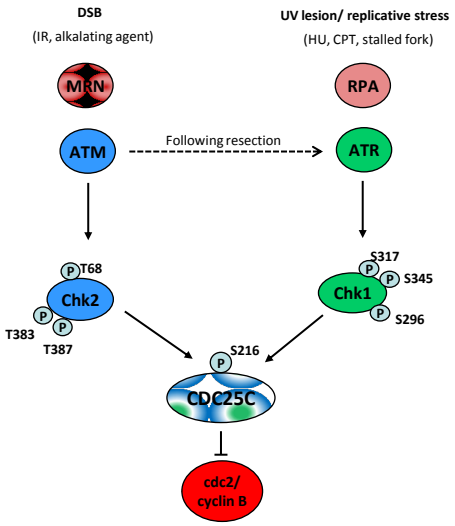

Figure 3.5: A schematic overview representing DNA damage signalling responses that function to initiate G2/M checkpoint arrest. DSBs generated following exposure to IR, oxidative stress or alkalayting agents activate ATM. Active ATM associated with DSBs via the MRN complex (Shiloh et al., 2003). ATM phosphorylates Chk2 on residue Thr68 which stimulates Chk2 autophosphorylation at residues Thr383 and Thr387, subsequently resulting in Chk2 kinase activation. ATM specifically and exclusively activates Chk2 at the damage site (Lukas et al., 2003). Active Chk2 phosphorylates CDC25C at Ser216, creating a binding site for 14-3-3 proteins. 14-3-3 bound CDC25C is catalytically inhibited or sequestered in the cytoplasm, where it is unable to activate cdc2/cyclin B. As a consequence cdc2/cyclin B remains phosphorylated and inactive. The G2/M checkpoint is then arrested. DSBs generated by replication associated damage such as stalled or collapsed replication forks or following treatment with crosslinking agents such as HU or CPT, generate ssDNA overhangs which ssDNA binding protein RPA can bind. RPA coated DNA recruits ATRIP along with ATR to the site of a lesion. Active ATR phosphorylates Chk1 at Ser317, resulting in Chk1 autophosphoryaltion at Ser345 and Ser296 and subsequent activation. Chk1 can also function like Chk2 to phosphorylate CDC25C at ser216 and mediate G2/M checkpoint arrest via inhibiting the dephosphorylation of cdc2/cyclin B. DSBs which undergo resection prior to RPA binding require ATM activity upstream of this process. Here ATM can phosphorylate either or both the MRN complex (Gatei et al., 2000, Stewart et al., 2001) and CtIP (Li et al., 2000) to initiate resection. In this pathway of G2/M arrest, ATM acts up stream of ATR in the activation of Chk1. For sufficient signalling mediated by Chk2 and Chk1 to initiate G2/M checkpoint arrest at least 15 DSBs are required.

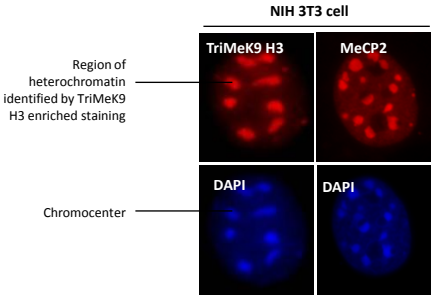

Figure 3.6: Visualization of heterochromatin by immunoflorescence
NIH 3T3 cells were immunostained for the heterochromatin marker TriMeK9 histone H3 (red) and DAPI (blue). DAPI dense chromocenters co-localize with regions of heterochromatin identified by TriMeK9 staining. MeCP2 also co-localizes with DAPI dense chromocenters.

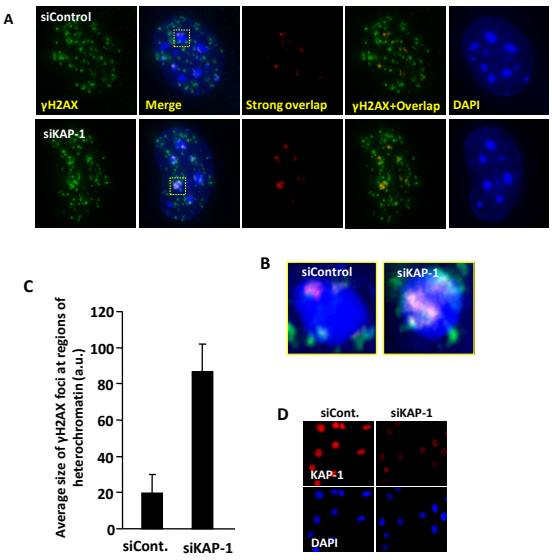

Figure 3.7: The size of IR induced γH2AX foci expansion at regions of heterochromatin increases following KAP-1 knockdown. (A) NIH 3T3 murine cells were transfected with control or KAP-1 siRNA for 48 hours. Cells were irradiated with 3 Gy IR and 30 minutes later immunostained for γH2AX (green) and DAPI (blue). Using the Delta Vision microscope, high resolution, deconvolved Z stack images were obtained. To analyze quantitatively regions of γH2AX and DAPI overlap, the co-localization tool on Sorftworx suite software was used. Red represents regions of strong DAPI (blue) and FITC (green) overlap. **(B)** Picture panel represents a close up of the region outlined in yellow in (A). **(C)** The relative size of γH2AX foci at regions of heterochromatin was assessed using ImageJ software. **(D)** Image of knockdown efficiency. NIH 3T3 cell were treated with KAP-1 siRNA as described in (A) and immunostained for KAP-1 (red) and DAPI (blue). Results are representative of 3 independent experiments.

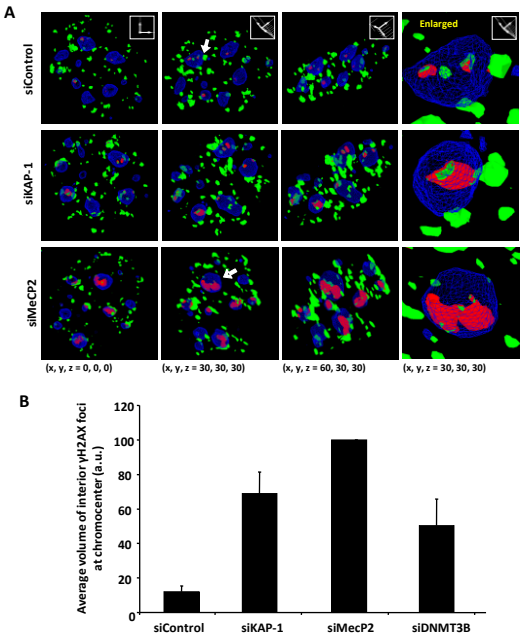

Figure 3.8: The volume of γH2AX signal expansion at regions of heterochromatin increases following KAP-1, MeCP2 or DNMT3B knockdown. (A) Representative images of NIH 3T3 cells following treatment with either control, KAP-1 or MeCP2 siRNA for 48 hours. 3D images were generated using the Delta vision softworx software. Pink represents regions of strong γH2AX and DAPI co-localization. γH2AX (green) and DAPI (blue) **(B)** Quantification of the volume of strong γH2AX and DAPI overlap was performed using Huygens co-localization analyzer software in cells treated as in (A). Values were normalized to the maximum volume of over-lap which was observed following MeCP2 knockdown. 100 chromocenters were analyzed per cell type. Results are representative of 3 independent experiments.

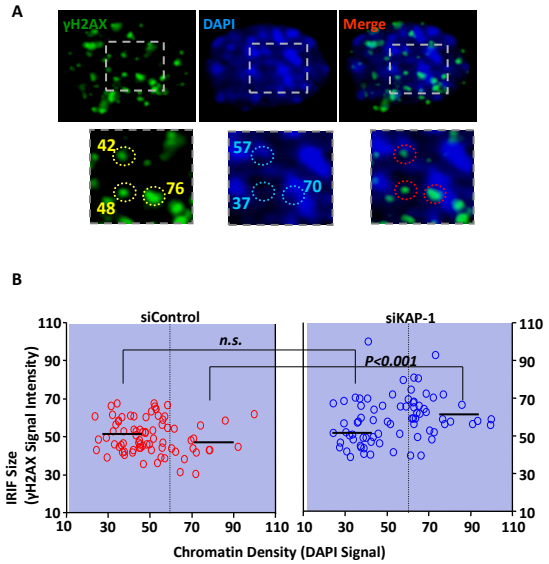

Figure 3.9: IR induced γH2AX signal intensity increases following KAP-1 knockdown. (**A)** To analyze γH2AX and DAPI signal intensity the Zeiss Axioplane microscope was used and exposure times kept constant. To measure signal intensity, each γH2AX foci and corresponding DAPI region was analyzed using ImageJ software. **(B)** NIH 3T3 cells were treated with either control or KAP-1 siRNA for 48 hours. 30 minutes post 3 Gy IR, cells were fixed and immunostained for γH2AX and DAPI. The x axis represents DAPI signal intensity and the y axis represents γH2AX signal intensity.

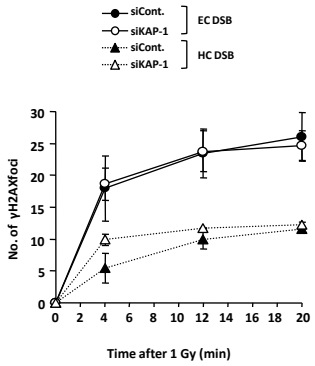

Figure 3.10: IR induced γH2AX foci form with faster kinetics in NIH 3T3 cells following KAP-1 knockdown. NIH 3T3 cells were treated with either control or KAP-1 siRNA for 48 hours. Following transfection, cells were irradiated with 1 Gy IR and fixed and immunostained for γH2AX at indicated time points. γH2AX foci co-localizing with DAPI dense regions (chromocenters) were scored as heterochromatin (HC) DSBs. γH2AX foci not co-localizing with DAPI dense regions were scored as euchromatin (EC) DSBs. Results are representative of 3 independent experiments.

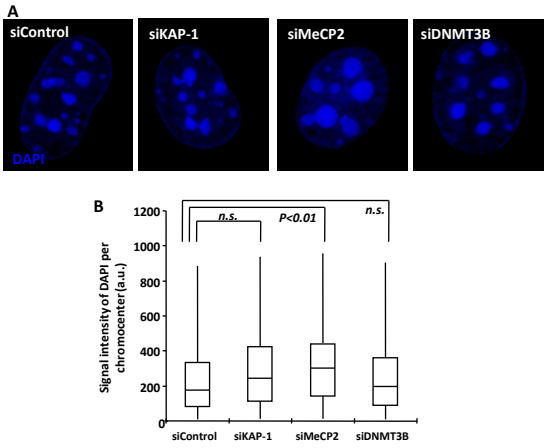

	siCont.	siKAP-1	siMeCP2	siDNMT3B
Max	885	936	957	903
Upper quartile (0.75)	334	422	439	360
Median	190	232	299	202
Lower quartile (0.75)	78	108	140	86
Min	7	12	12	8
Average	228	293	334	225
No. of chromocenter / nuclei	9.15	8.83	7.70	7.70

Figure 3.11: MeCP2 knockdown significantly affects the size of DAPI dense chromocentres in NIH 3T3 cells. (A) Representative delta vision images of NIH 3T3 cells following 48 hour incubation with either control, KAP-1, MeCP2 or DNMT3B siRNA. Cells were stained with DAPI (blue). **(B)** DAPI dense chromocentre intensity was analyzed using high resolution Delta vision images using Image J software. P values were calculated using a two sample t test assuming unequal variances. KAP-1: P(T<=t) = 0.073, MeCP2: P(T<=t) = 0.007, DNMT3B: P(T<=t) = 0.921.

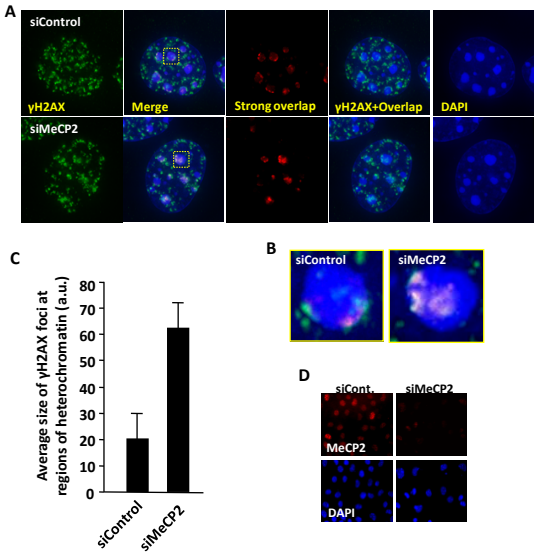

Figure 3.12: The size of IR induced γH2AX foci expansion at regions of heterochromatin increases following MeCP2 knockdown. (A) NIH 3T3 murine cells were transfected with control or MeCP2 siRNA for 48 hours. Cells were irradiated with 3 Gy IR and 30 minutes later immunostained for γH2AX (green) and DAPI (blue). Using the Delta Vision microscope, high resolution, deconvolved Z stack images were obtained. To analyze quantitatively regions of γH2AX and DAPI overlap, Sorftworx suite software was used. Red represents regions of strong DAPI (blue) and FITC (green) overlap. **(B)** Picture panel represent a close up of the region outlined in yellow in (A). **(C)** The relative size of γH2AX foci at regions of heterochromatin was assessed using ImageJ software. **(D) Image showing knockdown efficiency.** NIH 3T3 cell were treated with MeCP2 siRNA as described in (A) and immunostained for MeCP2 (red) and DAPI (blue). Results are representative of 3 independent experiments.

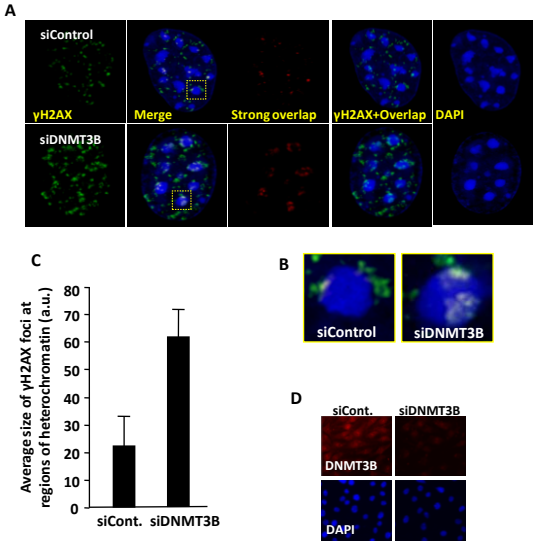

Figure 3.13: The size of IR induced γH2AX foci expansion at regions of heterochromatin increases following DNMT3B knockdown. (A) NIH 3T3 murine cells were transfected with control or DNMT3B siRNA for 48 hours. Cells were irradiated with 3 Gy IR and 30 minutes later immunostained for γH2AX (green) and DAPI (blue). Using the Delta Vision microscope, high resolution, deconvolved Z stack images were obtained. To analyze quantitatively regions of γH2AX and DAPI overlap, Sorftworx suite software was used. Red represents regions of strong DAPI (blue) and FITC (green) overlap. **(B)** Picture panel represent a close up of the region outlined in yellow in (A). **(C)** The relative size of γH2AX foci at regions of heterochromatin was assessed using ImageJ software. **(D)** NIH 3T3 cell were treated with DNMT3B siRNA as described in (A) and immunostained for DNMT3B (red) and DAPI (blue). Results are representative of 3 independent experiments.

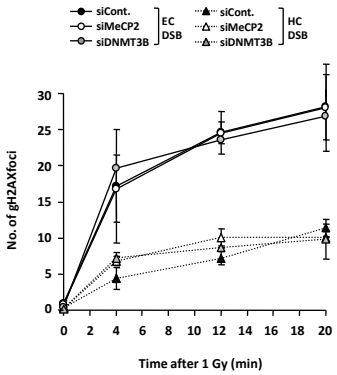

Figure 3.14: IR induced γH2AX foci form with faster kinetics in NIH 3T3 cells following MeCP2 or DNMT3B knockdown. NIH 3T3 cells were treated with either control, MeCP2 or DNMT3B siRNA for 48 hours. Following transfection, cells were irradiated with 1 Gy IR and fixed and immunostained for γH2AX at indicated time points. γH2AX foci co-localizing with DAPI dense regions (chromocenters) were scored as heterochromatin (HC) DSBs. γH2AX foci not co-localizing with DAPI dense regions were scored as euchromatin (EC) DSBs. Results are representative of 3 independent experiments.

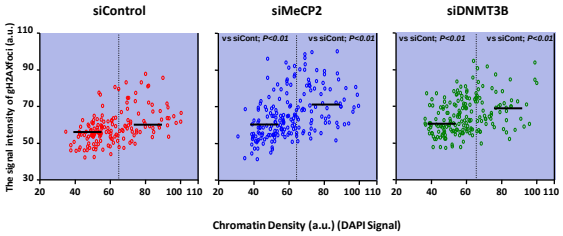

Figure 3.15: IR induced γH2AX signal intensity increases following MeCP2 or DNMT3B knockdown. NIH 3T3 cells were treated with either control, MeCP2 or DNMT3B siRNA for 48 hours. Following transfection, cells were fixed and immunostained for γH2AX 30 minutes post 3 Gy IR. To analyze γH2AX and DAPI signal intensity the Zeiss xeoplane microscope was used and exposure times kept constant. To measure signal intensity, each γH2AX foci and corresponding DAPI region was analyzed using ImageJ software. Black lines represent the median values. Statistical significance was determined using Student's two-tailed *t* test.

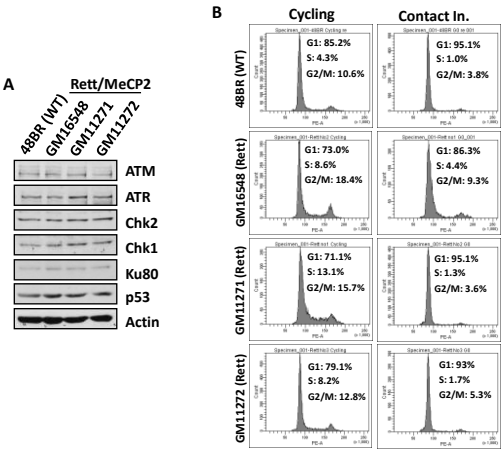

Figure 3.16: Protein expression of ATM, ATR, Chk2, Chk1, Ku80 and p53 in Rett syndrome patient GM16548 (Rett/MeCP2), GM11271 (Rett/MeCP2) and GM11272 (Rett/MeCP2) is normal. (A) Cycling populations of 48BR (WT), GM16548 (Rett/MeCP2), GM11271(Rett/MeCP2) and GM11272(Rett/MeCP2) primary fibroblast cells were harvested for whole cell protein extract. 50 µg of extract was resolved on a 8% denaturing SDS gel. Larger molecular weight proteins (ATM and ATR) were transferred to a nitrocellulose membrane at 12V overnight at 4°. The other molecular weight proteins were transferred as described in materials and methods. Membranes were immunoblotted for indicated antibodies. **(B) Cell cycle profile analysis of GM16548 (Rett/MeCP2) GM11271 (Rett/MeCP2) and GM11272 (Rett/MeCP2)**. Cycling and contact inhibited (more than 10 days confluent) G1 arrested 48BR (WT), and Rett syndrome (MeCP2) primary fibroblasts were prepared for FACS analysis as described in materials and methods. Results are representative of three independent experiments.

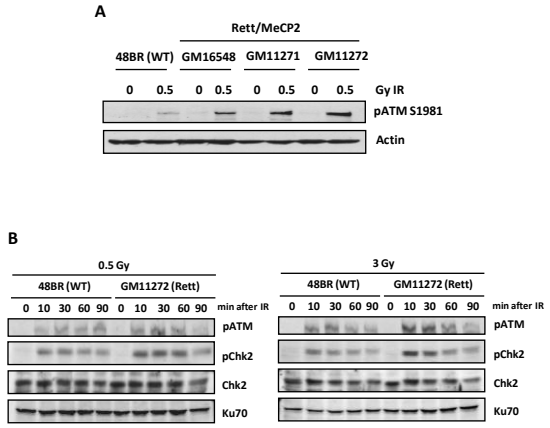

Figure 3.17: (A) Rett syndrome patient cells display hyperactive ATM activation in cycling cell populations following DNA damage. Cycling 48BR (WT), GM16548 (Rett/MeCP2), GM11271 (Rett/MeCP2) and GM1172 (Rett/MeCP2) primary fibroblasts were irradiated with either 0 or 0.5 Gy IR and harvested 0.5 hr later. Whole cell extracts were prepared and immunoblotted for indicated antibodies. **(B) ATM and Chk2 activation is also increased in G1 arrested Rett syndrome patient cells compared to WT cells following DNA damage.** G1 arrested, more than 10 days confluent, 48BR (WT) and GM11272 (Rett/MeCP2) primary fibroblasts were irradiated with either 0, 0.5 or 3 Gy IR and harvested at indicated time points post IR. Whole cell extracts were prepared and immunoblotted for indicated antibodies. Blots are representative of 3 independent experiments. 0 = no IR treatment.

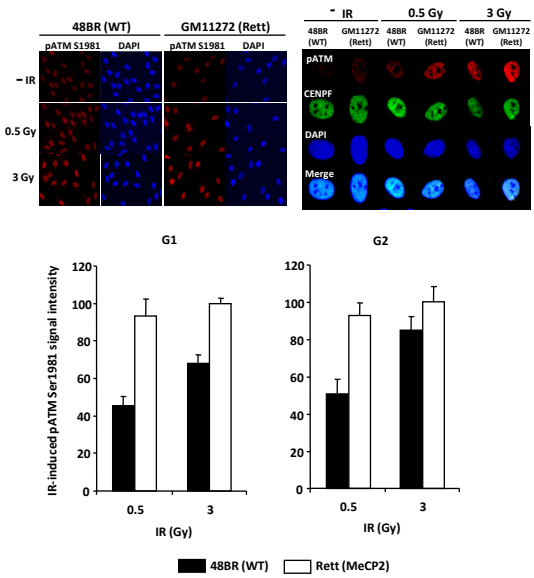

Figure 3.18: Rett syndrome cell lines exhibit enhanced ATM signalling after IR in G1 and G2 phase cells. Cycling 48BR (WT) and Rett syndrome (MeCP2) fibroblasts were irradiated with indicated doses IR. 30 minutes post IR cells were fixed and immunostained for pSer1981 ATM (red), DAPI (blue) and the G2 marker CENP-F (green). Pan nuclear pSer1981 ATM signal intensity in G1 phase (CENP-F negative) cells was analyzed using ImageJ software. **(B)** 48BR (WT) and Rett syndrome (MeCP2) fibroblast cells were treated as in (A). Pan nuclear pS1981 ATM signal intensity in G2 phase (CENP-F positive) cells was analyzed using ImageJ software. Results are representative of +/- SD of three independent experiments.

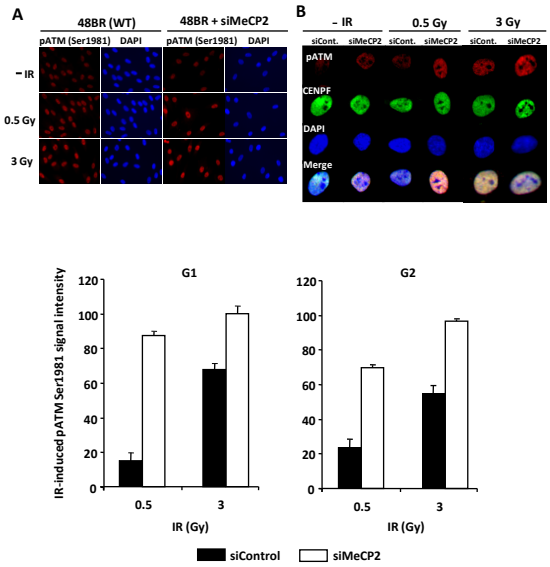

Figure 3.19: ATM phosphorylation is hyperactive in G1 and G2 phase 48BR (WT) primary cells knocked down for MeCP2. 48BR (WT) fibroblast cells were transfected with either control or MeCP2 siRNA for 48 hours. Cell were irradiated with indicated doses IR. 30 minutes post IR cells were fixed and immunostained for pSer1981 ATM (red), DAPI (blue) and the G2 marker CENP-F (green). Pan nuclear pSer1981 ATM signal intensity in G1 phase (CENP-F negative) cells was analyzed using ImageJ software. **(B)** 48BR (WT) fibroblast cells were treated as in (A). Pan nuclear pSer1981 ATM signal intensity in G2 phase (CENP-F positive) cells was analyzed using ImageJ software. Results are representative of +/- SD of three independent experiments.

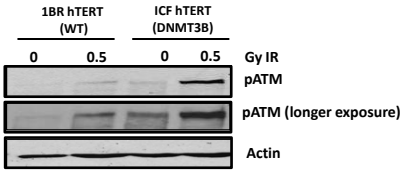

Figure 3.20: ATM activation is hyperactive in ICF (DNMT3B) syndrome hTERT cells. Contact inhibited G1 arrested 1BR (WT) and ICF (DNMT3B) hTERT cells were irradiated with either 0 or 0.5 Gy IR. Whole cell extracts were prepared and immunoblotted with the indicated antibodies. Of note, when over exposed the 0 hr signal for pSer1981 ATM activation in the ICF (DNMT3B) hTERT cells was as pronounced as that observed in the 1BR (WT) hTERT cells after 0.5 Gy IR.

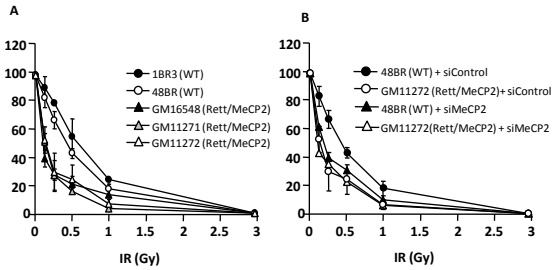

Figure 3.21: Rett syndrome patient cells initiate G2/M checkpoint arrest hypersensitively following IR. (A) 48BR (WT), GM16548 (Rett/MeCP2), GM11271 (Rett/MeCP2) and GM11272 (Rett/MeCP2) primary fibroblast cells were grown on cover slips for 48 hours and irradiated with indicated doses IR. 1 hour post IR, cells were fixed and immunostained for pS10 histone H3 (mitotic marker). The number of pS10 histone H3 positive cells were counted and normalized to the un-irradiated control. **(B)** 48BR (WT) and GM11272 (Rett/MeCP2) fibroblasts were treated with either control or MeCP2 siRNA for 24 hours, retransfected, and incubated with siRNA for a further 48 hours. Cells were irradiated with indicated doses and IR and fixed and immunostained for pS10 histone H3 1 hour later. No additive effect on checkpoint sensitivity was observed following MeCP2 knockdown in GM11272 (Rett/MeCP2) fibroblasts. Results represent the +/- SD of three experiments.

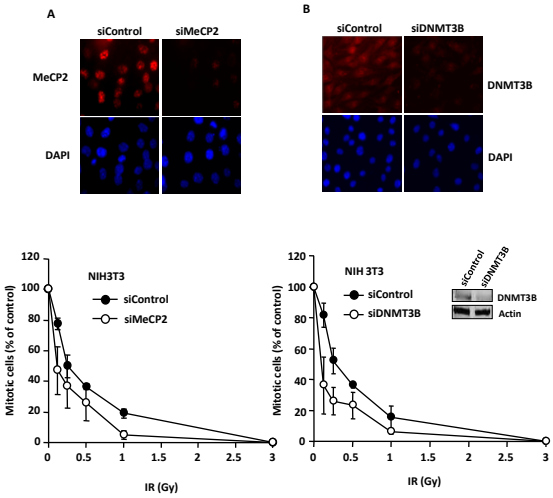

Figure 3.22: MeCP2 and DNMT3B knockdown confers a hypersensitive G2/M checkpoint arrest in NIH 3T3 cells following IR. (A) NIH 3T3 cells were transfected with MeCP2 siRNA for 48 hours. Cells were irradiated with indicated doses IR. 1 hour post IR cells were fixed and immunostained for pS10 histone H3. pS10 histone H3 positive cells were scored and normalized to the un-irradiated control. Representative immunofluorescent images of knockdown efficiency are shown: MeCP2 (red) and DAPI (blue). **(B)** NIH 3T3 cells were treated with DNMT3B siRNA for 48 hours, cells were treated as in (A). Western blot showing knockdown efficiency. Protein extracts were harvested from cells transfected with either control or DNMT3B siRNA. 60 µg of whole cell extract was immunoblotted for DNMT3B and Actin (loading control). Representative immunofluorescence images are shown of knockdown efficiency: DNMT3B (red) and DAPI (blue). Results are representative of three independent experiments.

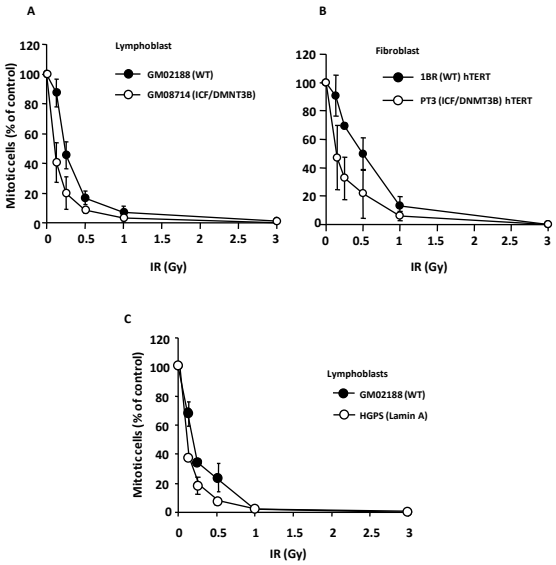

Figure 3.23: ICF (DNMT3B) syndrome and HGPS (Lamin A) cell lines also exhibit a hyperactive G2/M checkpoint response following IR. (A) 1BR (WT) and PT3 (ICF) hTERT cells were grown on cover slips for 48 hours and irradiated with indicated doses IR. 1 hour post IR cells were fixed and immunostained for pS10 histone H3. The number of pS10 histone H3 positive cell were counted and normalized to the un-irradiated control. **(B)** GM02188 (WT) and GM08714 (ICF) lymphoblast cells were treated as in (A). The number of pS10 histone H3 positive cells were scored and normalized to the un-irradiated control. **(C)** GM02188 (WT) and HGPS lymphoblast cells were irradiated with indicated doses IR and fixed and immunostained for pS10 histone H3 1 hour later. The number of pS10 histone H3 positive cells were counted and normalized to the un-irradiated control. Results represent the +/- SD of three experiments.

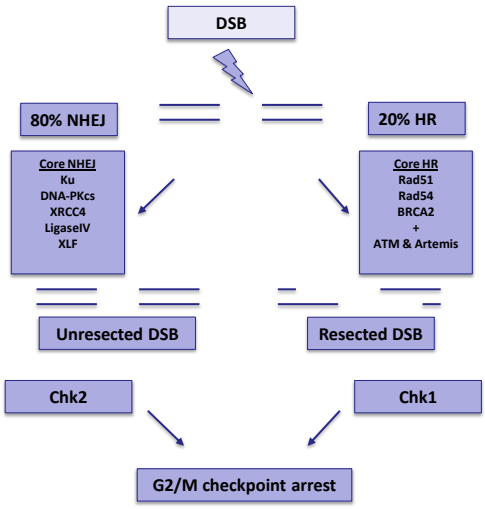

Figure 4.1: Model showing the mechanisms contributing to G2/M checkpoint arrest. In G2 phase, two DSB repair mechanisms exists, these being Non-Homologous end Joining (NHEJ) and Homologous Recombination (HR). Around 80% of DSB in G2 are repaired with fast kinetics by the core NHEJ machinery (Beucher et al., 2009). DSBs repaired by NHEJ are unresected and signal via ATM to Chk2 to initiate checkpoint arrest. A subcomponent (~20%) of DSBs in G2 undergo ATM dependent resection, generating RPA coated ssDNA that signals via ATR to Chk1 to mediate checkpoint arrest (Jazayeri et al., 2006). Resected DSBs are repaired with slow kinetics by HR (Beucher et al., 2009). Therefore at late time points after IR, arrest is mainly dependent on HR repair (Shibata et al., 2010). Therefore checkpoint arrest is maintained by ATR dependent Chk1 activation at resected DSBs and sustained ATM to Chk2 signalling at unrepaired DSBs (Shibata et al., 2010)

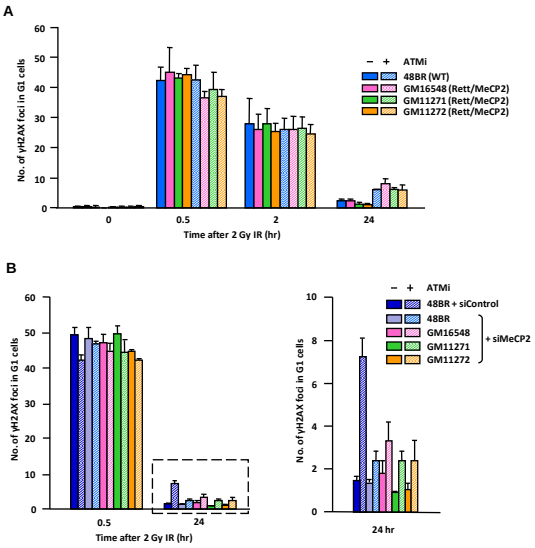

Figure 4.2: DSB repair is normal in G1 phase Rett syndrome primary cells and MeCP2 knockdown rescues the ATM dependent repair defect. (A) 48BR, Rett syndrome patient (GM16548, GM11271 & GM11272) primary fibroblasts were treated with -/+ ATMi 30 minutes prior to IR. Cells were irradiated with 3 Gy IR and fixed at indicated time points. Numbers of γH2AX foci were scored. **(B)** Cells were treated as in (A) with the addition of either control or MeCP2 siRNA for 48 hours prior to -/+ ATMi treatment. All results represent the +/- SD of three independent experiments.

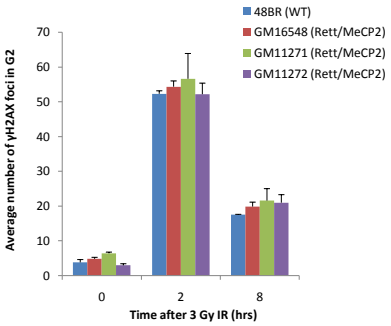

Figure 4.3: DSB repair is normal in G2 phase Rett syndrome primary cells (A) 48BR, Rett syndrome patient (GM16548, GM11271 & GM11272) primary fibroblasts were irradiated with with 3 Gy IR and fixed at indicated time points. Numbers of γH2AX foci were scored. All results represent the +/- SD of three independent experiments.

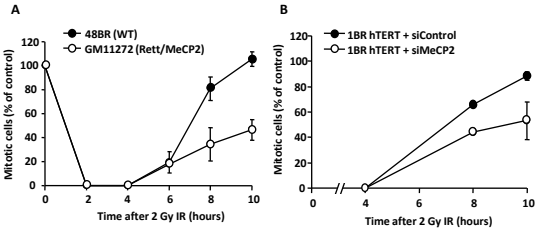

C

Average number of mitotic cells (%)				
Time after IR (hr)	48BR primary	GM11272 (Rett/MeCP2)	1BR hTERT + siControl	1BR hTERT + siMeCP2
0	2.9	3.5	2.7	3.1
4	0.0	0.0	0.0	0.0
8	2.2	1.2	1.9	1.4
10	3.5	1.5	2.5	1.8

Figure 4.4: **Rett and MeCP2 knockdown cells have a prolonged G2/M checkpoint arrest (A)** 48BR and Rett syndrome patient (GM11272) primary fibroblasts were irradiated with 2 Gy IR, treated with aphidicolin (4μM) and fixed at indicated time points. Cells were immunostained for pS10 histone H3. pS10 histone H3 positive mitotic cells were scored and expressed as a percentage of the control mitotic population. **(B)** 1BR hTERT cells were treated with either control or MeCP2 siRNA for 48 hours. Following transfection, cells were irradiated with 2 Gy IR, treated with aphidicolin (APH) and harvested at indicated time points. **(C)** Table of the average percentage of mitotic cells (without normalization) after IR for each cell type. All results represent the +/- SD of three experiments

A

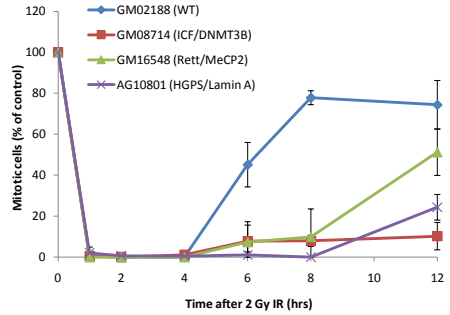

B

Average number of mitotic cells (%)				
Time after IR (hr)	GM02188 (WT)	GM08714 (ICF/DNMT3B)	GM16548 (Rett/MeCP2)	AH10801 (HGPS/Lamin A)
0	3.5	4.0	3.1	2.5
1	0.1	0.0	0.0	0.0
2	0.0	0.2	0.2	0.1
4	0.1	0.1	0.1	0.0
6	1.9	0.7	0.5	0.0
8	3.0	0.7	0.6	0.1
12	3.3	1.0	1.9	1.0

Figure 4.5: Rett, ICF and HPGS lymphoblastiod cells maintain a prolonged G2/M checkpoint arrest. (A) GM02188 (WT), GM08714 (ICF/DNMT3B), GM16548 (Rett/MeCP2) and AG10801 (HGPS/LaminA) lymphoblastiod cells were irradiated with 2 Gy IR and treated with aphidicolin (4μM) immediately after IR. At indicated times after IR cells were harvested by cytospin and immunostained for pS10 histone H3. pS10 histone H3 positive cells were scored and expressed as a percentage of the control mitotic population. **(B)** Table of the average percentage of mitotic cells (without normalization) after IR for each cell type. All results represent the +/- SD of three experiments

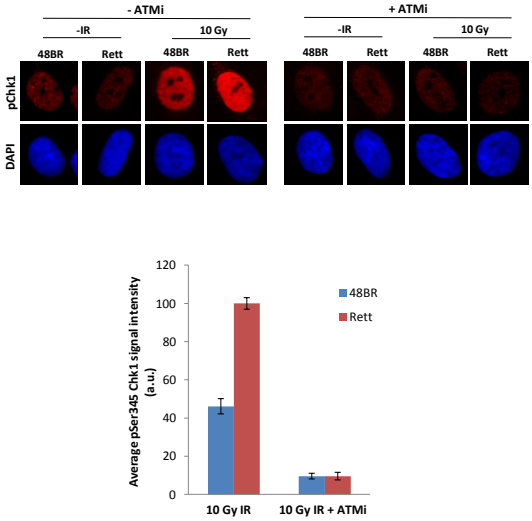

Figure 4.6: Hyperactive Chk1 activation in Rett syndrome patient GM11272 is ATM dependent. 48BR and Rett syndrome (GM12272) patient primary fibroblast cells were treated -/+ ATMi 30 minutes prior to IR. 1 hour post irradiating with either 0 or 10 Gy IR, cells were fixed and immunostained for pSer345 Chk1 (red) and DAPI (blue). Cells were also stained for CENP-F to select for G2 phase cells. 20 G2 phase cells were analyzed per condition. Results are representative of +/- SD of three independent experiments. a.u. = arbitrary units.

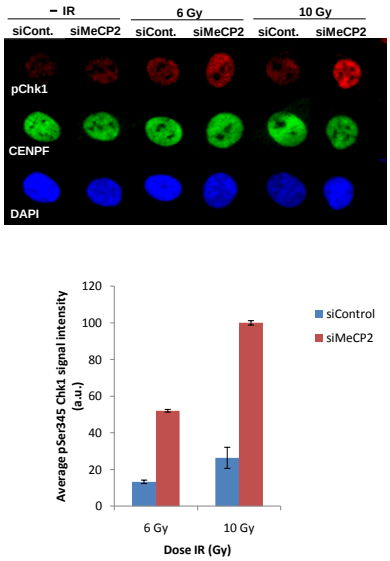

Figure 4.7: pSer345 Chk1 phosphorylation is hyperactive in 48BR primary cells knocked down for MeCP2. 48BR (WT) fibroblast cells were transfected with either control or MeCP2 siRNA for 48 hours. Cell were irradiated with indicated doses IR. 1 hour post IR cells were fixed and immunostained for pSer345 Chk1 (red), DAPI (blue) and the G2 marker CENP-F (green). Pan nuclear pSer345 Chk1 signal intensity in G2 phase (CENP-F positive) cells was analyzed using ImageJ software. 20 G2 phase cells were analyzed per condition. Results are representative of +/- SD of three independent experiments. a.u. = arbitrary units.

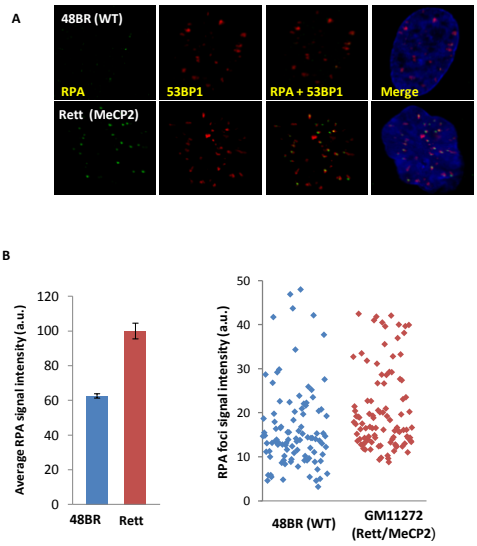

Figure 4.8: RPA foci signal intensity is enhanced in Rett syndrome patient cells(A) 48BR (WT) and Rett syndrome (GM11272) primary fibroblasts were irradiated with 3 Gy (IR). 1 hour following IR, cells were pre-extracted using 0.2% trition for 1 minute before fixing. Cells were immunostained for RPA (green), 53BP1 (red) and DAPI (blue). **(B)** Cells were treated as in (A). RPA signal intensity was analyzed for foci which co-localized with 53BP1 using Image J software.
a.u. = arbitrary units.

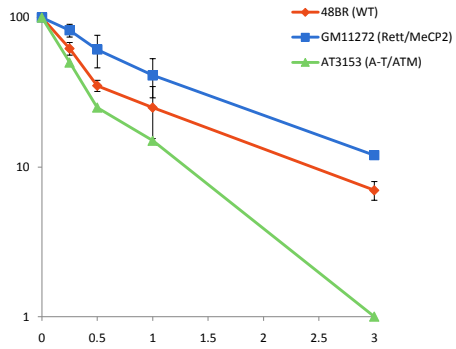

Figure 4.9: Rett syndrome cells have normal survival IR.
Radiosensitivity was assessed by colony survival analysis. 48BR (WT) and Rett syndrome (GM11272) cells were trypsinzed, irradiated with indicated doses IR and plated onto feeder cells prepared 24 hours earlier then left to form colonies for 3 weeks. The radiosensitivity of AT3153 (A-T/ATM) is also shown (take from M'Kacher et al., 2003).

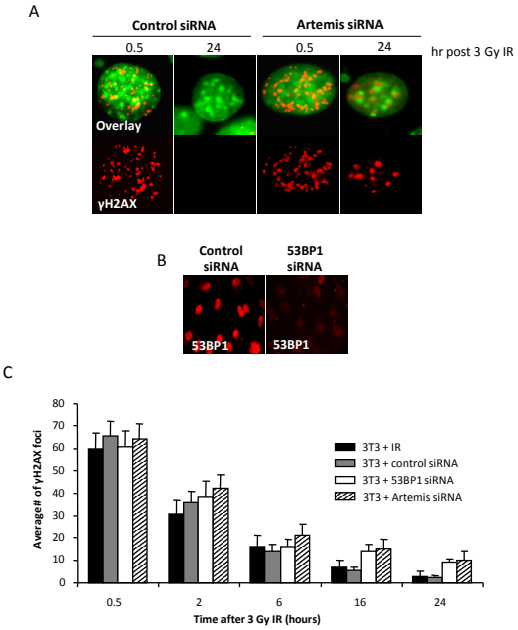

Figure 5.1: DSBs dependent on Artemis for repair reside within regions of heterochromatin. (A) NIH 3T3 cells were treated with either control or Artemis A & B siRNA oligo's for 48 hours before irradiating cells with 3 Gy IR and harvesting at time points indicated. Cells were fixed and immunostained for γH2AX (red) and DAPI (green). **(B)** 53BP1 knockdown in NIH 3T3 cells was confirmed by immunoflourescence. Cells were fixed and stained for 53BP1 (red) 48 hours following transfection. **(C)** NIH 3T3 cells were treated as in (A) with the indicated siRNA oligo's and harvested at indicated time points. Total γH2AX foci numbers were enumerated. More than 30 cells were randomly selected for each condition. All results represent the +/- SD of three experiments

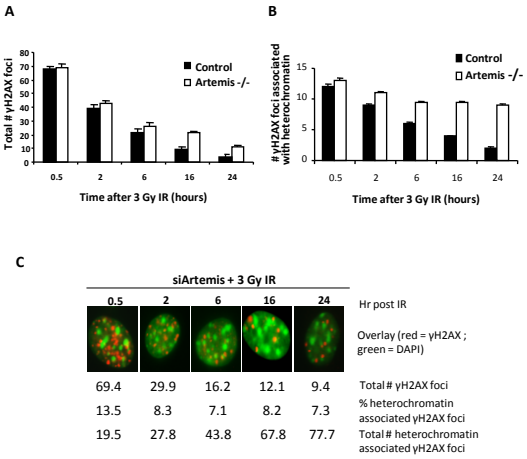

Figure 5.2: More than 70% of unrepaired IR induced DNA double stranded breaks are visibly associated with regions of heterochromatin in Artemis siRNA transfected NIH 3T3 cells. (A) NIH 3T3 cells were treated with Artemis A & B siRNA oligo's for 48 hours before irradiating cells with 3 Gy IR. Cells were fixed and harvested at indicated time points. Total γH2AX foci numbers were counted. **(B)** γH2AX foci localizing with dense DAPI staining regions (heterochromatin) were also scored. **(C)** NIH 3T3 cells were treated as in (A). The total number of γH2AX foci associated with regions of heterochromatin was counted for a minimum of 30 cells and the average of 3 experiments is shown. The percentage of breaks associated with heterochromatin has been calculated.

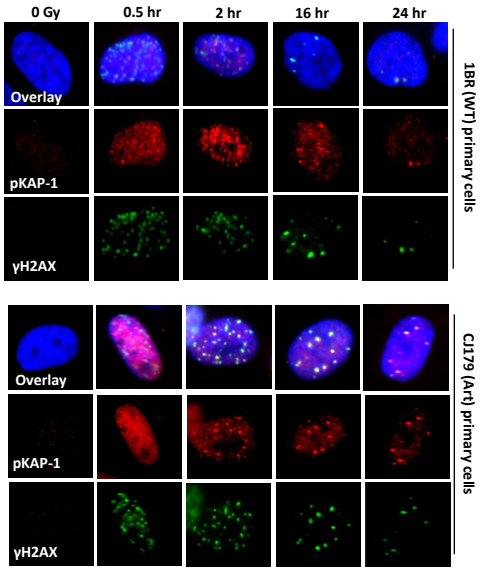

Figure 5.3: Phospho-KAP-1 co-localizes with late repairing γH2AX foci in Artemis defective human cells. 1BR (WT) and CJ179 (Art) primary cells were grown on cover-slips until confluent, irradiated with 3 Gy IR and harvested and indicated time points. Cells were fixed and stained for pKAP-1 (red), γH2AX (green) and DAPI (blue).

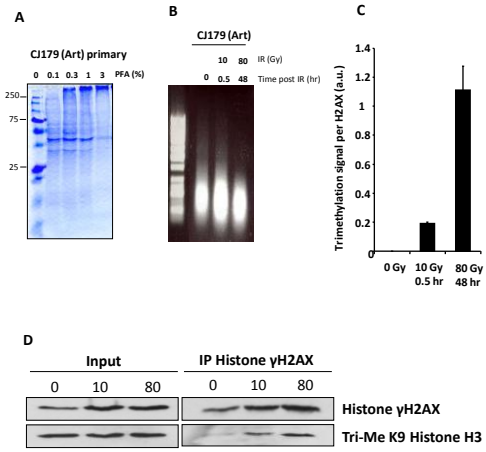

Figure 5.4: Artemis dependent DSBs are enriched for the heterochromatic marker Tri-Me K9 Histone H3. **(A)** First a suitable fixation condition was optimized for the IP. Protein extracts were prepared as described in materials and methods from CJ179 (Art) primary cells. Extracts were treated with indicated doses of PFA and fixed for 3 minutes prior to resolving on a 8% denaturing SDS gel, followed by commassie staining. 0.1% PFA was selected on the basis that no protein sample was fixed in the well after this concentration. **(B)** Next the size of DNA fragments generated after sonication was analysed. CJ179 (Art) primary cells were irradiated with either 10 Gy (30 minute recovery) or 80 Gy (48 hour recovery) IR. Whole cell DNA extracts (5 µg) were prepared as described in materials and methods and resolved on an agarose gel. **(C)** Quantification of 3 separate γH2AX immunoprecipitations in CJ179 (Art) primary cells. **(D)** CJ179 (Art) primary cells were irradiated and harvested at indicated time points. Cells were lysed and nucleosomes solubilized as described in materials and methods. Soluble nucleosome extracts (60 µg) were blotted for γH2AX and trimethylated K9 of histone 3 (Tri-Me K9 H3). γH2AX was immunoprecipitated from soluble nucleosome extract, and blotted for γH2AX and Tri-Me K9 H3 (IP Histone γH2AX sample). All results represent the +/- SD of three independent experiments

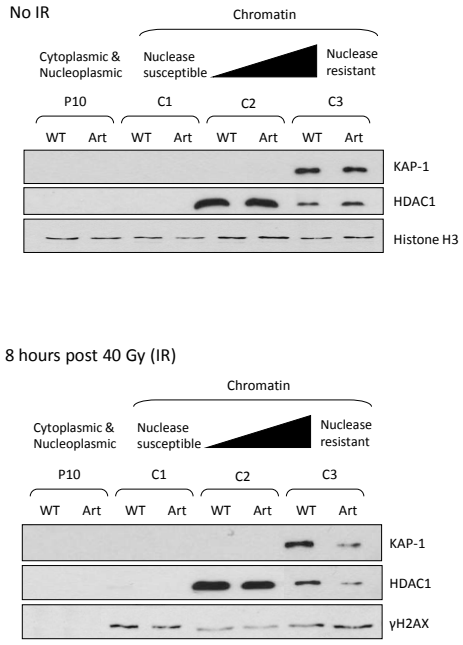

Figure 5.5: IR induced KAP-1 dissociation from chromatin enriched fractions is prolonged in Artemis defective cells. Confluent, contact inhibited wildtype or Artemis MEFs were irradiated with either 0 or 40 Gy IR and harvested 8 hours later. Cells were processed for chromatin fractionation as described in the materials and methods. Cell extracts were resolved on a split 7.5% and 17.5% denaturing SDS gel and immunoblotted for the indicated antibodies. Results are representative of three independent experiments.

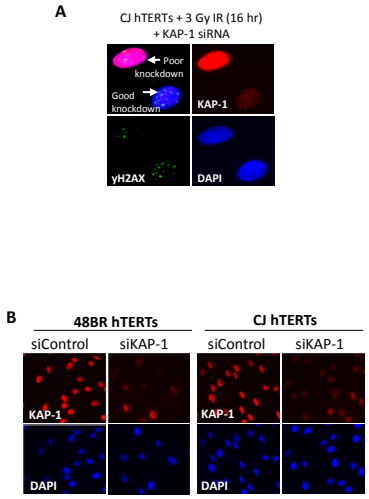

Figure 5.6: KAP-1 knockdown does not alleviate the requirement for Artemis in DSB repair. (A) A representative image of a CJ hTERT (Art) cell selected on the basis of successful knockdown. 24 hours post 3 Gy IR, following a 48 hour KAP-1 siRNA transfection incubation, cells were fixed and stained for KAP-1 (red), γH2AX (green) and DAPI (blue). Both a successful (faint red) and unsuccessful (bright red) KAP-1 knockdown cell is shown. 100x magnification is shown **(B)** 48BR (WT) hTERT and CJ (Art) hTERT cells were transfected with control or KAP-1 siRNA. At 48 hours post transfection, cells were harvested and stained for KAP-1 (red) and DAPI (blue). 40x magnification is shown.

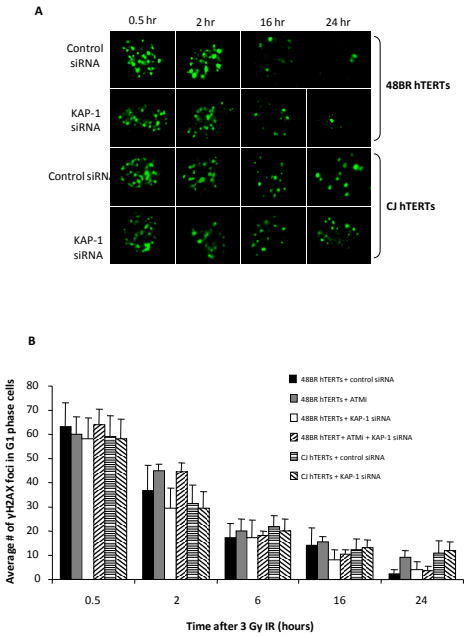

Figure 5.7: KAP-1 knockdown does not alleviate the requirement for Artemis in DSB repair. (A) Representative images of γH2AX foci (green) in successfully KAP-1 knocked down hTERT cells. **(B)** hTERT cells were transfected as in (A). Cells were fixed and stained for KAP-1, γH2AX and DAPI. Cells treated with ATMi were incubated with the drug 30 minutes prior to IR. Numbers of γH2AX foci were scored. All results represent the +/- SD of three experiments.

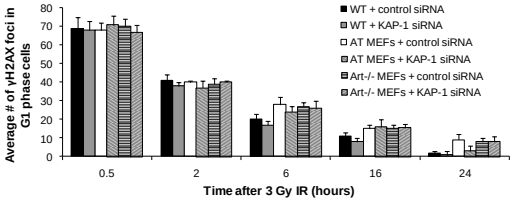

Figure 5.8: KAP-1 knockdown alleviates the DSB repair defect observed in AT MEFs but not Artemis defective MEFs. 48 hours following siRNA transfection, cells were irradiated with 3 Gy IR. Cells were harvested at time points indicated following IR, fixed and immunostained for KAP-1, γH2AX and DAPI. γH2AX foci were counted in cells successfully knockdown for KAP-1. All results represent the +/- SD of three independent experiments

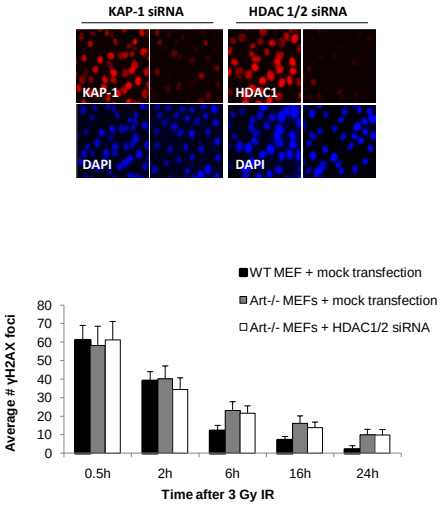

Figure 5.9: HDAC1 and HDAC2 knockdown does not alleviate the requirement for Artemis in DSB repair. (A) Art$^{-/-}$ MEFs were transfected with KAP-1 or HDAC1/2 siRNA for 48 hours. Cells were fixed and stained for KAP-1 (red) or HDAC2 (red) and DAPI (blue). **(B)** 48 hours following siRNA transfection cells were irradiated with 3 Gy IR. Cells were harvested at time points indicated following IR, fixed and immunostained for HDAC1, γH2AX and DAPI. γH2AX foci were counted in cells successfully knockdown for HDAC1/2. Results represent the +/- SD of three independent experiments.

Particle	LET (keV/μm) (ICRU Report 16, 1970)	Particle status after cellular absorption (Sekine et al., 2008)	Chromosome exchange frequency (Himada et al., 2010)	DNA fragment frequency (Himada et al., 2010)
X-ray	1.7	-	0.23	0.16
Carbon	68.3 – 70.0	C: ~87% dose contribution (~50% original, other nucleotides: He and H)	0.45	0.71
Iron	199.3 - 200.0	Fe: over 90% dose contribution (over 80% original)	0.61	0.88

Table 6.1: The frequency of chromosome aberrations increases with LET value. Chromosome aberration frequency was measured by premature chromosome condensation and fluorescence *in situ* hybridization (FISH) (Himada et al., 2010). Secondary particles such as H and He (lighter fragments) also contribute to ion induced damage after Fe ions (Sekine et al., 2008).

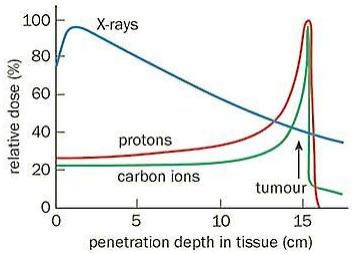

Figure 6.1: Heavy ions such as protons and Carbon ions have a bragg peak. X-rays (photons) lose energy rapidly by ionization as they travel through the body. Charged particles such as protons and carbon ions deposit most of their energy at a specific depth that depends on their energy (called the Bragg peak). This means that they can deliver a high radiation dose at a tumour site, while sparing the surrounding healthy tissue.

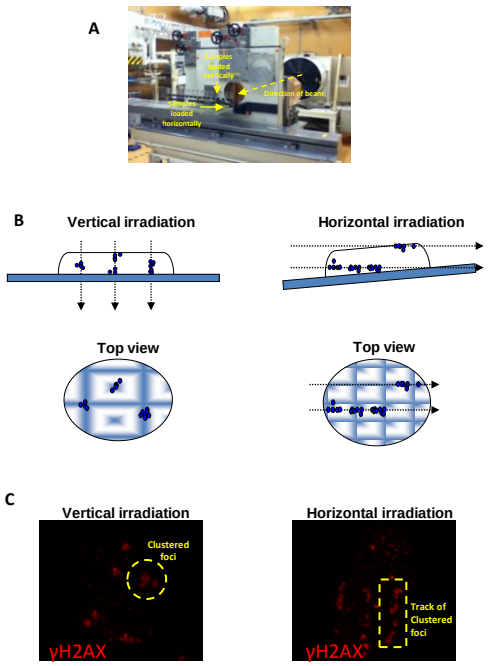

Figure 6.2: Fe ion irradiation can be administered either vertically or horizontally.
(A) Photograph of the HIMAC at the NIRS. Yellow dashed arrow indicated direction of ion beam. Solid yellow arrows indicate the directions that samples were loaded for horizontal or vertical IR. (B) Schematic representation of the direction the ion beam will hit cells when irradiating either vertically or horizontally. (C) 1BR hTERT cells irradiated with 1 Gy Fe ions either vertically or horizontally. Cells were fix and immunostained for γH2AX (red) 4 hours after IR.

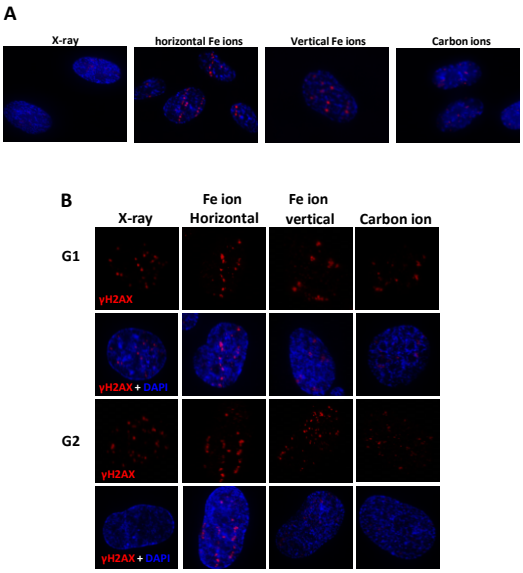

Figure 6.3: Heavy ion irradiation produces variation in the number of DSBs induced between cells, and the type of γH2AX foci formed differs from that after X-rays. (A) The number of DSBs induced after heavy ion irradiation varies between each cell. 1BR hTERT cells were fixed 1 hour after irradiating with 1 Gy either X-ray, Fe ions (horizontally or vertically) or Carbon ions and stained with γH2AX (red), DAPI (blue) and CENP-F (not shown). Images were obtained using a Delta vision microscope with deconvolution (60x). **(B) The shape and size of heavy ion induced γH2AX foci differ from that of X-ray induced foci**. Cells were treated as in (A). G2 phase cells were selected on the basis of staining positive for CENP-F.

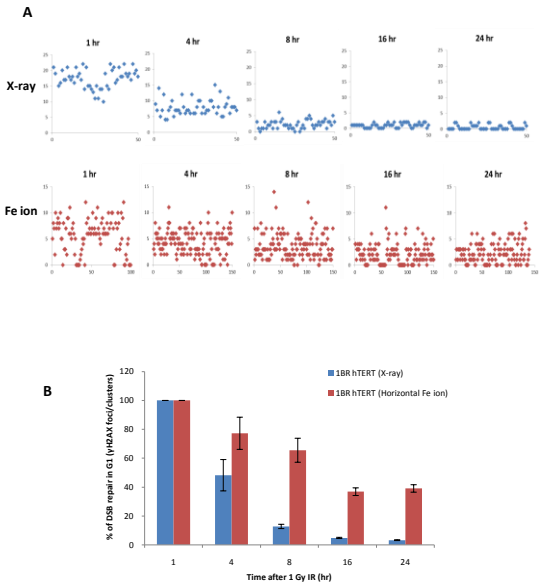

Figure 6.4: Horizontal Fe ion irradiation induces DSBs are repaired with slow kinetics in G1. (A) A large variation in the number of DSBs induced between cells after Fe ion irradiation is observed. Scatter blots represent the number of γH2AX foci per cell, with more than 30 cells scored for each time point. 1BR hTERT cells were irradiated with 1 Gy either X-ray or horizontal Fe ions. Cells were fixed at indicated time points after IR and immunostained for γH2AX, CENP-F and DAPI. γH2AX foci were quantified in G1 (CENP-F negative) cells. **(B)** Percentage rate of DSB repair after horizontal Fe ion and X-ray irradiation. Cells were treated as in (A). The number of γH2AX foci were normalized with the number of foci at 1 hour post IR. Error bars represent the standard deviation of the mean from 2 independent experiments

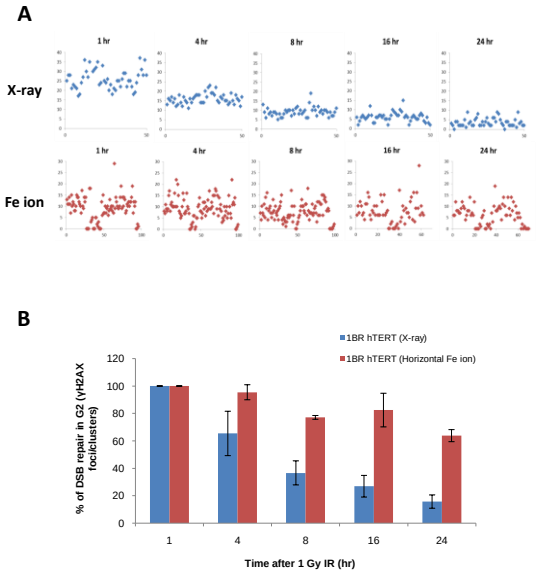

Figure 6.5: Horizontal Fe ion irradiation induces DSBs are repaired with slow kinetics in G2. (A) A large variation in the number of DSBs induced after Fe ion irradiation is observed. Scatter blots represent the number of γH2AX foci per cell, with more than 30 cells scored for each time point. 1BR hTERT cells were irradiated with 1 Gy either X-ray or horizontal Fe ions. Cells were fixed at indicated time points after IR and immunostained for γH2AX, CENP-F and DAPI. γH2AX foci were quantified in G2 (CENP-F positive) cells. **(B)** Percentage rate of DSB repair after horizontal Fe ion and X-ray irradiation. Cells were treated as in (A). The number of γH2AX foci were normalized with the number of foci at 1 hour post IR. Error bars represent the standard deviation of the mean from 2 independent experiments

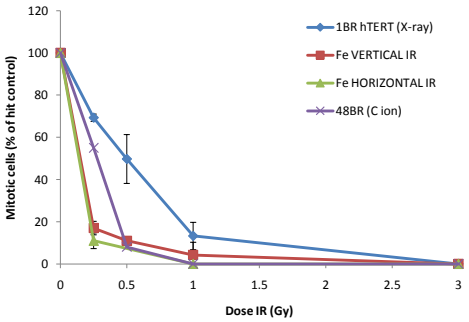

Figure 6.6: G2/M checkpoint arrest is initiated at lower doses after heavy ion irradiation. 48BR primary or 1BR hTRET cells were treated with APH and irradiated with either X-rays, Fe ions (vertically or horizontally) or Carbon ions at indicated doses of IR. One hour post IR, cells were fixed and immunostained for the mitotic marker pH3. pH3 positive cells were counted and normalized to the un-irradiated control. Error bars represent the standard deviation of the mean from 2 independent experiments

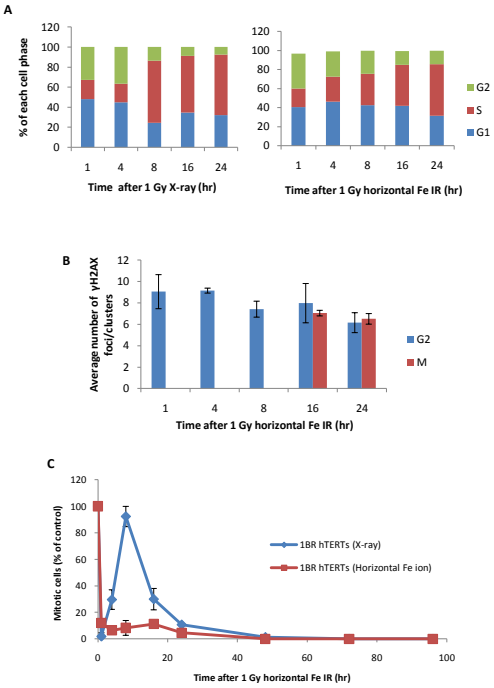

Figure 6.7: 1BR hTERT cells are released from the G2/M checkpoint with ~7-8 Fe (horizontal) ion induced DSBs. (A) Cell cycle progression after Fe ion irradiation is slowed. 1BR hTERT cells were treated with APH and irradiated with 1 Gy either X-ray or Fe ions. Prior to IR cells were treated with aphidicolin to prevent S phase cells progressing into G2 during analysis. Cells were fixed at indicated time points post IR and immunostained for γH2AX, pH3, CENP-F and DAPI. The percentage of G1 (CENP-F negative), G2 (CENP-F positive) and S (pan nuclear γH2AX) phase cells was calculated for a cell population containing at least 300 cells. (**B)** Cells released from the G2/M checkpoint manifest ~ 7 Fe ion induced DSBs. Cells were treated as in (A). γH2AX foci were counted in G2 and M phase cells at indicated time points. **(C)** Cells were treated as in (A). pH3 positive cells were counted and normalized to the un-irradiated control. Error bars represent the standard deviation of the mean from 2 independent experiments

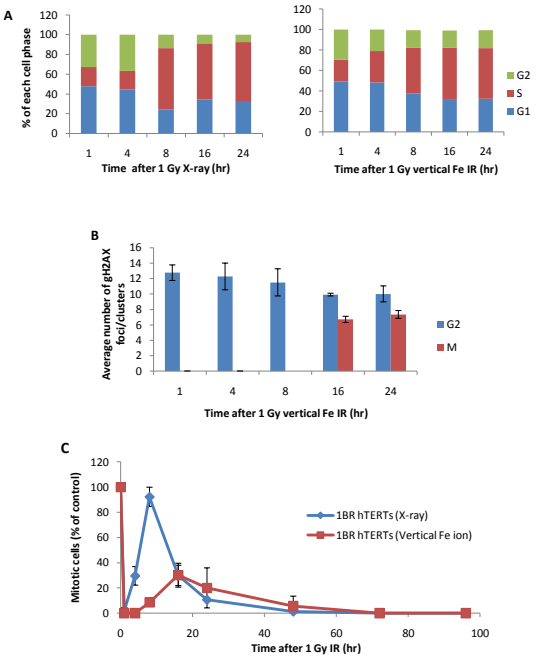

Figure 6.8: 1BR hTERT cells are released from the G2/M checkpoint with ~7 Fe (vertical) ion induced DSBs. (A) Cell cycle progression after Fe ion irradiation is slowed. 1BR hTERT cells were irradiated with 1 Gy either X-ray or Fe ions. Prior to IR cells were treated with aphidicolin to prevent S phase cells progressing into G2 during analysis. Cells were fixed at indicated time points post IR and immunostained for γH2AX, pH3, CENP-F and DAPI. The percentage of G1 (CENP-F negative), G2 (CENP-F positive) and S (pan nuclear γH2AX) phase cells was calculated for a cell population containing at least 300 cells. **(B)** Cells released from the G2/M checkpoint manifest ~ 7 Fe ion induced DSBs. Cells were treated as in (A). γH2AX foci were counted in G2 and M phase cells at indicated time points. **(C)** Cells were treated as in (A). pH3 positive cells were counted and normalized to the un-irradiated control. Error bars represent the standard deviation of the mean from 2 independent experiments

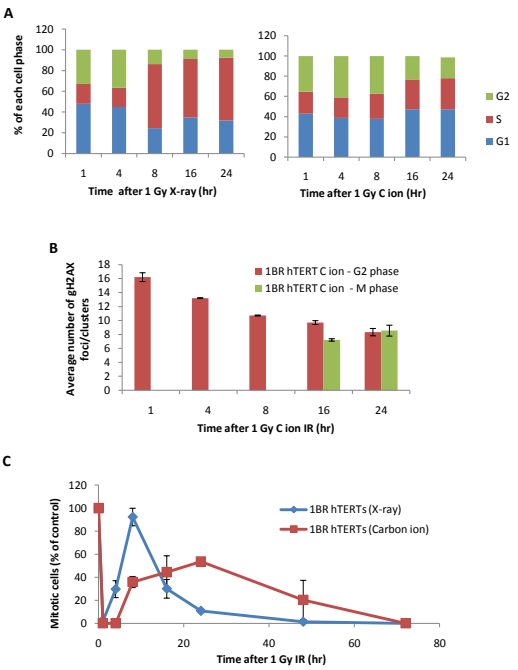

Figure 6.9: 1BR hTERT cells are released from the G2/M checkpoint with ~7 Carbon ion induced DSBs. (A) Cell cycle progression after Carbon ion irradiation is slowed. 1BR hTERT cells were irradiated with 1 Gy either X-ray or Carbon ions. Prior to IR cells were treated with aphidicolin to prevent S phase cells progressing into G2 during analysis. Cells were fixed at indicated time points post IR and immunostained for γH2AX, pH3, CENP-F and DAPI. The percentage of G1 (CENP-F negative), G2 (CENP-F positive) and S (pan nuclear γH2AX) phase cells was calculated for a cell population containing at least 300 cells. **(B)** Cells released from the G2/M checkpoint manifest ~ 7 Carbon ion induced DSBs. Cells were treated as in (A). γH2AX foci were counted in G2 and M phase cells at indicated time points. **(C)** Cells were treated as in (A). pH3 positive cells were counted and normalized to the un-irradiated control. Error bars represent the standard deviation of the mean from 2 independent experiments

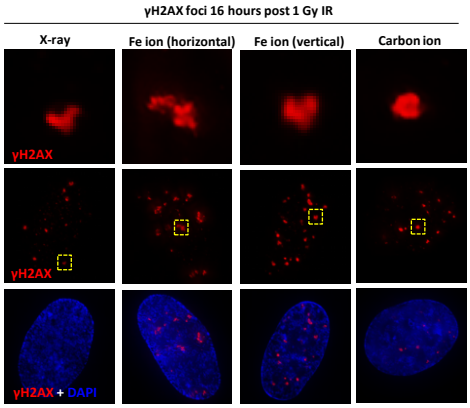

Figure 6.10: γH2AX foci 16 hours after irradiation with heavy ions.
1BR hTERT cells were irradiated with 1 Gy either X-ray, Fe ions (horizontal or vertical), or Carbon ions. 16 hours after irradiation cells were fixed and immunostained for γH2AX (red) and DAPI (blue)

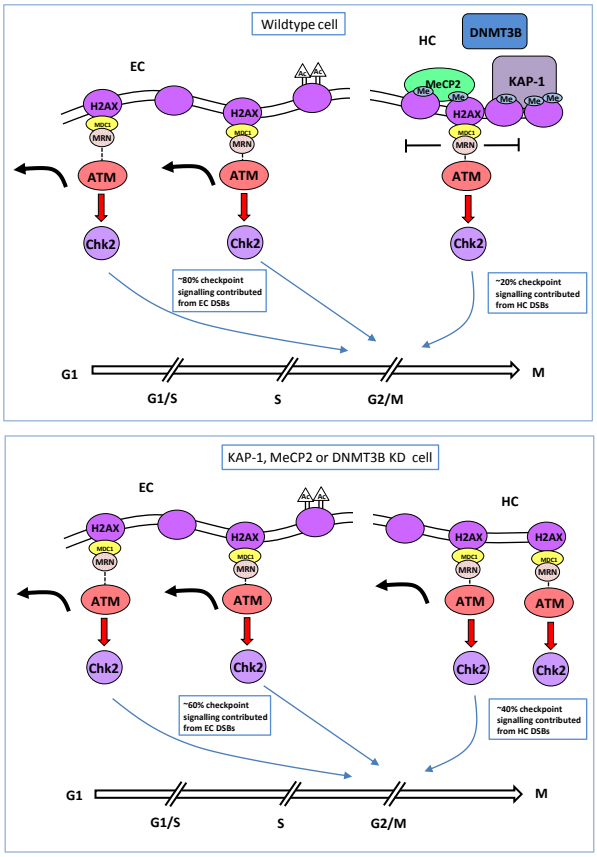

Figure 7.1: A model for hyperactive ATM signalling in the context of reduced higher order chromatin structure
(1) WILDTYPE CELL: Euchromatin (EC) - Sufficient γH2AX expansion occurs at EC-DSBs after IR which enables DSB repair with fast kinetics. However, γH2AX expansion at these regions is not indefinite, possibly due to repressive histone marks or rapid turnover of H2AX. Heterochromatin (HC) - Small localized chromatin relaxation occurs following H2AX phosphorylation. However, signalling from these DSBs at early times is modest until sufficient KAP-1 phosphorylation has been pursued following 53BP1 mediated tethering of ATM. **(2) KAP-1, MeCP2 or DNMT3B KD CELL:** Heterochromatin (HC) - More Chk2 signalling emanates from HC associated DSBs as a result of greater γH2AX expansion and hence more ATM activation. The repressive EC associated histone modifications may be absent in HC, and therefore γH2AX expansion is greater at HC in comparison to EC.